Lapped joints in reinforced concrete

R. C. B. Judge

LAPPED JOINTS
IN
REINFORCED CONCRETE

R.C.B. JUDGE

A Thesis submitted for the
Degree of PhD in the Faculty of
Science, University of Durham

October 1987

ABSTRACT

This thesis is concerned with an experimental investigation of the behaviour of lapped joints in reinforced concrete. A review of existing literature highlights the need to establish the longitudinal strain distribution along lap joints. This has been achieved experimentally, with detailed strain measurements being taken using a technique of internally gauging the reinforcing rods. In some specimens, strain concentration gauges were installed at the tip of the lap to permit the acquisition of particularly localised information. Computer programs were developed to process the substantial amounts of data generated during the course of each test.

Two series of tests were undertaken, both using axially loaded specimens, and dealing with tension and compression lap joints respectively. The laps ranged in length from 125 to 750 mm, and comprised bars of either 12 or 20 mm diameter. Transverse reinforcement was provided in two of the tension specimens.

Greater emphasis was placed on the first series, with fifteen tension specimens being tested. Thirteen of these tests were each completed within a single day but, additionally, two long-term tests were undertaken. In the latter, a constant load was sustained for up to 81 days. The measurements clearly showed the changing behaviour of the specimens, first as transverse cracks developed and subsequently as failure of the lap joint was approached. The comprehensive analysis of the test results includes a comparison of the ultimate behaviour of these joints with existing design proposals and regulations. The detailed information provided by the strain measurements enables the justification of design assumptions regarding lap joint behaviour, and thus lends greater confidence to existing design regulations.

The results from five compression specimens were analysed and compared with the tension tests. The significant contribution to force transfer made by the bearing of the free end of the steel against the concrete was evident. The specimens were loaded to the rig capacity without failing.

Additional strain measurements were taken in one tension and one compression specimen by casting embedment gauges within the concrete. These gauges were arranged to measure the circumferential strains in the specimen, and were complemented by strain gauges mounted on the surface of the concrete. The data thus obtained permitted a comparison of the bursting forces set up inside and outside the lap joints.

The work showed that some aspects of lap joint behaviour require clarification. Suggestions for further work are included.

ACKNOWLEDGEMENTS

I should like to thank my Supervisors, Dr. R.H. Scott and Dr. P.A.T. Gill for their advice and guidance over the last three years.

The project required considerable technical assistance, and I am grateful to Mr. T. Brown and Mr. B.P. Scurr for their help. I am also indebted to Mr. T.D. Harrison and Mr. S.M.P. Heseltine for the reliability of the strain gauge installations.

The analytical work, and subsequent presentation of results, involved the use of a number of computers. I am therefore much obliged to Mr. T. Nancarrow for his help in transferring data between various computing machines.

I wish to thank all those people whose helpful comments and suggestions contributed to this research, in particular Miss G. Quine for her considerable help with proof-reading this thesis.

Finally, I am pleased to acknowledge the financial support of the Science and Engineering Research Council.

STATEMENT OF COPYRIGHT

DECLARATION

No material in this thesis has previously been submitted for a degree in this or any other university.

CONTENTS

ABSTRACT i

ACKNOWLEDGEMENTS ii

STATEMENT OF COPYRIGHT iii

DECLARATION iii

CONTENTS iv

LIST OF FIGURES vi

NOTATION ix

1. INTRODUCTION 1

2. LITERATURE REVIEW 3

2.1 Introduction 3

2.2 Factors Influencing Lap Strength 6

2.3 Analyses of the Ultimate Strength of Lap Joints 10

2.4 Stress Distributions Along Lap Joints 16

2.5 Conclusion 21

3. STRAIN MEASUREMENTS 23

3.1 Strain Measurements in the Reinforcement 23

3.1.1 Strain gauging technique 23

3.1.2 Gauge layout 25

3.1.3 Strain concentration gauges 25

3.2 Other Strain Measurements 25

3.2.1 Surface strains 25

3.2.2 Embedment gauges 26

4. TEST SPECIMENS AND PROCEDURE 27

4.1 Specimen Dimensions 27

4.1.1 General 27

4.1.2 Short term tension specimens 28

4.1.3 Long term tension specimens 29

4.1.4 Short term compression specimens 29

4.2 Concrete Mix and Casting 30

4.3 Test Procedures 31

4.3.1 Short term tension tests 31

4.3.2 Long term tension tests 31

4.3.3 Short term compression tests 32

5. DATA ACQUISITION AND ANALYSIS 33
5.1 Data Acquisition 33
5.2 Data Analysis Program 34
5.2.1 General 34
5.2.2 Determination of rod cross-sectional area 35
5.2.3 Curve smoothing procedure 35
5.2.4 Determination of bond stresses 37
5.2.5 Determination of concrete stresses 39
5.2.6 Determination of slip 40
6. TENSION TEST RESULTS AND DISCUSSION 41
6.1 Tension Test Results 41
6.2 Steel Strain Distribution 48
6.2.1 Precrack strain distribution 48
6.2.2 Transverse cracks and postcrack strain distribution 52
6.3 Bond Stresses 57
6.3.1 Bond stress distribution 57
6.3.2 Ultimate bond stresses 61
6.4 Embedment Gauge Results 64
7. COMPRESSION TEST RESULTS AND DISCUSSION 67
7.1 Compression Test Results 67
7.2 Steel Strain Distribution 69
7.2.1 Comparison between loading methods 69
7.2.2 Longitudinal strain distribution 70
7.3 Bond Stresses 72
7.4 Embedment Gauge Results 74
8. CONCLUSIONS 78
8.1 Tension Specimens 78
8.2 Compression Specimens 79
9. FURTHER WORK 81
REFERENCES 83
FIGURES 89

FIGURES

1.1 Previous strain measurements in lap joints 90

2.1 Forces in a single bar anchorage 91
2.2 Typical splitting failure patterns 92
2.3 Proposed force distributions around lap joints 93
2.4 Bond stress/slip relationships 94
2.4.1 Typical bond stress/slip curves 94
2.4.2 Bond stress/slip and associated bursting stresses 94
2.5 Theoretical steel and bond stress distributions 95
2.6 Bond stress distribution in a compression lap 96

3.1 Section through reinforcing bar 97
3.2 Typical strain gauge layout 98
3.3 Concentration gauges 99
3.4 Embedment gauges 100

4.1 Specimen layout 101
4.2 Specimen details 102
4.3 Specimen properties 103
4.4 Link and embedment gauge layout 104
4.5 Tension rig 105
4.6 Dartec rig 106
4.7 Compression rig 107

5.1 Data logger 108
5.2 Example of cubic spline curve fit 109

6.1 Steel strain distributions 110
6.1.1 Specimen 125T12/12 110
6.1.2 Specimen 250T12/12 111
6.1.3 Specimen 500T12/12 112
6.1.4 Specimen 750T12/12 113
6.1.5 Specimen 250T20/20 114
6.1.6 Specimen 500T20/20 115
6.1.7 Specimen 750T20/20 116
6.1.8 Specimen 250T12/20(A) 117
6.1.9 Specimen 250T12/20(B) 118

6.1 Steel strain distributions (continued)
6.1.10 Specimen 500T12/20 119
6.1.11 Specimen 250T20/20(E) 120
6.1.12 Specimen 250T20/20(L) 121
6.1.13 Specimen 500T20/20(L) 122
6.1.14 Specimen 125D12/12 123
6.1.15 Specimen 125D12/12(L) 124
6.2 Rod, concrete and bond stresses at a crack 125
6.3 Typical concentration gauge result 126
6.4 Precrack reinforcement strain distributions 127
6.5 Reinforcement strains and loads at crack formation 128
6.6 Effect of longitudinal cracking on steel strain distribution 129
6.7 Failed specimens 130
6.7.1 Specimen 250T12/12 130
6.7.2 Specimen 250T20/20 131
6.7.3 Specimen 250T12/20(B) 132
6.8 Ultimate steel strain distribution along lap 133
6.8.1 Specimen 250T20/20 133
6.8.2 Specimen 500T20/20 133
6.8.3 Specimen 250T20/20(E) 134
6.8.4 Specimen 250T20/20(L) 134
6.8.5 Specimen 250T12/20(B) 135
6.8.6 Specimen 250T12/20(A) 135
6.9 Ultimate loads 136
6.10 Comparison of steel and concrete strains 137
6.11 Comparison of predicted and measured reinforcement strains 138
6.12 Distance required to develop percentage of average strain 139
6.13 Strains developed at lap end 140
6.14 Precrack concrete stress distributions 141
6.15 Reinforcement strains (Before and after crack formation) 142
6.16 Crack spacing 143
6.17 Applied load vs. force in steel 144
6.18 Variation in strains with time 145
6.19 Bond stress/ slip relationship 146
6.20 Steel strain distribution along the lap 147
6.21 Bond stresses at crack formation 148

6.22 Comparison of peak and average bond stresses near transverse cracks 149
6.23 Bond stress/ rod stress relationship 150
6.24 Bond breakdown at the specimen end 151
6.25 Bond stresses at maximum load 152
6.26 Ultimate bond stresses 153
6.27 Circumferential strains 154

7.1 Steel strain distributions 155
7.1.1 Specimen 125C12/12 155
7.1.2 Specimen 250C12/12(A) 156
7.1.3 Specimen 250C12/12(B) 157
7.1.4 Specimen 125C20/20 158
7.1.5 Specimen 250C20/20(E) 159
7.2 Comparison of loading methods 160
7.3 Comparison of steel and concrete strains 161
7.4 Steel strains at the lap ends 162
7.5 Bond stress/ rod stress relationship 163
7.6 Comparison of average and peak bond stresses 164
7.7 Circumferential strains 165

NOTATION

A_c Area of concrete.

A_e Area of engagement of one transverse rib.

A_s Area of steel reinforcement.

A_{tr} Area of transverse reinforcement.

a_l Height of longitudinal ribs.

B Bond influence length.

c Concrete cover.

E_c Modulus of elasticity of concrete.

E_s Modulus of elasticity of steel reinforcement.

F_b Longitudinal component of bond force.

F_o Applied force.

F_p Radial component of bond force.

f_{bave} Average bond stress between peak and trough steel strains.

f_{bc} Bond stress at which the cover cracks.

f_{bp} Peak bond stress.

f_{bs} Bond stress.

f_{bu} Ultimate bond stress.

f_c Concrete stress.

f_{ct} Ultimate tensile stress of concrete.

f_{cu} Ultimate compressive stress of concrete cubes.

f'_c Ultimate compressive stress of concrete cylinders.

f_p Bursting stress generated by bond.

f_s Reinforcement stress.

f_{sp} Peak reinforcement stress.

f_{st} Trough reinforcement stress.

f_y Yield stress of steel reinforcement.

f_{yt} Yield stress of transverse reinforcement.

i Number of longitudinal ribs.

j Pitch of longitudinal ribs.

K_1 A constant in bond strength equation.

K_d Modulus of displacement.

K_{pt} A constant in relationship between peak and trough stresses.

k_{tr} Number of transverse ribs around bar perimeter.

k_1, k_2 Constants in crack spacing equation.

l Lap length.

m Ratio of the elastic modulii (E_s/E_c).

S_{ave} Average crack spacing.

S_L Lap joint spacing - centre to centre.

S'_L Clear spacing between lap joints.

s_r Spacing of transverse ribs.

s_v Spacing of transverse reinforcement.

T Tension force in steel reinforcement.

u Perimeter of steel reinforcement.

x_n Distance along specimen, at position 'n'.

α Angle of inclination to bar axis of compressive force in concrete.

α_{sb} Specific rib area.

β Bond coefficient, dependent on bar type.

β_r Angle between transverse rib and longitudinal axis of bar.

ϵ_{ave} Average reinforcement strain.

ϵ_c Concrete strain.

$\epsilon_{c_{ave}}$ Average concrete strain along specimen.

ϵ_n Reinforcement strain, at position 'n'.

ϵ_s Reinforcement strain.

$\epsilon_{s_{ave}}$ Average reinforcement strain along specimen.

κ A constant used in expressions for longitudinal stress distributions along lap joints.

ρ Reinforcement percentage.

ϕ Diameter of steel reinforcement.

Δ Slip between steel reinforcement and concrete.

CHAPTER 1

INTRODUCTION

Recently a technique of mounting electric resistance strain gauges within steel reinforcing bars has been developed at the University of Durham [1,2]. While the concept of installing gauges in a duct milled along the length of the reinforcement was not original, the many advances in strain gauge technology and data acquisition systems since the technique was pioneered now enables measurements to be taken with greater detail. The earliest account of the technique appears to have been that published by Mains in 1951 [3], and the idea has since been adopted by a number of researchers [4,5,6].

The ability to accurately measure the strain distribution along the reinforcement means that the technique lends itself to a number of fundamental studies into the behaviour of reinforced concrete. It is particularly well suited to research into the bond between steel and concrete, as the steel's bond characteristics are maintained by internally gauging the bars. One aspect of bond research is the study of lap joints, in which the force is transferred between a pair of overlapping bars by bond.

The continuity of reinforcement in concrete structures has traditionally been achieved using lap joints. Overlapping the steel offers an economical and simple solution to the problem of continuity, but care must be taken over the detailing of such joints to ensure the satisfactory performance and safety of the structure.

Most of the bond in deformed reinforcing bars is developed by the bearing of the ribs against the concrete, with the wedging action of these ribs setting up radial forces around the steel. Hoop stresses are developed and longitudinal splitting cracks are formed when these stresses exceed the tensile strength of the concrete. In laps these cracks may extend rapidly along the joint, often leading to an explosive failure. Consequently, the strength of a lap is generally associated with bond strength, which in turn is related to the strain gradient in the reinforcing steel.

Both the British [7] and the American [8] design codes assume a constant bond stress along the lap joint. The commentary to the American code [9] considers this value to be more meaningful in design, partly because standard bond tests determine the average bond stress over a length of reinforcement, and partly because of the extreme variations in bond stress that exist near a transverse crack. Tepfers [10], amongst others [11], has reported the variation in bond stress that

exists along the lap, this increasing with lap length and being very pronounced at low loads. He also writes that 'to estimate the ultimate load of the splice it is important to know the distribution of bond stresses'. A detailed measurement of the longitudinal reinforcement strains would enable the determination of the bond stress distribution along the lap, and would demonstrate the manner in which the force is transferred from one reinforcing rod to the other. This investigation sought to further the understanding of both tension and compression lap joint behaviour by taking such measurements.

There have been previous attempts to establish the strain distribution over the lap length. A summary of lap joint research which has involved a measurement of the reinforcement strains is given in Figure 1.1. Whilst the list does not claim to be exhaustive, especially as no foreign language literature has been scanned, it is believed that it gives a representative, and balanced, picture of previous work.

Typically, fewer than twenty strain gauges have been installed in lap joints, at approximately 50 mm centres. The technique currently available enables the installation of about eighty gauges, with the use of strain concentration gauges permitting a minimum spacing of 2 mm. The technique clearly offers the potential for much greater detail than has previously been achieved.

The table (Figure 1.1) includes some brief notes reflecting the purpose of the measurements in previous studies. The impression gained from the literature was that researchers have tended to use the measurements as a means of demonstrating the linearity of the ultimate strain distribution, thus justifying the assumption of a uniform ultimate bond stress over the lap length, or to corroborate their analysis or modelling of lap joint behaviour.

It was believed that there remained a need to establish the precise nature of the strain distribution throughout the load range, and to assess the influence of variables such as bar diameter and lap length on the longitudinal strains. The measurement technique developed at Durham provided the means of achieving this.

CHAPTER 2

LITERATURE REVIEW

2.1 Introduction

The satisfactory performance of reinforced concrete structures depends upon the strength, and permanence, of bond between the steel and the concrete. The classical concept of bond has been as a shear force acting at the steel/concrete interface [20]. Force transfer between the two materials requires a stress to be generated at their interface; this stress is referred to as a 'bond stress' and is generally defined as the stress per unit area of the bar surface. Bond stress may be considered either in terms of the force transferred from concrete to bar, or as the rate of change of the steel stress along the bar, and in reinforced concrete there can be no bond stress unless the bar stress changes, and no change in bar stress without bond stress [20].

Bond performance has received considerable attention, with one of the first series of tests being conducted by Duff Abrams [21] at the University of Illinois in 1913. He, however, wrote of earlier studies, beginning in 1876 with the work of Thaddeus Hyatt (who investigated the bond between concrete and iron bars). Abrams noted that this field of research had attracted increasing attention; by the first decade of this century numerous bond tests were being reported. One aspect of this bond research was the study of lap joint behaviour and, according to Tepfers [10], some of the earliest work in this field was being carried out by Scheit and Wawczinick in 1912 and by Amos in 1913.

Following the introduction of deformed reinforcing steel in the 1930's, research into lap joints has generally been carried out using deformed reinforcement, and unless stated otherwise the rest of this review is concerned with the behaviour of such bars.

Much of the bond strength of a deformed bar is provided by the mechanical bearing of bar ribs against the concrete. Initially there is some adhesion between the steel and concrete (on which a plain bar depends for its bond strength), but this breaks down at bond stresses of between 0.5 and 1.5 N/mm^2 [11]. The subsequent bearing of the ribs leads to radial forces being set up in the concrete, and these are equilibrated by a hoop tension around the bar, as shown in Figure 2.1. Typically, bond failure of a deformed bar will be due to splitting of the concrete along the bar axis as the hoop tension forces exceed the tensile strength of the concrete. Consequently, research into the ultimate behaviour of lap joints has often been

concerned with splitting failures, seeking to identify factors which influence the magnitude of, and resistance to, splitting forces.

More generally, researchers have been interested in determining the value of the bond stress at which failure occurs. To facilitate the evaluation of ultimate bond stresses in lap joints, it has often been assumed that a constant bond stress exists along the lap length. However, as early as 1945 Kluge and Tuma [12] were able to conclude from measurements of the steel strains (using a mechanical strain gauge) that peaks existed in the bond stress distribution at the free ends of lapped reinforcing bars.

Early researchers were concerned with the arrangement of reinforcement in a lap joint. First Kluge and Tuma[12], and then Chamberlin during the 1950's[22,23], included a study of joints in which the lapped bars were either in contact or spaced. They agreed that the two methods of overlapping the steel gave comparable results.

In 1955 Chinn, Ferguson and Thompson[24] recognised the importance of splitting as far as lap strength was concerned, and sought to establish trends by investigating a number of variables. The significance of factors such as bar size and lap length in the development of hoop forces around the lap, and the influence of cover, transverse reinforcement and concrete strength in providing resistance to these forces, was noted and paved the way for subsequent research.

Much of the research into lap joints continued at the Center for Highway Research, at the University of Texas at Austin, with Ferguson, in particular, becoming involved in a number of further studies [13,20]. He carried out work with Breen [25] dealing with the performance of large diameter bars in lapped splices, and the need for longer laps as bar diameter increased was recognised. A limited number of tests were also carried out to demonstrate the beneficial effect of transverse reinforcement on the strength and ductility of lap joints. The influence of both links and bar diameter were further investigated by Ferguson and Krishnaswamy [13], and the resulting design proposals permitted the use of large bars (43 and 57 mm diameter) in lap joints, as long as transverse reinforcement was provided. Nonetheless, the American code[8] continues to prohibit the use of bars larger than 36 mm diameter in tension laps.

An extensive study into the behaviour of lapped joints, conducted at the Chalmers University of Technology, was reported in 1973 by Tepfers[10]. A comprehensive experimental programme was undertaken, permitting an empirical analysis of factors influencing lap strength. The nature of the force system along and around a lap joint was dealt with theoretically, and expressions thus derived were compared favourably with the experimental data. The work included an analysis

of the resistance provided by the concrete cover to splitting forces. In order to apply this theory to lapped bars, it was assumed that the radial forces around a lap would be double those around a single bar. This would appear to concur with a conclusion made by Roberts and Ho [26], at about the same time, that a lap was akin to a double-ended anchorage.

These conclusions were only applicable to tension laps, as the force transfer in a compression lap is due to both bond forces and the bearing of the free end of the rods against the concrete. Pfister and Mattock [18] were the first to report the effect of end bearing in lap joints, following a study into the behaviour of compression laps in reinforced concrete columns, undertaken at the Portland Cement Association's laboratories in the early 1960's. They considered the effect of bond and of end bearing to be additive, though more recent work by Cairns and Arthur, at Glasgow University in 1976, has suggested that this is not the case [15,27]. The latter also commented on the influence of the position of transverse reinforcement on compression lap strength, and suggested that links should be clustered at the lap ends where the splitting forces were most severe.

The emphasis has, however, continued to be on the behaviour of tension laps. There has been an increased activity in lap joint and bond research over the last decade, with the first two issues of the Journal of the American Concrete Institute in 1979 being concerned with the interaction between steel and concrete. In 1982 a major international conference on bond was held at the Paisley Institute of Technology [28]. Perhaps this increased interest in bond was precipitated by the American Concrete Institute publishing a paper on 'Opportunities in Bond Research' in 1970 [29].

In 1977 Orangun, Jirsa and Breen [30] collated the results from a number of investigations to develop an empirical design equation for lap length. The key parameters included concrete strength, bar diameter and cover, with an additional factor making allowance for the benefits arising from the provision of transverse reinforcement. A particularly interesting conclusion from this work was that lap and anchorage lengths could be equated, which contradicted both Tepfers' and Roberts and Ho's findings. Reynolds [31] developed a new theory for the force system in the concrete around a lap based on this conclusion. This theory and Tepfers' earlier one will be described in section 2.3.

Reynolds also commented on the inconsistencies in the existing design codes concerning links, and attempted to assess their contribution to lap strength experimentally at the Cement and Concrete Association. An equation for lap strength was derived, similar to that proposed by Orangun, Jirsa and Breen [30]. Reynolds

suggested that for design purposes it was adequate to deal with anchorage forces rather than bond stresses.

Another empirical formula, a 'mean prediction equation', was presented by Zsutty in 1985 [32]. The equation was based on a simplified empirical relationship between ultimate bond strength and concrete strength, bar diameter and lap length. Additional factors were then included to allow for the influence of cover and transverse reinforcement. The prediction equation was favourably compared with Orangun, Jirsa and Breen's design proposals [30], and the mean value prediction was used as a baseline for subsequent comparisons between the 'standard' beams and other test series. Confidence in the equation was provided by its ability to forecast data not included in the original regression analysis with a coefficient of variation of under 10%.

Recently, researchers have shown considerable interest in the behaviour of lapped joints subjected to non-monotonic loads [19,33,34]. Particular attention has been focussed upon the effect of seismic loads at Cornell University by White, Gergely and others [35,36]. Under seismic conditions lap joints may be subjected to both tensile and compressive forces, and this ongoing work demonstrates a continuing interest in the behaviour of both tension and compression lap joints.

2.2 Factors Influencing Lap Strength

In general, the ultimate aim of lap joint research has been to define a lap length capable of transferring the steel stresses efficiently. For design purposes, it is preferable to determine a lap length rather than an average ultimate bond stress [30]. Reynolds [31] argued that the concept of bond stress was itself unnecessary in design, and proposed equations that dealt with the force which had to be developed over an anchorage, or lap, length. Nonetheless, design equations are generally based upon the assumption that the ultimate bond stress is constant over the lap. If this was valid it might be expected that, all else being equal, the strength of a lap would be proportional to its length. However, the inefficiency of an excessively long joint has long been recognised [12,18], and as a splice becomes increasingly inefficient, so the influence of its length on lap strength decreases.

The relationship between the length and strength of a lap varies according to the diameter of the lapped bars. Tepfers [10] reported an almost linear relationship for bars of under 12 mm diameter, and a parabolic one for larger bars. The current British standard [7] tables lap length in terms of bar diameter, but Tepfers has commented that such a practice is unacceptable. This was prompted by the considerable scatter he observed when relating lap strength to the ratio of lap

length and bar diameter; a further scattering of the results was anticipated if the concrete cover was also varied in terms of bar diameter. In a previous investigation, Chinn and his colleagues [24] were surprised to find differences in joint strength when all the other parameters were equal in terms of bar diameter, and Tepfers' comments may help to explain this.

It is well documented that the size and type of reinforcement used in a lap joint will influence its strength [11]. Bond stress may be thought of in terms of a shear force acting at the steel/concrete interface, and so, for a given change of force along the bar, an increased steel surface area will result in a lower bursting force. If bars of mixed diameter are lapped, the design codes require the lap length to be based on the smaller rod [7,8], the size of which limits the force to be transferred. No tests appear to have been carried out on such laps. The American design code does not permit the use of bars larger than 36 mm diameter in tension laps, though Ferguson and Krishnaswamy [13] did find that such bars could be successfully lapped if transverse reinforcement was provided.

In both tension and compression laps the surface characteristics of the reinforcement will affect the bursting forces, though the influence of the rod characteristics will be limited by splitting of the concrete around the lap [10]. In general, better bond properties will be achieved by rods with a higher specific rib area (α_{sb}) [11], which has been defined to be:

$$\alpha_{sb} = \frac{k_{tr} A_e \sin \beta_r}{\pi \phi s_r} + \frac{i a_l}{j} \tag{2.1}$$

where:

ϕ	=	Diameter of steel reinforcement.
k_{tr}	=	Number of transverse ribs around the bar perimeter.
A_e	=	Area of engagement of one transverse rib.
β_r	=	Angle between transverse rib and longitudinal axis of bar.
s_r	=	Spacing of transverse ribs.
i	=	Number of longitudinal ribs.
a_l	=	Height of longitudinal ribs.
j	=	Pitch of longitudinal ribs.

Improved bond strength may be achieved by increasing the specific rib area, but the corresponding reduction in slip between the bar and the concrete may lead to a more brittle failure. There is also a play-off between the improvement in bond strength, and the increased bursting forces generated by a greater rib area. The optimum value of α_{sb} lies in the range 0.05–0.08, and as long as this value is kept reasonably constant, the rib height and spacing may be changed without

influencing bond behaviour [11]. It was concluded by Cairns and Jones [37] that the strength of a lap increases at approximately one fifth the rate of the specific rib area. This is in contrast to Tepfers' earlier comments that the two were not directly related [10].

Skorobogatov and Edwards [38] found that the inclination of the rib face had little influence on lap strength, as long as it was greater than a minimum value of between 30 and 40°. This is because a crushed wedge of concrete develops ahead of the rib due to a high local compressive force, and thereby standardises the angle α at which the compressive forces act in the concrete. Cairns and Jones [37], however, did find that rib inclination had a slight influence on the ultimate strength of a lap. They also noted a difference in the bond strength of twisted bars and rods with crescent shaped ribs. In the former, the bond stresses around the circumference are equal. In the latter, peaks exist in the bursting force where the rib height is at its greatest, and thus the alignment of the ribs will influence the force distribution around the lap joint and may affect lap strength. It was concluded that the influence of rib geometry is as great as that of concrete strength, which is one of the key factors affecting bond strength [39].

The tensile strength of the concrete is of major importance if failure is caused by splitting of the cover, but for design purposes it is more convenient to consider failure in terms of the concrete's compressive strength. The tensile strength has traditionally been equated to the square root of compressive strength [40], but a variety of equations have been proposed [41] and the apparent influence of the compressive strength on lap behaviour will depend upon the relationship chosen [37]. In general, raising the concrete strength will increase the failure load, but above a certain value (Tepfers [10] suggested 70 N/mm^2) the additional bursting forces associated with shrinkage of the concrete may reduce the ultimate bond strength.

The distribution of bond stress along a lap joint is influenced by concrete strength, partly because slip of the reinforcement is dependent upon the extent of the localised crushing ahead of the ribs, and partly due to a weaker concrete being able to adjust better to differential strains [25]. The inability of a stiffer concrete to distribute the effect of peak bond stresses has resulted in lower average bond stresses at failure [35]. In a separate investigation, it may have reduced the distance over which force was transferred between lapped bars [14].

A number of researchers [11] have concluded that their experimental results have indicated a certain 'plastification' of concrete under tension loading due to the formation of microcracks. The degree of plastification is influenced by the heterogeneity of the concrete, the specimen size and the strain gradient. Although

there is no generally accepted explanation for the phenomenon [11], the ability of the concrete to redistribute tensile stresses from highly to less stressed zones must be taken into account when analysing bond behaviour. It has been assumed that plastification will occur over a length varying from half to about three times the bar diameter, in analyses carried out by Eligehausen [42] and Tepfers [10] respectively.

Lap strength will also be influenced by the concrete cover, with this providing a significant resistance to the splitting forces. A non-linear relationship between minimum cover and lap strength was reported by Roberts and Ho [26]. They noted a 30% strength increase when the cover was increased from one to three bar diameters, and a further 10% improvement as the cover was raised to five bar diameters.

The spacing between adjacent lap joints will affect the lap strength in a manner similar to cover, and these two factors were considered as a single parameter by Orangun, Jirsa and Breen [30] in their design proposals. If the spacing between neighbouring laps is too small then failure may occur along the plane of the bars, thus reducing the influence of cover and defining the failure mode. The relationship between side and bottom cover will also affect the nature of the specimen failure. A number of failure types have been identified [11] which are dependent upon whether longitudinal cracks develop in the side or the bottom cover. Three typical failure patterns are illustrated in Figure 2.2. It may be seen that the use of excessive cover to resist the bursting forces may result in cracks running diagonally through the bottom cover, a 'V-notch' type failure. An upper bound for cover has therefore been introduced in some of the design equations [30,31].

It has been stated that the influence of cover becomes negligible once splitting cracks have formed [34]. Subsequent resistance to failure may be provided by transverse reinforcement carrying the tensile forces across a longitudinal crack. The effects of links and cover are not additive [26], though for design purposes they have generally been considered to be so [30]. The improvement in lap joint behaviour due to links has long been recognised, with a number of researchers reporting increased strength and ductility [11]. A detailed study into the benefits of links [31] showed that the most marked effect was on laps located in a zone of shear, whilst laps subjected to a constant moment showed only a small increase in strength, with the links not being fully used.

The failure of compression splices has been attributed to the failure of the confining reinforcement at the lap ends. Consequently, it was suggested that links should be clustered at these positions [27]. A similar distribution may be beneficial in a tensile splice, in which higher strains are found in the links at the lap ends [17].

Under a cyclic load, however, the links should be evenly distributed throughout the lap [35], as bond breakdown may move progressively away from the lap end, and therefore beyond any links positioned there.

In conclusion, there appears to be a general agreement that lap strength is influenced by the following factors:

i) Lap length (l).
ii) Diameter (ϕ) and surface characteristics of the lapped bars (typified by specific rib area, α_{sb}).
iii) Concrete strength (generally related to f_{cu}).
iv) Concrete cover (c), and spacing of the lap joints (S_L).
v) Transverse reinforcement (as typified by area A_{tr}, yield strength f_{yt} and spacing s_v).

However, the importance attached to the individual parameters in equations for lap strength varies considerably [39], and perhaps this is a consequence of some equations being derived analytically and others empirically.

The empirical approach favoured by Orangun, Jirsa and Breen [30] produced design proposals based on the results of numerous lap joint tests reported by various researchers. A non-linear regression analysis of the key parameters influencing lap strength yielded the following equation for ultimate bond stress (f_{bu}):

$$f_{bu} = \sqrt{f'_c}\left(1.2 + \frac{3c}{\phi} + \frac{50\phi}{l} + \frac{A_{tr}f_{yt}}{500s_v\phi}\right) \tag{2.2}$$

where:

All units are pounds and inches.

f'_c = Ultimate compressive stress of concrete cylinders.

This approach certainly embodied the ideas which had been propounded regarding lap joint behaviour. It also surmounted difficulties resulting from uncertainties about the relationship between bond and splitting forces, and about the degree of plastification of the concrete. Its purpose, however, was to be a design equation and some of the analytical formulae tend to be more precise, with Tepfers [10], for instance, developing separate equations for each of the possible crack patterns across a lapped section at failure.

2.3 Analyses of the Ultimate Strength of Lap Joints

Much of the analytical work on the ultimate strength of lap joints has been based on the bond behaviour of a single rod [10,31,43]. Therefore, in the first in-

stance, it is necessary to consider the situation around a single bar when no transverse reinforcement is present.

It has already been noted that the bearing of the bar ribs sets up compressive forces in the concrete, at an angle α to the reinforcement (Figure 2.1). These forces are balanced by a hoop tension acting around the bar, and bond failure of a deformed bar is often due to these bursting forces exceeding the tensile capacity of the concrete. Tepfers [44] modelled this situation by analysing a thick concrete cylinder loaded by internal pressure, with the wall thickness being equivalent to the concrete cover. He identified three different stages at which longitudinal cover cracks might form:

i) Elastic stage: A splitting crack is initiated as the maximum tensile stress exceeds the tensile strength of the concrete.

ii) Partly cracked elastic stage: Peaks in the tensile stress distribution exist in the vicinity of the reinforcing bar, and when the tensile capacity of the concrete is exceeded internal cracks are formed, radiating outwards from the rod. It was demonstrated analytically that if the cover/diameter ratio is greater than 0.53 these cracks will not propagate immediately to the surface of the concrete, but create a partially cracked specimen. The bond forces are then transferred by the concrete teeth between the internal cracks to the uncracked part of the cylinder. The load carrying capacity of the cylinder is not exhausted until the internal cracks reach an 'optimum depth' (which is dependent upon cover and bar diameter) and then failure will occur as the maximum tensile stress exceeds the tensile strength of the concrete.

iii) Plastic stage: The concrete is assumed to act plastically. Splitting ocurs when the tensile stress, uniform across the concrete cover, exceeds the tensile strength of the concrete.

Tepfers developed equations for each of these stages, relating the bond stress at which the cover cracked (f_{bc}) to the tensile strength of the concrete (f_{ct}), the cover (c) and the bar diameter (ϕ):

Elastic stage:

$$f_{bc} = \frac{f_{ct}}{\tan\alpha}\left(\frac{(c+\frac{\phi}{2})^2-(\frac{\phi}{2})^2}{(c+\frac{\phi}{2})^2+(\frac{\phi}{2})^2}\right) \tag{2.3}$$

Partly cracked elastic stage:

$$f_{bc} = \frac{f_{ct}\,(c+\frac{\phi}{2})}{1.664\,\phi\,\tan\alpha} \tag{2.4}$$

Plastic stage:

$$f_{bc} = \frac{2\, f_{ct}\, c}{\phi \tan \alpha} \tag{2.5}$$

In reality, the elastic stage gives the load at which internal cracks form near the steel, and the partly cracked elastic stage gives the load at which the cracks propagate to the surface of the concrete. Tepfers' comparison of experimental results with the theoretical bond stresses calculated from equations 2.3–2.5 showed the test values to lie between the partly cracked elastic and the plastic stages. Consequently, when Reynolds [31] developed a theoretical lower bound for bond strength, it was based on the equation for the partly cracked elastic stage (2.4).

Reynolds introduced a constant K_1, which was dependent upon α and upon the relationship between the tensile (f_{ct}) and compressive strength (f_{cu}) of concrete, and generalised Tepfers' equation such that:

$$f_{bc} = K_1 \sqrt{f_{cu}} \left(0.5 + \frac{c}{\phi}\right) \tag{2.6}$$

He was able to demonstrate, by changing the equation into an expression for force, that this equation (2.6) was of a similar nature to that proposed by Orangun, Jirsa and Breen [30] for the A.C.I. code (equation 2.2), and by Losberg and Olssen [45] for the Nordic code. He recommended that equation 2.6 should be used as the basis for design, using a constant value of 0.2 $\mathrm{N}^{\frac{1}{2}}/\mathrm{mm}$ for K_1. This figure was shown to give a reasonable lower bound to results gained experimentally.

Reynolds recognised a considerable variation in the allowance made for the contribution of transverse steel to anchorage strength in previous design proposals [31], and so included an assessment of the influence of links in his experimental study. He considered the contribution to be equal to the force carried by transverse bars and noted that these bars did not necessarily reach their yield stress. Consequently, he suggested that for design purposes it was reasonable to assume a stress of 70 $\mathrm{N/mm^2}$ in the links and, by converting this additional anchorage force to bond stress, he was able to add the contribution of transverse steel to his basic equation (2.6).

Reynolds' proposals have been adopted in BS8110:1985 [46], with the equation given in this standard for the design ultimate bond stress being:

$$f_{bu} = \beta \sqrt{f_{cu}} \tag{2.7}$$

The coefficient β is dependent upon bar type. The figure for a type 2 deformed bar [47] under tension is derived by assuming that $\frac{c}{\phi} = 1$ (giving $\beta = 0.3$ $\mathrm{N}^{\frac{1}{2}}/\mathrm{mm}$

from equation 2.6), and then making allowance for the presence of transverse steel to bring β up to 0.5 $N^{\frac{1}{2}}$/mm. Whilst the handbook to the code [46] acknowledges that this is a rather simplistic approach, it is argued that refining equation 2.7 to give a more realistic treatment of anchorage bond would add considerable complication to the design procedure for little economic gain.

In order to apply the aforementioned ideas for a single bar to a lapped pair of rods it is necessary to understand the force system around anchored and lapped bars. For a single bar the bursting force will be the same at all points on the rod circumference, if the rib area is constant. The relationship between bond stress (f_{bs}) and the bursting pressure (f_p) is based on the angle α which the compressive strut makes with the axis of the bar (Fig. 2.1), such that $f_p = f_{bs} \tan \alpha$. This angle need not remain constant. It has been suggested by Eligehausen [42] that the ratio f_p/f_{bs} varies from 0.5 to 1 as the bond stress increases and wedges of crushed concrete develop ahead of the bar ribs.

Tepfers [10] has proposed two possible force systems for laps which are illustrated in Figure 2.3. The first, Type A, is simply the addition of two single bar anchorages. The bursting forces perpendicular to the lap axis would be double the value for a single bar, and this would result in lap strength being dependent upon orientation of the lapped bars. If this were the case, then, for instance, a lap joint in a slab with bars placed side by side would need to be twice the length of a similar joint with the bars placed one above the other. There has been no evidence in the literature that lap orientation has such a significant effect, and in a more recent publication [48] Tepfers appears to have favoured the second of his proposed force systems, Type B.

In this system it is assumed that the displacement between the lapped bars will be twice the slip between each individual bar and the concrete. This may result in a breakdown of bond between the bars, thus leading to a reduction in longitudinal bond stresses in this area. In the extreme case, when the axial component of bond is totally lost, the compressive force between the bars may become perpendicular to the bar axis ($\alpha = 90°$). As may be seen in Figure 2.3, such a system results in the bursting forces around a lap being twice as high as those around a single bar, and therefore Tepfers recommended that the equations derived for the bond stress which causes the cover to crack (equations 2.3–2.5) should be halved if they are applied to lap joints.

However, it was established by Orangun, Jirsa and Breen [30], from a large amount of experimental data, that lap and anchorage lengths were equivalent. This contradicted Tepfers' findings, and an alternative force system, in which the

two lengths could be equated, was put forward by Reynolds [31]. He argued that the area between the rods provided the shortest and stiffest route for force transfer, and thus attracted much of the force. This is equivalent to a reduced value of the angle α in the area, with the decrease being just sufficient to ensure that the resulting distribution of bursting forces around a lap (Figure 2.3) is the same as that around a single bar. The proposals therefore agreed with the experimental evidence, and it is interesting to note that, for tensile loads, the most recent British Standard [7] equates lap and anchorage lengths.

Although Reynolds and Tepfers have differing ideas concerning the magnitude of the bond stress at which the cover splits around a lap, they do agree that the bursting forces in the plane of, and perpendicular to, the lapped bars are equal. The longitudinal crack will therefore develop in the smaller of the horizontal and vertical covers. Laps may continue to sustain loads after the formation of splitting cracks, and so the equations for the bond stress at which this occurs do not necessarily give the ultimate bond strength.

Tepfers [10] identified six possible failure patterns which, like those shown in Figure 2.2, varied according to the section geometry. Separate equations were developed for each failure type. He assumed that the concrete behaved plastically in the failure zone, and thus an estimate for ultimate strength could be obtained by multiplying the area of the failure surface by the tensile strength of the concrete. If required, the contribution of transverse reinforcement carrying stresses across the cracks could be added to this estimate [49]. The ultimate strength of the lap was determined by the failure pattern which offered least resistance to the splitting forces.

The discussion to date has centred upon the stress distribution around a tension lap, but a similar sort of system might be expected around a compression lap. It is clear that end bearing affects the force transfer in such laps, and consequently any analysis should include this. Cairns [43] investigated the behaviour of compression laps, and developed an expression for their ultimate strength. He treated the components of stress due to bond and to end bearing separately, and then combined them to form his final equation.

Compressive forces in the concrete parallel to the bar axis affect the bond behaviour of the reinforcement by restraining the growth of internal cracks. Cairns' analysis of the ultimate compressive bond strength of ribbed bars [43] was based on the premise that bond failure was due to a breakdown in the bearing of the ribs. This mode of failure is characterised by the formation of shear cracks on an inclined surface passing through the top of the ribs, and explains the concrete

wedges which were seen to adhere to the bar ribs after failure of his compression laps. The stresses acting on a wedge of concrete ahead of a rib were determined theoretically, and an equation was developed which related the steel stresses to the bursting forces. He demonstrated that the ultimate bond strength was the sum of two separate factors, one which dealt with the relationship between the splitting and the confining forces in a specimen and the other, a 'non-bursting' component, which was dependent upon the strength of the concrete and the total area of the failure surfaces. The key parameters were shown to be the concrete strength, the surface characteristics of the reinforcement and the confining force. Cairns' tests on full-scale columns had shown the concrete cover to be split over the entire lap length before failure occurred, and so it was assumed that links provided the entire confining force.

Cairns' experiments showed that when lapped bars fail in end bearing a cone of concrete is pushed out from the end of the rod. Consequently, he considered the stresses acting on such a failure cone, and showed that end bearing could also be thought of in terms of a 'bursting' and a 'non-bursting' component, related to the confining force on the cone and the concrete strength respectively.

Although Cairns initially treated the two mechanisms of force transfer separately, in a compression joint both bond and end bearing will be active[27]. The ultimate strength will not be the simple addition of equations derived for the two individual stress components because only a limited amount of confining force is available in a specimen, and so failure will depend on the relative value of the bursting forces associated with each. Since this varies according to the specimen characteristics, Cairns did not attempt a quantitative analysis, but instead demonstrated that the ratio of the confining force to the force developed by the bar was similar for both methods of force transfer. It was therefore possible to consider the ultimate compressive lap strength to be the sum of just three components:

i) non-bursting component of bond.
ii) non-bursting component of end bearing.
iii) bursting component of bond.

Two expressions were developed for the ultimate compressive lap strength, one being an upper limit in which the bursting forces were assumed to act over the entire lap length, and the other being a lower limit in which the forces were assumed to be concentrated at the lap ends. The results derived analytically compared favourably with those obtained experimentally, with the latter values lying between the upper and lower limits.

In spite of the two limiting conditions which make allowance for whether all the links, or just those at the lap ends, yield, it was assumed in the analysis that the total bursting force produced is the product of one rib's bursting force and the total number of ribs over the lap length. Implicit in this is the assumption that each rib exerts a similar bursting force, which seems unlikely from the measured distribution of bond stresses reported by Cairns [27] (see §2.4).

It should be remembered that the analyses described for both tension and compression laps are concerned with the behaviour across the section, and therefore deal with a unit length, along which the bond stress is assumed to be constant. This length could be considered to be the entire lap length, but in reality the bond stresses may vary along the joint [11], and so to predict the ultimate lap strength a knowledge of the bond stress distribution is required.

2.4 Stress Distributions Along Lap Joints

It is often assumed that the bond stress is constant over the lap length at failure, and therefore, by implication, that the force is evenly transferred between the lapped bars [7,8]. For design purposes this is usually adequate, particularly as standard bond tests [50] determine average bond stresses, but in reality variations do exist in the bond stress distribution, particularly at low loads [11]. It would seem probable that it is the peaks in this distribution which cause splitting of the concrete cover. Authors generally quote the average bond stress which results in a splitting crack and, even allowing for some plastification of the concrete, this figure might be expected to be lower than the true value of bond stress which initiated splitting. It is clear that if the behaviour of lap joints is to be fully understood then the stress distributions along the lapped bars must be determined.

This was first attempted in 1945 by Kluge and Tuma [12] who, by providing small openings in the concrete, were able to measure the steel strain distribution with a mechanical strain gauge. Although the gauge holes would have undoubtedly affected the local bond stresses, it was concluded that their presence did not adversely affect lap strength. Another unusual characteristic of the specimens was that the lapped bars were flanked by two continuous rods, and it was acknowledged that the results might have been slightly different in the absence of these rods. The lap joint consisted of a pair of high yield deformed steel rods, of either half or one inch diameter, and had a length ranging from twenty to fifty bar diameters.

The five inch gauge length of the mechanical strain gauge resulted in rather crude measurements but, nonetheless, it was established that peaks in the bond stress distribution existed at the free ends of the rods, with the bond stress then

generally decreasing over the lap length. In laps longer than forty rod diameters, negligible bond stresses were observed in the central portion of the lap, suggesting that such splices were inefficient. A comparison of the stress distribution for various lap lengths showed that the peak bond stress at the free end of the lap was independent of variations in lap length or bar type. A linear relationship existed between this peak stress and the tensile stress in the continuing rod. In general, failure was attributed to yield of the reinforcement, though longitudinal cracking was observed in some specimens near the maximum load. In a complementary series of tests, in which the average bond stress at failure was determined, laps shorter than twenty rod diameters exhibited bond failure. A comparison of maximum and average bond stresses along the lap showed that whilst the maximum value remained unaffected by changes in the lap length, higher average ultimate bond stresses were observed in shorter laps.

Although longitudinal cracks were observed in these early experiments, it was Chinn, Ferguson and Thompson [24], almost a decade later, who initially examined the phenomenon of splitting. They noted that longitudinal cracks generally propagated from transverse cracks, particularly from those at the lap ends, suggesting that splitting may be associated with the peak bond stresses found in this region. The lap was often able to continue transferring forces after the cover cracked. Consequently, the influence of splitting on the stress distribution is of interest. It was suggested in a report produced by the A.C.I. Committee 408 [20] that splitting could be one means by which some of the unnevenness in the bond stress distribution was smoothed out.

Tepfers, as part of his extensive analytical and experimental study of lap joints, considered the longitudinal stress distribution in the steel [51]. He developed theoretical expressions for the distribution which were then compared to values derived from the reinforcement strains measured in some of his specimens by electric resistance strain gauges.

Tepfers based his theory on the slip at the steel/concrete interface, using a constant 'modulus of displacement' (K_d) to linearize the initial portion of the bond stress/slip (f_{bs}/Δ) curve (Figure 2.4.1) such that:

$$f_{bs} = K_d \, \Delta. \tag{2.8}$$

It was assumed that the specimen behaved elastically, and the rate of change of bond stress was related to the difference in the steel and concrete strains, resulting in an equation of the form:

$$\frac{df_{bs}}{dx} = K_d \left(\frac{f_s}{E_s} - \frac{f_c}{E_c} \right). \tag{2.9}$$

The change in rod stress could be considered in terms of a bond stress:

$$\frac{df_s}{dx} = \frac{u}{A_s} f_{bs} \tag{2.10}$$

as could the concrete stress around a lap (in which two bars are present):

$$\frac{df_c}{dx} = -\frac{u}{A_s}(f_{bs1} + f_{bs2}). \tag{2.11}$$

where:

Subscripts 1, 2 refer to individual bars.

u = Perimeter of steel reinforcement.

A_s = Area of steel reinforcement.

f_c = Concrete stress.

f_s = Reinforcement stress.

Consideration of equilibrium conditions enabled the applied force to be related to the forces within the lap, and a relationship could thus be established for the stresses in the steel and the concrete.

Tepfers analysed a lap comprising bars of similar diameter and placed the joint in a constant moment zone, which meant that the stresses at both ends of the lap were the same. It was assumed that transverse cracks had formed and were located at the lap ends, due to the sudden change in specimen stiffness. Second order differential equations describing both the concrete and the steel stress distributions were evolved from equations 2.9–2.11. These were solved by consideration of the boundary conditions: that there was zero concrete stress at the lap ends (due to the assumed transverse cracks), and that the steel stress was zero at the free end of the rods, and at a maximum where it carried the applied force across the crack. The resulting equations for the steel stress distributions were differentiated to give the bond stresses along each rod. The theoretical steel and bond stress distributions along the lap have been plotted in Figure 2.5.

A plot of the stress distributions for one of the lapped bars revealed peak bond stresses at both ends of the lap. The curves (Figure 2.5), calculated for a typical range of reinforcement percentages (1–10%), presupposed that no cracks existed within the lap length. If transverse cracks did appear then the concrete stress would be zero at the crack position, and the steel and bond stresses could be determined by considering an infinite reinforcement percentage ($\rho = \infty$). This describes the situation which exists when there is no concrete area available to carry stresses, yet the bond between the bars is still active and maintains the constant modulus of displacement. Tepfers compared values for $\rho = 1$ and $\rho = \infty$, and demonstrated that, for normal crack spacings (from 50–200 mm), the concrete

acting between the cracks had a maximum influence of under 5% on the tensile stresses, and under 20% on the bond stresses. He also argued that plastic behaviour of the concrete was likely to result in an equalization of local bond stress peaks, so reducing this last figure.

The original stress equations were simplified by assuming that there was no interaction of the surrounding concrete ($\rho = \infty$), giving the following expressions for the variation of steel and bond stresses along the lap length:

$$f_{s1} = \frac{f_{s0}}{2}\left(1 - \frac{\sinh \kappa x}{\sinh\left(\frac{\kappa l}{2}\right)}\right) \tag{2.12}$$

$$f_{s2} = \frac{f_{s0}}{2}\left(1 + \frac{\sinh \kappa x}{\sinh\left(\frac{\kappa l}{2}\right)}\right) \tag{2.13}$$

$$f_{bs1} = -f_{bs2} = \frac{f_{s0} A_s \kappa}{2u}\left(\frac{\cosh \kappa x}{\sinh\left(\frac{\kappa l}{2}\right)}\right) \tag{2.14}$$

where:

Subscripts: 0 refers to single bar outside the lap joint, 1 and 2 refer to individual bars inside the lap.

κ = $\sqrt{\frac{uK_d}{E_s A_s}}$.

K_d = Modulus of displacement, generally taken as the secant modulus.

A comparison of stresses calculated from these simplified expressions with those measured experimentally showed that in the early stages of a test the two values differed due to the involvement of the concrete between cracks. However, this discrepancy became less apparent as the concrete reached its final, closest, crack spacing and at medium loads the theoretical and the experimental distributions were similar. Longitudinal cracks formed in the concrete cover before the specimen failed, and the resulting changes in the bond stress/slip relationship rendered the analysis invalid.

Tepfers observed, from pull-out tests, that splitting of the concrete cover led to an equalization of bond stresses due to increased slip between the steel and the concrete [10]. A limited measurement of the strains in the lapped bars showed the steel strain distribution to become increasingly linear as failure approached. Similar behaviour has been reported by other authors [16,17].

There has been some concern [52] regarding the assumption of a linear bond stress/slip relationship (equation 2.8 and Figure 2.4.1). Tepfers argued that as the cover generally cracked at bond stresses of between 2.0 and 4.0 N/mm^2 these values

represented an upper limit for the validity of the analysis. He commented that within this range the bond stress/slip curve for the Swedish Ks60 steel reinforcing bars used in his tests was linear. However, a 'realistic' bond stress/slip curve (Figure 2.4.2), derived by Eligehausen [42] for a similar analysis, is non-linear in the same range.

In order to calculate the stress distributions along laps, Eligehausen solved a system of differential equations (similar to those derived by Tepfers from equations 2.9–2.11) using an iterative technique to make allowance for non-linearities in the bond stress/slip curve. He also took into account the effect of the change in the ratio of the bursting force to the bond force. According to his finite element modelling of bond behaviour, this ranged from about 0.5, when the concrete between the ribs was undamaged, to about 1.0 as the crushed concrete wedges built up ahead of the steel ribs (Figure 2.4.2). This meant that although the bond stresses were reasonably constant over the lap length at maximum loads, the splitting forces increased considerably at the lap ends. He suggested that this would result in the development of longitudinal cracks from the lap ends when the splitting force reached a critical level. The critical value is that which, according to the force distributions around the reinforcement (described in §2.3.), will result in splitting of the cover.

This approach is similar to that adopted by Tepfers [48] for the estimation of the ultimate strength of the lap. Variations in the extent of splitting along the specimen resulted in the definition of three possible failure modes, in which the cover could be either completely, partly or not cracked over the lap length. The final bond stress distribution was either linear in regions where splitting had occurred, or could be determined using the simplified equations (2.12–2.14) if the cover was uncracked. The ultimate lap strength was estimated by considering the possible failure patterns, which are dependent on the section geometry (see §2.3 and Figure 2.2), and using either an average or a peak bond stress as appropriate.

The analytical work of Tepfers and Eligehausen has been restricted to the behaviour of tension splices, and to date, there appears to have been no theory established for the bond stress distribution in a compression lap. It was shown in measurements taken by Cairns [27] that considerable variation could be found in the bond stress along the lap, with a peak existing at the free end of a lapped bar due to end bearing. The absence of transverse cracks in a compression lap enabled some of the force to be transferred outside the lap joint. Cairns noted the presence of bond stresses over a distance of approximately three bar diameters beyond the lap end. The precise steel strain distribution was found to be dependent upon concrete stiffness and reinforcement percentage, tending to become more linear

over the lap length with a less stiff concrete and a higher precentage of steel in the specimen. It was clear from a distribution plotted for a lap length of twenty bar diameters (Figure 2.6) that low bond stresses existed in the central portion of the lap, and since failure would be initiated at points of peak bond stress, this caused the ultimate average bond stress of the specimen to appear relatively low.

2.5 Conclusion

It was concluded by the A.C.I. Committee [20], which reported on bond stress research previous to 1966, that 'the development of an adequate bond theory depends on the establishment of the real bond stress distribution, the real splitting forces developed and what factors affect these two'.

Much of the research into lap joints has been concerned with the phenomenon of splitting, and there is now general agreement about the key factors affecting lap strength, although the importance attached to each parameter does vary [39]. The problem of longitudinal cracking has been dealt with both theoretically and experimentally, and results thus obtained have been favourably compared. There has, however, been some disagreement concerning the force distribution around the lapped bars, with different force systems being proposed by Tepfers [10] and by Reynolds [31]. Measurement of the circumferential strains in the concrete may help to resolve this problem. It might also clarify the uncertainty that exists regarding the changing relationship between bursting force and bond stress as the applied load is increased.

Although a measurement of these strains is undoubtedly of interest, there is a greater need to deal with the first part of the A.C.I.'s conclusion, namely the establishment of the longitudinal bond stress distribution. Since Kluge and Tuma's early work [12], in which a five inch mechanical gauge was used to determine the reinforcement strains along tension laps, no experimental study has concentrated on this aspect of lap joint behaviour. More recently, researchers have demonstrated that the steel strain distribution becomes increasingly linear near ultimate loads, particularly if the cover cracks, and have consequently justified the use of average bond stresses in design codes. However, the existence of peak bond stresses was recognised by Tepfers [10], with one possible mode of lap failure being the rapid development of a splitting crack along the lap length. Although plastification of the concrete may help to distribute the effect of the peak stresses, the cracking of the concrete cover may be attributed to a peak, rather than an average, bond stress. It is of considerable interest to establish not only the value of the peak stress, but also the relationship between the peak and the average bond stresses,

if the use of an average bond stress for estimating the ultimate lap strength is to be justified. To date, strain measurements in lap joints (Figure 1.1) have been carried out using a gauge spacing in the order of 50 mm. There has consequently been insufficient detail in the measured distributions to determine the peak bond stresses with confidence.

The effect of transverse cracking of the concrete within the lap has not been assessed experimentally, although Tepfers [48] did make provision for the development of such cracks in his derivation of equations which describe the steel and bond stress distributions. The influence of specimen characteristics such as lap length and bar diameter on these distributions have not been determined, and lap joints which comprise bars of different diameter appear to have been totally neglected in previous work.

It is clear that to fully understand the behaviour of both tension and compression lap joints the stress distribution along the lap length, and the factors affecting this distribution, have to be established. This can be best achieved experimentally.

CHAPTER 3

STRAIN MEASUREMENTS

3.1 Strain Measurements in the Reinforcement

3.1.1 Strain gauging technique

A number of techniques have been developed to determine the strain distribution along reinforcing bars in concrete. These include photoelastic investigations [14], the use of the Moiré method [6] and, more commonly, measurement by electric resistance strain gauges. Various researchers have attached such gauges to the surface of the steel to determine strains along lap joints (Figure 1.1), but the presence of gauges, and the associated waterproofing compounds and lead wires, must modify the bond characteristics of the rod. To overcome this Bernander [53] placed strain gauges on the side walls of a slot cut longitudinally along the bar, arguing that the small opening thus created on the circumference would have little effect on bond behaviour. Mains [3], in 1951, developed an alternative technique which left the perimeter of the rod intact, and was therefore more satisfactory for bond research. A reinforcing bar was cut in two axially, and up to twenty gauges were mounted in a groove milled in one portion of the bar. The two pieces were then tack welded together to re-create a complete rod. This technique has since been used by a number of researchers [4,5,6], and a similar method, which took advantage of the many advances in strain gauge technology in the 35 years since Mains' work, was developed by Scott and Gill [1,2]. It was their technique which was employed in this research.

This method of strain measurement was particularly suited to bond research, the use of electric resistance strain gauges enabling localised readings to be taken along the reinforcement, without changing the steel's bond characteristics. Since lap joints rely on bond to transfer the force between the overlapping bars it was important that the integrity of the steel/concrete interface was preserved. An additional benefit of internally gauging the rods was that, by providing an exit route for the lead wires within the steel, the surrounding concrete remained undisturbed.

The strain gauged rods were formed by milling two reinforcing bars to a half-round and machining a longitudinal groove, 5 mm wide and 2.5 mm deep, in each. In the first six specimens this groove was stopped 5 mm short of the embedded end of the bar. It was felt that closing the groove in this manner would help to seal the gauge installation. This was later found to be unnecessary, and in the subsequent

specimens the groove ran the full length of the rod. Electric resistance strain gauges (3 mm gauge length, overall size 9 × 3.5 mm) were fixed in these grooves using a cyanoacrylic adhesive. Terminal strips, to which the leads were soldered, were glued alongside the gauges. Space limitations within the groove necessitated the use of very small diameter (0.224 mm) enamelled copper lead wires. The strain gauges were connected for quarter bridge operation, using a three wire, common dummy, arrangement. This wiring system, combined with a twin constant current energising circuit, was used to eliminate any change in resistance produced by thermal effects on the 3 m long lead wires. The gauge installation was protected, first with a polyurethane varnish and then, following the tacking down of the lead wires, with an acrylic solution. The gauge resistance, nominally 120 Ω, and the earth leakage (between the gauge and the reinforcing steel) were checked before joining the two half-bars with an epoxy resin, with this resin also serving to fill any remaining space in the groove. The finished arrangement is shown in Figure 3.1.

The completed bar was placed in the test rig and subjected to strain cycling from zero to 500 microstrain, to minimise hysterisis and to check the gauge installation. Confidence in the measurement technique was provided by the uniformity of the strain distribution along the rod at 500 microstrain. Slight deviations from the mean strain level were attributed to changes in the rod cross-sectional area. As a final part of the bedding-in operation the bar was loaded to either 10 or 35 kN, depending on rod diameter, in increments of either 2 or 5 kN. The bar was then unloaded using the same increments. The strain measurements at each load value were recorded to enable the determination of the rod cross-sectional area (see §5.2.2).

In order to ensure that the steel was not gripped at a gauge position during the bedding-in operation the rods initially extended beyond the gauge at the lap end, with the standard overall length being 2.6 m. Prior to casting, the bar had to be cut to the required length. The cut end of the rod was coated with both polyurethane varnish and an acrylic solution to ensure that the gauge installation was completely sealed.

The reliability of the strain gauging procedure was good, with an overall gauge failure rate of under 3%. It was noted that specimens which were subjected to a sustained load were more susceptible to gauge failure, with some gauges failing during the course of a test. This may have been a consequence of the cyanoacrylate adhesive breaking down over a period of time.

3.1.2 Gauge layout

The strain gauge layout varied slightly for each specimen, but each pair of lapped rods was gauged similarly. Up to 44 gauges could be installed in each rod, with all the lead wires coming out of one end. A typical layout is shown in Figure 3.2. In general, the gauges were equally spaced over the central metre or so of the specimen, and bonded to alternate sides of the rod. A pair of gauges measured the rod strains out of the concrete, and thus provided a correlation with the load measuring instrumentation. Greater detail in the strain distribution was sought at the lap ends by a closer spacing of the gauges, and in some of the later specimens by the use of strain concentration gauges.

3.1.3 Strain concentration gauges

Strain concentration gauges, which consisted of five 1 mm gauge elements at 2 mm centres, provided very detailed information at the lap ends (Figure 3.3). The gauge installation procedure was considerably complicated by the leads coming out to the sides of these gauges. These leads had to be insulated prior to being soldered to the terminal strips, which in this case were glued to the walls of the groove.

It was clear that great care was required to ensure reliable results with the concentration gauges. In particular, the end elements of these gauges appeared to be prone to failure. These had performed well during the bedding-in procedure, but during the test indicated a strain that was atypical of the trend shown by the other four elements in the gauge. This may have been due to a failure in the bond between the gauge and the steel reinforcement, either caused by the ingress of moisture and consequent breakdown of the cyanoacrylate adhesive, or by damage which occurred as the rod was cut to its correct length. Increased experience in the installation of the concentration gauges seemed to alleviate the situation, with there being no recurrence of this problem in the later specimens. The loss of these few gauges did not detract from the value of the measurements.

3.2 Other Strain Measurements

3.2.1 Surface strains

The average concrete surface strains were measured using a Demec gauge. It was decided that a 200 mm gauge length would give sufficient detail in these tests, and a single row of five or six (depending on the specimen length) Demec studs was glued centrally on each face of the specimen.

3.2.2 Embedment gauges

Two specimens contained embedment strain gauges (12 mm gauge length, overall size 30 × 9 × 2.5 mm) within the concrete to measure the strains around the reinforcement. There were three groups of gauges at 100 mm centres — one within the lap, one outside and one at the lap end. A single gauge was positioned on each face, midway between the bar and the concrete surface, using a grillage of fine wire, as shown in Figure 3.4. This was complemented by an electric resistance strain gauge (30 mm gauge length) attached, by epoxy resin, to the surface of the concrete immediately above the embedment gauge. The embedment gauges were restricted to one half of the specimen due to their potential behaviour as crack inducers, and to the disturbance caused by their presence in the concrete.

CHAPTER 4

TEST SPECIMENS AND PROCEDURE

4.1 Specimen Dimensions

4.1.1 General

Research into lapped joints has generally been carried out on beams subjected to a four-point loading system, with the joint lying in the constant moment zone. Cairns and Jones [37] have used axially loaded specimens, reinforced with two pairs of lapped rods to negate bending influences, and concluded that the results of such tests correlated well with those of beam tests. The availability of test rigs equipped to apply axial forces, in particular the Dartec testing machine, resulted in the use of axial specimens in this investigation. The cost of strain gauging the reinforcing bars meant that only a single pair of lapped rods was cast in each specimen.

Two series of tests were carried out, the first dealing with tension laps and the second with compression laps. The tension series was divided into two groups: short term tension tests, comprising thirteeen specimens, and long term tests, comprising two specimens. The compression series consisted of a single group of five short term tests. Each of these groups was tested in a different rig, which led to some variations in the specimen lengths. This was 885 mm for the long term tests, 1000 mm for the compression tests, and 1500 mm for the short term tension tests.

All the specimens were nominally 100 mm square. Previous work on axial specimens reinforced by a single continuous rod [54] had shown that with such a cross-section a considerable amount of information could be collected both before and after crack formation. The specimens were centrally reinforced with either 12 or 20 mm diameter high yield steel rods (Torbar). The size of the larger rod was dictated by the tension rig which, with its loading limit of 100 kN, was unable to yield a bar larger than 20 mm diameter. Whilst a large variation in the rod dimensions would help to emphasise the influence of rod diameter, the use of too small a rod might result in the internal groove exerting an undue influence on the stresses. The 12 mm rod, which when gauged had a nominal cross-sectional area of 78% of a solid bar, was considered satisfactory.

The lap joint was situated in the centre of the specimen, and varied in length from 125 to 750 mm. The typical specimen layout is illustrated in Figure 4.1. The

lengths were, in part, chosen to ensure that the lap joint would not be affected by the anticipated breakdown in bond at the specimen ends. The lap lengths were both above and below the minimum requirements of the design code in operation at the start of the work[55]†.

The specimens have been coded according to the variables. The first number refers to the lap length (mm). This is followed by the group letter — T for short term tension, D for long term tension and C for compression. The next numbers refer to diameters (mm) of the two lapped rods. A final letter in brackets may be used to differentiate between two specimens which are nominally the same (A or B), or to identify those specimens with either transverse reinforcement in the form of links (L) or embedment gauges (E). Thus specimen 125D12/12(L) refers to a 125 mm lap length in the long term tension group, the lap comprising a pair of 12 mm rods and being surrounded by links. A description of each of the twenty strain gauged specimens is given in Figure 4.2, and the following sections will give details relevant to each group.

The measured specimen properties are tabled in Figure 4.3. The slight variations from the nominal dimensions were due to tolerances in the specimen specification. The areas of the two rods lapped in each compression specimen were equal because the shorter overall length of these specimens enabled a single length of reinforcement to be gauged and bedded-in, which could then be cut in half to form a pair of rods.

4.1.2 Short term tension specimens

The thirteen specimens in this group encompassed a wide range of variables. Lap lengths of 125, 250, 500 and 750 mm were used, and both 12 and 20 mm diameter rods were lapped. Embedment gauges were cast in one specimen to measure the circumferential strains in the concrete. In two of the later specimens transverse reinforcement was provided to help contain the splitting forces caused by the wedging action of the reinforcing bars. It was hoped that this would increase

† Clause 3.11.6.5 in CP110[55] states, *inter alia*, that 'When bars are lapped, the length of the lap should at least equal the anchorage length (derived from 3.11.6.2) required to develop the stress in the smaller of the two bars lapped, except that for deformed bars in tension the length should be 25% greater than the anchorage length required for the smaller bar. The length of the lap provided, however, should neither be less than 25 times the bar size plus 150 mm in tension reinforcement nor be less than 20 times the bar size plus 150 mm in compression reinforcement'. Application of this code for a grade 30 concrete gave minimum values for the lap length required to develop the yield stress of the reinforcement (460 N/mm^2): these were 594 and 991 mm when in tension or 394 and 657 mm when in compression, for the 12 and 20 mm diameter bars respectively. The constraints of the tension test rig limited the applied load to 100 kN, and the lap length required to develop this force in a 20 mm rod was 686 mm.

the failure load and also reduce the rate at which the longitudinal cracks developed. The positioning of the embedment gauges and the layout of the transverse reinforcement is shown in Figure 4.4.

Three tests were included in which the lapped rods were of differing diameter, 'mixed' laps. In the first of these (250T12/20(A)) the minimum cover to the two rods was unequal. In the subsequent two tests the joint was offset by 4 mm so that the minimum cover to each rod was the same.

4.1.3 Long term tension specimens

The two specimens in this group comprised a pair of 12 mm rods, lapped over a length of 125 mm. The first specimen (125D12/12(A)) failed just two days into the test, and it was clear that some modification to the specimens would be required if a load was to be maintained over a long period. Consequently two exploratory tests were carried out, using ungauged rods. The first used a crack-inducer to lower the load at which the first crack formed, hence reducing the likelihood of immediate failure. The second used links to contain the splitting forces, thus preventing a sudden failure. Both methods appeared to work satisfactorily, but it was felt that the specimen with the crack-inducer would have failed had longitudinal cracks developed. Consequently transverse reinforcement was provided in the second specimen to ensure that sustained loads could be applied (Figure 4.4).

4.1.4 Short term compression specimens

The compression tests were carried out in a strengthened version of the tension rig, with the modifications raising the rig limit to 300 kN. In order to determine whether lap failure might be anticipated four ungauged specimens were tested, in all cases lapping a pair of 12 mm rods. Three of the specimens had a nominal cross-section of 100 $\times$ 100 mm, the lap lengths being 30, 62 and 125 mm. The 62 mm lap failed, at 298 kN, but the other two joints showed no visible sign of damage at the maximum load of 300 kN. A fourth specimen, with a 70 $\times$ 70 mm cross-section and a 125 mm lap length, failed at 190 kN. However, failure was initiated at the ends of the specimen, rather than over the lap length. In order to prevent this type of failure in subsequent tests, the concrete was externally clamped at the specimen ends. The results from these pilot tests, discussed further in section 7.1, indicated that lap failure could not be guaranteed. It was therefore decided to restrict the tests to specimens which were comparable to those used in the tension series. The five gauged specimens were 100 mm square, with lap lengths of either 125 or 250 mm.

Embedment gauges were cast around the reinforcement in one specimen. As in the tension series (Figure 4.4), these were placed at the end of the lap and 100 mm to either side of this position. Since failure of the specimens was not expected the presence of transverse reinforcement was deemed unnecessary.

4.2 Concrete Mix and Casting

A concrete mix was designed to have a 28-day cube strength of 30 N/mm^2 and a high workability, using 10 mm aggregate and a zone 2 sand. The mix had a water/cement ratio of 0.6, an aggregate/cement ratio of 5.5 and a coarse/fine aggregate ratio of 1.5.

The arrangement of the reinforcement within the specimen is shown in Figure 4.1. The rods were placed above each other in order to reduce the influence that any consolidation of the fresh concrete beneath the splice might have. This also helped with joint stability, though of much greater relevance in this respect was the clamping of the rods outside the mould. The reinforcement was tied in one or two places along the lap using fine wire. The concrete was placed in three layers of approximately equal depth.

The concrete was cured for seven days under damp hessian, and was then stored in the laboratory. The short term tests were carried out at approximately 28 days (Figure 4.3). Some three months elapsed before the start of the long term tests in order to minimise creep and shrinkage effects during these tests.

Test cubes and cylinders were cast with the specimen for the determination of the compressive and indirect tensile strength of the concrete. The results from these tests are included in Figure 4.3. It is clear from this table that the true value of the concrete's compressive strength was considerably higher than the design value of 30 N/mm^2. The mean cube compressive strength of 52.3 N/mm^2, with a standard deviation of 5.1 N/mm^2, gave a characteristic strength† of 43.8 N/mm^2. The splitting tests on the cylinders yielded a mean indirect tensile strength of 2.9 N/mm^2, with a standard deviation of 0.3 N/mm^2. Traditional empirical relationships express the concrete's tensile strength in terms of the square root of the compressive strength [40]. An equation of this form was derived from the test

† The characteristic cube strength is defined as that value below which 5% of all possible test results would be expected to fall [7].

results, giving:

$$f_{ct} = 0.4\sqrt{f_{cu}} \tag{4.1}$$

4.3 Test Procedures

4.3.1 Short term tension tests

These tests were carried out in a rig which had been built to load axial specimens to 100 kN (Figure 4.5). The specimen was loaded through the reinforcing steel, with the load being applied by a manually operated hydraulic jack and measured by a flat load cell. The load cell output was displayed as a direct reading on a meter and sent to the data collection system as a voltage.

The 12 mm rods were sufficiently flexible to allow the jack and the load cell to be placed co-linearly. However, the stiffer section of the 20 mm rods prevented this arrangement, and when these bars were tested the jack had to be displaced by 20 mm. The provision of spherical seatings at the loading points permitted some rotation of the specimen in the rig.

The loads were applied incrementally, the increment size varying between 0.5 and 2 kN according to the strain changes and cracking taking place in the specimen. The load values and the strain gauge readings were recorded at each load stage. The loading was halted at 50 kN for the 12 mm rods, and at 100 kN for the 20 mm rods, unless the reinforcement had fully yielded or the specimen had failed earlier. Each test was completed within a day.

The Demec readings were taken at regular intervals, typically 5 kN, and also after the formation of each crack. Safety considerations precluded the carrying out of these measurements at the higher load levels.

4.3.2 Long term tension tests

The Dartec servo-hydraulic testing machine, illustrated in Figure 4.5, was used for the long term tension tests. A feature of its control system allowed the application of sustained loads. The specimen was loaded through the reinforcing steel, at increments of 1 kN, until a crack formed. It was envisaged that the load would then be maintained at this level for a period of approximately three months. The first specimen, however, failed after just two days. The second test was halted after 81 days, due to failure of the Dartec test rig.

The load value and the strain readings were initially recorded at two-hourly intervals. In the second specimen these intervals were lengthened as the test progressed, until the data was scanned on a daily basis. The Demec readings were taken twice a week.

4.3.3 Short term compression tests

The compression tests were carried out in a modified, and strengthened, version of the short term tension rig (Figure 4.7). To obtain an exact reversal of the tension situation would have necessitated the application of loads through the reinforcing bars. This would have limited the loads in specimens reinforced by 12 mm rods to approximately 70 kN, before the onset of yield in the steel. Consequently the first two specimens in this series, whilst being nominally the same, were subjected to different loading arrangements. It was demonstrated that loads of up to 300 kN could be applied through the concrete, and that the strain distribution in the lapped region was similar in these two specimens, irrespective of the loading mechanism (see §7.2.1). This method of loading the specimens was adopted, with spherical seatings again being provided at the loading points.

Strain and load measurements were taken at 5 kN increments. The Demec readings were taken every 15 kN, until 75 kN when a safety cage was placed around the specimen. The loading was halted at 300 kN, this being the capacity of the hydraulic jack, and each test was completed within a few hours.

CHAPTER 5

DATA ACQUISITION AND ANALYSIS

5.1 Data Acquisition

The numerous readings taken in the course of a test were recorded by a computer controlled data collection system. This consisted of an Intercole Spectra-ms data logger linked to a Cifer microcomputer. The system is illustrated in Figure 5.1.

The logger was constructed in modular form, with separate modules existing for the microprocessor unit, the analogue to digital converter and the instrumentation amplifier. A further thirteen modules were available for the input wiring, allowing up to 208 channels of data to be scanned.

Reed relay scanners were used to switch sequentially between the input channels, with the input signal being measured by the instrumentation amplifier and the associated analogue to digital converter (ADC). The high speed at which the ADC operated enabled a digital integration of the data, which was of value when rejecting spurious signals. Numerous values of a contaminated signal were sampled over a period of 20 milliseconds. These values were then digitised and integrated, and since, over this period, the integral of a 50 Hz sinusoidal signal is zero, mains interference was effectively eliminated.

The integration period influenced the scanning speed which, at 8 channels/ second, was low but adequate for the quasi-static conditions prevailing during the tests. This did, however, permit a sensitivity of ± 1 microstrain for the data logger. The accuracy of the sytem was maintained by its twin constant current energising circuits which, combined with the three lead wire system, enabled the measured voltages to be independent of the resistance of the lead wires. The readings from the entire strain gauge installation were accurate to better than ± 5 microstrain.

It would have been possible to instruct the data logger from a standard keyboard, via an RS232 link. However, greater flexibility could be achieved by the use of a supervising microcomputer, in this case a Cifer 2684.

A port which was connected directly to the keyboard was available on the computer. This enabled simultaneous output from the keyboard to the data logger, the VDU screen and the interfacing software. The logger would only respond to commands commencing with ';', and so it was possible to communicate with

the computer without activating the logger. The software made use of this, and commands intended specifically for the computer began with a '*'.

The interfacing program was developed as a series of FORTRAN subroutines. It enhanced communications with the data logger, with both the input and output becoming more comprehensible. More importantly, it introduced sophisticated file handling procedures, which were of particular value during the long term tests. A detailed description of this software has been published by its author [56].

The test data was initially stored on a $5\frac{1}{4}$ inch floppy disk, using the Cifer's external disk drive. Following the completion of the test the data was transferred to a Perkin-Elmer 3230 minicomputer, using file transfer programs available within the University. The considerable power of this machine was thus available for the subsequent analysis of the results.

5.2 Data Analysis Program

5.2.1 General

It was clear that computer programs were required to analyse the several thousand readings taken during each test. Two programs were written, in FORTRAN, to deal with the test results.

The first program reorganised the original data, and put it into a form suitable for further computation. Surplus readings were omitted, and the strain data was modified by removal of any zero error. It was possible to use this program to output the strain values to the screen or the printer, but its main role was to build a data file which contained all the parameters required for subsequent analysis. These included all the specimen dimensions; thus one of its requirements was that it should determine the cross-sectional area of the rod (see §5.2.2).

The second program undertook the preliminary analysis of the test data. It dealt primarily with the curve smoothing procedures, and the determination of the bond and concrete stresses, using techniques described in later sections of this chapter. These values were output either individually or in pairs (for instance bond/rod stresses), to the screen or to the printer. If graphic routines and curve fitting procedures were required for further analysis then the results could be output to another data file.

5.2.2 Determination of rod cross-sectional area

It was necessary to determine the rod cross-sectional area which, due to manufacturing tolerances, deviated from its nominal value of 88 and 289 mm^2 for the 12 and 20 mm rods respectively. On completion of the strain cycling procedure the rod was loaded incrementally, taking the steel strains to approximately 500 microstrain, well within the elastic limit (see §3.1.1). The rod was then unloaded, using the same increments. The strain values at each load stage were recorded.

The computer program used the method of least squares to fit a line to the stress/strain curve. A value for the Young's modulus of the rod was determined, using the nominal cross-sectional area, for both the loading and the unloading cases. The actual cross-sectional area was calculated by comparing the average of these two values with the Young's modulus of Torbar, which was determined experimentally to be 207 kN/mm^2. The influence of the epoxy resin was neglected as its Young's modulus was, at 2.7 kN/mm^2, two orders of magnitude below that of the steel.

It was possible to carry out the same operation for individual gauges to evaluate the area at each gauged point along the rod. The coefficient of variation† of the area along the bar was typically under 5%, and reached a maximum of 10% in one bar. Although it was useful to be able to note the changes in the rod area, the additional complication introduced if these variations were incorporated into the computation was not justified. The average cross-sectional area for the rod was therefore used in the subsequent programs.

5.2.3 Curve smoothing procedure

All the specimens exhibited the presence of bending, characterised by higher strains on one half of the rod than the other. An attempt was made to reduce the influence of bending upon the strain distribution by using a curve smoothing procedure.

A simple averaging technique was tried first, using the following equation to

† A measure of relative variation, defined as the standard deviation divided by the mean, and expressed here as a percentage.

smooth the distribution:

$$\epsilon_{ave} = \frac{1}{2} \times \left(\epsilon_n + \epsilon_{n-1} + \frac{(x_n - x_{n-1})(\epsilon_{n+1} - \epsilon_{n-1})}{(x_{n+1} - x_{n-1})} \right) \tag{5.1}$$

where:

ϵ_{ave}	=	Average reinforcement strain.
ϵ	=	Reinforcement strain, at positions 'n', 'n+1' and 'n-1'.
x	=	Distance along specimen, at positions 'n', 'n+1' and 'n-1'.

This worked reasonably well, but suffered from the disadvantage that it was not possible to obtain an averaged value for the points to either side of a faulty gauge. Thus, for every defective gauge three averaged results would be lost. However, this technique proved to be a useful yardstick by which to judge other procedures.

The first trials were carried out using a single low-degree polynomial. Unfortunately, this method proved to be unreliable, with the fitted curve occasionally oscillating between the data points. Consequently, attention was focussed upon the cubic spline technique. This held considerable promise of success; cubic splines are capable of approximating a wider variety of curves than a single polynomial, and are quicker to evaluate [57].

In this approximation the raw strain distribution was divided into a number of regions with common end-points, called knots, and then a cubic polynomial was fitted to the readings between each pair of knots. By keeping the first and second derivatives consistent at each knot, the individual curves could be joined, resulting in a single, continuous curve being fitted to the entire distribution. The algorithms required to apply this technique were available in the NAG subroutine library [58]. It was found helpful to have the strain readings displayed graphically on the screen as the knot positions were defined. The user was thus able to check that each curve was acceptable before proceeding further.

A typical result from the application of this technique is shown in Figure 5.2, which illustrates both the curve fitted through the raw data and the 'averaged' strains determined using equation 5.1. The positions of the user-defined knots are also shown (these exclude the knots automatically placed at the ends of the distribution within the NAG subroutine). In general, a single knot was placed where clear changes in the gradient of the original strain distribution existed, typically near the peaks and the troughs. The precise positioning of the knot was not critical and, for convenience, the knot was situated mid-way between adjacent gauges. On occasion, two knots, placed between separate, but neighbouring, pairs of gauges, were required to improve the fitted curve. Different knot positions could have been defined at each load stage, but in this work the knot positions

were generally maintained until the form of the curve changed. Although the above is a guideline to the positioning of the knots, the rules were not applied dogmatically, each case being judged on its own merits.

A comparison of the cubic spline procedure with the averaging technique described earlier (equation 5.1) showed that values obtained by the two methods were similar, generally differing by under 10% (Figure 5.2). The spline technique required greater effort on the part of the operator, but enabled interpolation between the strain gauged points, which was useful when strains at an ungauged position were required (for instance, in the evaluation of concrete stresses, §5.2.5). It also determined the first and second derivatives of the curve which permitted the bond stresses to be calculated.

5.2.4 Determination of bond stresses

In order to satisfy equilibrium conditions, a change in force along the reinforcing bar must be balanced by a corresponding bond force at the steel/concrete interface. Consideration of this condition leads to the following equation for bond stress:

$$f_{bs} = \frac{dT}{u\,dx} \tag{5.2}$$

where:

f_{bs}	=	Bond stress.
u	=	Perimeter of steel reinforcement.
dT	=	Change in force over length dx of rod.

As long as the steel behaves elastically, the change in force may be considered in terms of a change in strain. Equation 5.2 may be re-written to give:

$$f_{bs} = \frac{E_s\,A_s}{u} \times \frac{d\epsilon}{dx} \tag{5.3}$$

where:

E_s	=	Modulus of elasticity of steel reinforcement.
A_s	=	Area of steel reinforcement.
$\frac{d\epsilon}{dx}$	=	Strain gradient.

Thus, to obtain a value for the bond stress along the specimen it was necessary to determine the gradient of the strain distribution. It should be noted that equation 5.3 gives an average value of bond stress around the perimeter of the rod. The exact nature of the force system around a lap joint has not been resolved, although a variety of proposals have been put forward (see §2.3), and it was decided that an average value was satisfactory.

It was clear from the plots of the strain values along the specimen that there existed regions along which the strain could be seen to be varying linearly (Figure 5.2). The first technique used for the calculation of bond stresses relied on the visual identification of the end points of zones of approximately constant stress. A linear regression procedure was applied to the strain data from within these regions, and an average bond stress calculated. This method was extremely time consuming, with the result that the calculations were only carried out for a limited number of load stages. It was therefore possible that some valuable data was being neglected, and consequently an alternative, more time-effective, technique was sought.

The determination of strain gradients formed an integral part of the cubic spline curve fitting procedure, which enabled the easy evaluation of the bond stress at any point along the steel. However, the results indicated variations in the bond stress distribution where, previously, a constant bond stress had been assumed. There was concern that the apparent variation in bond stress was a feature of the curve smoothing procedure; as cubic polynomials were being fitted to the data the first derivative of the curve was constantly varying. To overcome this, a method of establishing regions of linearity was developed.

Regions of constant bond stress were delimited by considering the second derivative of the spline function, which is related to the rate of change of the strain gradient. The value below which this derivative had to lie varied according to the maximum strain in the rod, and was defined so that the end-points chosen by the computer program were comparable to those obtained by eye. If the length of the zone exceeded 10 mm then the bond stresses therein were averaged. The computed regions of linearity have been included in the strain distribution plotted in Figure 5.2, from which it may be seen that the delineation procedure tended to err slightly on the side of pessimism.

Another potential problem arising from the cubic spline procedure was that the calculated value of the peak bond stress could be curve fit dependent, because the gradient was being determined for single points along the distribution. In the region of the peak bond stress, the strain gradient tended to be varying sufficiently to remain unaffected by the delineation procedure outlined above. It was believed that greater confidence could be felt in the value of the peak bond stress if it could be established that this value was consistent over a length of rod. A suitable length was considered to be one gauge spacing, which lay within the range of half to three times the bar diameter over which, according to previous researchers [11], plastic behaviour of the concrete could serve to equalise the peak bond stresses. The mean of the two highest values of bond stress at adjacent gauges was thus

taken to represent the peak bond stress. Although it is acknowledged that this figure will be slightly lower than the true peak, greater confidence was placed in a value which was representative of the situation between adjacent strain gauges than one determined for a single point on the distribution.

The absence of strain concentration gauges in the earliest specimens created difficulties when trying to assess the bond stress at the tip of the tension laps. The strain measurements clearly showed the strain distribution tending to zero at the free end of the bar, and the results from the strain concentration gauges showed the distribution over the last 10 mm of the rod to be reasonably linear, particularly at higher loads. The bond stress was calculated by assuming a linear variation in strains from the value measured 10 mm from the lap end to zero at the tip of the lap. The values thus obtained compared favourably with the mean of the concentration gauge results. In order to standardise the bond stress calculations, this method of determining the bond stress at the lap end was adopted for all the specimens.

It is clearly apparent that the bond stress calculations involved more than a conversion of the first derivative of fitted curve into a figure for bond stress. The additional procedures outlined above were developed as a precautionary measure against the data being unduly curve fit dependent. The development of a computer based technique for the evaluation of bond stress enabled the processing of all the strain measurements, and thus made more information available than there may have otherwise been.

5.2.5 Determination of concrete stresses

The average concrete stress across a section was determined by equating the internal forces (those in the steel and in the concrete) to the external forces.

While the steel was behaving elastically the force in the bar was proportional to strain and the force in each lapped rod could be evaluated from the averaged strains. The cubic spline procedure enabled the interpolation of the steel strain distribution, which was of value when estimating the force in the ungauged part of the rod. Such an estimation was necessary within the lap joint when the gauges were not directly opposite each other.

In the two tension series the external forces were determined from the mean of the strains read by the external gauges. The applied load, as measured by the load cell, was used for the compression series as these specimens did not have external gauges.

The internal and external forces were balanced to give the average concrete force at a section. The concrete stress was thus calculated at each gauge position for all load stages. A warning was output next to the concrete stress value if the steel strain exceeded 1500 microstrain.

5.2.6 Determination of slip

Once the strain distribution along the reinforcement has been established, it is possible to estimate the slip between the steel bar and the concrete. The slip is the difference between the steel and concrete displacements over a given length, and the displacements may be calculated by integrating the respective strain distributions. Thus, for the length a – b, the slip at point 'b' may be determined from the following equation:

$$\Delta_b = \Delta_a + \int_a^b \epsilon_s dx - \int_a^b \epsilon_c dx \tag{5.4}$$

where:

Δ_b = Desired value of slip at point 'b'.

Δ_a = Known value of slip at point 'a'.

As no measurements of slip were taken, point 'a' was always positioned at a trough in the steel strain distribution, where zero slip was assumed. The integrals of the strain distributions were determined numerically using the trapezoidal rule.

The value of the reinforcement strain at the gauge position was obtained from the measurements. The concrete strain was estimated by assuming a typical Young's modulus of 27.6 kN/mm^2 for the concrete, and thus converting the average stress across the section into strain. Errors in the estimation of this strain were insignificant when calculating the slip near a crack, where the steel strains were much higher than the concrete strains. At the lap end, however, where the two strains were often very similar, the influence of the concrete strain was more significant.

From the outset the calculations seemed fraught with danger, especially as to determine the slip at the lap end it was necessary to use the Demec results to estimate the displacement of the concrete across a crack. Consequently, the procedure was not incorporated in the main data analysis program, instead being carried out by hand on selected groups of data.

CHAPTER 6

TENSION TEST RESULTS AND DISCUSSION

6.1 Tension Test Results

The test measurements clearly showed the distribution of strains along the lapped reinforcing bars. It was apparent from these results that some bending was present in the specimen. This was characterised by the strains in one half of the rod being slightly greater than the other. Although the bending may have influenced the cracking pattern, its effect on the strain distribution was less significant, particularly within the stiffer section of the lap. As the strain distributions were of prime interest in this work, the curve smoothing procedure described in section 5.2.3 was employed. Henceforth, it is implicit that any strains referred to have been subjected to this procedure.

The steel strain distributions for each of the fifteen tension specimens are plotted in Figures 6.1.1 – 6.1.15. In general, the plots show the strains measured immediately following crack formation, and at the higher load stages. In the case of the two long term specimens, in which the load was maintained at a constant level, the plots show the variation in the reinforcement strains over a period of time.

The manner in which the strains peaked at a crack, where the reinforcement carried the entire load, was evident. The situation around a single crack has been highlighted in Figure 6.2 in order to describe the relationship between the reinforcement, concrete and bond stresses. It is clear that the concrete stress was negligible at the crack. To either side of this position, the concrete carried an increasing share of the load, reaching a maximum stress at the position which corresponded with the trough in the steel stress distribution. In the early stages of the test the steel and concrete strains would have been comparable at this position, the bond between the two materials remaining unimpaired. Bond stresses were associated with the strain gradient set up on each side of the crack in the reinforcement. The steel strain distributions here were often linear, thus demonstrating the existence of zones of constant bond stress. Gross bond breakdown in the immediate vicinity of the crack resulted in negligible bond stresses, and caused the peak bond stress to be found a small distance away from the crack.

The magnitude of the peak steel strain at a crack was dependent on the reinforcement percentage. In those specimens reinforced by bars of similar diameter the peak strains at cracks outside the lap were therefore of similar magnitude. This

often resulted in the strain distribution being almost symmetrical about the centre of the specimen. In the mixed laps, different values of peak strain were associated with each rod, the values being dependent on the size of the reinforcement. The increased reinforcement area within the lap joint resulted in smaller peaks in this region, with the value of these peaks also being dependent on the position of the crack. In general, the steel strains in each half of the lap joint were lower in the terminating rod. This was particularly noticeable at the highest load stages.

Negligible strain exists at the free end of a reinforcing bar in a tension lap joint. This was corroborated by the test measurements which clearly showed the strain distribution tending to zero at this point. This resulted in steep strain gradients being developed at the lap end, particularly if a crack formed just inside the lap region, as in specimen 750T12/12 Rod A. The nature of the distribution at the lap end depended, to a large extent, on the proximity of the neighbouring crack, and on the value of the reinforcement strain at this crack. A steeper gradient would therefore be expected for the smaller size reinforcement, in which the peak strains were higher. This was confirmed by the results from the tests on mixed laps. If no cracks developed near the lap ends, the distribution here could remain virtually unchanged as the applied load was increased. Such behaviour was measured by the concentration gauges in specimen 500T12/20.

The measurements taken in the early specimens indicated a particularly sharp fall in the strains at the ends of the rods before crack formation. Strain concentration gauges were installed at the tip of the lap to investigate this effect, with a typical result being shown in Figure 6.3. Before cracking, the measurements demonstrated that the force was being transferred from one bar to the other over a remarkably short length of steel.

The development of transverse cracks along the specimen considerably modified the steel strain distribution. Before these cracks appeared the steel strains were constant along much of the specimen, as may be seen from the three typical precrack strain distributions illustrated in Figure 6.4. The form of this distribution was consistent for all the specimens, irrespective of lap length or bar diameter.

It is clear from Figure 6.4 that the strain gradient, and hence the bond stress, was negligible over much of the specimen prior to crack formation. Breakdown in the bond between the steel and concrete was only observed at the specimen ends, where the reinforcement entered the concrete, and at the ends of the lap joint.

The variation in the reinforcement percentage along the specimen resulted in a higher steel strain level outside the lap joint. Consequently, the first crack in each specimen generally formed out of the lap. On the two occasions when the

initial crack formed well within the lap joint, it was attributed to the crack being induced by tie-wire (500T20/20), or by an embedment gauge (250T20/20(E)).

Development of microcracks within the concrete was associated with the observed breakdown in bond at the specimen ends. Consequently, the earliest crack often originated at the end of the debond zone, where high, localised, tensile stresses coincided with a weakened section. This was consistent with the findings of Illston and Stevens [59], who carried out tension tests on axial specimens. However, the first crack in specimens subjected to four point loading typically develops at the ends of the lap joint, due to the discontinuity in specimen stiffness [17,25]. Such behaviour was not observed in the specimens tested here, with it being common for the lap ends to remain uncracked until late in the tests. This may be a consequence of using an axial rather than a four-point loading system.

In general, the cracks initially opened on just three faces of the specimen, putting the fourth into compression. In the specimens comprising a pair of 12 mm rods, the cracks were dominant on the A and C faces of the concrete (see Figure 4.1). Although the Demec measurements showed the effect of bending to be most pronounced on these two faces, the data was insufficient to correlate the crack pattern with the bending. However, the greater number of cracks in those specimens reinforced by a pair of 20 mm bars enabled such a comparison to be made, with the magnitude and distribution of the bending forces being assessed from the Demec results. A consistent pattern to the cracking was only observed out of the lap joint. No trend was apparent inside the lap where, despite the differences in cover, the cracks initiated on any one of the four faces.

In the early stages of the test the cracks generally dominated face A at the top of the specimen, and face C at the base. This was consistent with the distribution of the bending forces, which were initially greatest near the ends of the specimen due to the couples set up by curving the rods beyond the specimen ends (this enabled the load to be applied colinearly, see §4.3.1). The effect was less evident in specimens reinforced by 20 mm rods, in which the increased stiffness of the steel section required the offsetting of the hydraulic jack. The realignment of the specimen after the formation of cracks reduced the curvature of the rod outside the concrete, thus relieving the associated bending moment.

Many of the cracks (78%) which followed this pattern reversed at some later stage in the test, thus opening on face C above the lap and face A below it. This was attributed to the effect of the couples induced in the specimen by the offset of the overlapped bars becoming more apparent. One failure characteristic was the

visible widening of cracks at the lap ends; since these were on opposite faces the specimen tended to hinge at these points.

The majority of the cracks formed within the load range 10 – 30 kN, with it not being unusual for several cracks to appear at the same load. Details of the applied load and steel strains at crack formation are given in Figure 6.5. The value of the strain subsequent to cracking is included in this table to illustrate the extent of the change in strains. At times, in the case of the 12 mm rods outside the lap, the steel yielded as soon as cracks formed. It may also be seen that the two sizes of reinforcing bar behaved differently, with more cracks and lower strains being observed for the 20 mm rods.

The load in the short term tests was applied manually, and therefore crack formation was generally associated with a reduction in load. The frequent absence of such a fall was one manifestation of the gentle nature by which cracks formed in specimens reinforced by 20 mm rods. It appeared that these cracks were not opening fully until later in the test, when they often propagated around the specimen. A substantial rise in strains was noted as this occurred.

The reinforcement strain at crack formation typically lay between 40 and 175 microstrain (Figure 6.5). The lowest values of strains were often associated with some form of crack inducement, such as links or embedment gauges. Compatibility of the strains across the specimen in the early stages of the test would result in similar strains being found in the concrete. Neville [41] has commented that a concrete strain ranging from 100 to 200 microstrain generally results in cracking. A favourable comparison between this and the measured range may be made if the effect of bending is taken into account. This would result in the peak strain across the section being higher than was measured by the gauges in the reinforcement.

Some specimens developed cracks at much higher strains. Whereas a consistent pattern had been observed for the earlier cracks, the high strain cracks seemed to be specimen dependent. Many of the late cracks developed at the ends of the lap joint. These were probably a consequence of the bending forces set up in the specimen by existing cracks and by couples induced by the offset in the overlapping bars. Two of the high strain cracks may have been akin to Goto's [60] secondary cracks, which were the result of internal cracks reaching the surface. This type of behaviour was similar to that noted by Scott and Gill [54] in their tests on axial specimens.

The mean value of the strain at crack formation differed slightly for the two bar sizes. Excluding those cracks which developed at strains in excess of 175 microstrain, the average values for the 12 and 20 mm rods were 120 and 91 microstrain, with a standard deviation of 14 and 28 microstrain respectively. The overall mean of 97.6 microstrain agrees with the figure of 99.1 microstrain obtained by Scott [61] from tests on specimens reinforced by a single rod. In spite of a considerable range of results, particularly in the case of the 20 mm reinforcement, the strains at crack formation inside and outside the lap were similar, with overall averages of 95.0 and 99.5 microstrain respectively.

The concrete stress associated with these values of steel strain varied considerably, depending on the reinforcement percentage at the cracked section. Thus, whilst successive cracks generally formed at increasing values of steel strain, the value of concrete stress at crack formation could fall. The results agreed with Neville's [41] comment that it is a limiting tensile strain, rather than tensile stress, that determines the strength of concrete under static loading.

Longitudinal splitting cracks developed in some of the specimens at higher load stages. These cracks were associated with high bond stresses, their presence being a clear sign of bond distress. The cracks tended to be found at peaks in the bond stress distribution, either at the lap end or adjacent to a transverse crack.

Longitudinal cracks occasionally formed outside the lap, with these cracks being peculiar to those specimens reinforced by 20 mm rods. The cracks extended to a maximum length of approximately 60 mm by the highest load stage. It was interesting to note that these splitting cracks generally formed on the B and D faces (Figure 4.1), and therefore not on the face with the least cover. Longitudinal cracking resulted in a flattening of the reinforcement strains at the crack position. This indicated a greater length of gross bond deterioration adjacent to the transverse crack. Although the immediate consequence of splitting was a slight fall in the bond stress, as further load was applied the peak bond stress continued to rise.

Splitting cracks are generally associated with deformed reinforcement [11]. It was therefore intriguing to note the development of longitudinal cracks, near a transverse crack, over the plain mild steel corner bars which were used to locate the links in specimen 250T20/20(L). The splitting only occurred at one location, out of the strain gauged zone. This may have been a feature of the small (12 mm) cover above these bars. Alternatively, the bars may have created a plane of weakness along which splitting cracks associated with the 20 mm reinforcement chose to develop.

The development of a longitudinal crack at the end of the lap (rod B, specimen 750T20/20) had a marked effect on the strain distribution, as may be seen in Figure 6.6. Splitting extended over a length of approximately 70 mm, between two transverse cracks, on face A of the concrete, the face with minimum cover and the nearest to the bar with the higher bond stress. The crack resulted in an increased linearity of the strains, and a sudden fall in the bond stresses at the lap end. Thereafter, in spite of an increase in the applied load, the bond stresses remained stable.

Although the formation of longitudinal cracks did not always result in failure of the specimen, failure was always associated with the rapid propagation of splitting over the lap length on the A and C faces of the concrete. On one occasion, a specimen (250T20/20(E)) failed whilst the strain gauges were being scanned. Successive gauges showed typical pre- and post-failure values. This demonstrated that failure occurred in less than $\frac{1}{8}^{\text{th}}$ second, the time taken to record two strain readings. The explosive nature of failure resulted in substantial pieces of concrete being thrown from the specimen, although the presence of secondary reinforcement helped to contain this spalling. Photographs of the failed specimens (Figures 6.7.1 – 6.7.3) illustrate the longitudinal cracks. It is clear from these photographs that failure was confined to a region delimited by the transverse cracks at the lap ends.

The ultimate strain distribution over the lap length has been plotted in Figures 6.8.1 – 6.8.6. These diagrams include the results from specimen 250T12/20(A) which, although it did not fail, was believed to have been loaded to near capacity. On occasion failure coincided with the development of transverse cracks at the lap ends, and the final strain distribution was not recorded. Unfortunately, this occurred with the three specimens comprising bars of 12 mm diameter which failed, and thus no detailed information regarding ultimate strains was available for these tests.

It was clear from the strain measurements that the distribution over the lap length became increasingly linear as failure was approached. This was partly due to the dominating effects of the cracks at the lap ends. It was intriguing that cracks which had formed within the lap length had such little effect at high loads. The results suggested that bond stresses were being carried across the cracks within the lap, which would seem unlikely. It is more probable that, due to the severe bond breakdown adjacent to each crack, the reinforcement was unaffected by the concrete. The distribution would therefore be defined by the different levels of steel strain found to either side of the crack, rather than by the bond stresses.

The overall impression of the ultimate strain distributions was one of linearity (Figures 6.8.1 – 6.8.6). Such behaviour was consistent with the findings of previous researchers [11]. It should, however, be noted that the detail provided by these measurements showed that variations in the strain gradient still existed at failure. This will be discussed further in section 6.3.2.

The capacities of the lap joints in the specimens were compared to values predicted using equations developed by Orangun, Jirsa and Breen [30] (equation 2.2) and by Reynolds [31] (equation 2.6). The former has been put forward for the American Concrete Institute design recommendations. The latter has been used as the basis for the most recent British Standard (BS8110:1985) [46].

A comparison of measured and predicted ultimate loads has been made in Figure 6.9. The test results were generally lower than anticipated, due, in part, to the effect of crack-induced bending on the reinforcement strains. The true force carried by the steel was higher than was indicated by the applied load. This, combined with the varying capacities of specimens of nominally the same dimensions, made comparison difficult. However, some trends were clearly apparent.

The specimens which failed did not meet the requirements of BS8110, with the 20 mm rods not even being able to develop their yield stress. From the standpoint of ductility, not one of the lap lengths used here was satisfactory as failure was invariably both sudden and violent. The longer laps were able to carry a greater load, with the longest (750 mm) laps showing an ability to sustain a splitting crack within the lap length. The strength of a lap is often, usually implicitly, considered to be proportional to its length. This was not indicated by these results, and only the proposals for the American code [30] reflect such behaviour. However, making allowance for such non-proportionality renders equation 2.2 susceptible to errors, as it implies that a zero lap length can transfer force.

These tests clearly demonstrated that lap joints comprising a pair of 12 mm diameter bars failed at a lower load. The change in the cover/bar diameter ratio of the specimens resulted in Reynolds predicting the capacity of the 12 mm laps to be slightly higher than the 20 mm lapped bars. This was not borne out by the measured maximum loads. A lower ultimate bond stress was observed in the larger rods, which may have been due to the slight decrease in cover. The failure load of the mixed laps showed the smaller of the lapped bars to be the more relevant.

The values of ultimate load over-emphasise the benefits to be gained from using secondary reinforcement. Much of the apparent 45% increase in capacity may be attributed to the additional 40% in steel area provided by the mild steel corner bars which held the links in position. The assistance of these rods in carrying load

across transverse cracks resulted in a high maximum load. However, the ultimate bond stress was comparable to specimens without links. The British code, in agreement with numerous researchers [11], suggests a more marked improvement. It would, however, be foolhardy to even attempt to draw conclusions on the basis of this single result.

It is common for the value of the failure load to be based on a figure for ultimate bond stress. A comparison of the average bond stress along the lap joint at failure with the design proposals put forward by Orangun, Jirsa and Breen [30] and by Reynolds [31] was also undertaken. This will be discussed in section 6.3.2.

6.2 Steel Strain Distribution

6.2.1 Precrack strain distribution

In the early stages of the test, before cracks formed, two regions of constant strain generally existed in each rod, one inside and one, at a slightly higher level, outside the lap joint. Although the presence of links, or embedment gauges, in the specimen often created small, localised peaks in the distribution, the overall pattern remained unchanged.

The regions of constant strain were delimited by considering the rate of change of the strain gradient, a similar technique to that used to define zones of constant bond stress (see §5.2.4). The strain readings were averaged over a length in which the second derivative of the spline function remained below 0.01. This figure was chosen so that the lengths defined by the computer were similar to those previously defined visually. An average value for the reinforcement strain inside and outside the lap joint was thus determined for every rod. The difference between these two values was most pronounced at high precrack loads, and for larger bars. This suggested that the change in levels might be attributed to the variation in the reinforcement percentage along the specimen.

In order to examine the influence of the change in steel area along the specimen, an equation for estimating the reinforcement strains was developed. Balancing the applied force with the stresses within the specimen gives:

$$F_o = A_s f_s + A_c f_c \tag{6.1}$$

Assuming a compatibility of strains across the section, and elastic behaviour, this

equation may be rearranged to give an expression for the steel strain:

$$\epsilon_s = \frac{F_o}{E_s A_s} \frac{(m\rho)}{(1+m\rho)} \tag{6.2}$$

where:

ϵ_s	=	Reinforcement strain.
F_o	=	Applied force.
m	=	Ratio of the elastic modulii ($\frac{E_s}{E_c}$).
ρ	=	Reinforcement percentage ($\frac{A_s}{A_c}$).

The assumption of strain compatibility was valid as long as the bond between the steel and the concrete remained unimpaired. Although the strains varied across the section, due to bending in the specimen, the average value determined by the Demec gauge was similar to that measured in the reinforcement. This may be seen in Figure 6.10, in which the average reinforcement and concrete strains along the specimens are compared. A least squares analysis of the data showed the Demec readings to be slightly higher, with the equation of the line of best fit being:

$$\epsilon_{c_{ave}} = 1.04\,\epsilon_{s_{ave}} + 6.0 \tag{6.3}$$

where:

$$16.0 \leq \epsilon_{s_{ave}} \leq 91.0.$$

These results confirmed that it was reasonable to assume equal steel and concrete strains within the specimen at low loads.

The modulus of elasticity of the concrete was not measured. The traditional figure taken in short term tests for the modular ratio (m) is 7.5, and this value was used in the calculations. Thus the assumed Young's modulus of the concrete (E_c) was 27.6 kN/mm^2. The mean value of E_c quoted in BS8110:pt.2:1985 [7] (Table 7.2) for concretes with a characteristic compressive strength of 40 N/mm^2 is 28.0 kN/mm^2, with the typical range of results being ± 6.0 kN/mm^2 about the mean. Such a range might result in a variation in the predicted strains of up to $\pm 20\%$ about the mean, for specimens with nominal dimensions. However, it has a much smaller effect on the ratio of the strain levels in/out of the lap joint. The absolute variation about the mean of this ratio is below 0.02. The elastic modulus of concrete is partly dependent upon the modulus of the aggregate [41]. It is probable that as the same aggregate was used throughout the test series, the range of E_c in these specimens, and the subsequent effect on the predicted strains, was considerably smaller than the previous figures suggest.

The theoretical and measured reinforcement strains were initially compared on the basis of the ratio of the mean strain inside/outside the lap joint. The

breakdown in bond at the ends of the specimen meant that, on occasion, there was too short a length to average the strains out of the lap region with confidence. This resulted in the values from the two 750 mm laps (750T12/12 and 750T20/20) and from rod B in the first of the long term specimens (125D12/12) being excluded from the comparison.

The theoretical ratio of strains in/out of the lap, for specimens with nominal dimensions, were 0.95 for a pair of 12 mm bars, 0.86 for 20 mm rods and either 0.96 or 0.84 in a mixed lap. The predicted figure varied slightly, according to the true specimen dimensions. The measured ratio was generally within 5% of the prediction, and the difference between the two values did not exceed 11%. The measured value remained stable throughout the precrack load range, thus as the load increased the difference in the strain levels became more apparent. These results indicated that the reduction in steel strain within the lap region is a function of the change in the reinforcement percentage.

A plot of the measured strains in the reinforcement against those derived using equation 6.2 is shown in Figure 6.11. The two values agreed until approximately 40 microstrain. Beyond this figure the experimental reinforcement strains became increasingly greater than the predicted figure. The pattern was similar for the two bar sizes, and for the strains inside and outside the lap joint. An improved agreement between the two values was noted when a similar analysis was carried out using a lower value for the concrete's modulus of elasticity (taking E_c to be 24.0 kN/mm^2). Nevertheless, the tendency of the measurements to be greater than predicted at higher strain levels was maintained. Such an effect would be anticipated if microcracking occurred in the concrete, which implied a gradual breakdown in the applicability of equation 6.2. However, the results showed that a reasonable estimate of the strains in the reinforcement may be made on the basis of strain compatibility across the specimen.

A sharp fall from the average strain level was observed at the lap ends, with the concentration gauge results confirming that zero strain existed at the free ends of the reinforcing bars (Figure 6.3). The detail provided by the strain measurements enabled the estimation of the length of the transition from zero to the average strain level. A value of zero strain was assumed at the lap end in order to be able to fit a curve, using a cubic spline approximation technique, over the entire end region, and thus gain maximum information from this exercise.

The distance at which the rod carried a certain percentage of the average strain was derived from the fitted curve. At the lowest load stages, when dealing with strains of below 20 microstrain, there was a considerable scatter of results. At

the highest precrack load levels the development of localised peaks in the strain distribution, and the consequent variation in strains along the lap length, made it difficult to estimate the relevant distance. The results from the lowest and the highest precrack load levels were therefore atypical of the trend, and were excluded from the subsequent analysis. Small variations from the mean strain level also influenced the estimate of the distance to 90 and 100% this value, and consequently these figures have not been presented. The distance required to develop up to 80% of the average strain within the lap could be confidently pin-pointed, with consistent results being obtained. A plot of some typical results (Figure 6.12) shows that this distance remained constant for a given rod, irrespective of the applied load. The bond stresses were therefore continually increasing at the lap end. No upper limit to this behaviour was observed within the precrack load range.

The consistent nature of the results enabled the distances estimated at the different strain levels to be averaged. The results thus obtained were subsequently ignored if their standard deviation exceeded an arbitrary 5 mm. This occurred in two specimens in which localised strain peaks developed early in the test: the first, 250T20/20(L) rod A, due to the presence of links and the second, 250T20/20(E) rod A, due to the disturbance caused by embedment gauges. The failure of a gauge at the tip of the lap in specimen 500T12/12, rod B, created difficulties for the curve fitting procedures, as did the encroachment of the debond zone into the lap end in specimen 750T12/12, rod A. The analysis of these two specimens also yielded atypical figures. The results from the remaining thirteen specimens (twenty-six bars) are plotted in Figure 6.13.

Although some scatter was apparent, the general pattern was unaffected by lap length, the position of the rod, whether the end of the internal groove was closed or open, or by the diameter of the continuing rod. Thus a 12 or 20 mm rod in a mixed lap behaved similarly to its counterpart in a lap joint comprising bars of equal diameter. This suggested that the distance over which strains were developed was not related to the continuing rod. Curves fitted through the mean of the points for the 12 and 20 mm bars demonstrated that a greater length of bar was involved in force transfer in the larger rod.

The ratio between the average value for the 12 and 20 mm bars varied slightly over the percentage range, but typically lay between 0.63 and 0.73[†], with the average ratio being 0.67. The ratio of the bar diameters was 0.6, and the results demonstrated that the length over which force was transferred was a function of bar

[†] A value of 0.9 and 0.78 was recorded at 10 and 20% of the average strain respectively. However, the distances involved here were so small that these ratios were unlikely to be representative.

diameter. It is not possible to be more specific as many of the bond characteristics of Torbar, such as bar perimeter, rib spacing and rib dimensions, are themselves a function of bar diameter [62]. Both bar sizes developed 60% of the average strain within one bar diameter of the lap end, and approximately 80% within two diameters.

The curvature of the strain distribution at the ends of the lap joints in the transition from zero to the average strain level (Figure 6.13) corresponded to variations in the bond stress. The concentration gauges showed the strain distribution to be sensibly linear over the last 10 mm of the reinforcing bars (Figure 6.3). On the basis of the average strain distributions plotted in Figure 6.13, maximum bond stresses of 3.4 and 2.6 N/mm^2 were developed in the 12 and 20 mm rods respectively.

6.2.2 Transverse cracks and postcrack strain distribution

It has already been noted that plateaux of constant steel strain were found along the specimen before crack formation. The form of the concrete stress distribution was similar to that of the reinforcement strain, in that regions of constant stress existed to either side of the lap. The steel strain distributions shown in Figure 6.4 have been replotted in terms of concrete stress, Figure 6.14. A slight peak in the distribution was noted at the tip of the laps where, although there was a reduction in concrete area, most of the strain was being carried by a single rod. In those specimens reinforced by bars of differing diameter, the stress increased along the lap joint due to the larger value of concrete stress associated with the smaller bar. At the ends of the specimen, in the debonding zone, the concrete stresses were low.

The initial cracks generally formed outside the lap joint, where both the steel and the concrete strains were higher. It was unusual for the first crack to appear at a lap end, in spite of the localised peak concrete stresses found here.

In general, the cracks propagated very rapidly across the concrete section, resulting in a sudden jump in the strain levels at the crack position (Figure 6.5). On occasion, however, a slight peak developed in the reinforcement strains before the crack reached the surface of the concrete. The effect is illustrated in Figure 6.15. The growth of such a peak was suggestive of a crack developing within the specimen. There was no evidence from the rod area calculations that the peaks were due to a local reduction in reinforcement cross-sectional area. The presence of a localised peak could be attributed to any one, or a combination, of possibilities. The crack might be initiated at the bar surface due to localised flaws such as tie

wires or poor compaction. Alternatively, the crack could be caused by the linking of a system of microcracks at the aggregate/cement interface or by irregularities within the specimen such as embedment gauges or links. A further consequence of the links would be a reduction in the concrete area, and therefore a higher localised concrete stress. The results from the specimens including links showed their crack inducing properties, with lower loads and strains being recorded at crack formation (Figure 6.5).

The formation of transverse cracks considerably modified the steel strain distribution. The strains peaked at a crack, where the reinforcement carried most of the load, and fell to either side of this position. Consequently, as cracks developed along the specimen, the zones of constant strain shortened, and the distribution became a succession of peaks and troughs (Figure 6.1.1 – 6.1.15). The maximum values of concrete stress coincided with the troughs in the reinforcement strain distribution. Later cracks tended to form at these well defined positions.

Successive cracks usually developed midway between existing cracks, provided the steel strains at the adjacent cracks were similar. This was the system of crack formation suggested by Tepfers[51]. However, if the neighbouring cracks exhibited very different strains, for instance if one was inside and the other outside the lap, then the trough, and hence the next crack, tended to be formed away from the midpoints.

Other influences, such as the discontinuity in the specimen at the lap ends, or the weaknesses in the section introduced by using embedment gauges or links, also served to define the crack positions. Specimens which included such crack inducers exhibited the greatest number of transverse cracks. The number of primary cracks observed in each specimen, and the associated crack spacings, are tabled in Figure 6.16.

According to Beeby[63], the mean crack spacing in axially reinforced tension members may be predicted by an equation of the form:

$$S_{ave} = k_1 c_{min} + k_2 \frac{\phi}{\rho} \tag{6.4}$$

where:

S_{ave}	=	Average crack spacing.
c_{min}	=	Minimum cover.
ϕ	=	Diameter of steel reinforcement.
ρ	=	Reinforcement percentage.
k_1, k_2	=	Constants.

The first component of this equation reflects the distance required for the transition from zero concrete stress at a crack to the general level of stress. This is considered to be proportional to cover. The second component was concerned with the ratio of the concrete area under tensile stress to the bar perimeter. This assesses the contribution of the bond stress found to either side of a crack. The combination of these two effects served to explain the greater number of cracks, and the smaller crack spacing, observed in specimens reinforced by 20 mm rods.

One implication of the equation was that a smaller crack spacing should be observed within the lap joint, because of the increased reinforcement percentage in this area. An average ratio of 0.8 (standard deviation 0.2) was calculated for the crack spacing inside/outside the lap. However, for the purpose of the crack spacing calculations the ends of the specimen were considered to be equivalent to cracks. It was generally the case that the greatest crack spacing was found here, in the initial debond zone, and this may have exacerbated the difference between crack spacing in and out of the lap. The true ratio may have been nearer unity.

A considerable variation in the spacing of cracks within each specimen was noted, and figures for the maximum and minimum observed crack spacings are included in Figure 6.16. A commonly quoted value for the ratio between maximum and minimum spacing is 2.0 [60,64]. A greater variability of crack spacing in axial specimens has been noted by Beeby [65]. Thus, the mean ratio of 2.5 observed in these tests did not seem unduly high.

As the reinforcement carried the entire load across the transverse cracks, the peak strains would be expected to correlate with those measured by the strain gauges out of the concrete. The value of load carried by the steel, as determined from the strain measurements, was generally between 10 and 30% higher than the applied load. This was mainly due to crack induced bending, but the slight variations in rod area may have exacerbated the effect. Typical relationships between the applied and the measured load at a crack are shown in Figure 6.17. The comparison was not attempted for steel strains of over 2500 microstrain, when gross yield of the reinforcement occurred. It may be seen that the ratio between these two loads remained stable as the test progressed and the applied load increased.

It was interesting to note that in the 20 mm rods, in the case of those cracks which formed at low strains, the steel initially carried less than the applied load. This was consistent with the gentle nature of crack formation in these specimens, which suggested that the crack had not fully developed. At some higher load these cracks suddenly opened fully, often propagating around the entire specimen.

Thereafter, the characteristic pattern of a higher than anticipated stress in the steel emerged.

Figure 6.17 also includes a similar comparison carried out for the troughs in the distribution. In this case, the ratio between the apparent load in the steel and the applied load rose as the test progressed. This culminated in the entire load apparently being carried by the reinforcement at the higher load levels. The implication was that as the load increased there was a corresponding reduction in the stress carried by the concrete, which might have been expected as microcracks formed. Similar behaviour was observed for both bar sizes. The situation was analagous to that described by Tepfers[51] for an infinite reinforcement percentage, in which the concrete acted as an adhesive, yet carried no tensile force.

Changes in strain distribution along the specimen were noted when the load was maintained over a period of time. The effect was measured in all the specimens as the Demec readings were being taken, which took approximately fifteen minutes. Creep of the concrete led to a slight equalisation of the bond stresses between the cracks, and to a noticeable increase in the strain values at the troughs. Such behaviour is apparent in Figure 6.17.

The long term tests were carried out to ascertain the influence of sustained loads on the strain distribution. Only one of these specimens (125D12/12(L)) provided information on the postcrack strains. The other was concerned with the precrack behaviour, and the only effect of time was the encroachment of the debond zone into the specimen.

The change in the value of strains at the peaks and the troughs over a period of time is illustrated in Figure 6.18. It was clear that the greatest change occurred in the initial stages of the test, over approximately the first week. A rise in the strains throughout the specimen was noted, which may have been symptomatic of the cracks developing to their fullest extent. Thereafter the peak values remained relatively stable, with the sole exception being the sudden rise observed at one position after 43 days. This was due to the crack extending around the specimen, for no obvious reason. The troughs, however, continued to change, albeit at a slower rate. It was unfortunate that the failure of the Dartec rig precluded the continuation of this test. A problem of this test rig was the tendency of an electrical spike to activate the trips, resulting in total loss of load. This occurred on a number of occasions during the test. On reloading, the specimen re-adopted its previous strain distribution. However, tripping of the Dartec appeared to affect specimen behaviour, as the values of strain found at the troughs in the distribution often changed more rapidly for a few days after the specimen had been reloaded.

It was clear that in both the short- and the long-term specimens the difference between the peaks and the troughs in the strain distribution became less pronounced as the tests progressed. It has already been commented that, as this occurred, the situation in the specimen became analogous to that described by Tepfers [51] for an infinite reinforcement percentage. The measured strain distributions were therefore compared to those predicted using Tepfers' simplified equations (2.12 – 2.14). The equations were produced for bars of similar diameter, and consequently no comparison could be made for the mixed laps.

In order to determine an appropriate value for the modulus of displacement (K_d), an attempt was made to establish the bond stress/slip relationship for these specimens. The results from the calculations were disappointing, with the considerable scatter of the results making it difficult to fit a straight line with confidence. K_d was therefore chosen to be 100.0 N/mm^3, which lay in the centre of the range suggested by Tepfers. It may be seen from Figure 6.19, in which the bond stress/slip relationship has been plotted, that such a value for K_d was not unreasonable. Typical results from the comparison of the predicted and the measured strain distributions are shown in Figure 6.20.

At low loads Tepfers' equations overestimated the strains, as the contribution of the concrete in carrying tensile force was neglected. In general, the predicted and measured strains compared most favourably once a close crack spacing had developed, by which stage the concrete played a minor role. The assumption of an infinite reinforcement percentage resulted in the absence of troughs in the predicted distribution but, according to Tepfers [51], this would result in a maximum error of 5%. The theory also makes no allowance for the severe bond breakdown found adjacent to the transverse cracks.

Tepfers' analysis was based on a lap joint with cracks at both ends, and the predicted curves naturally compared better when this was the case. In those specimens which had few cracks within the lap length, or in which the strains in the continuing rod were unaffected by cracks at the lap ends, Tepfers' analysis did not apply. The influence of bending in the test specimens, which caused higher strains than predicted at the cracks, caused further discrepancies. The plots (Fig. 6.20) compare the measured and analytical values for linked specimens, in which the peak strains were comparable to those anticipated on the basis of the applied load. It is clear from these diagrams that a close correlation existed between the theoretical and the actual distributions.

In spite of its limitations as a means of precisely describing the strain distribution, Tepfers' analysis was able to describe the peak strains which might be

expected at the crack position in the individual rods. In the load range between the formation of transverse cracks and the development of longitudinal splitting cracks the equations provide a valuable means of estimating the strains along a lap joint.

6.3 Bond Stresses

6.3.1 Bond stress distribution

It has already been noted that before crack formation the strain gradient, and hence bond stress, was negligible over much of the specimen. Bond stresses only existed at the ends of the specimen, where the steel bars entered the concrete, and at the tip of the lap joint, where the strains fell sharply to zero. The bond stress distribution became more pronounced as cracks developed in the specimen.

The bond stresses on each side of a crack were usually of the same order, with their magnitude being significantly influenced by the value of the peak rod stress at the crack. This is apparent from Figure 6.21, which tables both the rod stress at the crack following its formation and the bond stresses observed to either side of this position. Bond stresses were not calculated for rod stresses exceeding 310 N/mm^2, above which the steel stress/strain relationship became non-linear. The italicised figures in the table refer to those cracks which were unduly influenced either by the lap end or by neighbouring cracks. The former resulted in an artificial rise in the bond stress, due to the strain having to decrease to zero at the free end of the bar and the lap end thus defining the length over which the bond stresses could act. The latter led to a reduction in the bond stresses, due to the deterioration of the concrete which existed in the proximity of previous cracks.

A typical bond stress distribution around a crack was shown in Figure 6.2. There was a complete breakdown in bond at the crack position, and peak bond stresses were observed adjacent to the crack. A region of constant bond stress was apparent to either side of the crack, represented by the linear distribution of steel strains. On the few occasions when this region of constant bond stress crossed the end of the lap, a situation which could only occur in the continuing rod, the bond stress remained unchanged. The bond stress decreased as the trough in the steel strain distribution was approached.

The peak bond stress was compared to the average value determined over the length from the peak to the trough in the steel strain distribution. The comparison was made for all the bond stresses listed in Figure 6.21. The results were therefore independent of crack position. A clear relationship between the peak and the

average bond stress emerged, this is illustrated in Figure 6.22. The coefficient of correlation between these two stresses was 0.98†. A least squares regression analysis of the data yielded the following equation:

$$f_{bp} = 1.5\, f_{bave} + 0.02 \tag{6.5}$$

where:

$0.5 \leq f_{bave} \leq 4.6.$

f_{bp} = Peak bond stress adjacent to a crack.

f_{bave} = Average bond stress between peak and trough steel strains.

The peak was therefore typically 50% greater than the average value, with the standard deviation from the line of best fit being 0.6 N/mm^2. The relationship was clearest at lower bond stresses, with the distribution tending away from the line represented by equation 6.5 at higher values of bond stress.

It was noted in section 6.2.2 that the ratio between the steel strains at the troughs and the peaks in the distribution increased as the load was applied. Assuming that the distance between the peaks and the troughs remained constant, which was generally the case, then the following equations relate the average bond stress to the peak rod stress:

$$\frac{f_{bs}}{f_{sp}} = \frac{A_s}{u\, dx}\left(\frac{f_{sp} - f_{st}}{f_{sp}}\right) \tag{6.6}$$

Rearranging this equation gives:

$$\frac{f_{bs}}{f_{sp}} = K_{pt}\left(1 - \frac{f_{st}}{f_{sp}}\right) \tag{6.7}$$

where:

f_{sp} = Peak reinforcement stress.

f_{st} = Trough reinforcement stress.

K_{pt} = Constant.

Thus, an increase in the ratio between f_{st} and f_{sp}, corresponded to a decrease in the average bond stress/rod stress ratio. The relationship between the latter would seem to vary according to the ability of the concrete to sustain the high stresses associated with the troughs in the reinforcement strain distribution.

As the peak and the average bond stresses next to a crack were related (equation 6.5), similar behaviour would be anticipated when comparing the peak bond

† The coefficient of correlation measures the degree of linear association between two variables. A value of +1 represents perfect positive correlation, -1 represents perfect negative correlation and 0 represents no correlation.

stress to rod stress. The relationships for the two bar diameters are plotted in Figure 6.23. Those results considered to be influenced by the presence of neighbouring cracks, or the lap end, have been excluded. It was not uncommon for the bond stresses found to either side of the crack to differ slightly, which led to two distinct bands of results for each crack. Although the figures showed considerable scatter, a consistent trend was apparent.

In the first instance, an almost linear relationship existed between the two stresses. However, at higher rod stresses the relationship became increasingly curved. The two bar sizes exhibited similar behaviour. The figures determined for the individual bars in a mixed lap were the same as their counterparts in the other specimens. There was also no difference in the behaviour at cracks inside and outside the lap joint.

A quadratic was fitted to both sets of data, using the method of least squares. The ratio of the values for the 12 and 20 mm rods varied slightly, according to position along the curve, but was approximately 0.62. This confirmed that the results were proportional to bar perimeter, as might be expected from the equation for bond stress (equation 5.2). The results were consistent with the findings reported by Snowdon [66] following his extensive survey of the bond behaviour of a variety of reinforcing bars.

The non-linearity of the bond stress/rod stress relationship was indicative of a breakdown in the peak bond stresses found at higher rod stresses. This may have been a sign of the concrete's inability to develop a greater stress, possibly due to the development of microcracks within the material. The increased plasticity associated with microcracking would result in the peak bond stress being carried by a greater length of rod. This would cause an apparent reduction in the peak bond stress/rod stress ratio. The flattening of the curves could also be attributed to the changing relationship between the peak and the trough reinforcement strains.

The bond stress/rod stress relationship has been considered for cracks which formed in isolation. This provided an understanding of the bond stress distribution around a single crack. However, it was evident from the strain measurements that there was some interaction between neighbouring cracks. It is consequently of interest to gain an understanding of the influence lengths of the individual cracks, as represented by the distance required to transfer the stresses from the reinforcement into the concrete. The influence lengths of cracks which formed in isolation, and of the ends of the specimen, were estimated from the bond stress results.

The situation at the ends of the specimen, just beyond the limits of the concrete, in many respects resembled that at a crack. The entire load was carried by the steel reinforcement, and bond stresses developed in the area. This zone of bond breakdown thus illustrated the behaviour of the bond influence length in the absence of further cracks.

The results from the long term tests, in which the full length of the specimen was gauged, are shown in Figure 6.24. These figures were typical of the tension specimens, and although there was a considerable scatter of results, a consistent pattern of behaviour was displayed by the individual rods. The most rapid breakdown in bond occurred in the early stages of the test. This was followed by a sporadic lengthening of the debond zone, and a gradual rise in the average bond stress over this length. Maintaining the load over a period of time led to an increased length of bond breakdown, this corresponding to a reduction in the mean bond stress.

It is clear from Figure 6.24 that the rate at which the bond influence length extended was dependent on the level of the peak rod stress. Cracking of the specimen raised the rod stresses to such a level that much of the influence length was developed at crack formation. Consequently, the effect of an increase in applied load was less apparent thereafter, as may be seen in Figure 6.1.1. This figure shows the slight extension of the influence lengths in specimen 125T12/12 as the load rose from 23 to 32 kN. The results from specimen 125D12/12 demonstrated that the length of bond breakdown also increased when the load was sustained over a period of time. The rate of change of the influence length decreased as the test progressed, with time taken for incremental extensions of 12.5 mm being approximately 1, 7 and 53 days.

The influence lengths did not appear to differ inside and outside the lap, although the different peak stresses associated with these regions might be expected to have a slight effect. The diameter of the reinforcing bars and cover dimensions appeared to be more significant. An equation relating the bond influence length (B) to the concrete cover (c), making allowance for bar diameter (ϕ), was proposed by Scott [61] for specimens reinforced by Torbar:

$$\frac{B}{\phi} = 4.45\,\frac{c}{\phi} - 4.14 \tag{6.8}$$

where:

$$2.0 \leq \tfrac{c}{\phi} \leq 16.0$$

An average value of the concrete cover (40 and 44 mm, out of the lap) gives an influence length of 95 and 146 for the 20 and 12 mm bars respectively, with

the ratio between the two being 0.65. Excluding the results from the mixed laps, the corresponding figures determined from these tests were 108, 170 and a ratio of 0.63. The predicted and measured ratios between the two bar sizes showed excellent agreement. The consistently higher values observed in these specimens may be due, in part, to the different methods used to establish the influence length.

The influence length generally exceeded the closest crack spacing. Consequently, once a number of cracks had formed, the bond influence length became increasingly insignificant, and the bond stress distribution was predominantly influenced by the position of the cracks. As these became closer spaced, the gross breakdown in bond adjacent to each crack resulted in lower bond stresses between the cracks. Peak bond stresses were observed at the lap end and adjacent to those cracks which remained unaffected by their neighbours.

The value of the bond stress at the free end of the bars depended on the proximity of the nearest crack. If this was distant then the stresses could remain relatively stable as load was applied, with only small changes being observed as the test progressed. However, if the peak rod stress at a neighbouring crack increased, then the bond stress would also rise. The peak bond stresses along the specimen are discussed more fully in the next section, which deals with the ultimate behaviour of the lap joints.

6.3.2 Ultimate bond stresses

The ultimate steel strain distribution is generally considered to be linear and, by implication, the ultimate bond stress is assumed to be uniform over the lap length. The detail provided by the strain measurements (Figure 6.8) showed that variations still existed in the bond stress at failure.

The variation in bond stress along the lap length was assessed by determining the mean and the coefficient of variation of the distribution for each rod. These values are tabled in Figure 6.25 for the highest load stages. In general, the coefficient of variation was lowest for those specimens which failed. The exception to the rule was specimen 250T12/20(A), but this specimen was believed to have been close to failure. Similar calculations were undertaken for the lower load levels. These showed a reduction in the coefficient of variation of the bond stress as the applied load was raised. Increased microcracking of the concrete at the higher loads may help to distribute the effect of the peak bond stresses, thus increasing the linearity of the strain distribution. The magnitude of the coefficient of variation was such that it warranted the consideration of peak bond stresses when dealing with ultimate behaviour.

Peak bond stresses were located either next to a transverse crack or at the lap end. It has already been noted that longitudinal cracks are associated with high bond stresses, and that the rapid growth of such cracks often resulted in failure of the lap joints. It is therefore of interest to consider the level of bond stress which results in splitting of the concrete cover. The values of this bond stress (f_{bc}) were normalised with respect to the tensile strength of the concrete (f_{ct}) in order to be consistent with Tepfers [44]. They are referred to in terms of 'f_{ct}'.

In general, longitudinal cracks formed at bond stresses within the range 1.8 – 2.7 f_{ct} N/mm^2. The sole exception was the atypically high bond stress of 5.1 f_{ct} N/mm^2 observed at one lap end in specimen 250T20/20. With the exclusion of this figure, the ten longitudinal cracks which developed in specimens reinforced by a pair of 20 mm rods formed at an average value of 2.3 f_{ct} N/mm^2, with a standard deviation of 0.3 f_{ct} N/mm^2. The measured values of bond stress which led to splitting of the concrete cover were therefore within the range 1.2 – 3.0 f_{ct} N/mm^2 derived from Tepfers' equations for a single bar (equations 2.4 and 2.5). The lower of these values referred to a partly-cracked elastic section, the higher to a fully plastified section. It should, however, be noted that the bond stresses at the lap ends occasionally far exceeded the upper limit proposed by Tepfers, one being the value already noted at the end of specimen 250T20/20. This resulted in failure, but other specimens, notably 750T12/12 with a peak stress of 7.7 f_{ct} N/mm^2, developed high bond stresses at the lap end with no apparent distress.

Tepfers' [44] suggested that the figures from his equations should be halved when dealing with lap joints, his argument being that the bursting forces around a lap joint was double that around a single bar. This clearly is unnecessary, and the results therefore suggest that the total bursting force around a lap joint is similar to that around a single bar. There was no significant difference in the bond stress at which the cover cracked inside and outside the lap joint. The results thus agreed with the conclusions of Orangun, Jirsa and Breen [30], who equated lap and anchorage lengths.

The development of a splitting crack within the lap length generally resulted in failure. Only one specimen (750T20/20) was able to sustain a longitudinal crack within the lap, and in this case the central portion of the lap remained unaffected by either the longitudinal splitting or the tranverse cracks which formed at each end of the joint. A zone of negligible bond stress thus existed over much of the lap. In two of the shorter laps (specimens 250T20/20(L) and 500T20/20), the bond stress rose at the tip of the lap in the few load stages immediately prior to failure. Since the stresses at the lap ends had previously been stable, it may be

that the effects of the dominant transverse cracks were only just reaching the free end of the rods. Consequently, by the time the peak bond stresses were sufficient to initiate splitting, the entire lap length was being used to transfer force. The specimens were therefore unable to resist the propagation of the splitting cracks, resulting in the characteristic 'zipper' mode of failure.

The results from these tests suggested that the ability to withstand the effect of splitting is dependent upon the nature of the bond stress distribution over the entire lap. The average bond stress over the lap length is thus indicative of a lap's resistance to failure. It is therefore not unreasonable to use an average value of ultimate bond stress for design purposes.

The average bond stress was usually highest in those specimens which failed. With the exception of the mixed laps, the ultimate bond stress in the individual rods of a specimen were similar. The longitudinal cracks developed on the A and C faces, those nearest to the individual bars. This implied that failure was initiated by just one of the rods. Thus, the higher of the values determined for each bar in a specimen was more relevant than the mean of the two figures. There was, unfortunately, insufficient information to be able to compare the results from the two rod diameters. The readings from the mixed laps, in which the bond stress for the 12 mm bar was higher, were an indication that higher bond stresses were associated with the smaller reinforcement. Further evidence of such an association is provided in Figure 6.7.3, in which it is clear that the splitting crack which formed on the A face (the nearest to the 12 mm bar) was more severe than the one found on the C face.

It is common for the value of the failure load to be based on a figure for bond stress, the load being estimated by assuming a constant value of ultimate bond stress over the lap length. This is the approach favoured by BS8110[7]. The mean of the bond stresses calculated over the lap length, and the ultimate bond stress estimated on the basis of various design equations have been tabled in Figure 6.26.

The ultimate bond stresses proposed in the British code appear conservative, with the smallest of the measured values being some 30% higher than required. This would be further emphasised if the partial safety factor of 1.4 was included. The conservatism was partly due to deformed rods in specimens without links having to be treated as if they were plain reinforcement. A more comparable result was obtained by the specimen which included secondary reinforcement. The assumption of a value of unity for the cover/bar diameter ratio[46] resulted in the code requirements not reflecting the variations attributed to the changes in specimen dimensions.

Reynolds' work [31] formed the basis of the British Standard, and it is therefore not surprising to note that the test values were higher than his proposals. The latter were, in turn, based on Tepfers' analysis of the bond stress required to cause longitudinal cracking of the concrete cover [44]. Reynolds noted that his results lay within the range delimited by the values for a partly-cracked elastic and a plastic analysis (equations 2.4 and 2.5). It was therefore concluded that the former, the lower of these two values, could be used as a 'lower bound' for the bond stress which initiated failure. Although average values of bond stress were used by Reynolds, it would seem more appropriate to deal with the peak values which initiate the splitting cracks. It has been shown that the peak bond stresses measured in these test specimens lay well above the lower limit. Reynolds, by measuring average ultimate bond stresses , was consistent in his use of an average bond stress. It would seem to be implicit in this approach that some form of relationship existed between the peak and average values of bond stress. Although the detailed information provided by the strain measurements failed to show any correlation between the peak and the ultimate bond stress in these specimens, it has been noted that the average bond stress gives a useful indication of a lap's ability to resist failure. Consequently the average values produced by Reynolds are adequate for design purposes.

A favourable comparison was made with the results from Orangun, Jirsa and Breen's multi-variable analysis [30]. Their equation, based on the results from a number of sources, appears to reflect most accurately the results from these tests. However, once again, the beneficial effect of links was not apparent in these specimens.

Although this series of one-off tests was not geared towards the production of design recommendations, it was encouraging to note the agreement shown between the test results and existing design proposals. One point which can be made on the basis of the correlation of the results from axial specimens with equations based on four-point bending tests concerns the design of lap joints in tension tie members. The commentary to the A.C.I. design recommendations [9] notes that the lapping requirements for such members were initially made excessively severe because of the lack of specific research data. It would appear that such caution is unnecessary.

6.4 Embedment Gauge Results

Embedment gauges were cast in the final tension test specimen to measure the circumferential strains around the lap joint (Figure 4.4). The technique of casting

the gauges proved successful, with just a single gauge giving dubious results. The internal readings were complemented by electric resistance strain gauges mounted on the surface of the concrete. The measured circumferential strains, at representative load stages, are plotted in Figure 6.27.

Before cracks formed, a small compressive strain was shown by most gauges. This was due to the effect of the Poisson's ratio of the concrete. The influence of a tensile bursting force was, like the bond stress, negligible. The embedment gauges typically showed a higher tensile strain than the surface gauges, which was attributed to their being closer to the reinforcing bar. Similarly, variations in the distance from the reinforcement accounted for some of the differences in the strains measured by individual gauges. In general, however, the strains measured on all four faces of the specimen were consistent, and the influence of the lap joint was not apparent.

The crack-inducing properties of the embedment gauges have already been documented (see §6.1), and early cracks were observed at the gauge groups within and at the end of the lap. The strain readings subsequently appeared to be more affected by these cracks than by bursting forces, with the peak strains being observed on the uncracked face (face D, on both occasions). It seemed probable that some debonding of the embedment gauges occurred when a transverse crack ran along their length. As a consequence of the cracking, the gauges were of little assistance in establishing the strain distribution around a lap joint.

The effect of distance from the reinforcement remained apparent after crack formation. Within the lap, the ultimate mean of the strains measured by the embedment and surface gauges was 305 and 183 microstrain respectively, at an average distance of 20 and 35 mm. Assuming a Youngs' modulus for the concrete of 27.6 kN/mm^2, these circumferential strains corresponded to a bursting stress of 8.4 and 5.0 N/mm^2. The bond stress in both bars was approximately 5.4 N/mm^2. It is clear from Figure 2.1 that this (f_{bs}) may be related to the bursting stress (f_p):

$$f_p = f_{bs} \tan \alpha \tag{6.9}$$

The resulting values of α, 57° and 42°, corresponded to the typical figure quoted, 45° [31]. The higher strains measured near the bar was consistent with the concept of internal cracks developing near the reinforcement [60]. It was possible that the embedment gauges, to a limited extent, served to bridge these cracks. The internal gauges would have exaggerated the strains; greater credence may therefore be attached to the latter value. This bridging effect, combined with the ability of concrete to redistribute the peak stresses, enabled the bursting force to be considerably higher than the tensile strength of the material.

The measurements taken outside the lap joint consistently showed a compressive stress acting around the reinforcement. This was initially attributed to Poisson's effect. At the lowest load stages the circumferential and longitudinal stresses could be related by assuming a typical Poisson's ratio of 0.2 [7] for the concrete. As further load was applied, a greater proportion of the load was carried by the steel. A decrease in the circumferential strains, corresponding to the reduction in concrete stress, was anticipated. However, the circumferential strains became increasingly compressive. The bond stress remained consistently low, and the associated bursting force had no apparent effect on the distribution. It is possible that the phenomenon was a symptom of the transverse cracks releasing shrinkage stresses which had been locked into the concrete. There is, however, no evidence to support this suggestion.

The results from this single test were encouraging in that the technique of measuring the circumferential strains proved successful. It was unfortunate that the readings were dominated by the effect of cracking, and that it was not possible to gain more information about the strain distribution around the rods. It is suggested that should the test be repeated, a specimen with a greater cross-section be used. This would help to prevent the formation of transverse cracks, and would enable a greater number of embedment gauges to be cast within the specimen.

CHAPTER 7

COMPRESSION TEST RESULTS AND DISCUSSION

7.1 Compression Test Results

A fundamental difference between this series and the earlier tension tests was that none of the gauged compression specimens cracked or failed. Consequently the available information pertained to pre-crack behaviour, and no data concerning the ultimate behaviour of compression lap joints was acquired.

Some pilot compression tests were undertaken, loading four ungauged specimens up to the rig limit of 300 kN. Three of these specimens had a nominal concrete cross-section of 100 × 100 mm, the lap lengths being 125, 62 and 30 mm. Only the 62 mm lap failed, with an extremely violent failure occurring at 298 kN. The concrete cover split along the joint and transverse cracks, probably a consequence of bending, formed at the ends of the lap. It was not possible to determine the order of the cracks. Failure may therefore have been initiated either by excess bursting forces around the reinforcement or by bending forces in the specimen. The fourth test was carried out on a smaller 70 × 70 mm cross-section, using a 125 mm lap length. This failed explosively at 190 kN but, in this case, the failure was attributed to longitudinal cracks developing from the ends of the specimen, rather than to splitting over the lap region. This type of failure was prevented in subsequent tests by external links clamped to both ends of the specimens. The pilot tests indicated that compression failure could not be guaranteed by 300 kN. The gauged specimens were therefore chosen to be comparable to those used in the tension series.

The test measurements clearly showed the distribution of the reinforcement strains in the five compression specimens. The influence of bending was reduced by application of the cubic spline procedure (see §5.2.3) and the resulting distributions have been plotted in Figures 7.1.1 – 7.1.5.

In the early stages of the test the strain distributions were of a similar nature to those measured before crack formation in the tension specimens (see §6.1). Levels of almost constant strain existed inside and outside the lap joint, and a breakdown in the bond between the steel and the concrete was observed at the ends of the specimen. The two rods in each lap behaved similarly, which resulted in the distributions being symmetrical about the centre of the specimen.

Within the lap joint, the strains in each of the reinforcing bars tended to equalise as close to the ends of the lap as possible. The transfer of force was thus concentrated near the ends of the lap, resulting in steeper strain gradients at these positions. This was consistent with the findings of previous researchers[11]. As the applied load rose, a greater length of reinforcement was required to transfer force. Thus, the steeper strain gradients at the ends of the bars affected an increasing proportion of the joint, and the strain distribution along the lap became more linear.

It was clear from the strain measurements that the lengths of bond breakdown at the specimen ends were related to the applied load. However, the scatter of the results prevented any correlation of debond length and load. The encroachment of bond stresses into the specimen resulted in a shortening of the region of constant strain found outside the lap. The extreme situation, in which the debond zone reached the end of the lap joint before the maximum load of 300 kN, was noted in specimen 250C20/20(E). Localised peak strains observed at the end of these regions of bond breakdown were believed to have been a symptom of the damaged concrete found here.

The most significant difference between these tests and the earlier tension specimens was probably the presence of strains at the free ends of the reinforcing bars in the compression laps. These strains were due to the bearing of the steel against the concrete. It was evident from the rising value of strain measured at this position that end bearing played a significant role in the transfer of force between the rods. A comparison of the strains developed in individual bars showed the values at the ends of the 12 and the 20 mm rods to be similar. This consistent level of strain implied that the force transferred by end bearing was proportional to rod area. In general terms, approximately 20% of the peak steel strain found in these specimens was developed within the first 10 mm of the lap joint. A slightly reduced contribution was noted at the highest load stages, and the behaviour beyond 300 kN is therefore uncertain.

The strains developed at the lap end could be quite substantial. In one specimen (125C20/20) a peak strain of 370 microstrain was measured by the final concentration gauge element, 2 mm from the lap end. This corresponded to a stress of about 75 N/mm^2, and thus exceeded the ultimate uniaxial compressive stress of the concrete. The confinement of the surrounding cover, and of transverse reinforcement when this is provided, enables end bearing stresses of approximately three times the compressive strength of the concrete to be developed[11].

Peaks in the strain distribution also existed just beyond the ends of the lap joint, in the continuing rod. These peaks, being located at the end of lengths of bond breakdown, may be partly due to localised cracking of the concrete. They were probably also a consequence of the additional forces set up in the concrete by the end bearing of the terminating rod. In the 125 mm lap joints, these peaks were found up to six bar diameters beyond the tip of the lap. These specimens clearly showed that the length of reinforcement involved in force transfer was not limited by the lap length. Up to 20% of the steel strains were transferred outside the lap joint in specimen 125C20/20 at 300 kN. Such behaviour was consistent with that reported by Cairns and Arthur [27], who noted a transfer of force occurring between three and five bar diameters beyond the lap end. This is another way in which compression and tension laps differ; in the latter, transverse cracks at the ends of the joint delimit the transfer length.

7.2 Steel Strain Distribution

7.2.1 Comparison between loading methods

The load in the tension tests was applied through the steel reinforcement. If this loading arrangement was to be duplicated in the compression tests, then yield of the steel would severely limit the maximum load. In order to take advantage of the compression rig limit of 300 kN, the specimen had to be loaded through the concrete.

A comparison of the two loading methods was undertaken, with the first two compression specimens each being loaded twice:

i) 250C12/12(A): The steel was loaded to 25 kN, this value being chosen to prevent yield of the reinforcement. The specimen was subsequently reloaded to 300 kN through the concrete.

ii) 250C12/12(B): The specimen was initially loaded through the concrete, to 300 kN. The load was then re-applied through the steel, the maximum value of 65 kN being defined by gross yield of the bar outside the concrete.

The strain distributions along these two specimens are compared in Figure 7.2. In both cases the reinforcement strain at a given load was approximately 10% higher when the specimen was loaded through the steel. The results from the Demec readings indicated that the concrete strains were about 10% higher when the load was applied through the concrete. These generalisations were valid for both specimens, and were therefore unaffected by the loading history.

The difference in the strain distributions at the ends of the specimen illustrate another advantage of loading through the concrete. The length of bond breakdown in these regions was significantly affected by the loading arrangement. This was due to the relative dimensions of the steel and the concrete affecting the distance required to develop strain throughout the unloaded material. Reduced debonding was therefore observed when the load was applied through the concrete.

It was thus established that the two methods of loading produced similar results and later specimens were loaded through the concrete. Subsequent discussion of the first two specimens will deal only with their behaviour when loaded in this manner to 300 kN.

7.2.2 Longitudinal strain distribution

An estimate of the strains expected for different reinforcement percentages was made by assuming a modular ratio (m) of 7.5, elastic behaviour for both materials and a compatibility of strains across the section. This last assumption was confirmed by comparing the mean of the Demec readings ($\epsilon_{c_{ave}}$) to the average of the reinforcement strains ($\epsilon_{s_{ave}}$) for each specimen. The relationship is plotted in Figure 7.3. A least squares analysis of the data yielded the following equation for the line of best fit:

$$\epsilon_{c_{ave}} = 0.95\,\epsilon_{s_{ave}} - 0.75 \tag{7.1}$$

where:

$$43.0 \leq \epsilon_{s_{ave}} \leq 314.0.$$

The close correlation between these values demonstrated strain compatibility across the specimen, at low strain levels.

The measured reinforcement strains were averaged over lengths of the specimen in which the bond was unimpaired. These lengths became shorter due to the growth of the debond zone out of the lap, and to the increasing linearity of the distribution within the joint. The comparison between the predicted and measured ratio of the strains inside and outside the joint could therefore only be carried out at the lower load stages. The values of the ratio thus obtained remained constant, and typically lay within 5% of the predicted values of 0.95 and 0.86 for the 12 and 20 mm rods, respectively. The exception, specimen 250C12/12(B) rod B, was about 10% lower than expected which, although clear from the plot of the steel strain distribution (Figure 7.1.3), occurred for no apparent reason.

It has been stated by previous researchers [11] that the strain level inside a compression lap will tend to a higher proportion of the strain level found outside

the joint than those in a tension lap. The results from these specimens showed the ratio of the strains in/out of the lap to be related to the reinforcement percentage, and therefore similar in both test series. However, bond stresses within the lap joint prevented the comparison being made for the entire range of loads, and the ratio may have changed by the ultimate strain levels.

The above approach was also used to predict the level of strain which existed outside the lap at various load stages. The measured strains at the maximum load, 300 kN, exceeded the predicted values by over 50%. Some improvement in the comparison was achieved by taking the Young's modulus of the concrete as 24.0 kN/mm^2. This raised the value of the estimated strain, and lowered the ratio of the strains inside/outside the lap joint. This choice of E_c also proved beneficial in the analysis of the tension results (§6.2.1). In this case, however, the predicted strains were still 30% awry.

The typical relationship between the peak reinforcement strains at the start of the lap joint and the applied load is shown in Figure 7.4. The plots of the entire strain distribution showed these peak values to be representative of the average strain found outside the 250 mm laps (Figures 7.1.3 and 7.1.5). Figure 7.4 demonstrates that up to a strain of approximately 250 microstrain the measurements were consistent with figures anticipated from strain compatibility considerations. Beyond this level, the curvature of the relationship resulted in an increasingly poor correlation between measured and predicted strains. This behaviour was believed to be the consequence of a breakdown in strain compatibility, due to microcracking of the concrete.

The relationship between applied load and strain at the free end of the lap has been included in Figure 7.4. The measurements were taken at the final gauge position, 5 mm from the free end of the bar, and are thus indicative of the contribution of end bearing to force transfer. It was clear that, within this load range, end bearing was proportional to load.

It was evident from the strains measured at the lap end that, at a given load, end bearing was more active in the shorter laps. Typically, the end strain in the 125 mm lap lengths was about 70% higher than in the 250 mm laps. However, this situation may change at ultimate loads. Cairns and Arthur[27] concluded that the contribution of end bearing to joint strength was not significantly affected by lap length.

The relationship between the steel strain at the ends of the lap and the applied load also served to highlight the effect of time on the strain distributions. A sudden fall in the strain at the tip of rod B at 75 kN, whilst the Demec readings were

being taken, was observed in all the specimens. A less substantial reduction in strains was also noted in some specimens at 60 kN, the previous level of Demec measurement. Maintaining this level of load for a period of approximately ten minutes (the time taken to read the surface strains) clearly had a significant effect on the distribution in rod B, although rod A remained largely unaffected. The concrete stress calculations showed the concrete stress to fall outside the lap, and rise within it, over this period of time. The reverse effect would be observed in the reinforcement, thus within the lap joint the steel strains fell. This equalisation of the concrete stresses was most noticeable in the specimens comprising a pair of 20 mm bars, in which the stress difference in and out of the lap joint was greatest. The weaker concrete found at the top of the specimen, nearest the cast face, would result in the effect being most apparent in rod B. Similar behaviour was observed in specimen 250C20/20(E) at 190 kN, when electrical interference necessitated the re-initialisation of the data logger. The load was held at this level for approximately 30 minutes, resulting in reduced strains within the lap for both rods. It would appear from this behaviour that long-term tests of compression lap joints would prove to be a fruitful area of further research.

7.3 Bond stresses

It was evident from the longitudinal reinforcement strains (Figures 7.1.1 – 7.1.5) that regions of bond stress extended from the lap ends and from the ends of the specimen. The subsequent discussion deals only with the former, as the latter, a feature of the bond breakdown near the loading point, were not pertinent to lap behaviour.

Steeper strain gradients were generally found at the free end of the bar due to the equalisation of the steel stresses in the individual rods near the splice ends. The peak bond stresses were therefore located here. A secondary peak in the bond stress distribution existed at the lap end in the continuing rod, due to the different strain levels associated with the change in reinforcement percentage and end bearing effects. The form of this distribution was similar to that measured by Cairns and Arthur in their tests on compression lap joints [27] (Figure 2.6). The presence of peak bond stresses at the lap ends led to their recommendation that transverse reinforcement should be clustered at this position.

As the applied load was increased there was a general rise in the level of bond stress inside the lap, with the zone of peak bond stress influencing a greater length of reinforcement. If the length of the regions of peak bond stress is considered in terms of the applied load, then these zones developed at a greater rate in

the 125 mm laps and in the laps comprising a pair of 20 mm rods. This would be expected as the bond stresses associated with each of these specimen characteristics would be higher at a given load. This behaviour resulted in an increasing linearity of the steel strain distribution, evidenced by the reduced coefficient of variation of bond stress along the lap at higher loads.

The relationship between peak bond stress and peak rod stress has been plotted in Figure 7.5. The results were similar to those derived from the tension specimen data (Figure 6.23), the main difference being the level at which the peak bond stress stabilised. The influence of the bar diameter was less evident in the compression tests, the ratio between the bond stresses in the 12 and 20 mm diameter rods being approximately 0.75. In spite of these slight differences the results demonstrated the bond behaviour in both test series to be consistent.

The relationship between the peak (f_{bp}) and the mean bond stress (f_{bave}) along the lap length is shown in Figure 7.6. There was a clear correlation between the two stresses, with the relationship being independent of lap length and bar diameter. A least squares linear regression analysis yielded the following equation:

$$f_{bp} = 1.17\, f_{bave} + 1.47 \tag{7.2}$$

where:

$$0.3 \leq f_{bave} \leq 6.6.$$

The effect of the constant was to emphasise the influence of the peak bond stress only at low loads. Thus, the peak/average bond stress ratio at average bond stresses of 1.0 and 6.0 N/mm^2 was 3.6 and 1.4, respectively. This was consistent with the reduction in the coefficient of variation, and the extending influence of the peak bond stress, observed in these specimens at higher loads.

The equation (7.2), and more specifically the value of the constant, was different to that determined for the tension specimens (equation 6.5 and Figure 6.22). However, in the tension specimens the data was concerned with the local variation of bond stresses found adjacent to a transverse crack, rather than with the entire lap length. Aspects of compression lap behaviour, for instance the lengthening of the region of peak bond stress and end bearing effects, were therefore not evident in the tension results.

The average bond stress of approximately 6.0 N/mm^2 developed along the lap in specimen 125C20/20 at 300 kN exceeded the ultimate bond stress quoted in BS8110 [7]. This figure, calculated using $0.65\sqrt{f_{cu}}$†, is 4.1 N/mm^2. The code

† BS8110:pt. 1:1985 [7], §3.12.8, table 3.28. The constant includes a partial safety factor of 1.4.

uses the same basic equation (equation 2.7) to evaluate the average bond stress in a tension and a compression lap, the only allowance for the contribution of end bearing being the different value of the constant.

Although none of these specimens were loaded to capacity, it was interesting to note that the peak bond stresses developed in the 20 mm diameter rods reached the value at which cracking of the concrete cover occurred in the tension tests (see §6.3.2). However, the peak values of about 2.1 f_{ct} N/mm^2 were still considerably lower than the theoretical maximum level of stress which could be sustained by the cross-section. This was determined, on the basis of Tepfers' equations, to be approximately 9.0 N/mm^2 if the concrete behaved plastically (equations 2.4 and 2.5).

7.4 Embedment Gauge Results

The circumferential concrete strains were measured in the final compression test (250C20/20(E)). Embedment gaugés were cast at the end of rod A, and 100 mm to either side of this position. These were complemented by electric resistance strain gauges mounted on the surface of the concrete. This arrangement was similar to that used in the equivalent tension specimen (250T20/20(E) and Figure 4.4). The satisfactory performance of these additional strain gauges was maintained, with just a single gauge failure. The absence of cracking in the compression specimens enabled the results from the whole test to be considered. The circumferential strains measured at 100, 200 and 300 kN are plotted in Figure 7.7.

Although the embedment gauges consistently displayed a higher strain than their counterpart on the surface, the influence of distance from the reinforcement was not readily apparent around the compression lap. This differed from the situation in the tension specimens, in which the measurements indicated the circumferential strains to be almost inversely proportional to the distance from the reinforcement (see §6.4). In the compression laps the concrete carried a greater load and thus the effect of Poisson's ratio was more significant. The resulting tensile strains would be almost constant across the specimen. However, the circumferential strains attributed to the bond at the steel/concrete interface decreased with distance from the reinforcement. Thus, the difference between the embedment and the surface gauge readings became more pronounced as the load was raised.

The strains resulting from Poisson's ratio effect were estimated by assuming a typical value of 0.2 for the ratio [7] and a Young's modulus of 27.6 kN/mm^2

for the concrete. The longitudinal concrete strains were determined from the concrete stress calculations. The circumferential strains corresponding to the resulting figures were estimated to be 57, 110 and 162 microstrain at 100, 200, and 300 kN.

The strains due to the bursting effect of the bond stress were evaluated by assuming E_c to be 27.6 kN/mm^2, and the angle of incidence of the bond forces to the reinforcing bar (α) to be 45°. At the maximum load of 300 kN the bond stresses within the lap joint were approximately 4.0 N/mm^2 in each bar. This represented a circumferential strain of about 145 microstrain.

The addition of the two components of circumferential strain resulted in an overall figure of 307 microstrain. This corresponded to a mean measured strain of 279 and 222 microstrain in the embedment and the surface gauges, respectively. Removing the influence of strains due to the Poisson's ratio (162 microstrain) left values of 67 and 124 microstrain in the two groups of gauges. The ratio of these two figures, 0.54, compared favourably to the inverse of the ratio of the average distance of the gauges from the steel, 0.57. The results were thus consistent with the existence of two separate components of circumferential strain, only one of which was significantly affected by position from the reinforcement.

The comparison was best undertaken within the lap, where similar strains were measured on all four faces of the specimen. The slightly higher readings from the embedment gauges on the A and C faces were attributed to the reduced distance from the bar. The measurements indicated that the bursting forces around the overlapping bars were similar to those around an individual rod.

Out of the lap region, a greater scatter of results was observed, with the measurements from faces C and D being considerably higher than those taken on the A and B faces. Cairns [43] commented on the end-bearing in a compression lap pushing out a cone of concrete. Such a conical force system may have caused an imbalance in the strains around the specimen, clearest some distance beyond the end of the lap joint. This effect would have been most apparent on the C face. It does not, however, readily explain the different readings from the B and D faces of the specimen. It was unfortunate that the failure of an embedment gauge on face D prevented the confirmation of the trend shown by the surface measurements.

The procedure outlined above was used to estimate the circumferential strains outside the lap at 300 kN. The predicted value of 318 microstrain corresponded to measurements of 297† and 155 microstrain for embedment and surface gauges. The latter figure was inexplicably low.

---

† The strain on face D was estimated by considering the pattern around the specimen shown by the surface gauges.

At the end of the lap, the gauges indicated lower strains on face A. This side of the specimen, being the nearest to the continuing bar (in which the bond stresses were low), would be expected to be the least stressed. Such behaviour was consistent with Cairns and Arthur's [27] observation that the first longitudinal crack in his compression lap joints formed over the discontinued bar. The small influence of the bond stress on face A implied that much of the circumferential strain may be attributed to Poisson's ratio effects. The embedment and surface gauges showed consistent results throughout the test, with the maximum strains being in the order of 60 microstrain at 300 kN. This was considerably lower than anticipated and, most surprisingly, at a load of 100 kN the embedment gauges indicated compressive strains of about 40 microstrain. It appeared that some secondary effect, perhaps the release of shrinkage stresses, significantly affected the strains around the bar.

The results from the remaining three faces were somewhat scattered, but the mean values of strain, 298 and 294 microstrain, lay within the estimated range of 237–416 microstrain. These limiting values represented the difference between the bond stress at this position in the continuing and the terminating rod.

The test measurements indicated that the circumferential strains were due to a combination of Poisson's ratio effect and bond stresses. It would appear that any analysis dealing with the ultimate bond stress in compression laps should make allowance for both effects. Hitherto the effect of Poisson's ratio has been neglected, but as none of these compression laps reached their capacity it was not possible to compare the ultimate strength of these specimens to predictions which omitted this influence.

The mean strain measured on the surface of the specimen within the lap region, 222 microstrain, corresponded to a stress of approximately double the tensile strength of the concrete if a value of 27.6 kN/mm^2 was assumed for E_c. A higher value of strain, and hence stress, was measured by the embedment gauges. Thus, although longitudinal compression in the concrete resulted in additional circumferential strains, it seems to have increased the resistance to splitting cracks.

The reduced influence of distance from the reinforcement on the circumferential strains suggests that the effect of cover will be less significant in compression laps. This agrees with the experimental findings of Leonhardt and Teichen, discussed in the C.E.B. report on bond behaviour [11].

It was shown in this test that, up to the limiting load of 300 kN, comparable stresses were found around the specimen in and out of the lap region. The additional 25% of reinforcement required by BS8110 [7] in a compression lap, as

compared to a compression anchorage, thus appears surprising. It was interesting to note that the American design recommendations [8] equates compression anchorage and lap lengths. Although this single test is obviously not sufficient to warrant a change in the design code, it could form the basis of some very interesting further work.

CHAPTER 8

CONCLUSIONS

8.1 Tension Specimens

8.1.1 The technique of internally gauging the reinforcing bars proved a successful and reliable method of determining the longitudinal strain distribution. The use of strain concentration gauges enabled the acquisition of particularly detailed information from the tip of the lap joint.

8.1.2 Before crack formation, regions of constant steel strain existed inside and outside the lap joint. The difference between these two strain levels was a function of the change in the reinforcement percentage.

8.1.3 The precrack strain distribution tended to zero at the free end of the reinforcing steel. The length of the transition from zero strain to the average strain level inside the lap was dependent on the diameter of the terminating bar. Approximately 60% of the average strain had been developed within one bar diameter of the lap end, and 80% within two bar diameters.

8.1.4 The steel strain at crack formation was similar for cracks which formed inside and outside the lap joint. The development of cracks was more dependent on the magnitude of concrete strain than on the concrete stress.

8.1.5 The formation of transverse cracks in the concrete considerably modified the steel strain distribution, with peaks being found at the crack positions. Although the strains still fell to zero at the lap end, the distribution in this area became dependent on the proximity of the nearest crack.

8.1.6 The individual bars in a mixed lap behaved in a similar manner to their counterparts in a lap comprising bars of equal diameter.

8.1.7 The greatest changes in the strain distribution in the long term test occurred over the first week. Once the transverse cracks had fully extended, the values of the peak strains remained stable. The strains at the troughs were still rising slowly when the test terminated after 81 days.

8.1.8 Splitting cracks were associated with peak bond stresses in the range 1.8 – 2.7 f_{ct} N/mm^2. The bond stress which caused longitudinal cracking of the cover was similar inside and outside the lap joint. The bursting force around a lap may be equated to that around a single bar.

8.1.9 No generally applicable relationship between the peak and the average ultimate bond stress over the full lap length was found.

8.1.10 Although longitudinal cracks were initiated by a peak bond stress, the resistance to failure was partly dependent on the ability of the specimen to withstand their effects. The average value of the bond stress was indicative of such resistance; it is therefore not unreasonable to base design regulations on a mean figure.

8.1.11 The shorter lap lengths failed at lower loads. These tests indicated that the strength of a lap was not directly proportional to its length.

8.1.12 Laps comprising bars of 12 mm diameter failed at lower loads. The capacity of a mixed lap was determined by the smaller of the two bars.

8.1.13 The results from these tests were favourably compared to existing design proposals [30,31] and regulations [7]. The specimens which failed did not meet the requirements of the current British Standard, BS8110:1985. The agreement between these axial specimens and design equations based on beam tests showed that standard procedures may be used for the design of lap joints in tension ties.

8.2 Compression Specimens

8.2.1 No gauged compression specimen failed. Consequently the conclusions pertain to the behaviour of these specimens up to 300 kN.

8.2.2 Different strain levels were found inside and outside the lap joint, with the ratio between the two being similar to those found before crack formation in the tension series. The strain levels along the specimen were a function of the reinforcement percentage.

8.2.3 The bearing of the free end of the reinforcing steel against the concrete assisted in the transfer of force between the overlapping bars. Strains of up to 370 microstrain were measured in the steel close to the tip of the lap. The confinement provided by the cover to the reinforcement enabled the ultimate uniaxial compressive stress of the concrete to be exceeded.

8.2.4 The length of steel used to transfer force was not limited by transverse cracks at the ends of the lap joint. The tests showed that as much as 20% of the stress could be transferred over a distance of up to six bar diameters beyond the lap end.

CHAPTER 9

FURTHER WORK

A substantial proportion of this work was directed towards furthering the understanding of tension lap behaviour. The relative absence of work on compression specimens, both here and in general[11], leaves considerable scope for future work. In particular, there is a need to extend the compression test series, using a testing machine with a capacity greater than the 300 kN rig available. The ability to fail a compression lap would help to define the applicability of the reported results.

Both the tension and the compression test series were predominantly concerned with short-term loads. Maintaining the applied load for even the short period of time required to measure surface strains influenced the steel strain distribution. Although one long-term tension test was successfully completed, it is believed that further long-term tests would provide valuable data. This is particularly true in compression laps, as there appears to be no information available regarding their behaviour under a sustained load.

Scope remains to investigate the influence of various loading histories, for instance cyclic or quasi-seismic loads, on the strain distribution along lap joints. The strains could also be measured in a different type of specimen. A similar, though more limited, programme of beam tests would provide a correlation between axially loaded specimens and the work of previous researchers.

The opportunities for further research are not limited to an extension of the experimental programme. The detailed information provided by the strain measurements offers a valuable means of testing the computer modelling of bond behaviour.

An attempt was made to measure the circumferential strains in two of the specimens, around one tension and one compression lap joint. The technique of casting embedment gauges into the concrete proved very successful although, unfortunately, the development of transverse cracks at the gauge positions caused severe problems in the tension specimen. The small amount of information gleaned from this test effectively left the distribution around a tension lap joint unmeasured. It would be of great interest, though considerably more complicated, to measure the strains around the perimeter of the reinforcement, and thus establish the nature of the force system around lapped bars.

There were no problems with transverse cracking when measuring circumferential strains in the compression specimen, although further measurements are required to corroborate the results from this single test. In particular, the relationship between the anchorage and the lap length required in compression has yet to be ascertained. This could, however, be achieved without the need for circumferential strain measurements.

The overall impression is that the scarcity of the work on compression lap joints has left much to be done in this field. It is hoped that some of the questions left unanswered by the five specimens tested here will provide the impetus for further research.

REFERENCES

1. SCOTT R.H. and GILL P.A.T. "Developments in the measurement of reinforcement strain distributions in reinforced concrete members", Strain, Vol. 18, No. 2, May 1982, pp. 61,63,79.

2. SCOTT R.H. and GILL P.A.T. "Techniques in experimental stress analysis for reinforced concrete structures", in "Experimental stress analysis: Proceedings of an international conference", Amsterdam, May 1986, (ed. WIERINGA H.), Martinus Nijhoff Publishers, The Netherlands, 1986, pp. 87–96.

3. MAINS R.M. "Measurement of the distribution of tensile and bond stresses along reinforcing bars", Journal of the American Concrete Institute, Proc. Vol. 48, No. 11, Nov. 1951, pp. 225–252.

4. PERRY E.S. and THOMPSON J.N. "Bond stress distribution on reinforcing steel in beams and pull-out specimens", Journal of the American Concrete Institute, Proc. Vol. 63, No. 8, August 1966, pp. 865–874.

5. NILSON A.H. "Internal measurement of bond slip", Journal of the American Concrete Institute, Proc. Vol. 69, No. 7, July 1972, pp. 439–441.

6. JIANG D.H., ANDONIAN A.T. and SHAH S.P. "A new type of bond test specimen", in "Bond in concrete: Proceedings of an international conference", Paisley College of Technology, June 1982, (ed. BARTOS P.), Applied Science Publishers, London, 1982, pp. 127–139.

7. BRITISH STANDARDS INSTITUTION "Structural use of concrete", BS8110: Parts 1 and 2:1985, B.S.I., London, 1985.

8. AMERICAN CONCRETE INSTITUTE 318-83 "Standard building requirements for reinforced concrete", American Concrete Institute, Detroit, 1983.

9. AMERICAN CONCRETE INSTITUTE 318-83 "Commentary to the standard building requirements for reinforced concrete", American Concrete Institute, Detroit, 1983.

10. TEPFERS R. "A theory of bond applied to overlapped tensile reinforcement splices for deformed bars", Chalmers University of Technology, Division of Concrete Structures, Publication 73:2, Göteborg, 1973, 328 pp.

11. COMITE EURO-INTERNATIONAL DU BETON "Bond action and bond behaviour of reinforcement", C.E.B. Bulletin d'Information No. 151, Paris, April 1982, 153 pp.

12. KLUGE R.W. and TUMA E.C. "Lapped bar splices in concrete beams", Journal of the American Concrete Institute, Proc. Vol. 17, No. 1, Sept. 1945, pp. 13–33.

13. FERGUSON P.M. and KRISHNASWAMY C.N. "Tensile lap splices – Pt.2: design recommendations for retaining wall splices and large bar splices", Research report No. 113-3, Center for Highway Research, The University of Texas at Austin, April 1971, 60 pp.

14. BETZLE M. "Bond slip and strength of lapped bar splices", in A.C.I. Douglas McHenry International Symposium on Concrete and Concrete Structures, Mexico City, Oct. 1976, pp. 493–514.

15. CAIRNS J. "The strength of lapped joints in reinforced concrete columns", A thesis submitted for the degree of PhD, University of Glasgow, October 1976, 171 pp.

16. ORR D.M.F. "Lap splicing of deformed reinforcing bars", Journal of the American Concrete Institute, Proc. Vol. 73, No. 11, Nov. 1976, pp. 622–627.

17. THOMPSON M.A., JIRSA J.O., BREEN J.E. and MEINHEIT D.F. "Behavior of multiple lap splices in wide sections", Journal of the American Concrete Institute, Proc. Vol. 76, No. 2, Feb. 1979, pp. 227–248.

18. PFISTER J.S. and MATTOCK A.H. "High strength bars as concrete reinforcement, part 5 – lapped splices in concentrically loaded columns", Journal of the Portland Cement Association, Vol. 5, No. 2, May 1963, pp. 27–40.

19. REZANSOFF T. "Performance of lapped splices in reinforced concrete loaded beyond yielding of the steel", Canadian Journal of Civil Engineering, Vol. 5, No. 4, Dec. 1978, pp. 489–496.

20. A.C.I. COMMITTEE 408 "Bond stress – the state of the art", Journal of the American Concrete Institute, Proc. Vol. 63, No. 11, Nov. 1966, pp. 1161–1190.

21. ABRAMS D. "Tests of bond between concrete and steel", University of Illinois, Engineering Experiment Station, Bulletin 71, Dec. 1913, 238 pp.

22. CHAMBERLIN S.J. "Spacing of spliced bars in tension pull-out specimens", Journal of the American Concrete Institute, Proc. Vol. 49, No. 4, Dec. 1952, pp. 261–274.

23. CHAMBERLIN S.J. "Spacing of spliced bars in beams", Journal of the American Concrete Institute, Proc. Vol. 54, No. 8, Feb. 1958, pp. 689–697.

24. CHINN J., FERGUSON P.M. and THOMPSON J.N. "Lapped splices in reinforced concrete beams", Journal of the American Concrete Institute, Proc. Vol. 52, No. 2, Oct. 1955, pp. 201–213.

25. FERGUSON P.M. and BREEN J.E. "Lapped splices for high strength reinforcing bars", (Pt. 1 of a two-part paper), Journal of the American Concrete Institute, Proc. Vol. 62, No. 9, Sept. 1965, pp. 1063–1078.

26. ROBERTS N.P. and HO R.C.T. "Behaviour and design of tensile lapped joints in reinforced concrete beams", Civil Engineering and Public Works Review, Vol. 68, No. 1, Jan. 1973, pp. 33–45.

27. CAIRNS J. and ARTHUR P.D. "Strength of lapped splices in reinforced concrete columns", Journal of the American Concrete Institute, Proc. Vol. 76, No. 2, Feb. 1979, pp. 277–296.

28. BARTOS P. (editor) "Bond in concrete: Proceedings of an international conference", Paisley College of Technology, June 1982, Applied Science Publishers, London, 1982.

29. A.C.I. COMMITTEE 408 "Opportunities in bond research", Journal of the American Concrete Institute, Proc. Vol. 67, No. 11, Nov. 1970, pp. 857–867.

30. ORANGUN C.O., JIRSA J.O. and BREEN J.E. "A re-evaluation of test data on development length and splices", Journal of the American Concrete Institute, Proc. Vol. 74, No. 3, March 1977, pp. 114–122.

31. REYNOLDS G.C. "Bond strength of deformed bars in tension", C. & C.A. Tech. Report 42.548, Cement and Concrete Association, Slough, May 1982, 23 pp.

32. ZSUTTY T. "Empirical study of bar development behaviour", Proc. A.S.C.E., Journal of the Structural Division, Vol. 111, No. 1, Jan. 1985, pp. 205–219.

33. PAULAY T. "Lapped splices in earthquake resisting columns", Journal of the American Concrete Institute, Proc. Vol. 79, No. 6, Nov. 1982, pp. 458–469.

34. ARISTIZABAL-OCHOA J.D. "Earthquake resistant tensile lap splices", Proc. A.S.C.E., Journal of the Structural Division, Vol. 109, No. 4, April 1983, pp. 843–858.

35. LUKOSE K., GERGELY P. and WHITE R.N. "Behaviour of reinforced concrete lapped splices for inelastic cyclic loading", Journal of the American Concrete Institute, Proc. Vol. 79, No. 5, Sept. 1982, pp. 355–365.

36. SIVAKUMAR B., GERGELY P. and WHITE R.N. "Suggestions for the design of R/C lapped splices for seismic loading", Concrete International: Design & Construction, Vol. 5, No. 2, Feb. 83, pp. 46–50.

37. CAIRNS J. and JONES K. "Bond performance of ribbed reinforcing bars in lapped joints", in "Bond in concrete: Proceedings of an international conference", Paisley College of Technology, June 1982, (ed. BARTOS P.), Applied Science Publishers, London, 1982, pp. 342–352.

38. SKOROBOGATOV S.M. and EDWARDS A.D. "The influence of the geometry of deformed steel bars on their bond strength in concrete", Proc. Institution of Civil Engineers, Pt. 2, Vol. 67, June 1979, pp. 327–329.

39. REYNOLDS G.C. and BEEBY A.W. "Bond strength of deformed bars", in "Bond in concrete: Proceedings of an international conference", Paisley College of Technology, June 1982, (ed. BARTOS P.), Applied Science Publishers, London, 1982, pp. 434–445.

40. CARINO N.J. and LEW H.S. "Re-examination of the relation between splitting tensile and compressive strength of normal weight concrete", Journal of the American Concrete Institute, Proc. Vol. 79, No. 3, May 1982, pp. 214–219.

41. NEVILLE A.M. "Properties of concrete", 3rd edition, Pitman, London, 1981, 779 pp.

42. ELIGEHAUSEN R. Personal communication, March 1987.

43. CAIRNS J. "An analysis of the ultimate strength of lapped joints of compression reinforcement", Magazine of Concrete Research, Vol. 31, No. 106, March 1979, pp. 19–27.

44. TEPFERS R. "Cracking of concrete cover along anchored deformed reinforcing bars", Magazine of Concrete Research, Vol. 31, No. 106, March 1979, pp. 3–12.

45. LOSBERG A. and OLSSON P.A. "Bond failure of deformed reinforcing bars, based on the longitudinal splitting effect of the bars", Journal of the American Concrete Institute, Proc. Vol. 76, No. 1, Jan. 1979, pp. 5–18.

46. ROWE R.E. *et al* "Handbook to BS8110:1985", 1st edition, Viewpoint Publications, London, 1986, 206 pp.

47. BRITISH STANDARDS INSTITUTION "Specification for cold worked bars for the reinforcement of concrete", BS4461:1978, B.S.I., London, 1978.

48. TEPFERS R. "Lapped tensile reinforcement splices", Proc. A.S.C.E., Journal of the Structural Division, Vol. 108, No. 1, Jan. 1982, pp. 283–301.

49. TEPFERS R. "Tensile lapped splices with confining reinforcement", in "Bond in concrete: Proceedings of an international conference", Paisley College of Technology, June 1982, (ed. BARTOS P.), Applied Science Publishers, London, 1982, pp. 318–330.

50. R.I.L.E.M./C.E.B./F.I.P. "Recommendations R.C.5 and R.C.6 – bond tests for reinforcing steel: (1) Beam test and (2) Pull-out test", Materials and Structures, Vol. 6, No. 32, 1973, pp. 97–105.

51. TEPFERS R. "Bond stress along lapped reinforcing bars", Magazine of Concrete Research, Vol. 32, No. 112, Sept. 1980, pp. 135–142.

52. BROCK G., Discussion to TEPFERS R. "Bond stress along lapped reinforcing bars", Magazine of Concrete Research, Vol. 32, No. 112, Sept. 1980, pp. 135–142, *ibid.*, Vol. 33, No. 116, Sept. 1981, pp. 184–186.

53. BERNANDER K.G. "An investigation of bond by means of strain measurements in high tensile bars embedded in long cylindrical pull-out specimens", in R.I.L.E.M. Symposium on Bond and Crack Formation in Reinforced Concrete, Vol. 1, Stockholm, 1957, pp. 203–210.

54. SCOTT R.H. and GILL P.A.T. "Short-term distributions of strain and bond stress along tension reinforcement", The Structural Engineer, Vol. 65B, No. 2, June 1987, pp. 39–43,48.

55. BRITISH STANDARDS INSTITUTION "The structural use of concrete", CP110: Part 1:1972, B.S.I., London, 1972.

56. SCOTT R.H. and GILL P.A.T. "A modern data collection system", Strain, Vol. 20, No. 2, May 1984, pp. 63–68.

57. COX M.G. and HAYES J.G. "Curve fitting: a guide and suite of algorithms for the non-specialist user", N.P.L. Report NAC26, National Physical Laboratory, Teddington, Dec. 1973, 54 pp.

58. NUMERICAL ALGORITHMS GROUP, Fortran Library Manual Mark 11, Oxford, 1984.

59. ILLSTON J.M. and STEVENS R.F. "Internal cracking in reinforced concrete", Concrete, Vol. 6, No. 7, July 1972, pp. 28–31.

60. GOTO Y. "Cracks formed in concrete around deformed tension bars", Journal of the American Concrete Institute, Proc. Vol. 68, No. 4, April 1971, pp. 244–251.

61. SCOTT R.H. "Tension stiffening effects in reinforced concrete members", A thesis submitted for the degree of PhD, University of Durham, July 1985, 193 pp.

62. PERCY J. (BarFab Reinforcements, Cardiff), Personal Communication, March 1987.

63. BEEBY A.W. "The prediction of crack widths in hardened concrete", The Structural Engineer, Vol. 57A, No. 1, Jan. 1979, pp. 9–17.

64. RIZKALLA S.H. and HWANG L.S. "Crack prediction for members in uniaxial tension", Journal of the American Concrete Institute, Proc. Vol. 81, No. 6, Nov. 1984, pp. 572–579.

65. BEEBY A.W. "A study of cracking in members subjected to pure tension", C. & C.A. Tech. Report 42.468, Cement and Concrete Association, Slough, June 1972, 25 pp.

66. SNOWDON L.C. "Classifying reinforcing bars for bond strength", Building Research Station, Current paper 36/70, London, April 1970, 30 pp.

FIGURES

Author	Measurement technique	Notes
KLUGE & TUMA[12] 1945	Openings in concrete gave access to steel. Strains at 2.5 and 5 inch intervals measured by mechanical gauge. 26 specimens.	Demonstrated existence of peak bond stress at lap end. This value was independent of lap length.
NILSON[5] 1971	Steel internally gauged. 23 e.s.r.g. at a spacing of about 25 mm. 2 lap joint specimens.	Measurements used to assess bond stress/slip relationship for a lapped bar.
FERGUSON and KRISHNASWAMY[13] 1971	Gauges mounted on bar surface. Typically, 16 e.s.r.g. at a spacing of about 75 – 225 mm. 32 specimens.	Measurements showed an almost linear ultimate strain distribution along laps comprising bars of 43 & 57 mm diameter. A steepening strain gradient was noted at the lap end.
TEPFERS[10] 1973	Gauges mounted in slot cut into bar. Typically, 13 e.s.r.g. at a spacing of about 50 – 200 mm. Only some of the 193 specimens were gauged.	Measurements provided correlation with theoretical analysis. An almost uniform bond stress along the lap was observed near failure.
BETZLE[14] 1976	Gauges mounted on bar surface. Typically, 8 e.s.r.g. at a spacing of about 80 – 480 mm. 5 specimens. Complemented by photoelastic investigation.	Concentrations of bond stress and force transfer were observed at the lap ends. The local bond/stress slip relationship was seen to vary along the lap.
CAIRNS[15] 1976	Gauges mounted on bar surface. Typically, 9 e.s.r.g. at a spacing of about 40 – 200 mm. 4 gauged specimens.	The contribution of end bearing in compression lap joints was assessed. Noted transfer of force outside the lap, and a non-uniform bond stress distribution along it.
ORR[16] 1976	Gauges mounted on bar surface. Up to 16 e.s.r.g. at a spacing of 114 – 152 mm. 4 specimens.	Ultimate steel strain distribution observed to be almost linear. Related steel stress at the lap end to the applied moment.
THOMPSON *et al*[17] 1979	Gauges mounted on bar surface. Number of gauges varied. Generally around 15 e.s.r.g. per lap, at a spacing of about 40 – 60 mm. 25 specimens.	Below failure load, the bond stress distribution was similar in each of six laps across a wide section. Near ultimate, cracking above the outer laps reduced the bond stress in these joints.

Note: Other researchers[18,19] have mounted electric resistance strain gauges (e.s.r.g.) on the bar surface to relate the steel stress to the applied load.

Fig. 1.1 Previous Strain Measurements in Lap Joints

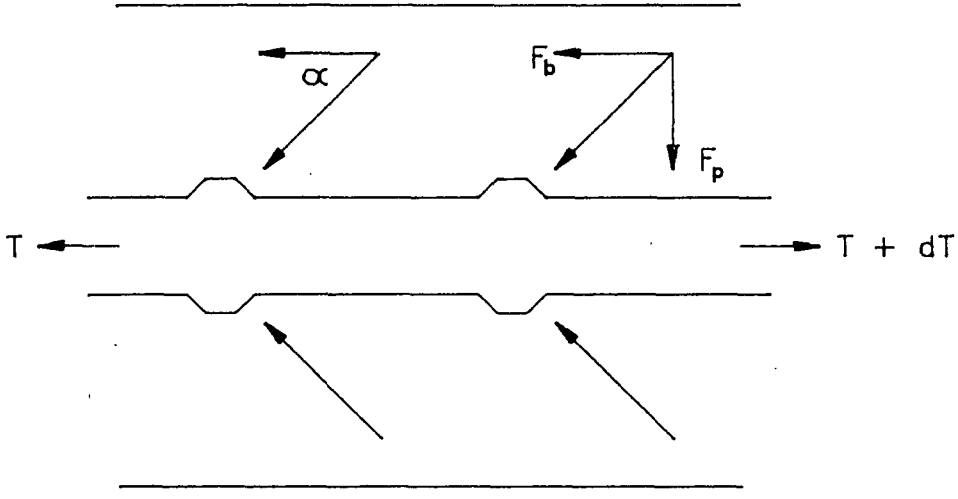

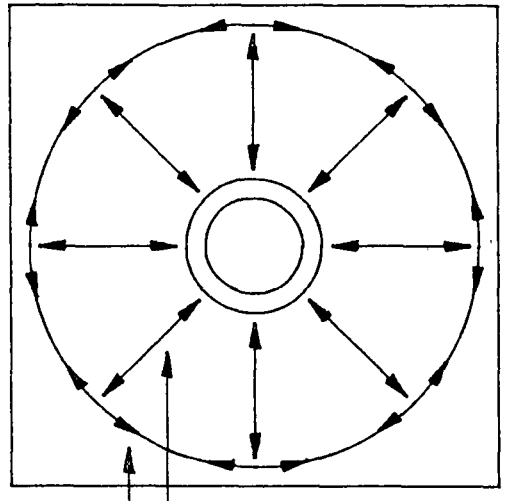

T : Tensile force in the reinforcement.
dT : Change in tensile force.
F_b : Longitudinal component of bond force.
F_p : Radial component of bond force.
α : Angle of compressive force.

Fig. 2.1 Forces in a Single Bar Anchorage

Side split ($S'_L/c < 1.4$)

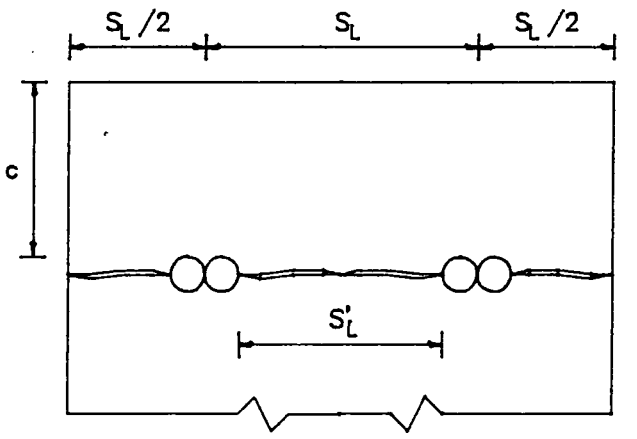

Face and side split ($1.6 < S'_L/c < 7.5$)

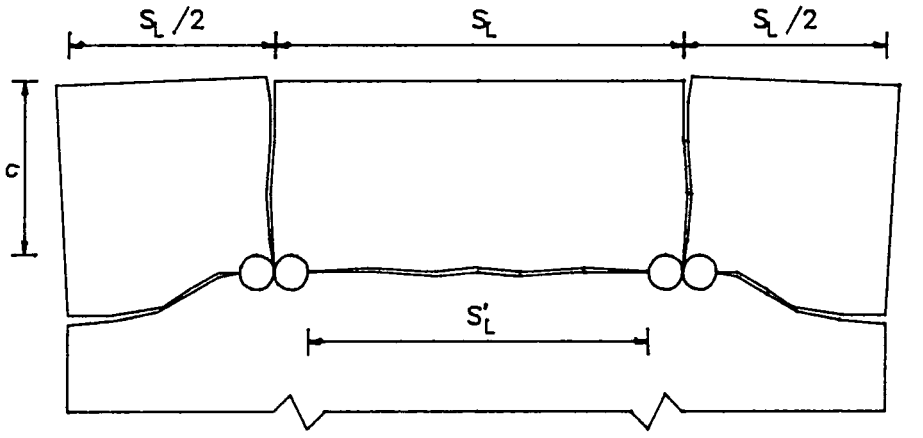

V–notch split ($S'_L/c > 8.0$)

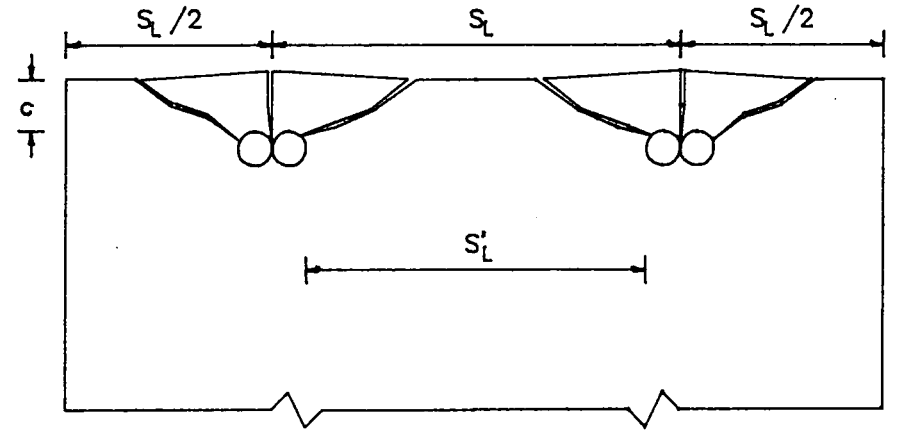

Fig. 2.2 Typical Splitting Failure Patterns (Ferguson and Krishnaswamy [13])

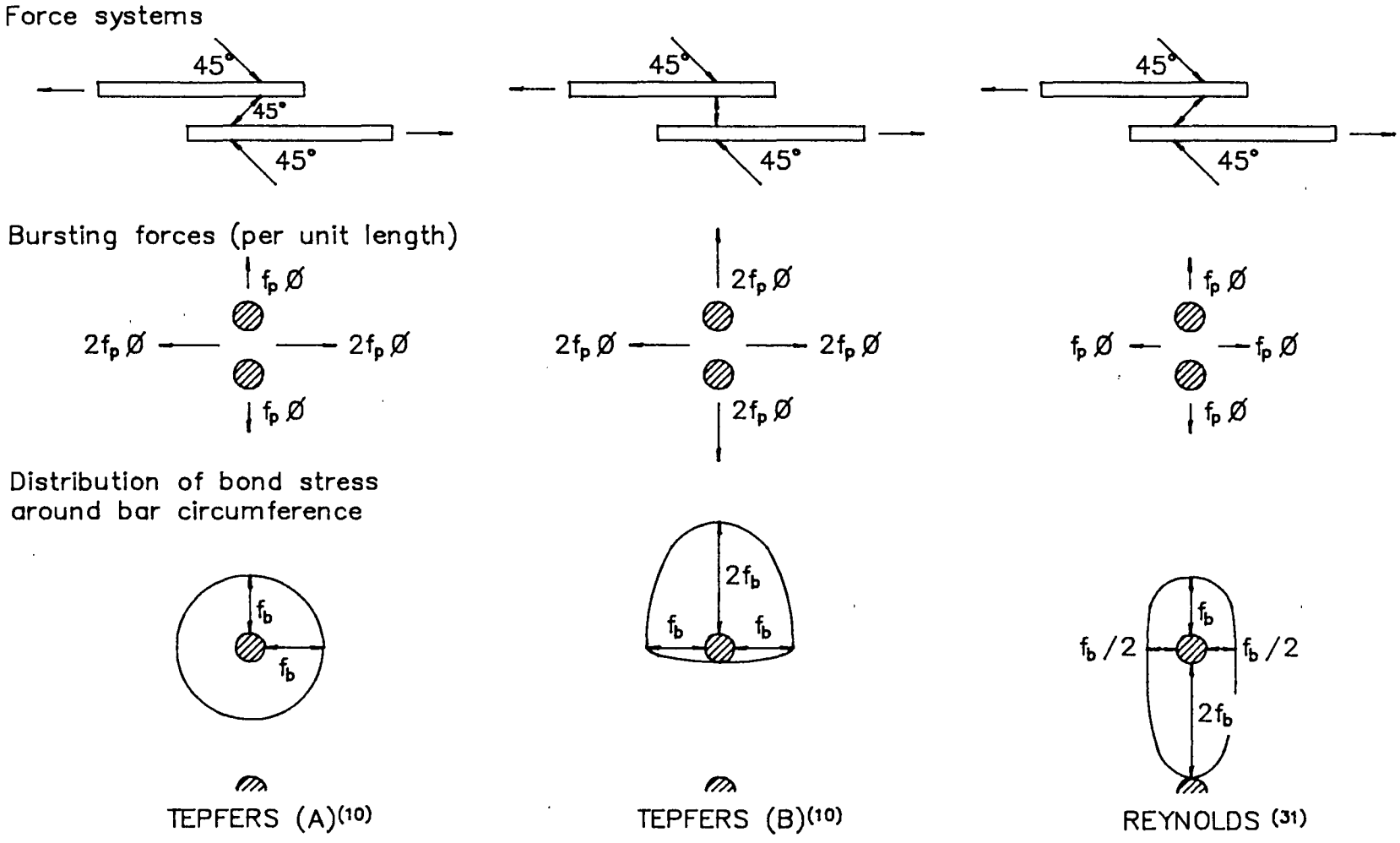

Fig. 2.3 Proposed Force Distributions Around Lap Joints

Fig. 2.4.1 Typical bond stress/slip curves (Tepfers[10])

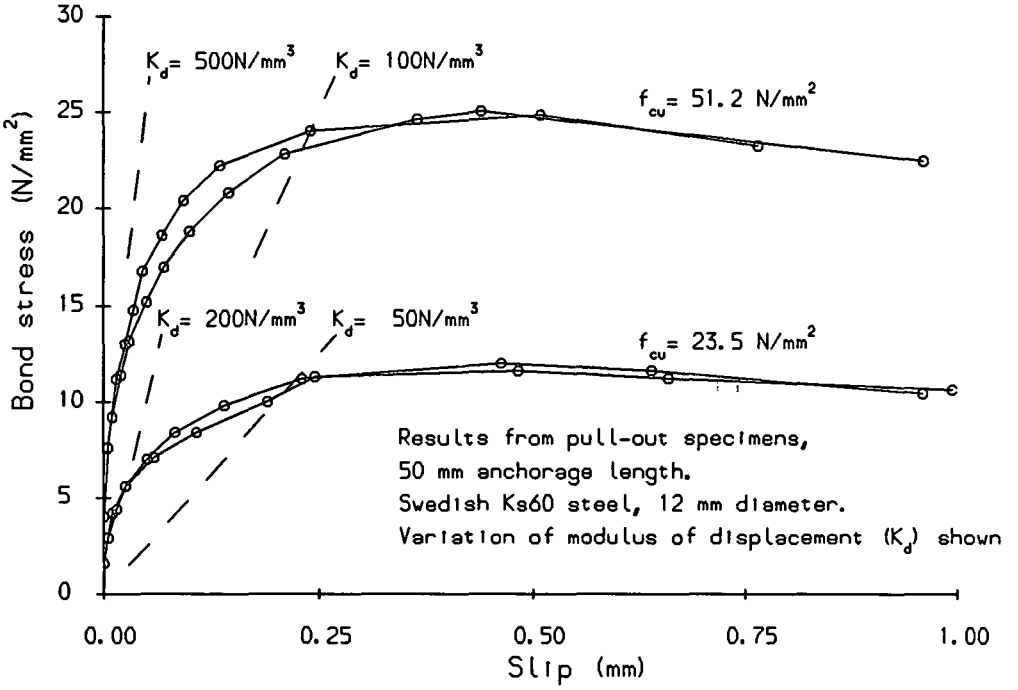

Fig. 2.4.2 Bond stress/slip and associated bursting stresses (Eligehausen[42])

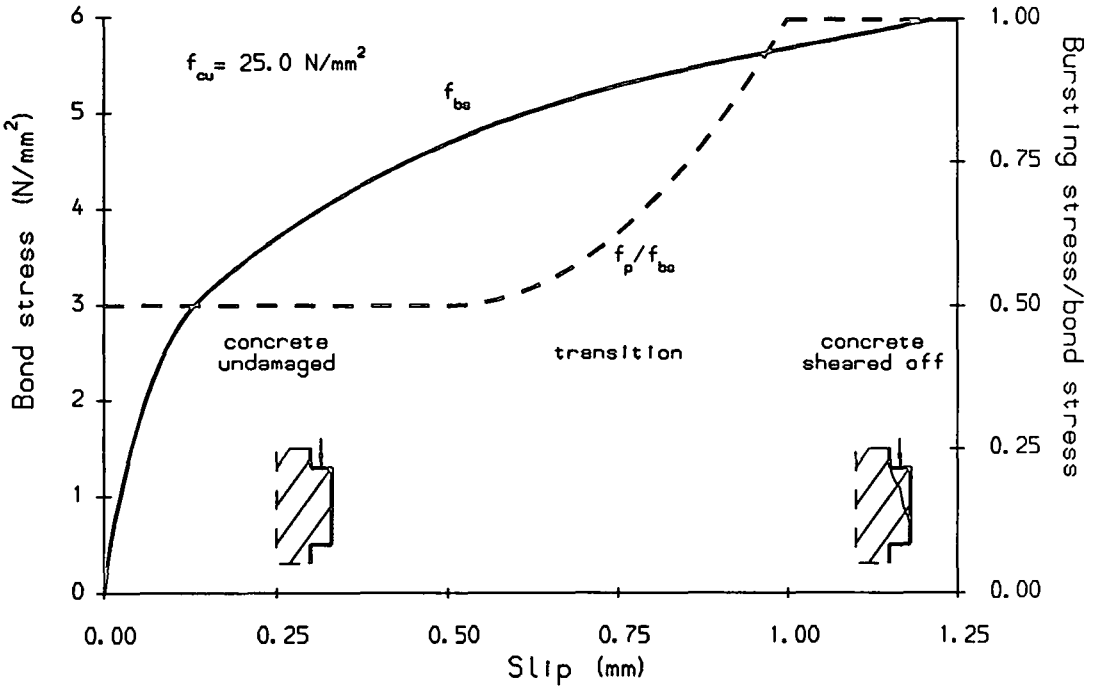

Fig. 2.4 Bond Stress/Slip Relationships

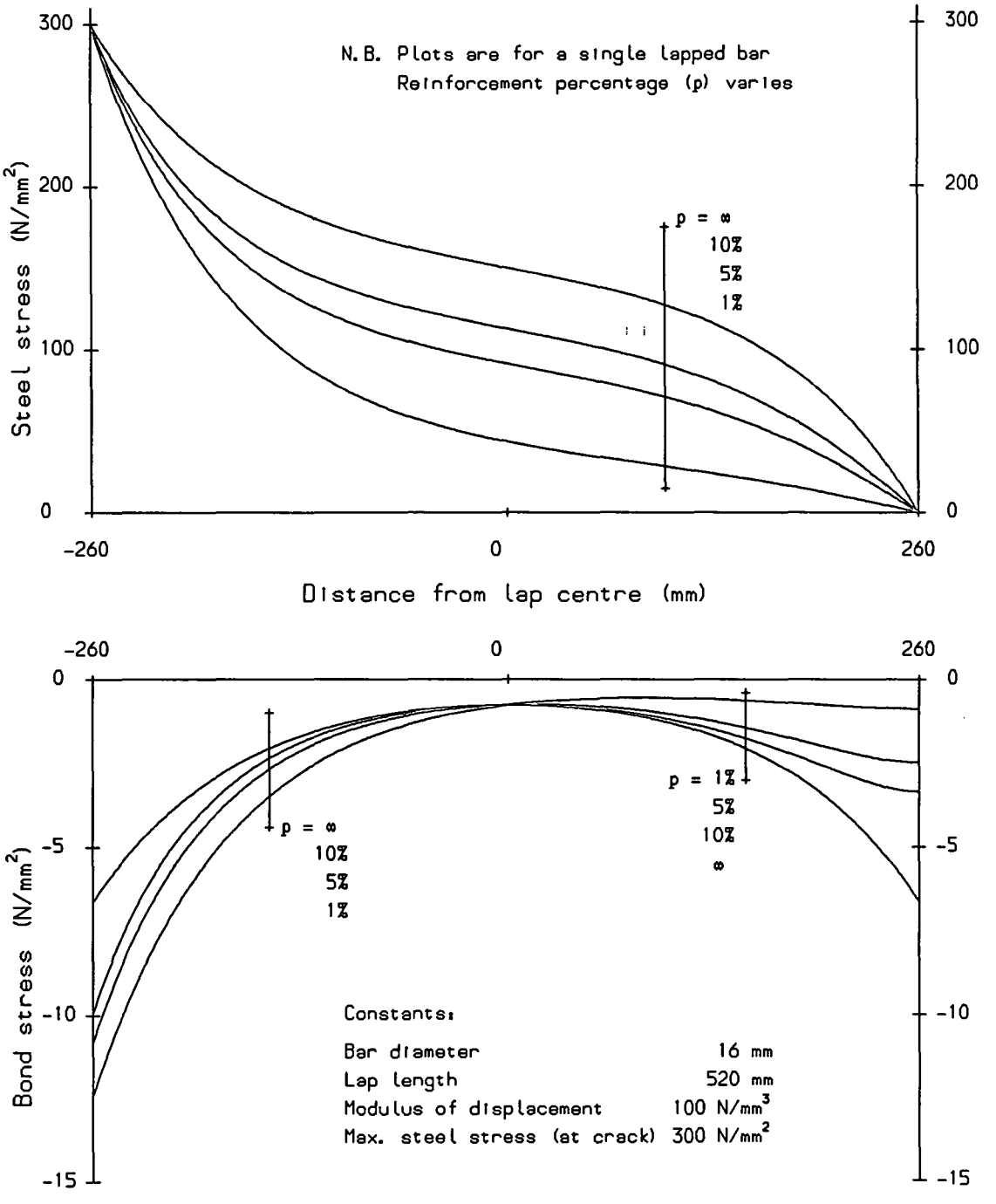

Fig. 2.5 Theoretical Steel and Bond Stress Distributions (Tepfers[51])

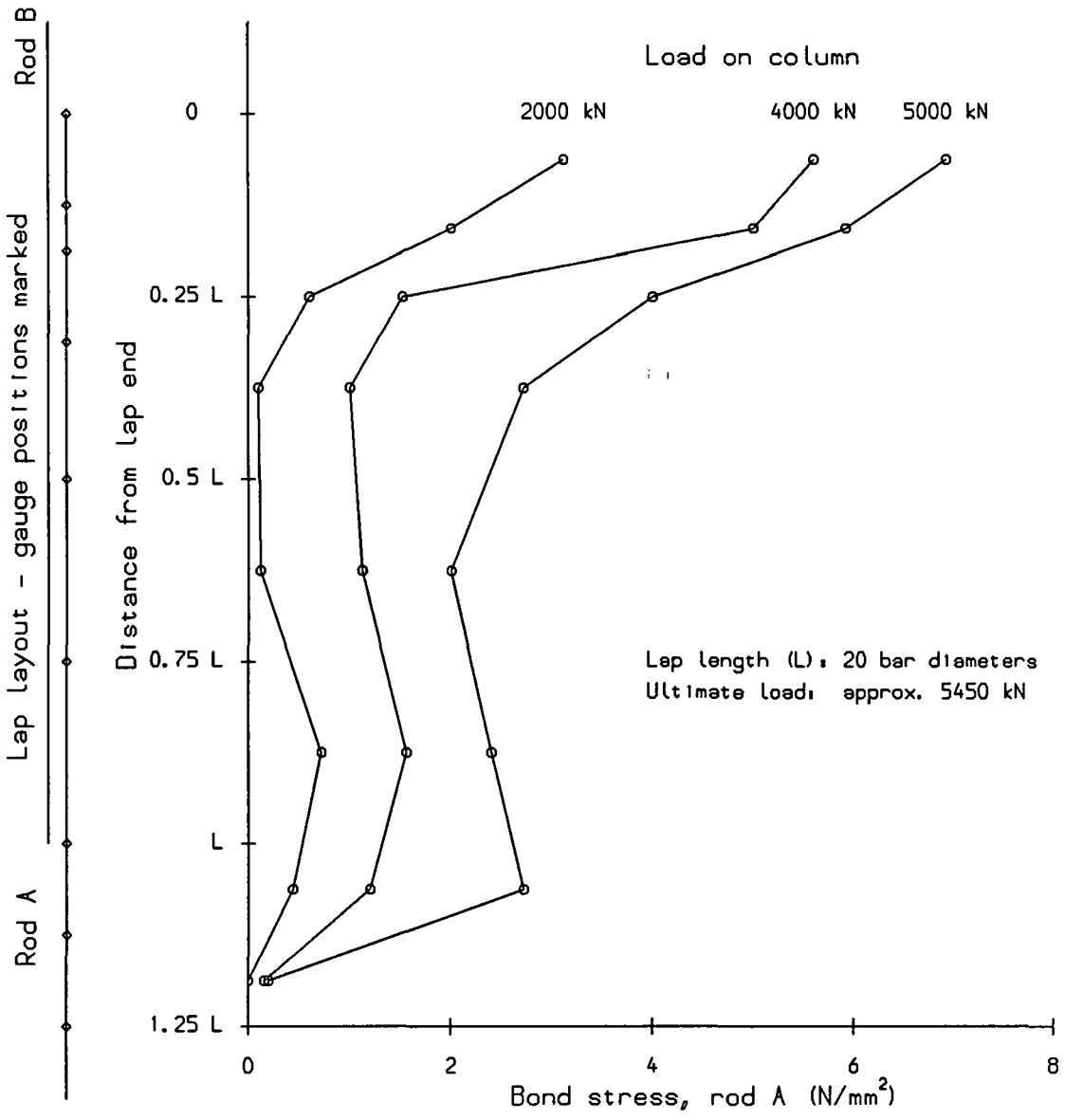

Fig. 2.6 Bond Stress Distribution in a Compression Lap (Cairns & Arthur[27])

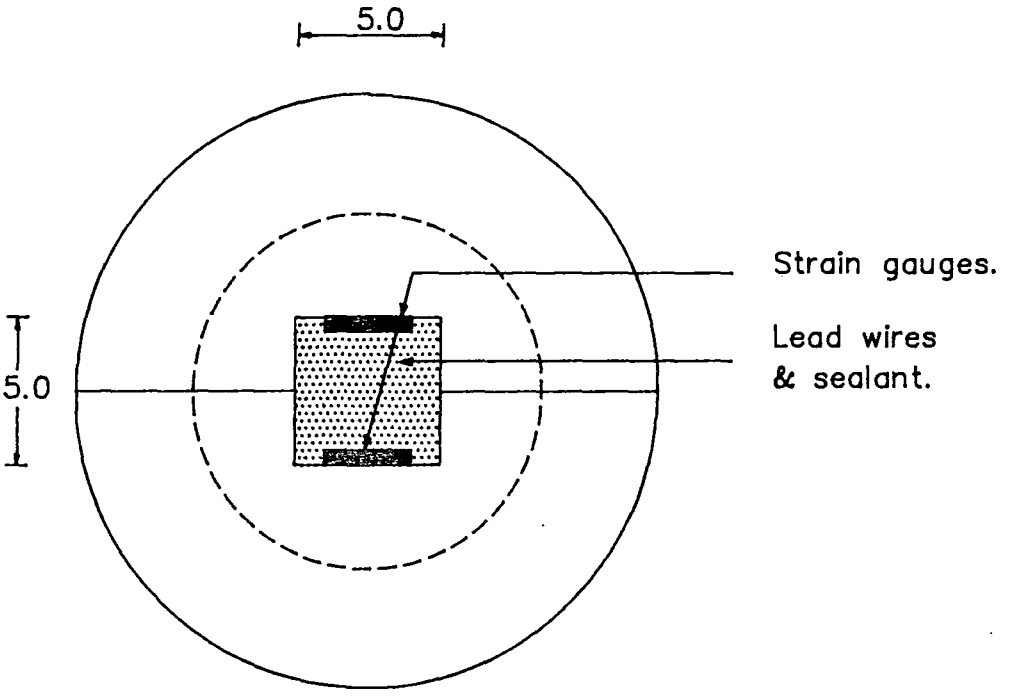

Rod diameter either 12 or 20 mm.

Fig. 3.1 Section Through Reinforcing Bar

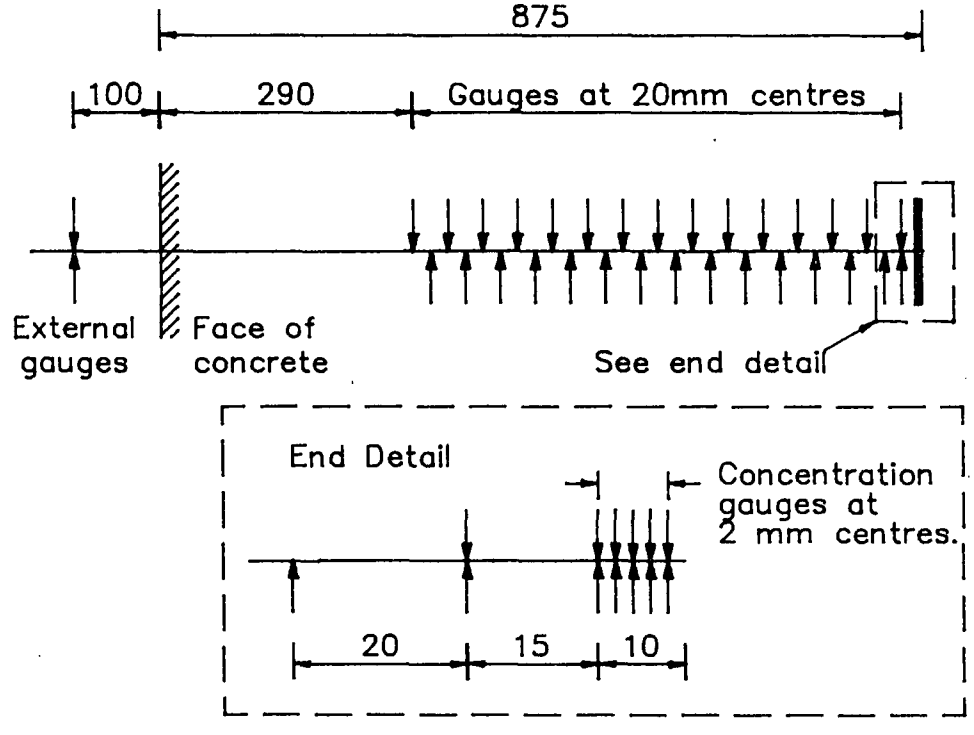

All dimensions mm

Rod A: 250mm lap length, with concentration gauges.

Rod B: Gauged similarly.

Fig. 3.2 Typical Strain Gauge Layout

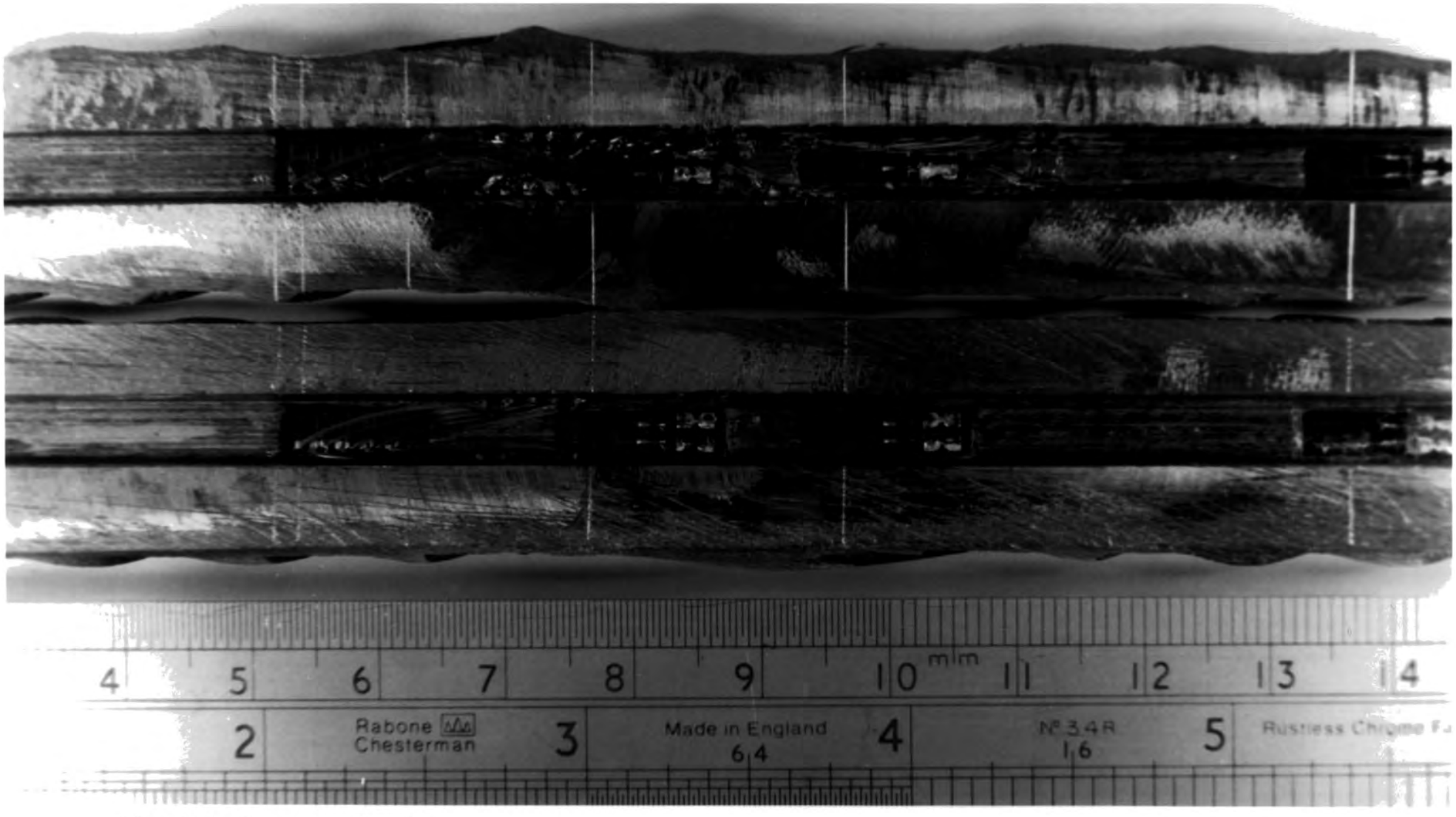

Fig. 3.3 Concentration Gauges

Fig. 3.4 Embedment Gauges

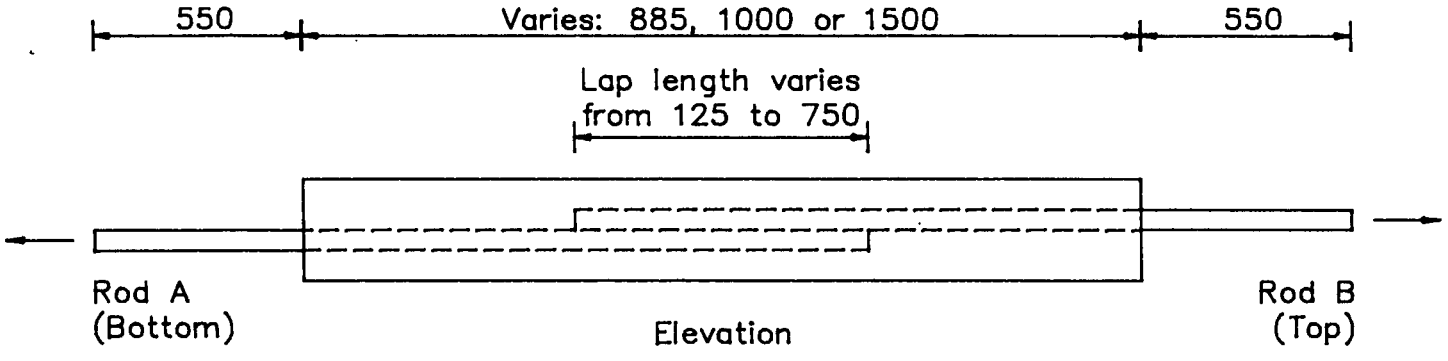

Specimen length:

Short term tension	1500
Long term tension	885
Compression	1000

All dimensions mm
Not to scale.

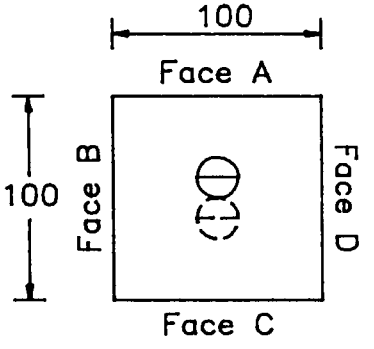

View from the top

Face A is the cast face.

Fig. 4.1 Specimen Layout

Specimen	Lap length (mm)	Rod diameter (mm)		Specimen length (mm)	Order tested
		A	B		
125T12/12	125	12	12	1500	10
250T12/12*	250	12	12	1500	3
500T12/12*	500	12	12	1500	1
750T12/12*	750	12	12	1500	2
250T20/20*	250	20	20	1500	4
500T20/20*	500	20	20	1500	5
750T20/20*	750	20	20	1500	6
250T12/20(A)†	250	20	12	1500	7
250T12/20(B)	250	20	12	1500	9
500T12/20	500	20	12	1500	8
250T20/20(E)	250	20	20	1500	14
250T20/20(L)	250	20	20	1500	12
500T20/20(L)	500	20	20	1500	13
125D12/12	125	12	12	885	11
125D12/12(L)	125	12	12	885	19
125C12/12	125	12	12	1000	17
250C12/12(A)	250	12	12	1000	15
250C12/12(B)	250	12	12	1000	16
125C20/20	125	20	20	1000	18
250C20/20(E)	250	20	20	1000	20

* Groove stopped 5 mm short of lap end.

† Cover to 12 and 20 mm rods differed

Fig. 4.2 Specimen Details

Specimen	Rod area (mm^2) A	B	Concrete dimensions (mm)	Compressive strength (N/mm^2)	Tensile strength (N/mm^2)	Age at test (Days)
125T12/12	77.7	88.8	101 × 101	51.4	3.1	27
250T12/12	96.7	80.2	103 × 100	51.2	2.6	29
500T12/12	88.4	88.7	101 × 101	48.1	2.7	29
750T12/12	89.2	105.1	103 × 100	50.1	2.8	30
250T20/20	317.5	328.5	101 × 101	46.2	2.5	27
500T20/20	308.6	296.5	102 × 101	48.8	2.3	27
750T20/20	319.4	312.1	101 × 101	49.5	2.4	29
250T12/20(A)	321.1	80.8	101 × 101	41.9	2.5	29
250T12/20(B)	319.4	86.8	101 × 102	53.8	3.0	28
500T12/20	295.8	87.8	101 × 102	49.3	2.8	29
250T20/20(E)	261.6	272.6	101 × 102	55.3	2.8	28
250T20/20(L)	283.8	259.6	101 × 102	58.4	2.9	27
500T20/20(L)	256.6	244.1	101 × 102	61.2	3.1	27
125D12/12	84.5	81.4	101 × 102	47.0	3.0	140
125D12/12(L)	67.2	91.5	101 × 102	60.8	3.6	100
125C12/12	87.8	87.8	100 × 101	53.4	3.0	29
250C12/12(A)	91.6	91.6	101 × 102	51.5	3.1	28
250C12/12(B)	90.5	90.5	104 × 101	54.3	3.0	33
125C20/20	309.6	309.6	101 × 102	60.4	3.2	29
250C20/20(E)	314.3	314.3	101 × 100	54.2	3.0	27

Fig. 4.3 Specimen Properties

Specimen 125D12/12(L)

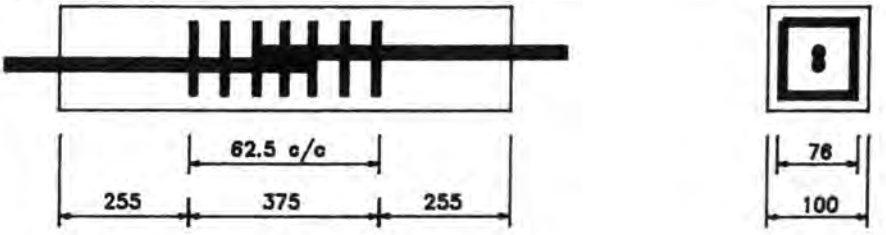

Specimen 250T20/20(L)

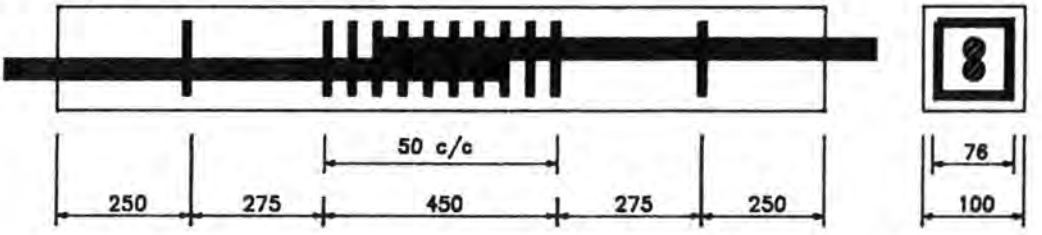

Specimen 500T20/20(L)

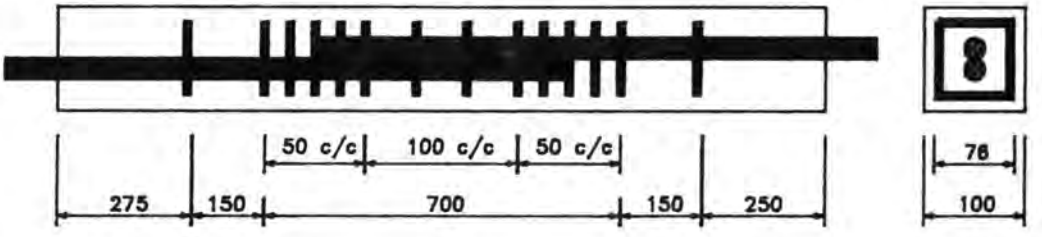

Specimen 250T20/20(E)

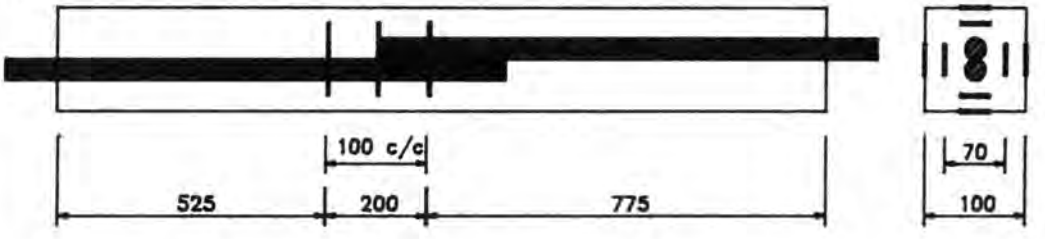

Links: 6mm diameter mild steel.

All dimensions mm

6mm diameter corner bars, supporting links, not shown.

Not to scale

Fig. 4.4 Link and Embedment Gauge Layout

Fig. 4.5 Tension Rig

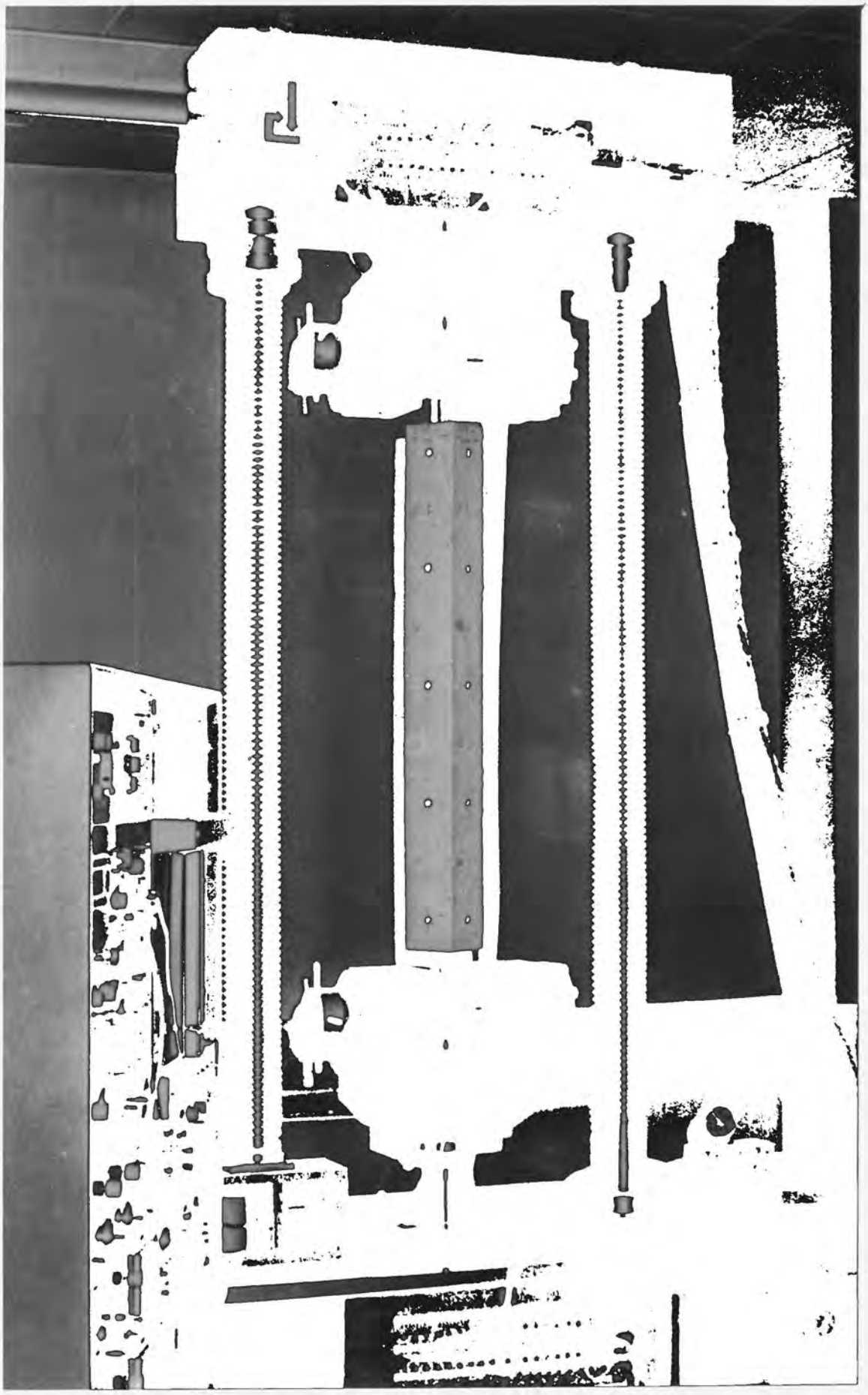

Fig. 4.6 Dartec Rig

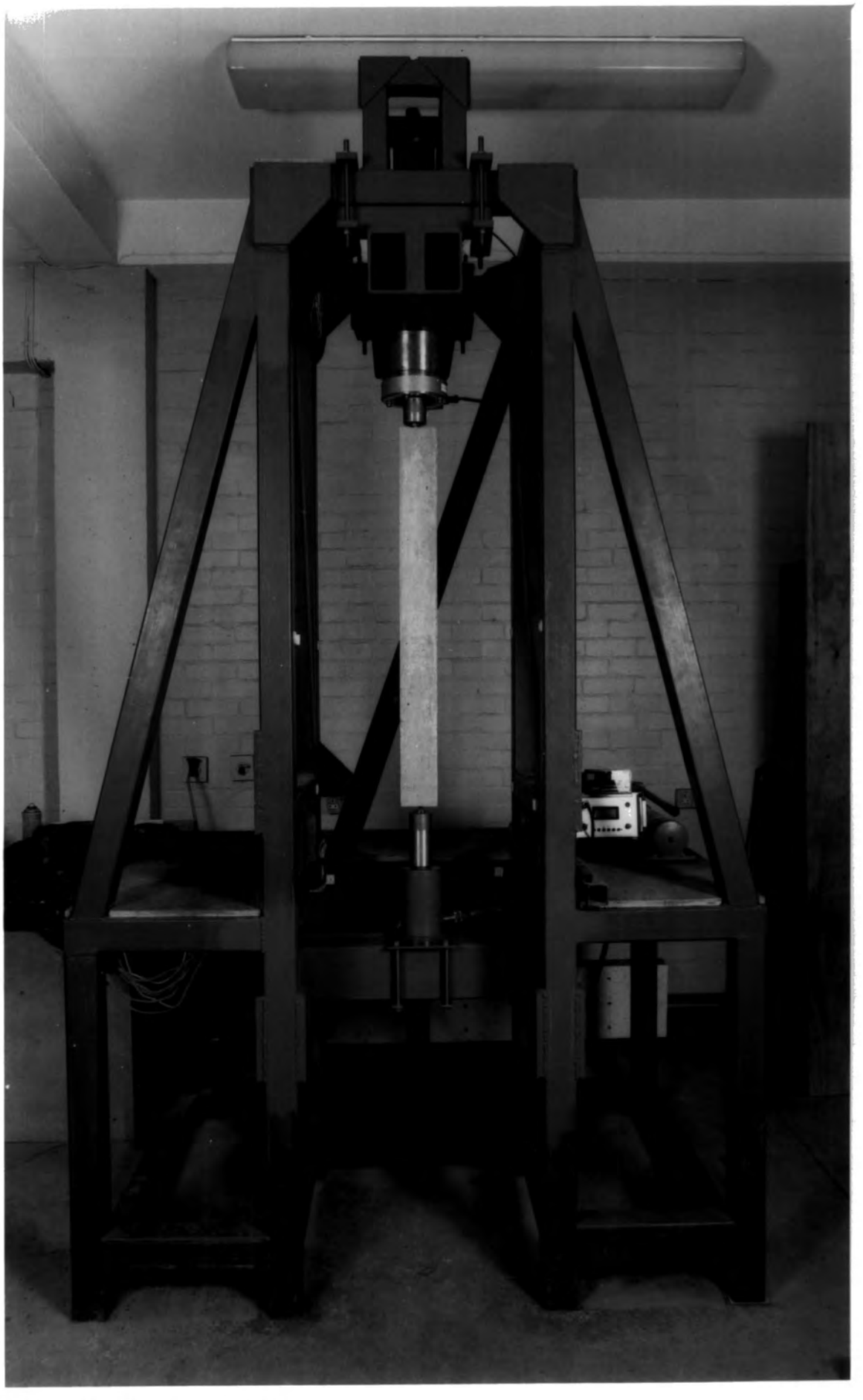

Fig. 4.7 Compression Rig

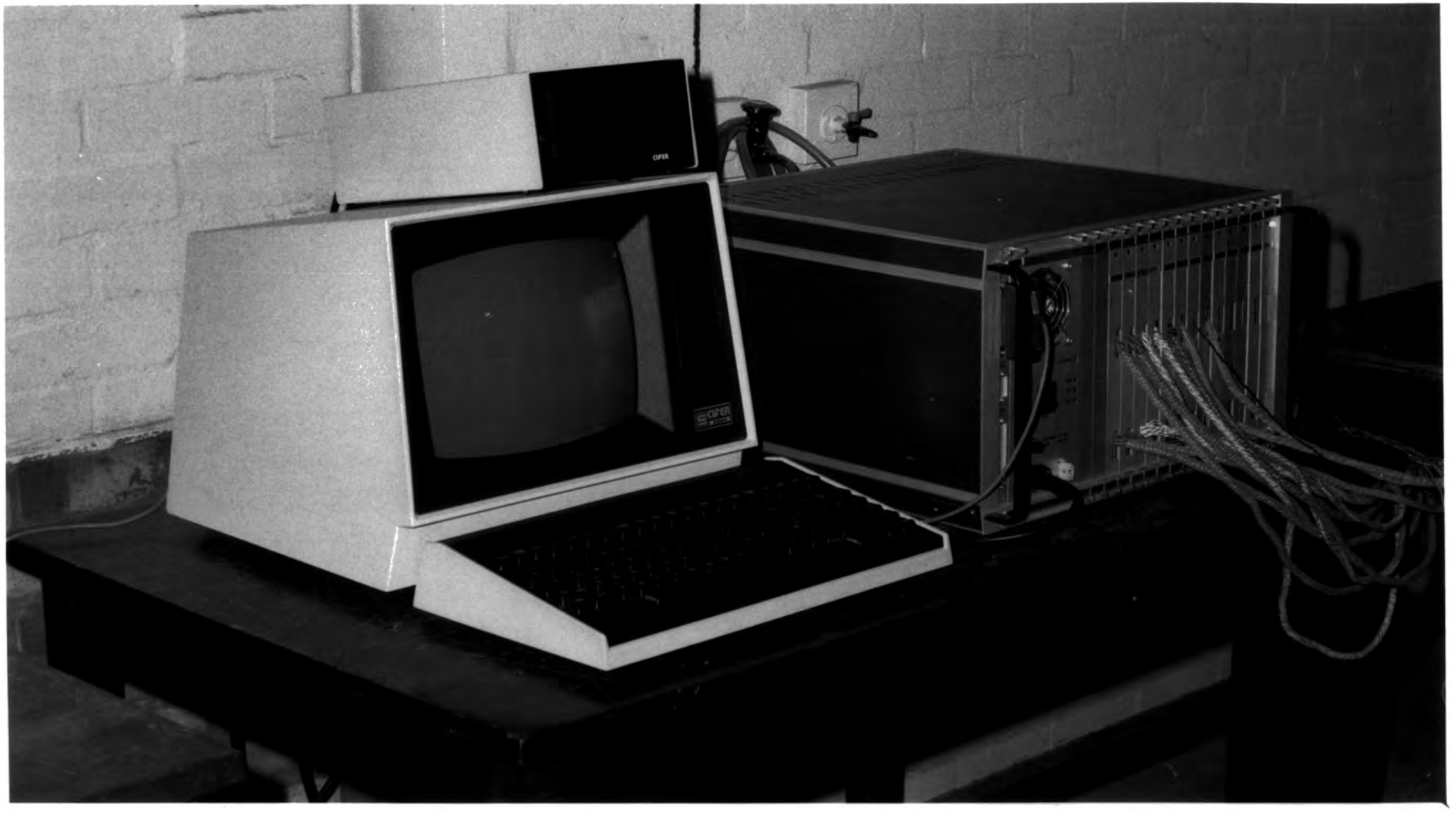

Fig. 5.1 Data Logger

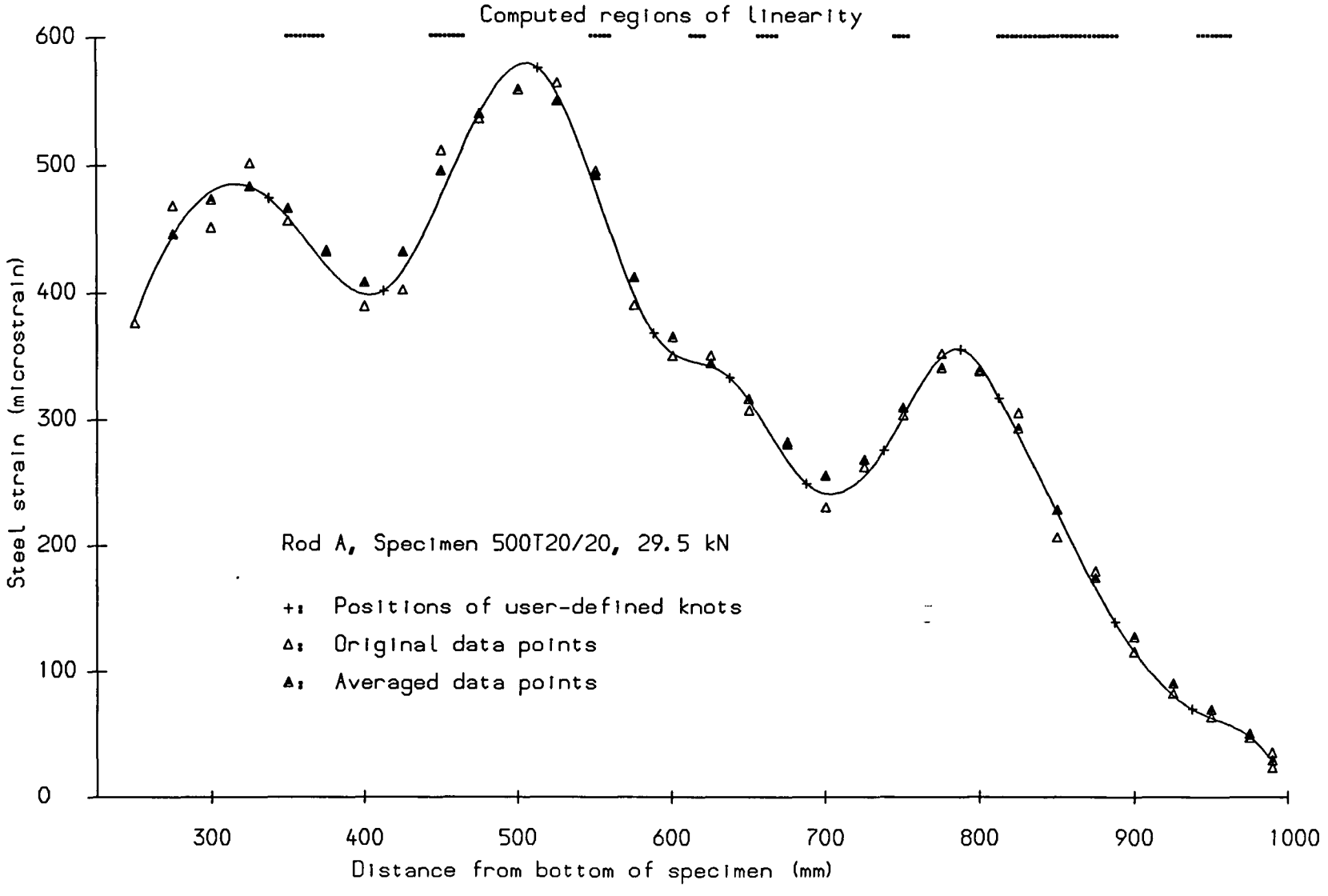

Fig. 5.2 Example of Cubic Spline Curve Fit

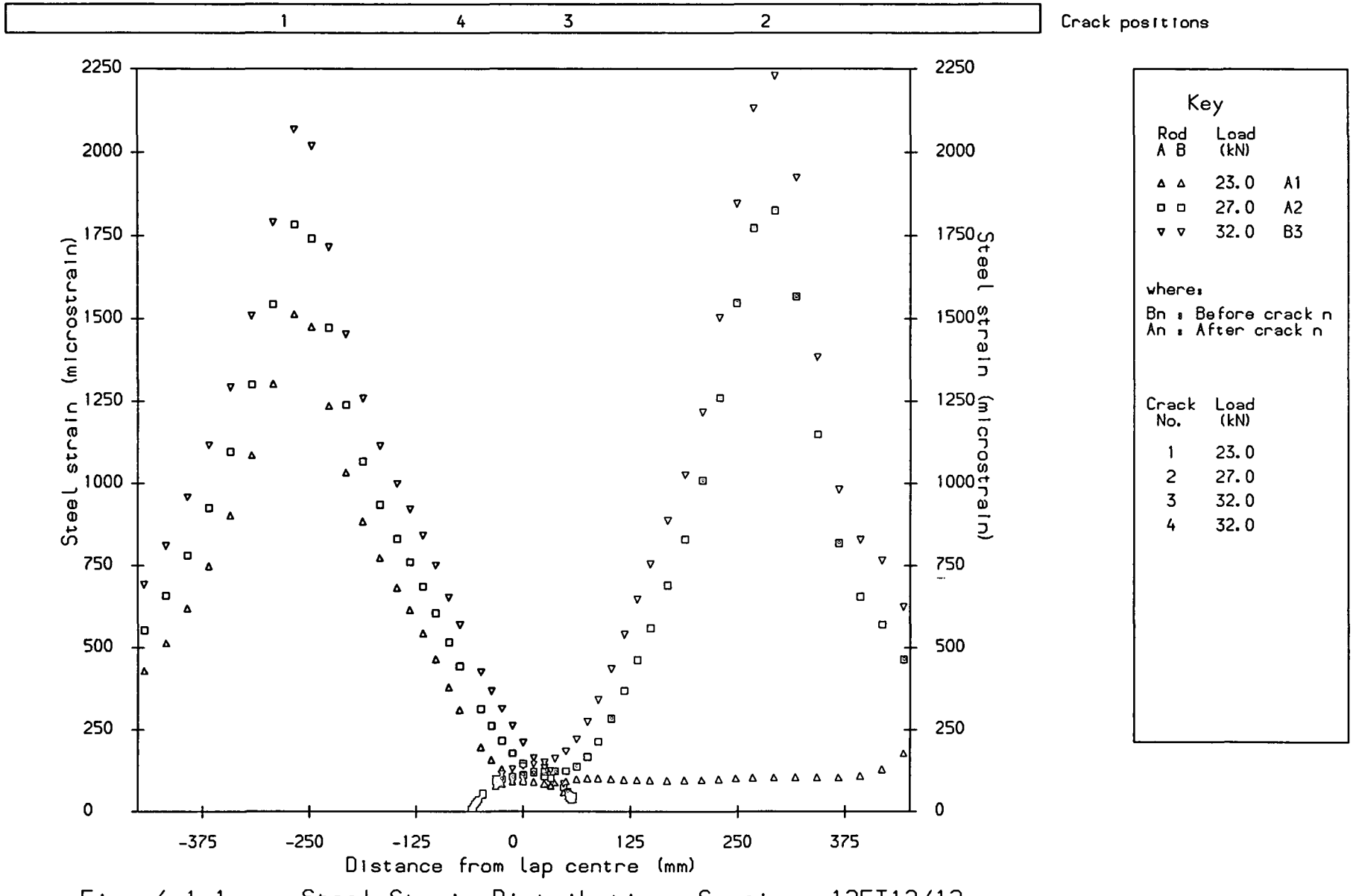

Fig. 6.1.1 Steel Strain Distribution Specimen 125T12/12

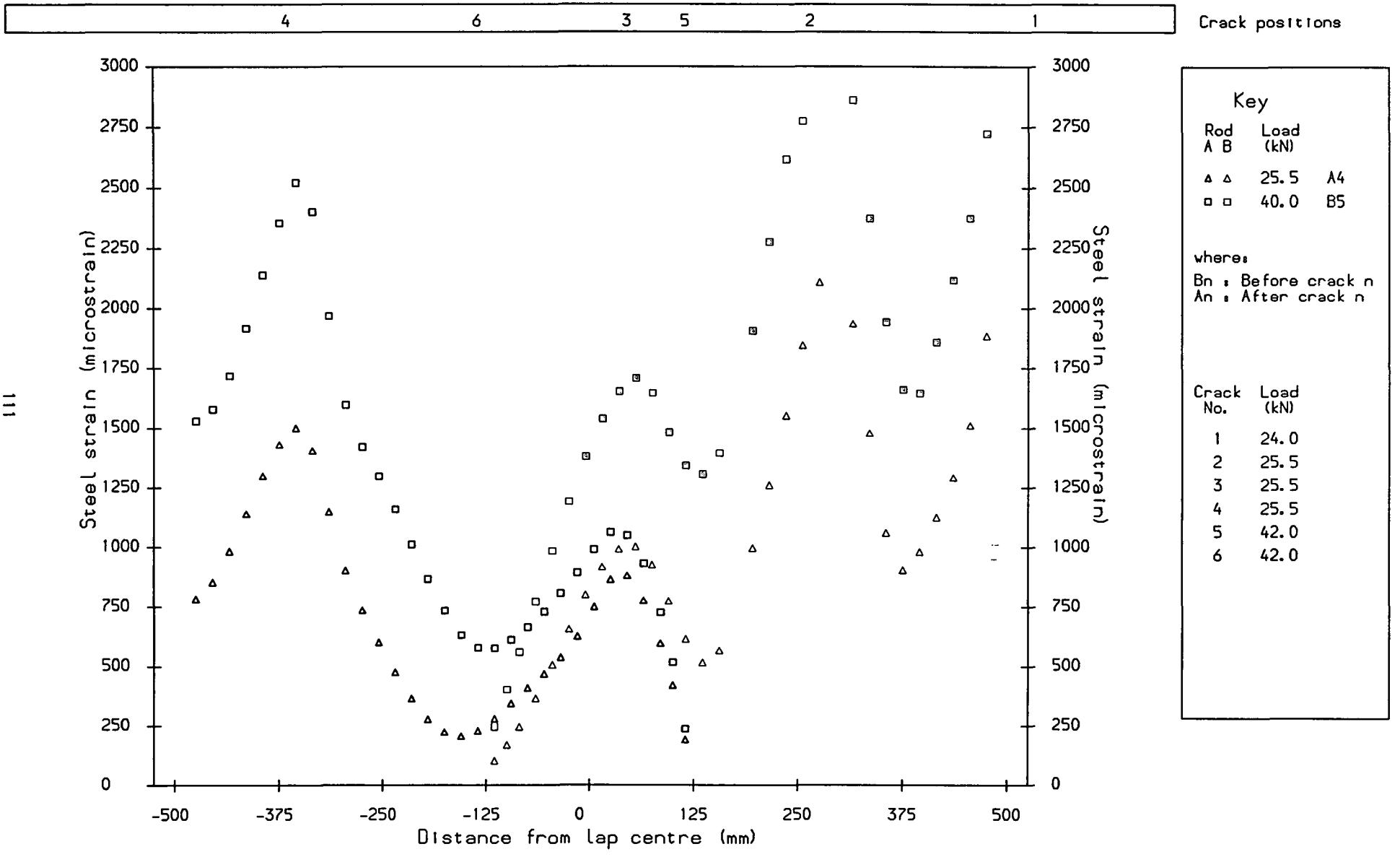

Fig. 6.1.2 Steel Strain Distribution Specimen 250T12/12

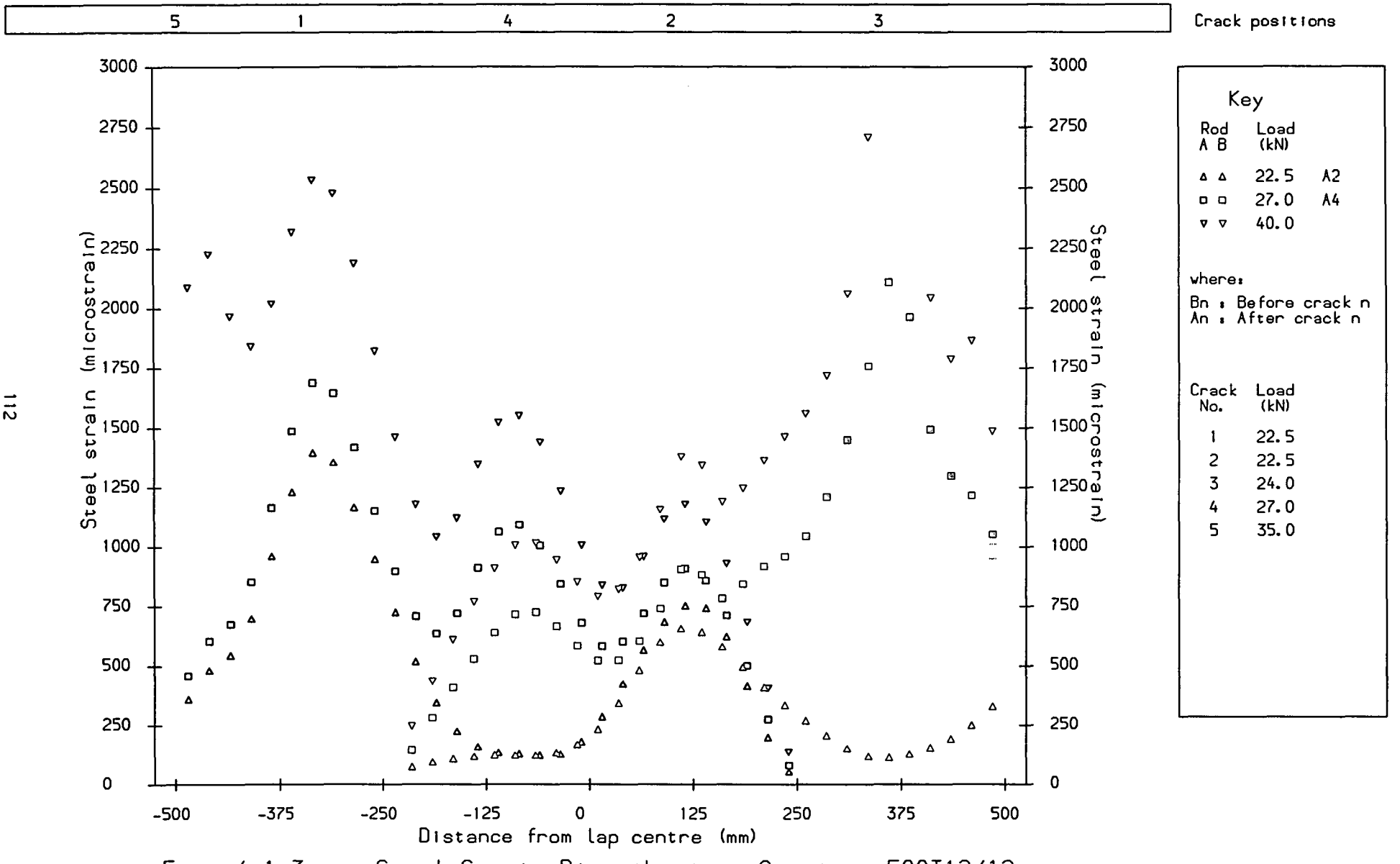

Fig. 6.1.3 Steel Strain Distribution Specimen 500T12/12

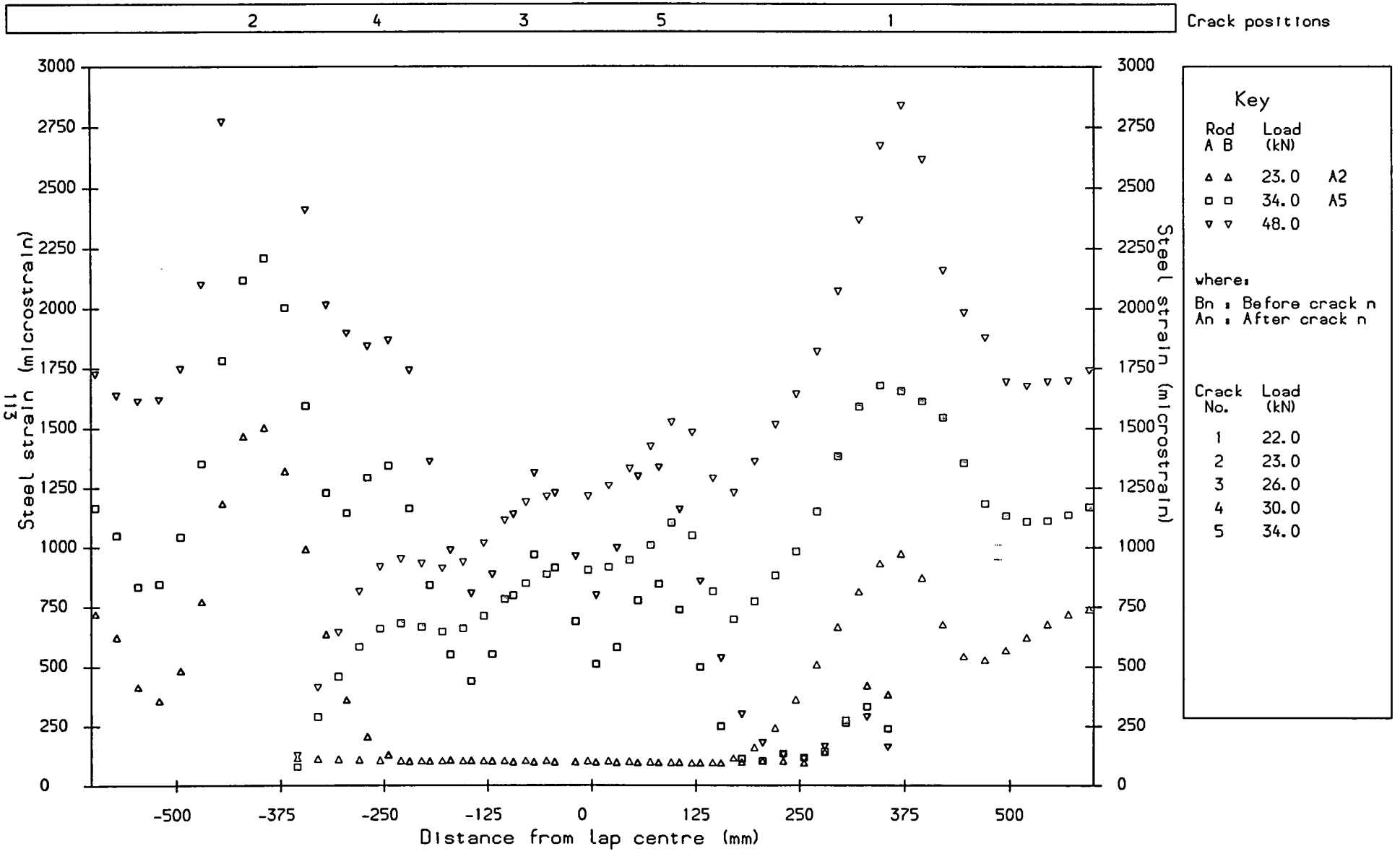

Fig. 6.1.4 Steel Strain Distribution Specimen 750T12/12

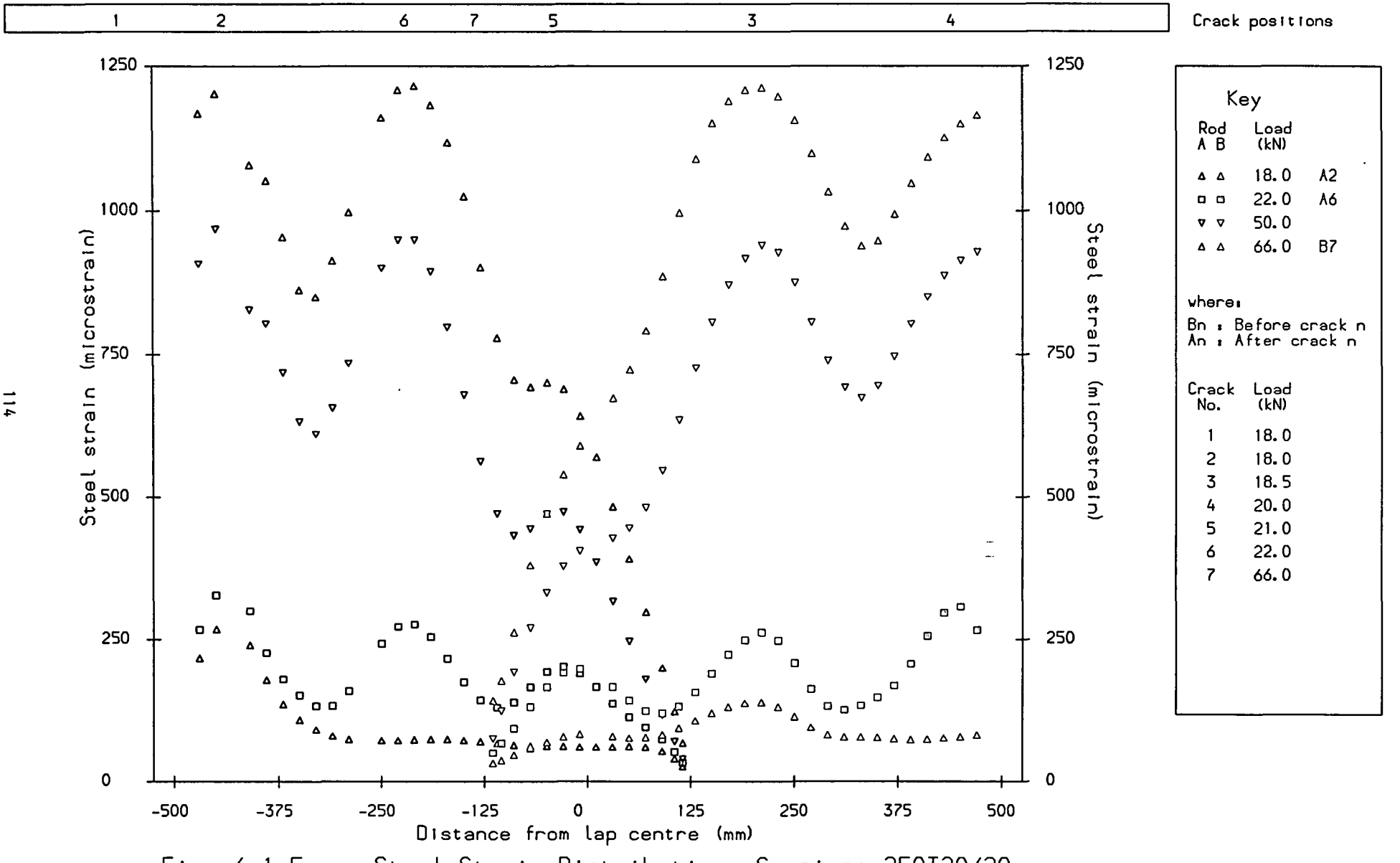

Fig. 6.1.5 Steel Strain Distribution Specimen 250T20/20

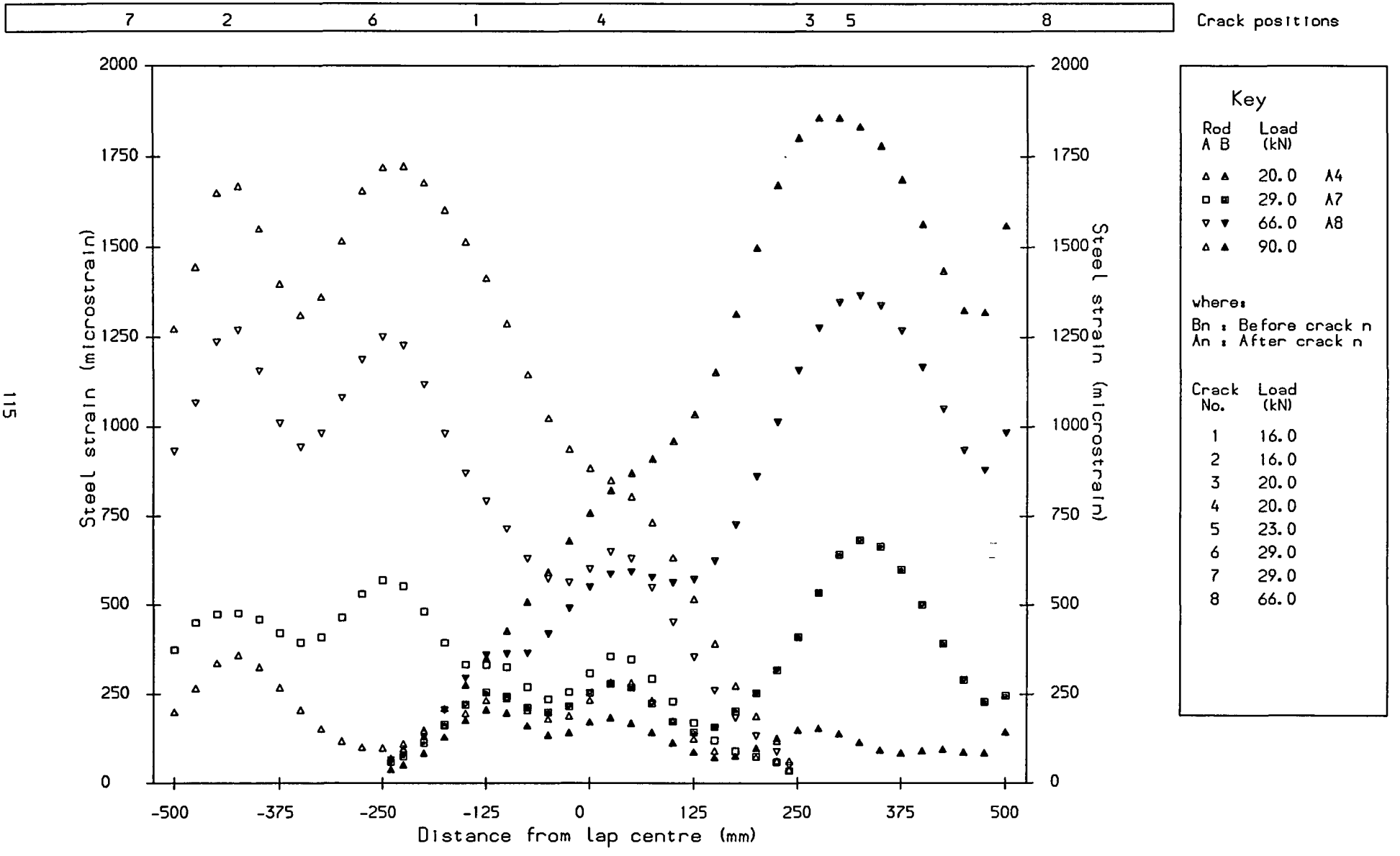

Fig. 6.1.6 Steel Strain Distribution Specimen 500T20/20

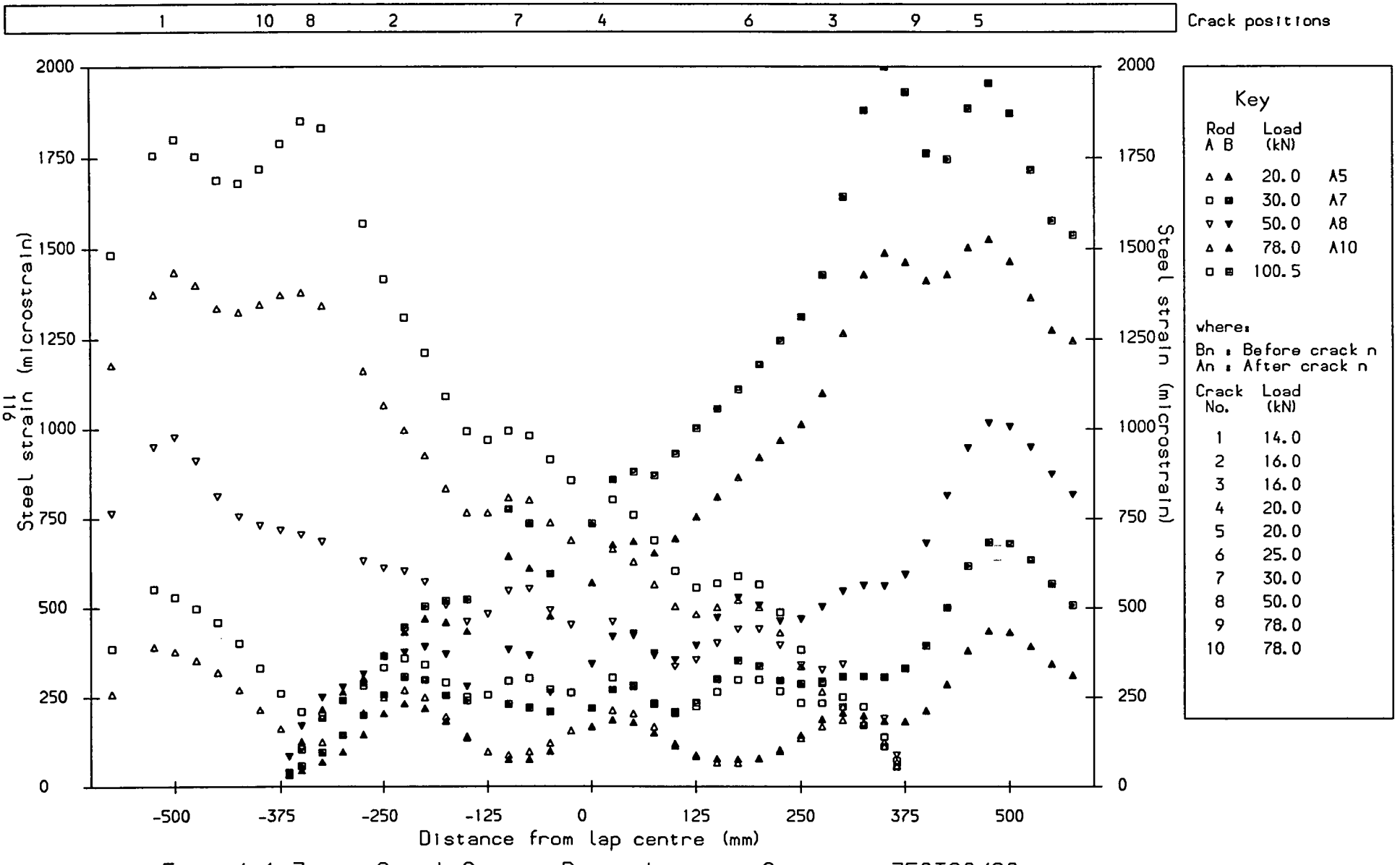

Fig. 6.1.7 Steel Strain Distribution Specimen 750T20/20

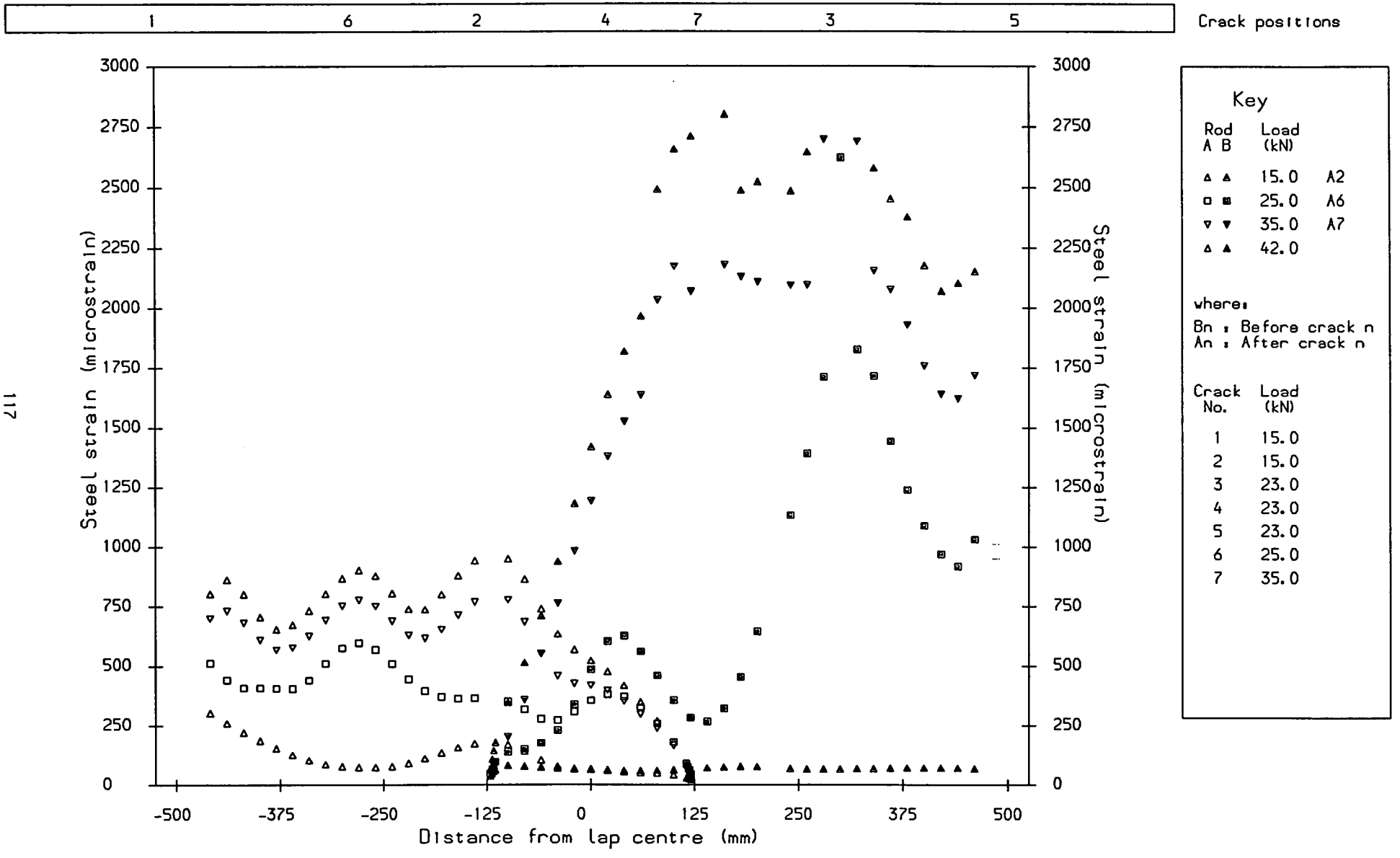

Fig. 6.1.8 Steel Strain Distribution Specimen 250T12/20(A)

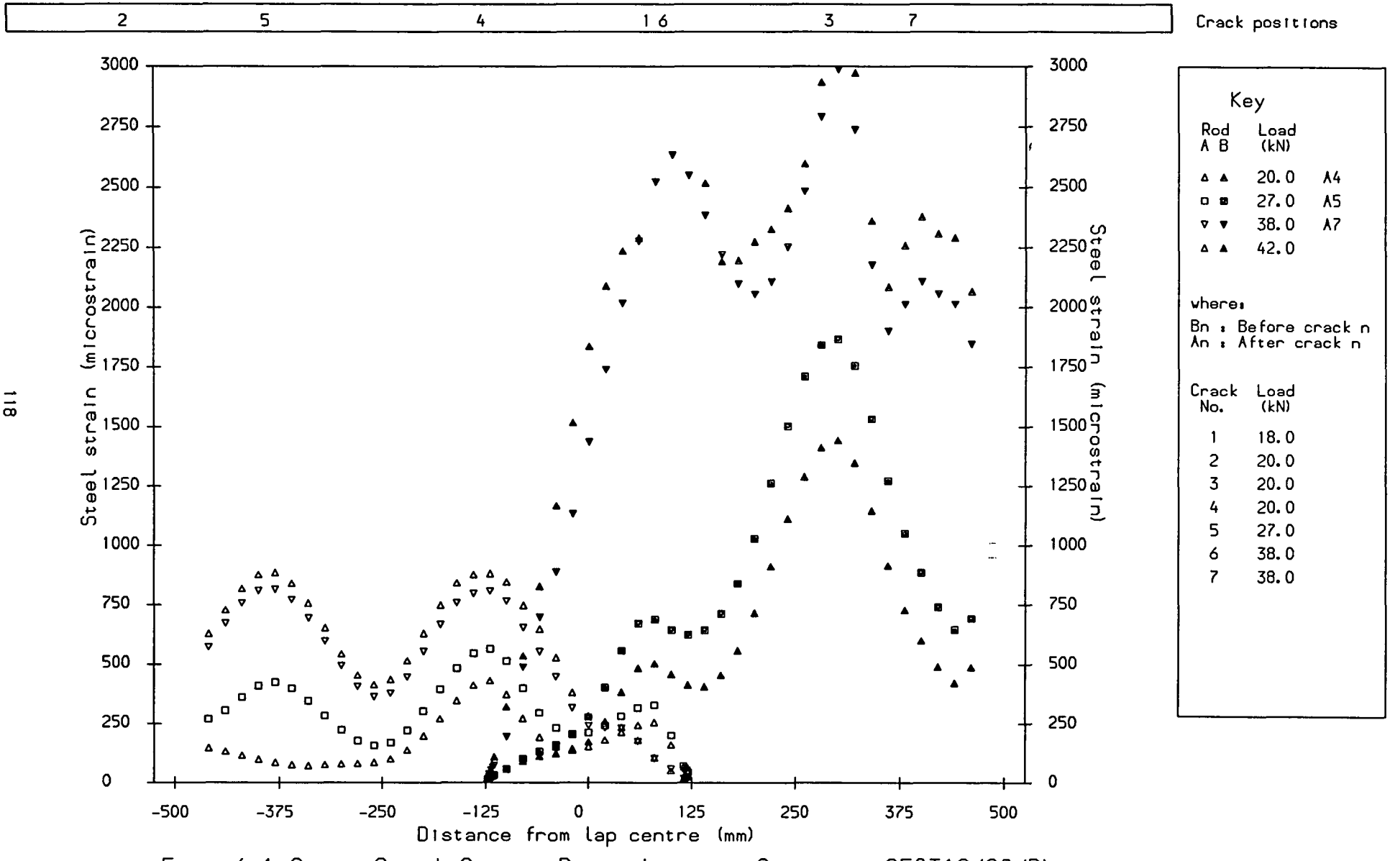

Fig. 6.1.9 Steel Strain Distribution Specimen 250T12/20(B)

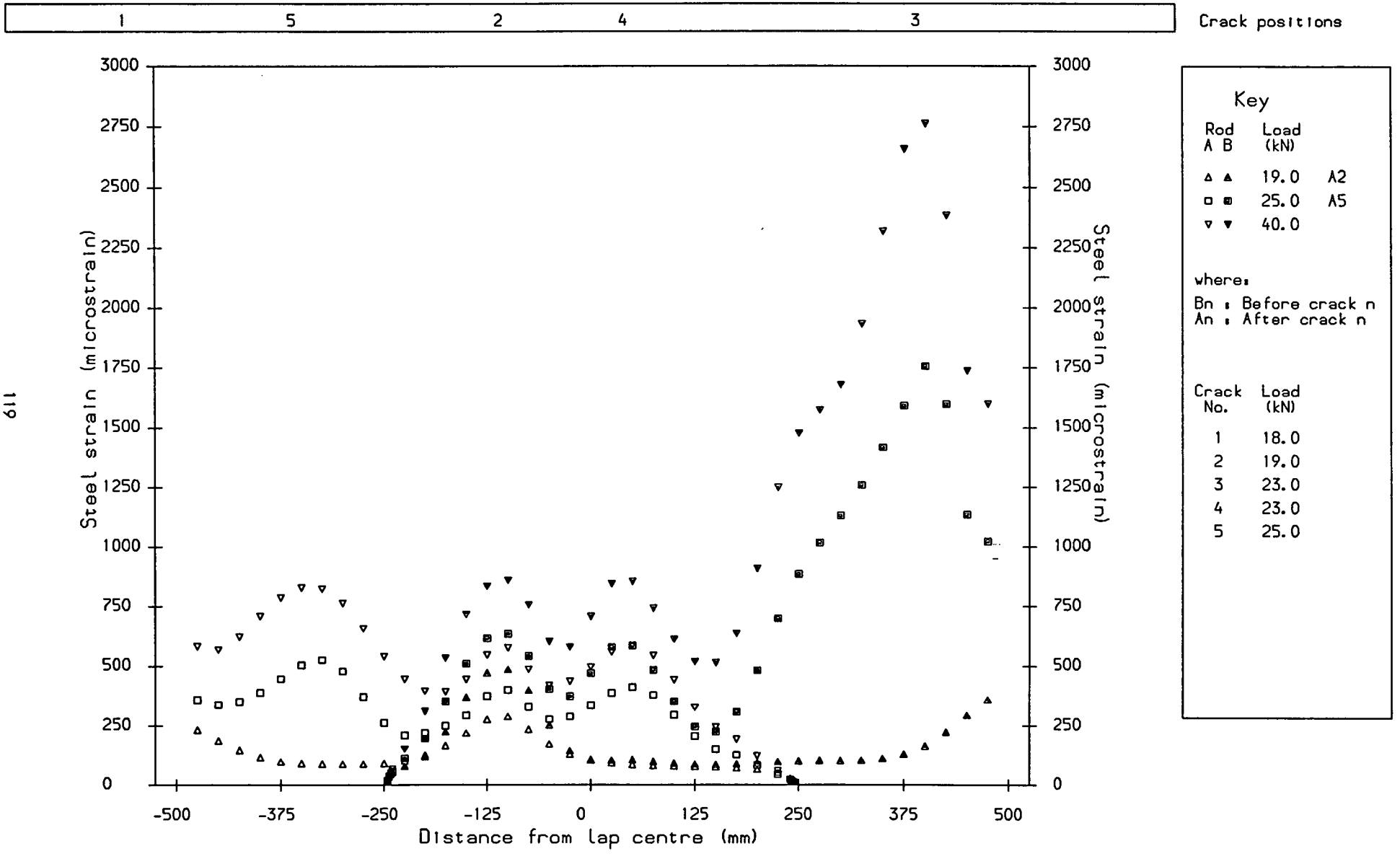

Fig. 6.1.10 Steel Strain Distribution Specimen 500T12/20

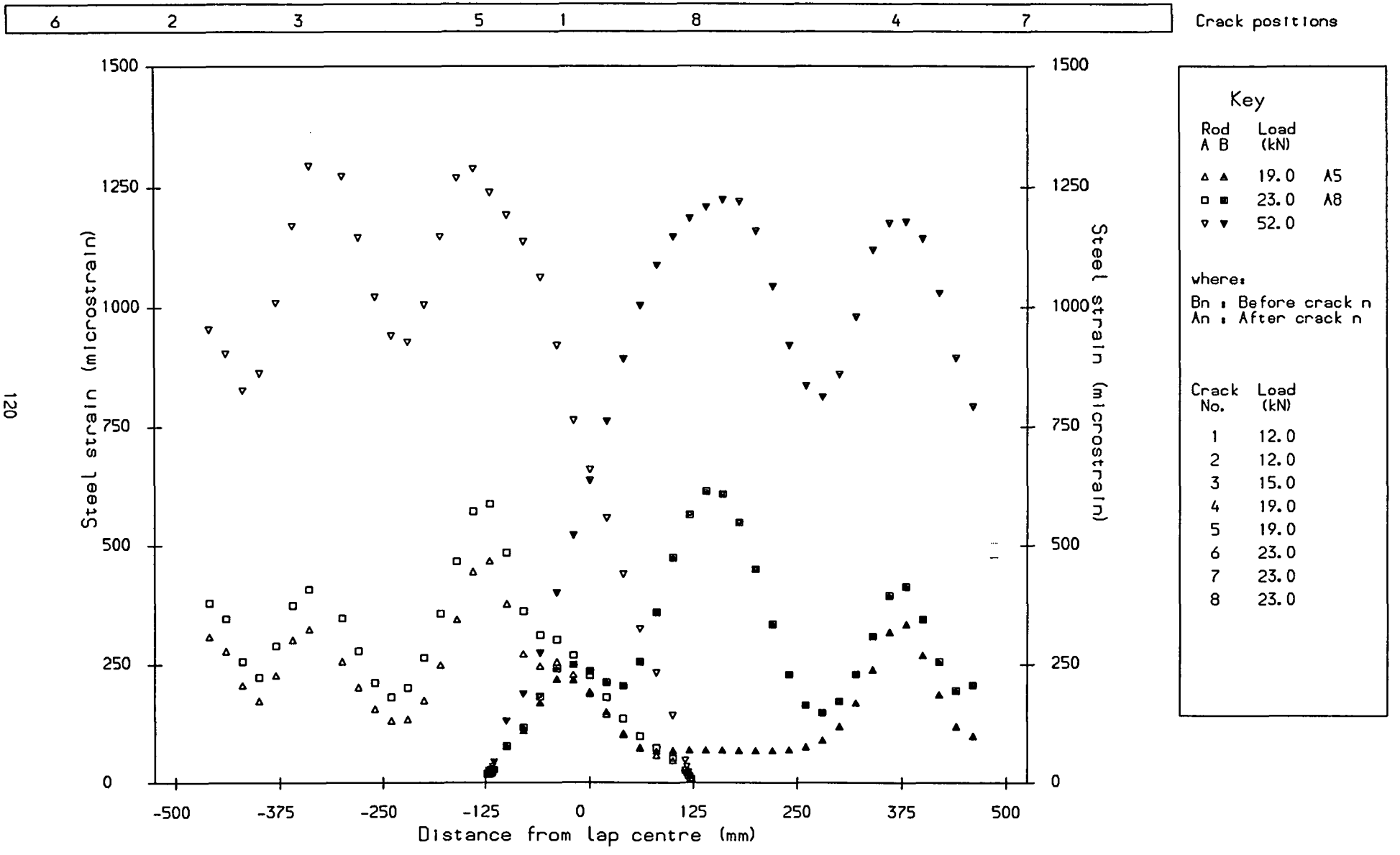

Fig. 6.1.11 Steel Strain Distribution Specimen 250T20/20(E)

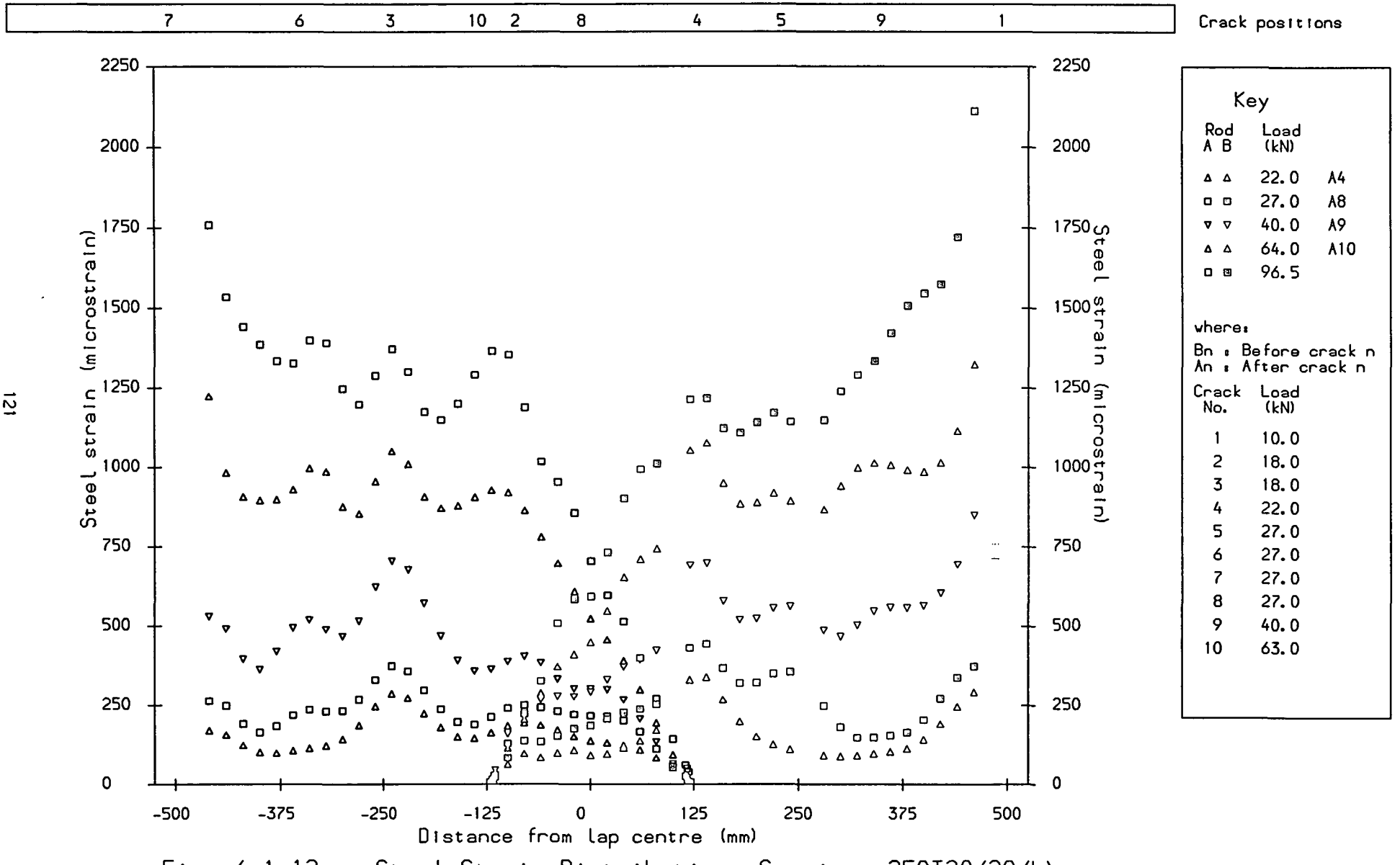

Fig. 6.1.12 Steel Strain Distribution Specimen 250T20/20(L)

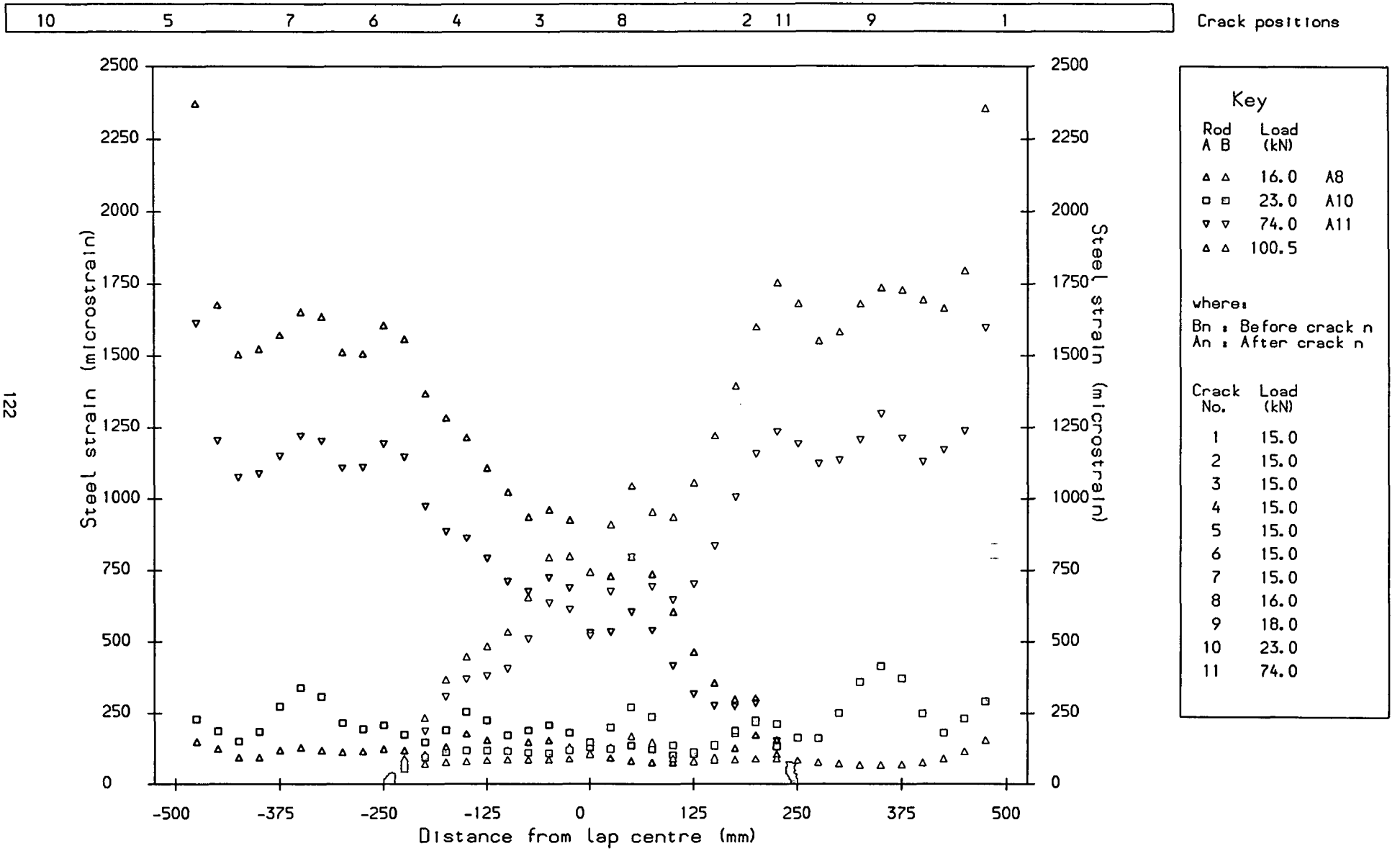

Fig. 6.1.13 Steel Strain Distribution Specimen 500T20/20(L)

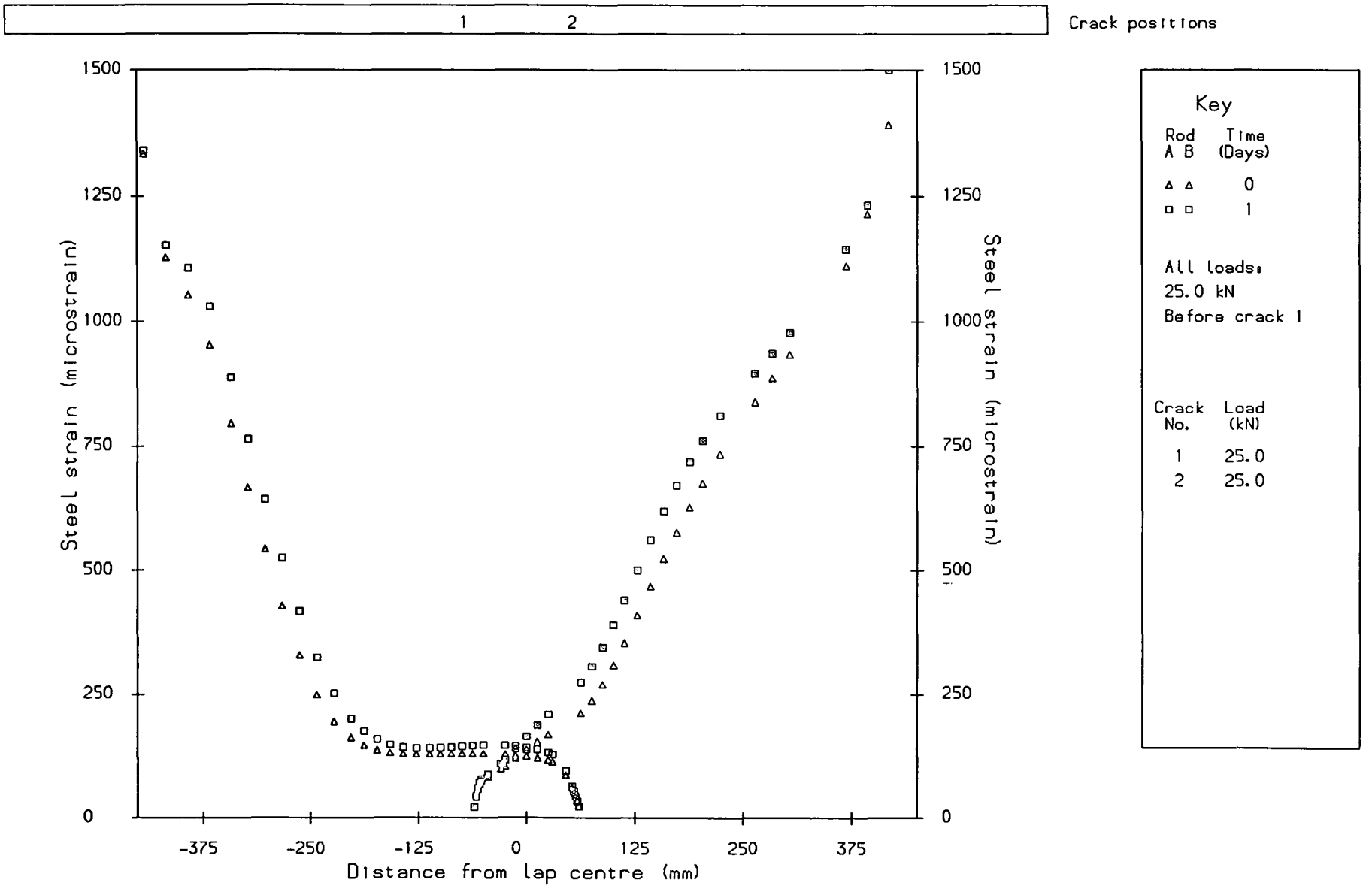

Fig. 6.1.14 Steel Strain Distribution Specimen 125D12/12

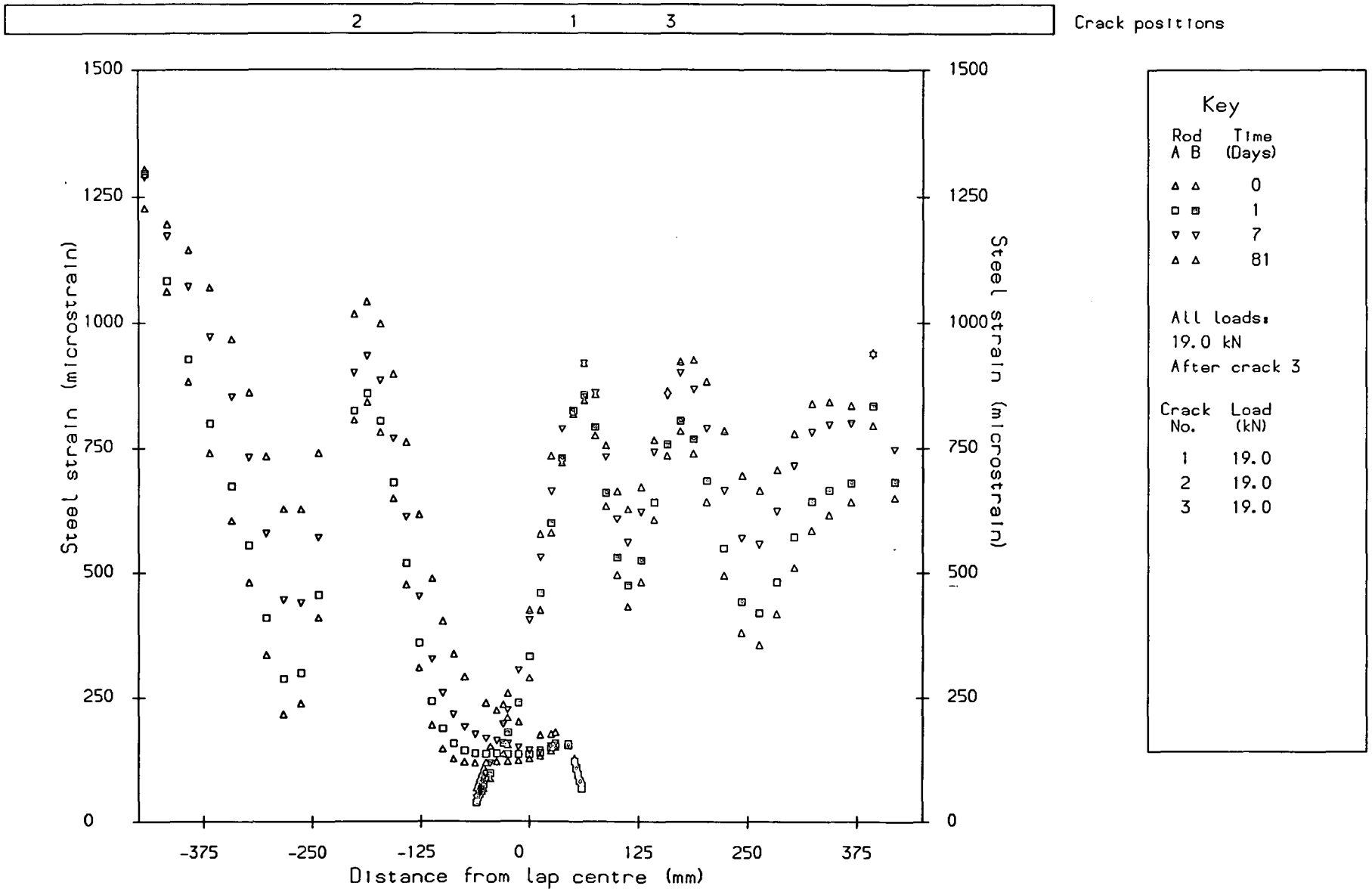

Fig. 6.1.15 Steel Strain Distribution Specimen 125D12/12(L)

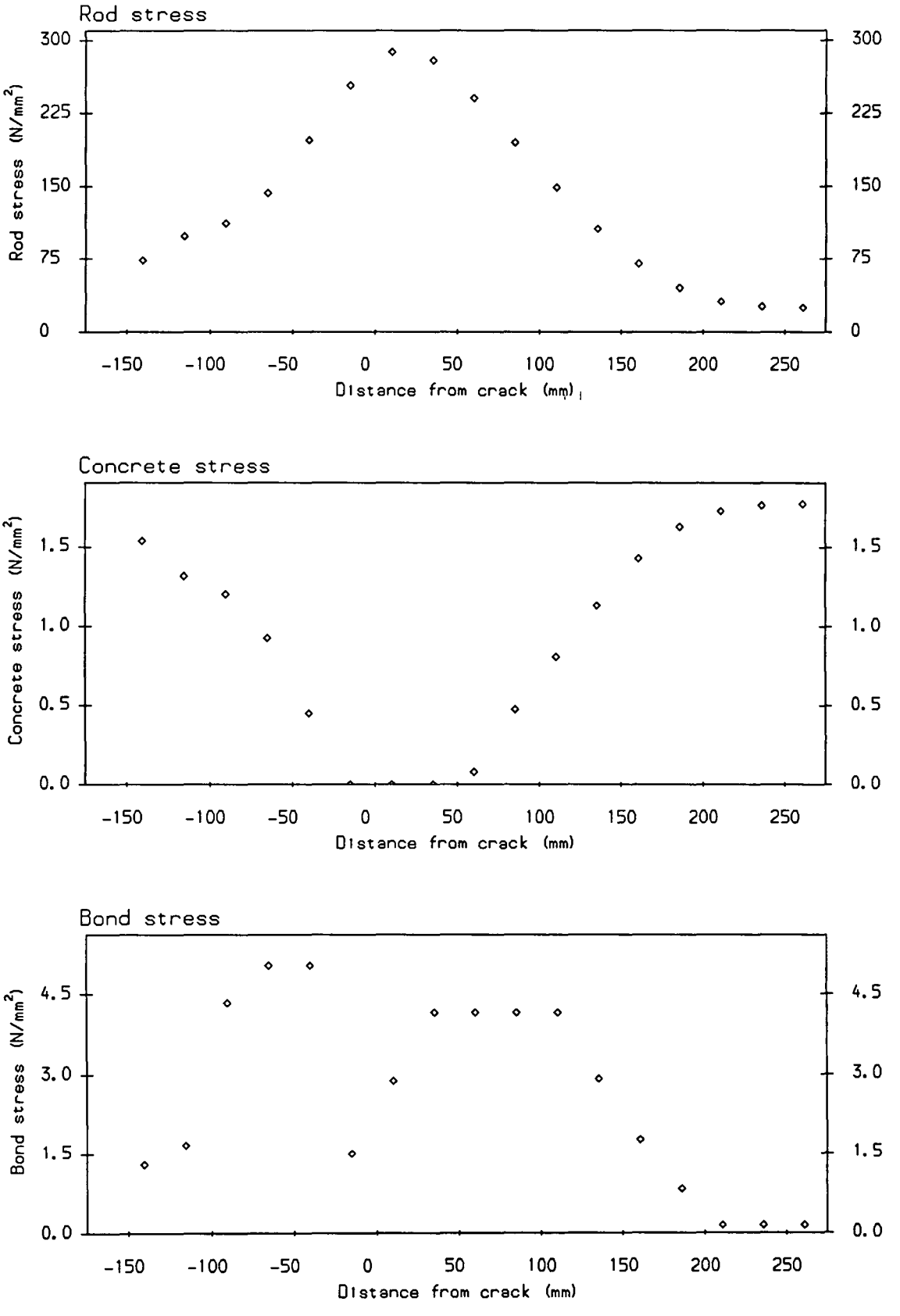

All plots: Crack 1, 500T12/12, 22.5kN

Fig. 6.2 Rod, Concrete and Bond Stresses at a Crack

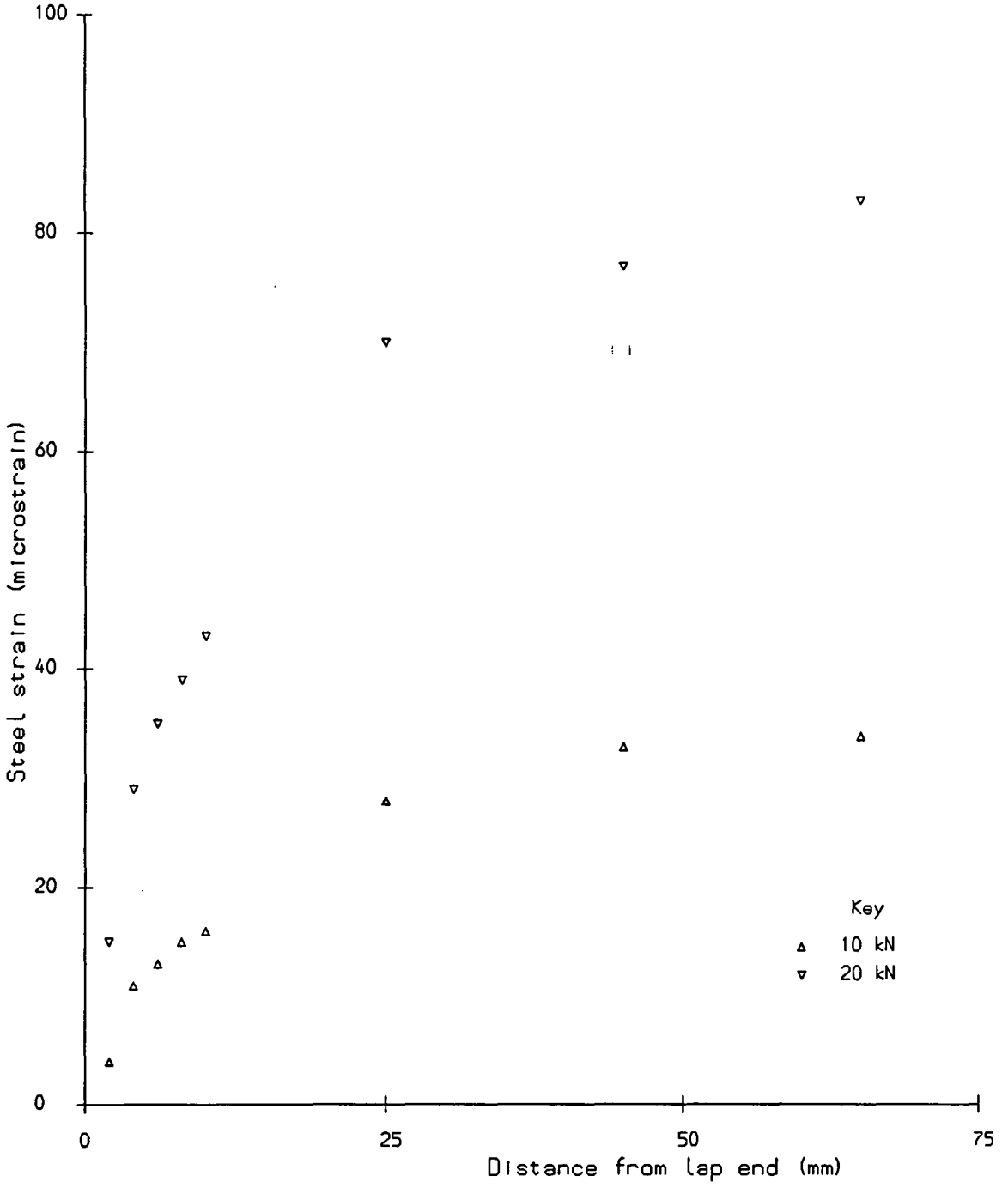

Fig. 6.3 Typical Concentration Gauge Result
Specimen 250T12/20(B), rod B (T12)

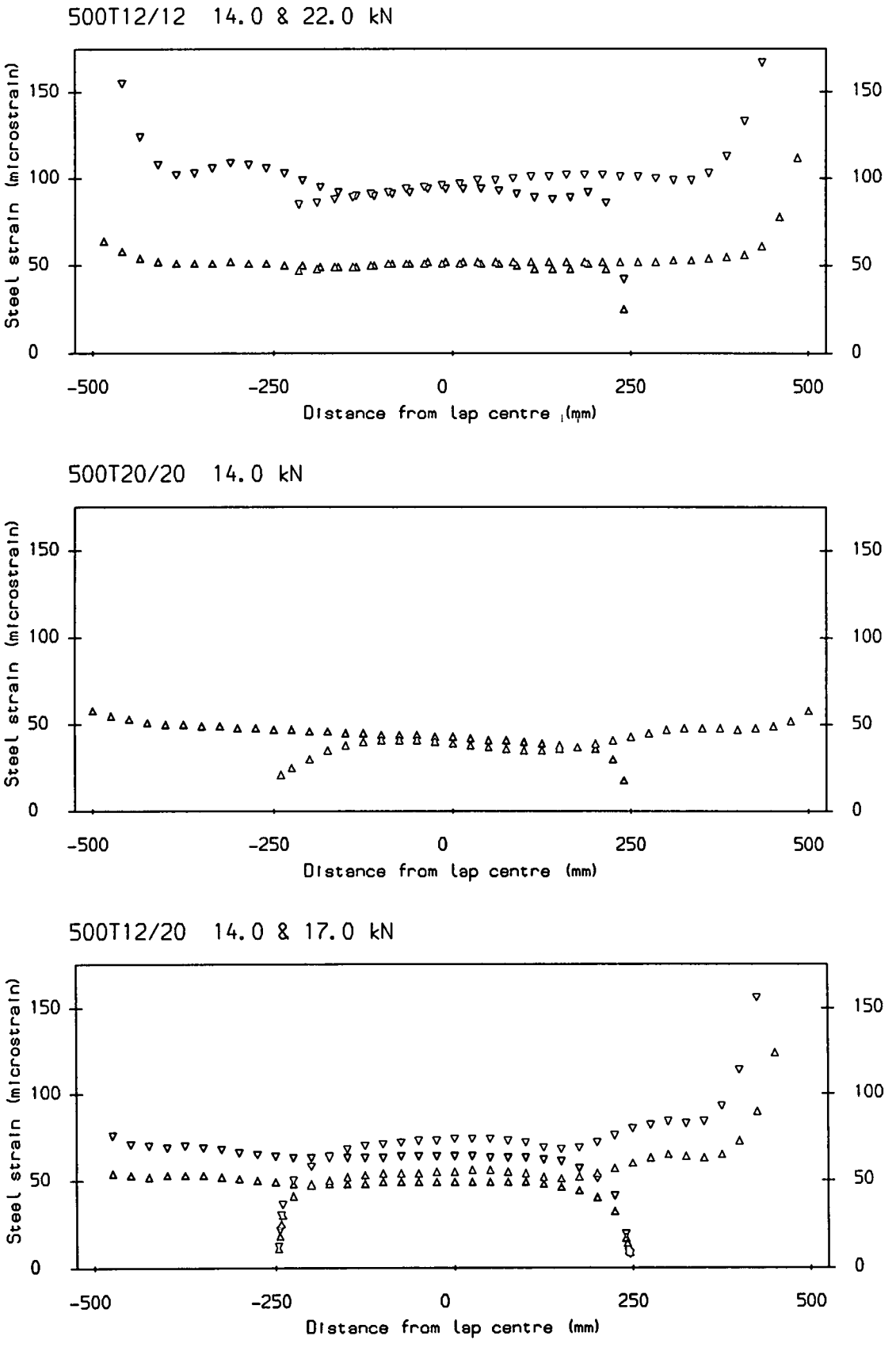

Fig. 6.4 Precrack Reinforcement Strain Distributions

Specimen	Crack number 1		2		3		4		5		6		7		8		9		10		11	
125T12/12	23.0		27.0		32.0		32.0															
	103	1509	117	1821	216	–	–	–														
250T12/12	24.0		25.5		25.5	L	25.5		42.0		42.0											
	–	–	112	2089	123	971	120	1495	1301	–	571	–										
500T12/12	22.5		22.5	L	24.0		27.0	L	35.0													
	135	1375	117	652	122	1918	159	1087	701	1803												
750T12/12	22.0		23.0		26.0	L	30.0	L	34.0	L												
	107	916	122	1497	121	725	231	1175	228	1099												
250T20/20	18.0		18.0		18.5		20.0		21.0	L	22.0		66.0									
	–	–	–	–	83	138	97	253	97	174	121	275	–	–								
500T20/20	16.0	L	16.0		20.0		20.0	L	23.0		29.0		29.0		66.0							
	44	173	64	289	95	119	91	278	125	562	129	565	–	–	–	–						
750T20/20	14.0		16.0	L	16.0	L	20.0	L	20.0		25.0	L	30.0	L	50.0	L	78.0		78.0			
	59	261	49	222	57	143	69	201	111	428	98	298	138	299	392	680	1001	1484	1183	1375		
250T12/20(A)	15.0		15.0		23.0		23.0	L	23.0		25.0		35.0									
	–	–	62	170	111	2360	96	546	–	–	136	592	617	–								
250T12/20(B)	18.0	L	20.0		20.0		20.0		27.0		38.0	L	38.0									
	56	408	–	–	112	1437	69	425	109	419	1218	2569	1471	2100								
500T12/20	18.0		19.0	L	23.0		23.0	L	25.0													
	–	–	88	481	231	1636	125	530	118	521												
250T20/20(E)	12.0	L	12.0		15.0		19.0		19.0		23.0		23.0		23.0							
	81	147	–	–	88	227	67	303	77	464	–	–	–	–	94	611						
250T20/20(L)	10.0		18.0	L	18.0		22.0		27.0		27.0		27.0		27.0	L	40.0		63.0			
	–	–	114	136	111	188	79	317	132	330	136	190	–	–	169	212	386	554	736	923		
500T20/20(L)	15.0		15.0	L	15.0	L	15.0	L	15.0		15.0		15.0		16.0	L	18.0		23.0		74.0	
	–	–	48	119	105	139	74	161	–	–	60	111	51	109	86	163	68	323	–	–	977	1186
125D12/12	25.5		25.5																			
	–	–	–	–																		
125D12/12(L)	19.0		19.0		19.0																	
	74	804	101	821	121	779																
KEY	A	B	A : Load (kN)										B : L – denotes crack within lap									
	C	D	C : Pre-crack strain (microstrain)										D : Post-crack strain (microstrain)									

Fig. 6.5 Reinforcement Strains and Loads at Crack Formation

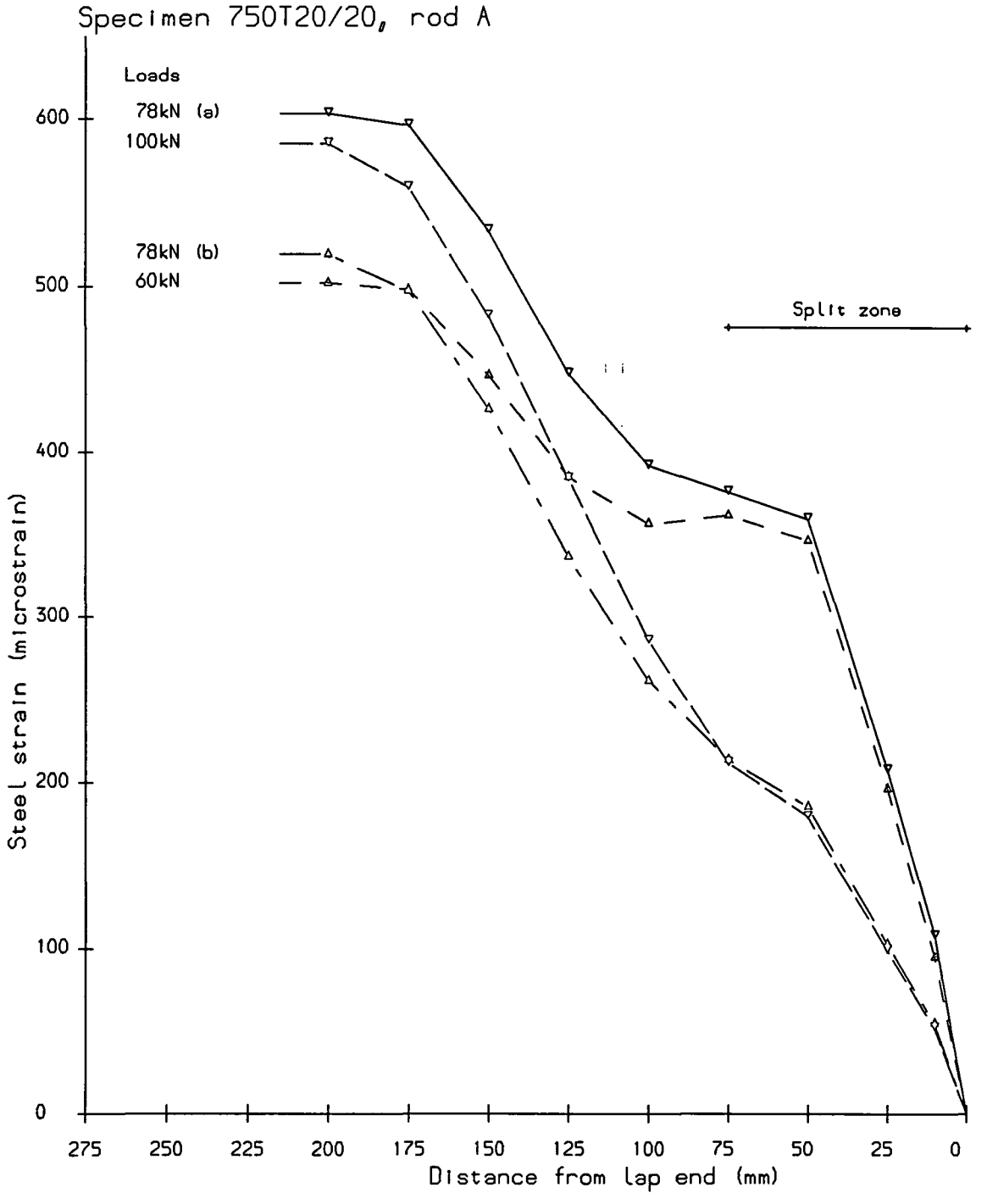

Fig. 6.6 Effect of Longitudinal Cracking on Steel Strain Distribution

Faces D & A

Face D

Fig. 6.7.1 Failed specimens Specimen 250T12/12

Faces B & C

Face B

Fig. 6.7.2 Failed specimens Specimen 250T20/20

Faces A & B

Face C

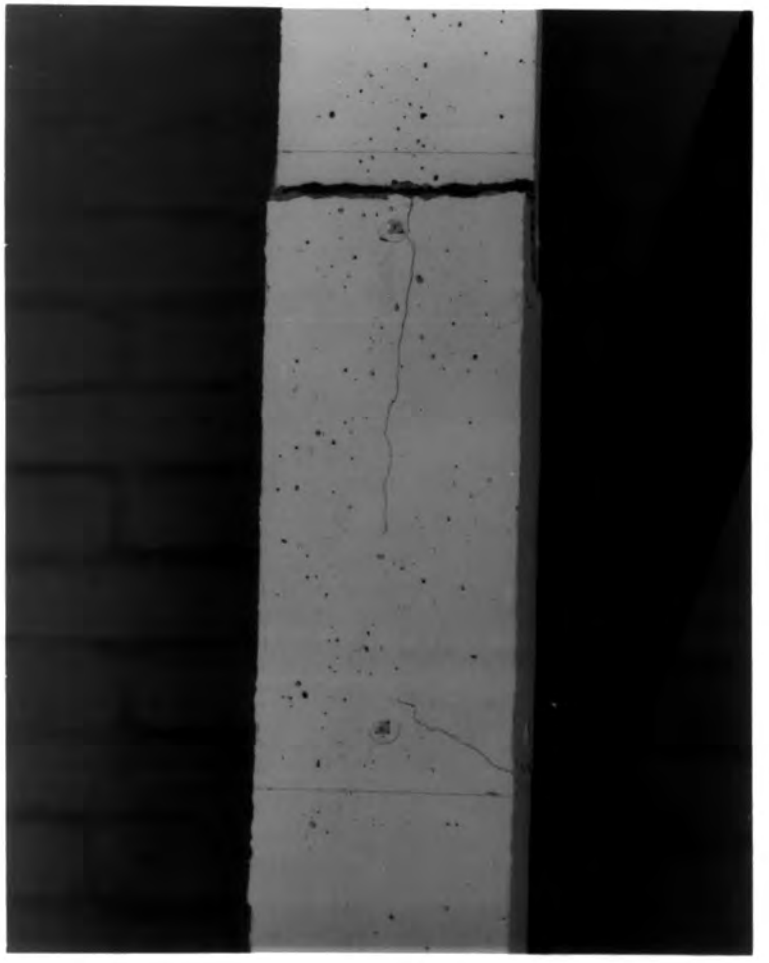

Fig. 6.7.3 Failed specimens Specimen 250T12/20(B)

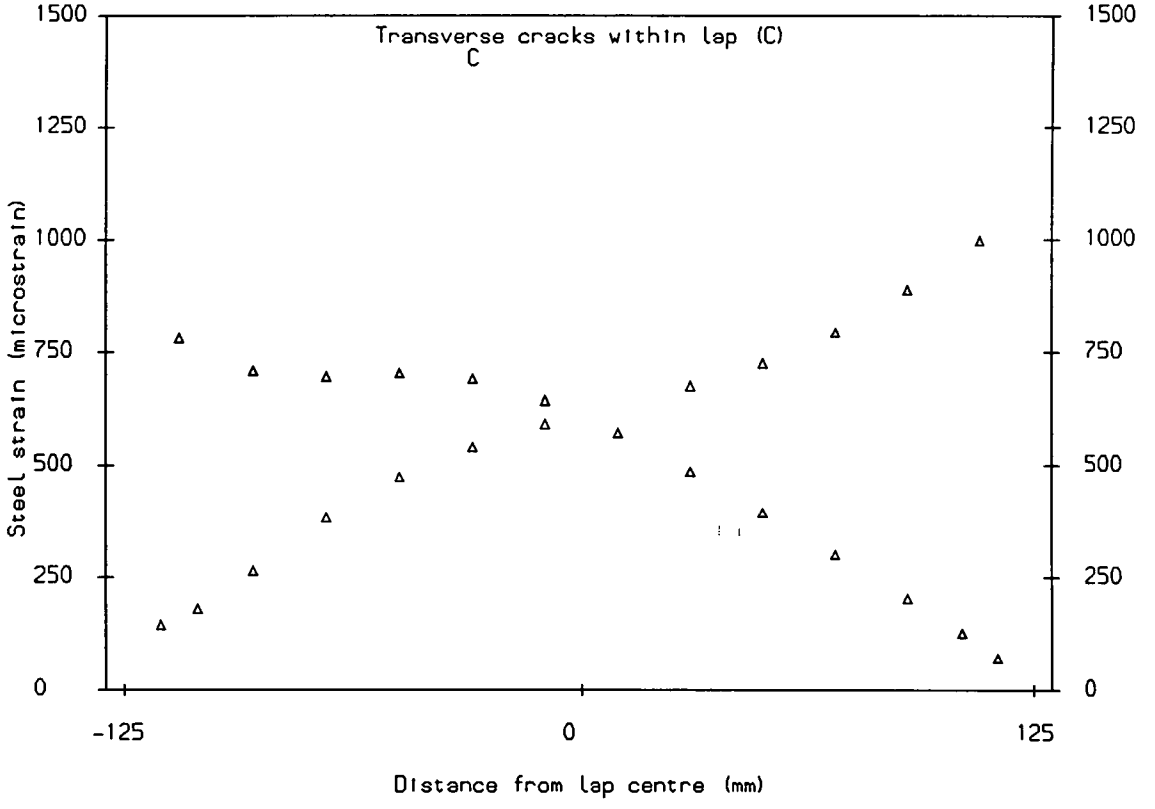

Fig. 6.8.1 Ultimate Steel Strain Distribution Along Lap
Specimen 250T20/20 Load: 66.0 kN

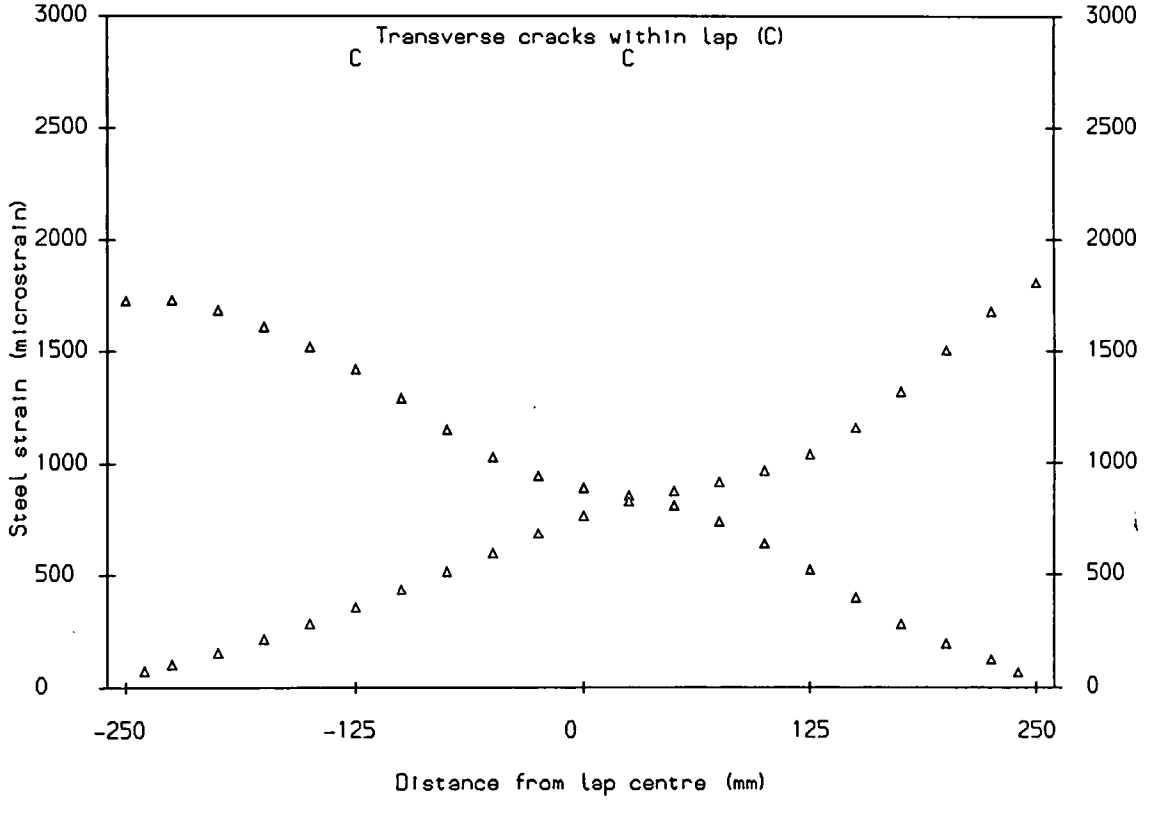

Fig. 6.8.2 Ultimate Steel Strain Distribution Along Lap
Specimen 500T20/20 Load: 90.3 kN

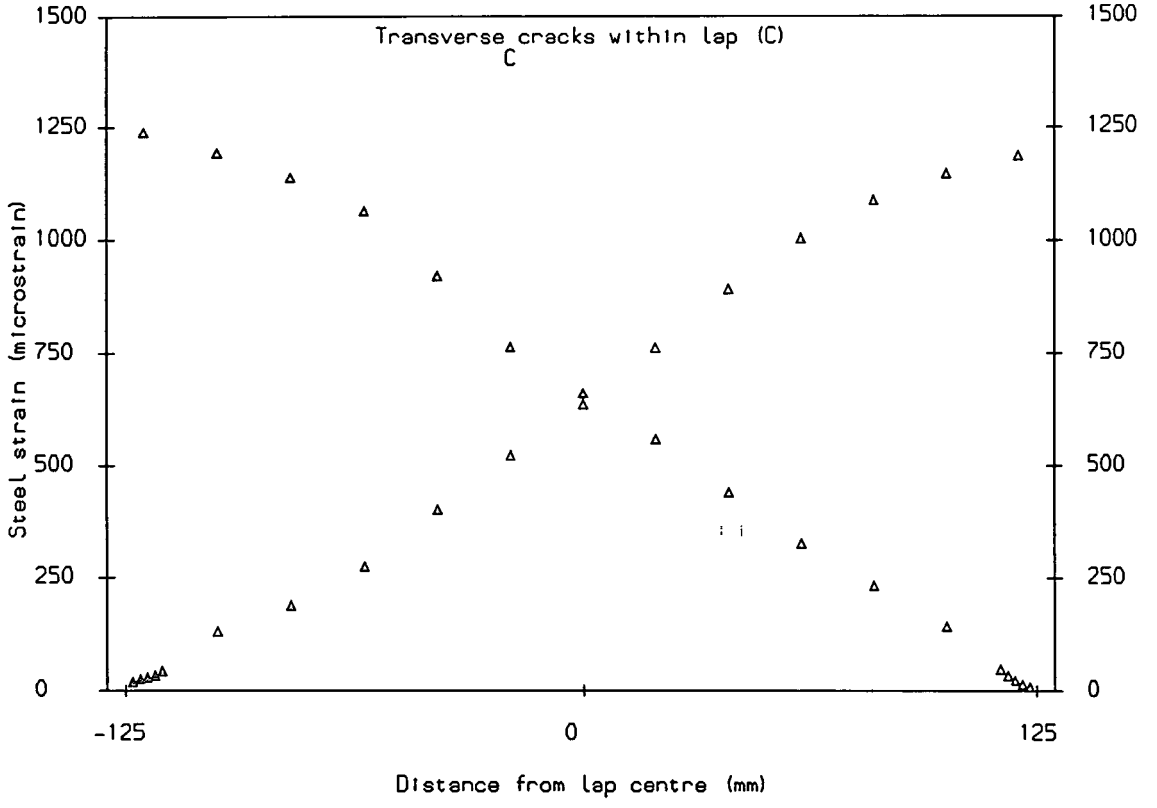

Fig. 6.8.3 Ultimate Steel Strain Distribution Along Lap
Specimen 250T20/20(E) Load: 52.0 kN

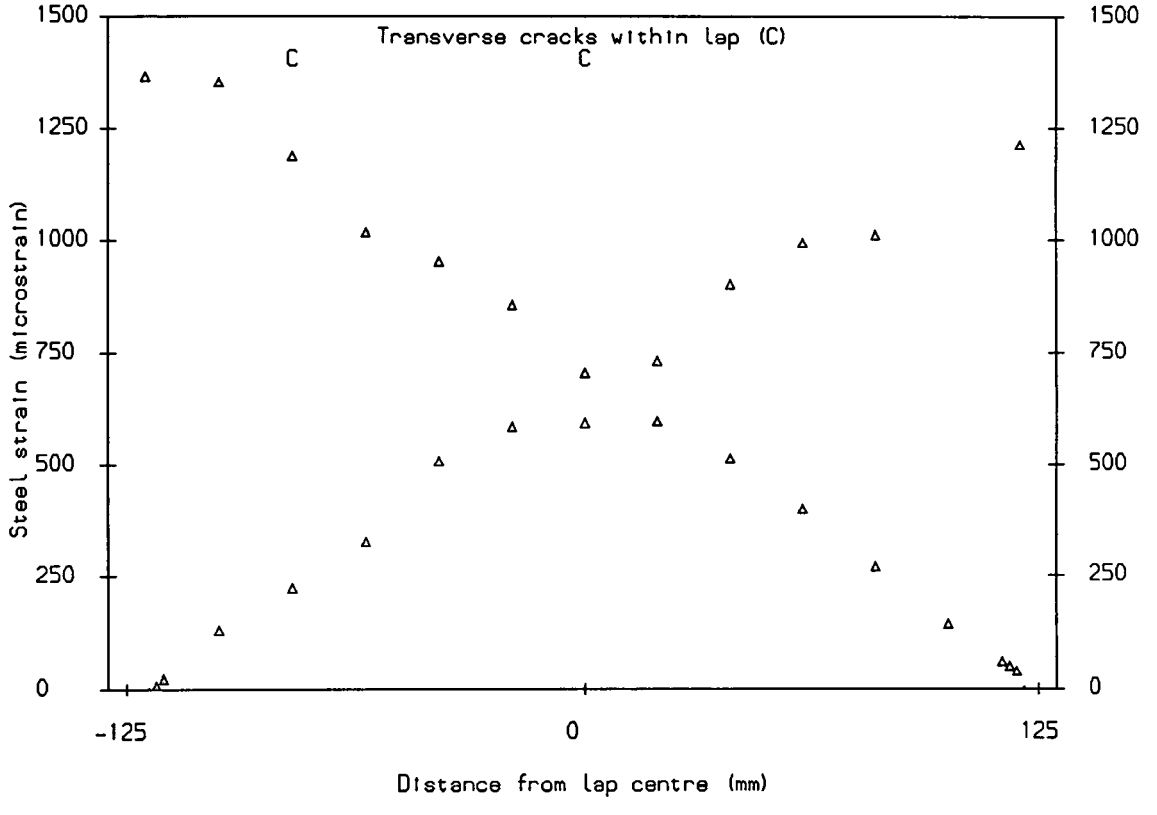

Fig. 6.8.4 Ultimate Steel Strain Distribution Along Lap
Specimen 250T20/20(L) Load: 96.5 kN

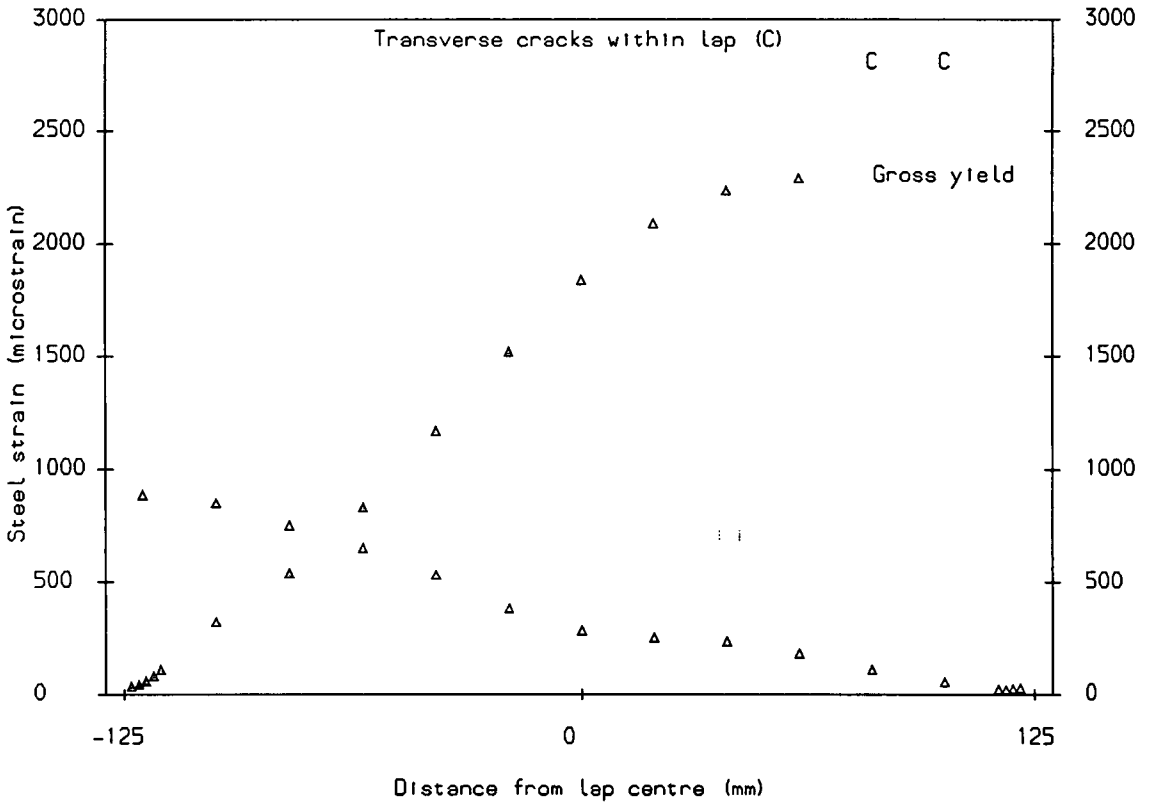

Fig. 6.8.5 Ultimate Steel Strain Distribution Along Lap
Specimen 250T12/20(B) Load: 42.0 kN

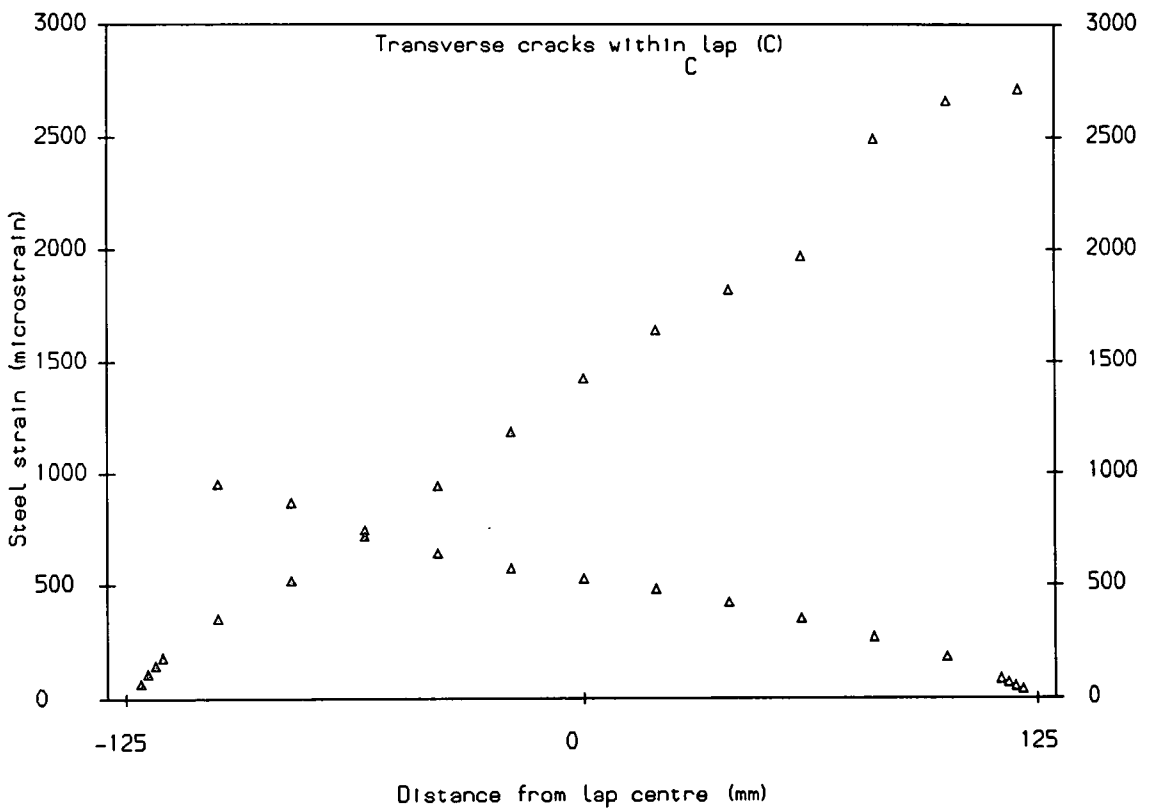

Fig. 6.8.6 Ultimate Steel Strain Distribution Along Lap
Specimen 250T12/20(A) Load: 42.0 kN

Specimen	Failure (Yes/No)	Maximum load (kN)	Ultimate load (kN) BS8110	Reynolds	O.J.& B.
125T12/12	Yes	32.0	13.2	31.6	39.7
250T12/12	Yes	42.0	26.4	62.9	67.2
500T12/12	No	40.0	51.2	122.1	118.5
750T12/12	No	48.0	78.4	186.9	175.4
250T20/20	Yes	66.0	41.8	54.4	79.4
500T20/20	Yes	90.3	86.0	111.8	130.5
750T20/20	No	100.5	129.9	168.9	180.7
250T12/20(A)	No	42.0	23.9	56.9	60.8
250T12/20(B)	Yes	42.0	27.0	61.6	66.3
500T12/20	No	40.0	51.9	117.9	115.0
250T20/20(E)	Yes	52.0	45.8	59.5	86.9
250T20/20(L)	Yes	96.5	84.0	80.9	132.5
500T20/20(L)	No	100.5	172.0	152.9	208.1
125D12/12	Yes	25.5	12.6	30.2	37.9
125D12/12(L)	No	19.0	25.7	42.2	60.8

British Code (BS8110:1985:§3.12.8)[7]:

$$F = 0.392\sqrt{f_{cu}}\pi\,\phi\,l \qquad \text{(without links)}$$

$$F = 0.7\sqrt{f_{cu}}\pi\,\phi\,l \qquad \text{(with links)}$$

These figures exclude the partial safety factor of 1.4.

Reynolds[31]:

$$F = 0.8\,l\sqrt{f_{cu}}\,(0.5\phi + c) + 70\left(\frac{A_{tr}\,l}{s_v}\right)$$

Orangun, Jirsa & Breen[30]:

$$F = 0.7\,l\sqrt{f_{cu}}\,(0.5\phi + c) + 11.7\,\phi^2\sqrt{f_{cu}} + 0.08\sqrt{f_{cu}}\,f_{yt}\left(\frac{A_{tr}\,l}{s_v}\right)$$

Constants have been converted from imperial units.

It is assumed that $f'_c = 0.8\sqrt{f_{cu}}$.

Fig. 6.9 Ultimate Loads

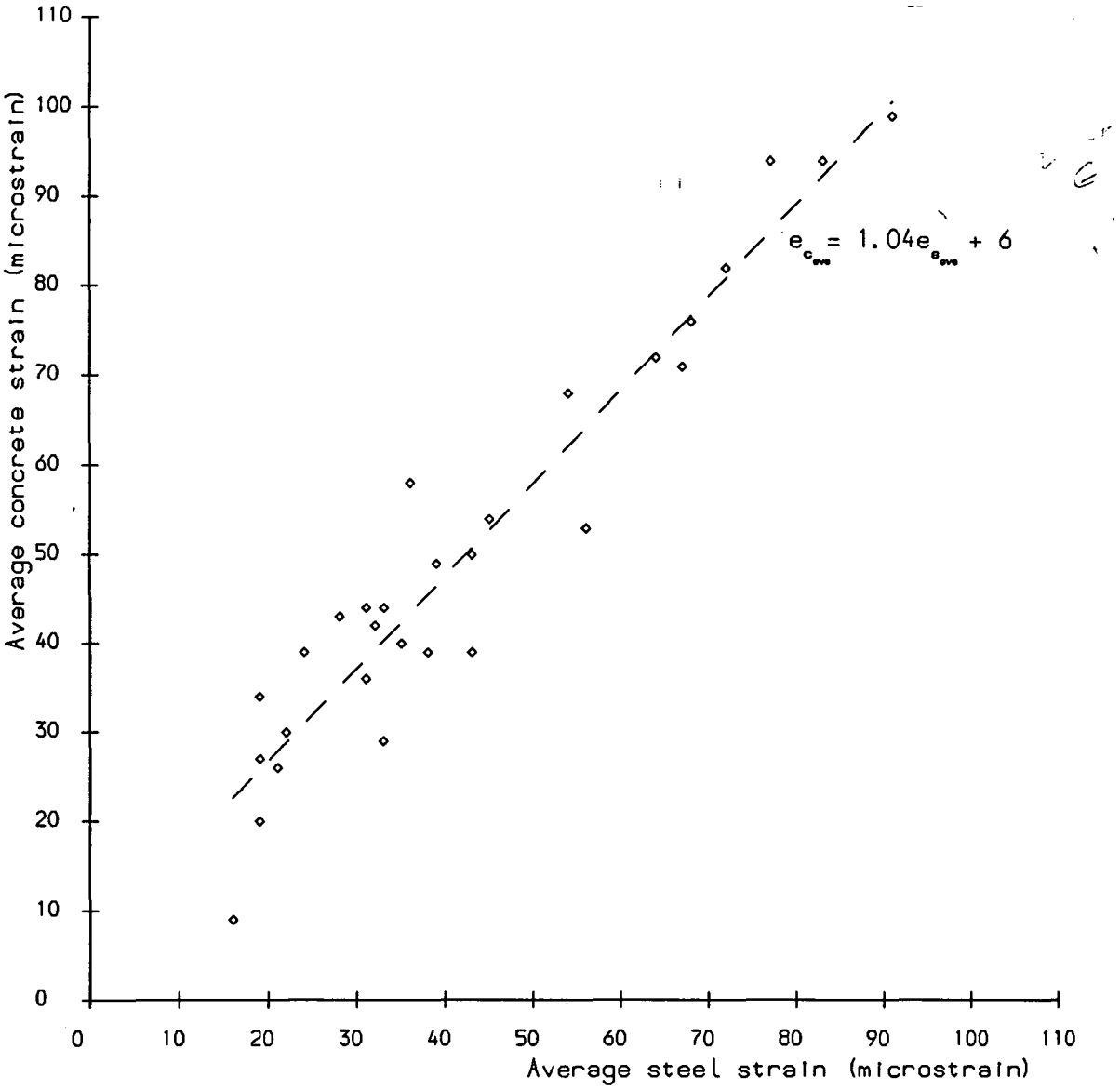

Fig. 6.10 Comparison of Steel and Concrete Strains

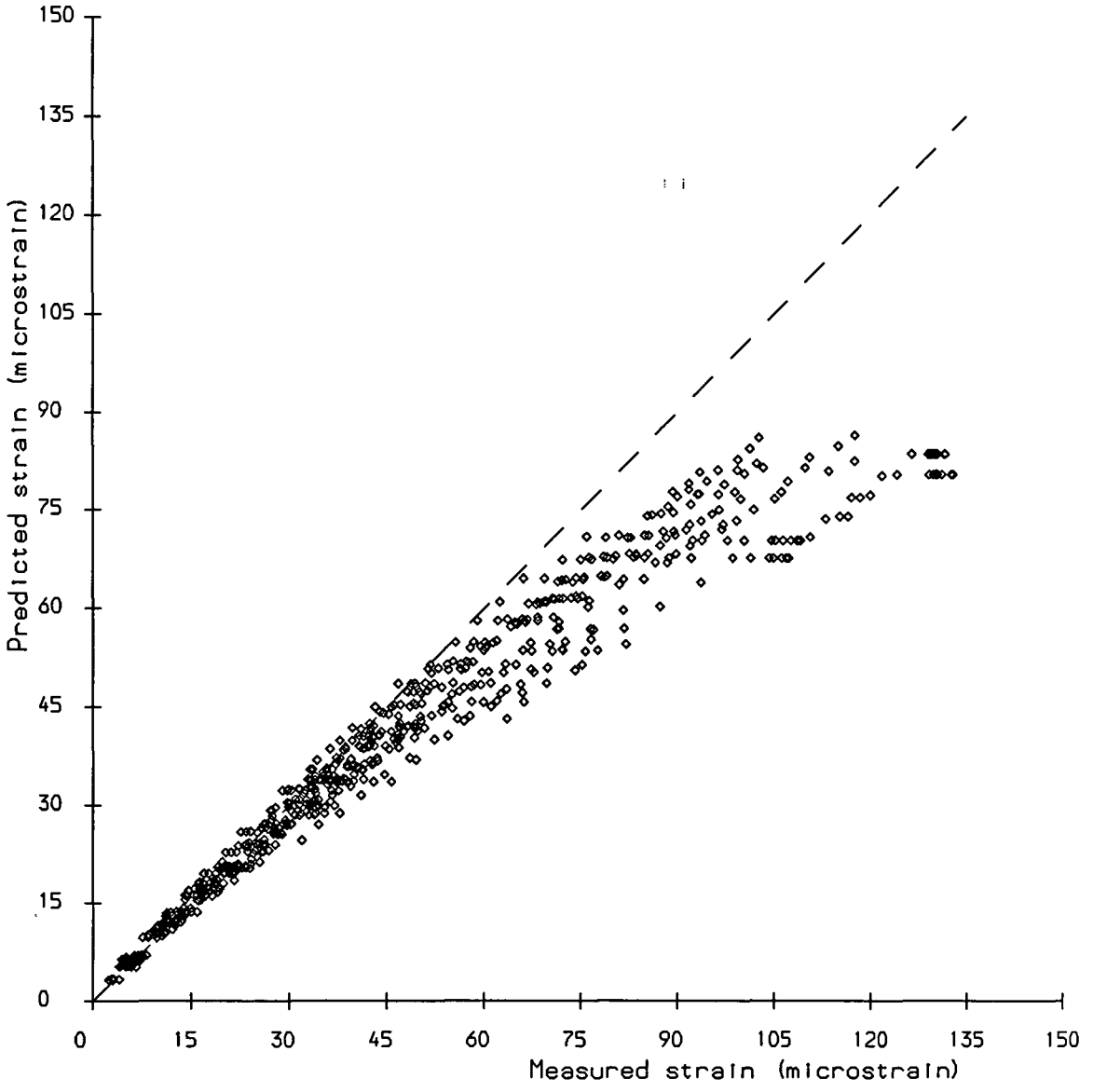

Fig. 6.11 Comparison of Predicted and Measured Reinforcement Strains

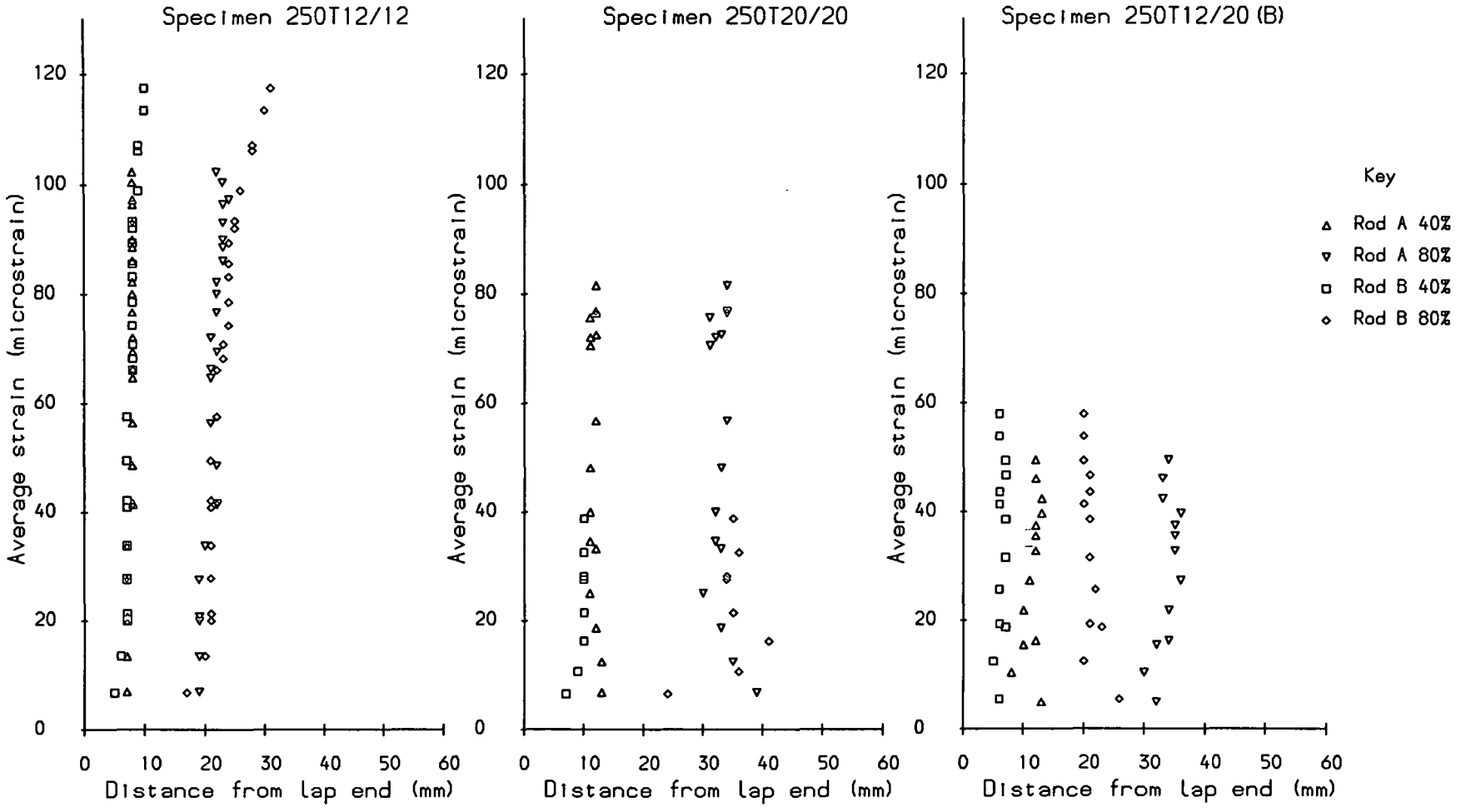

Fig. 6.12 Distance Required to Develop Percentage of Average Strain

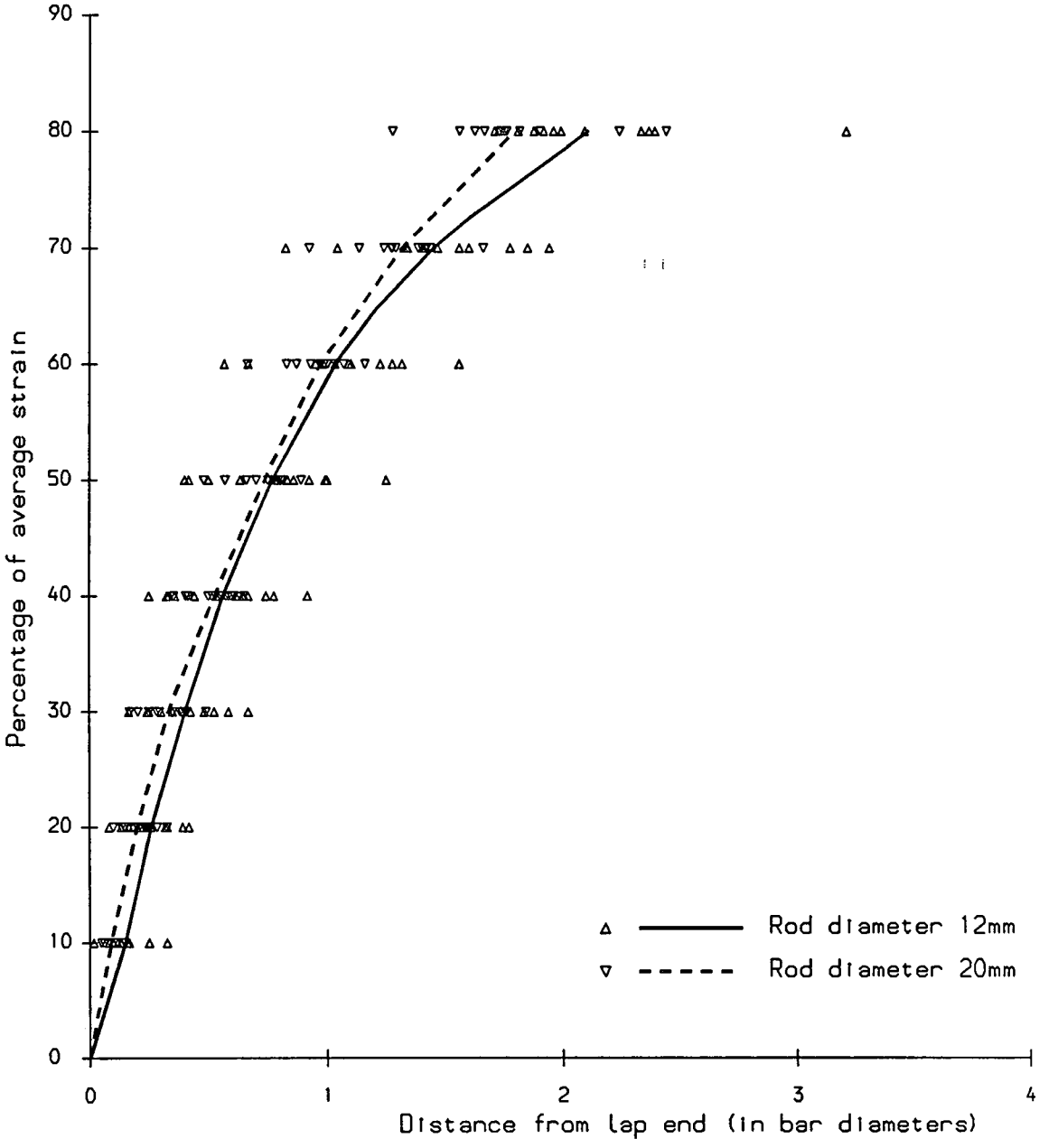

Fig. 6.13 Strains Developed at Lap End

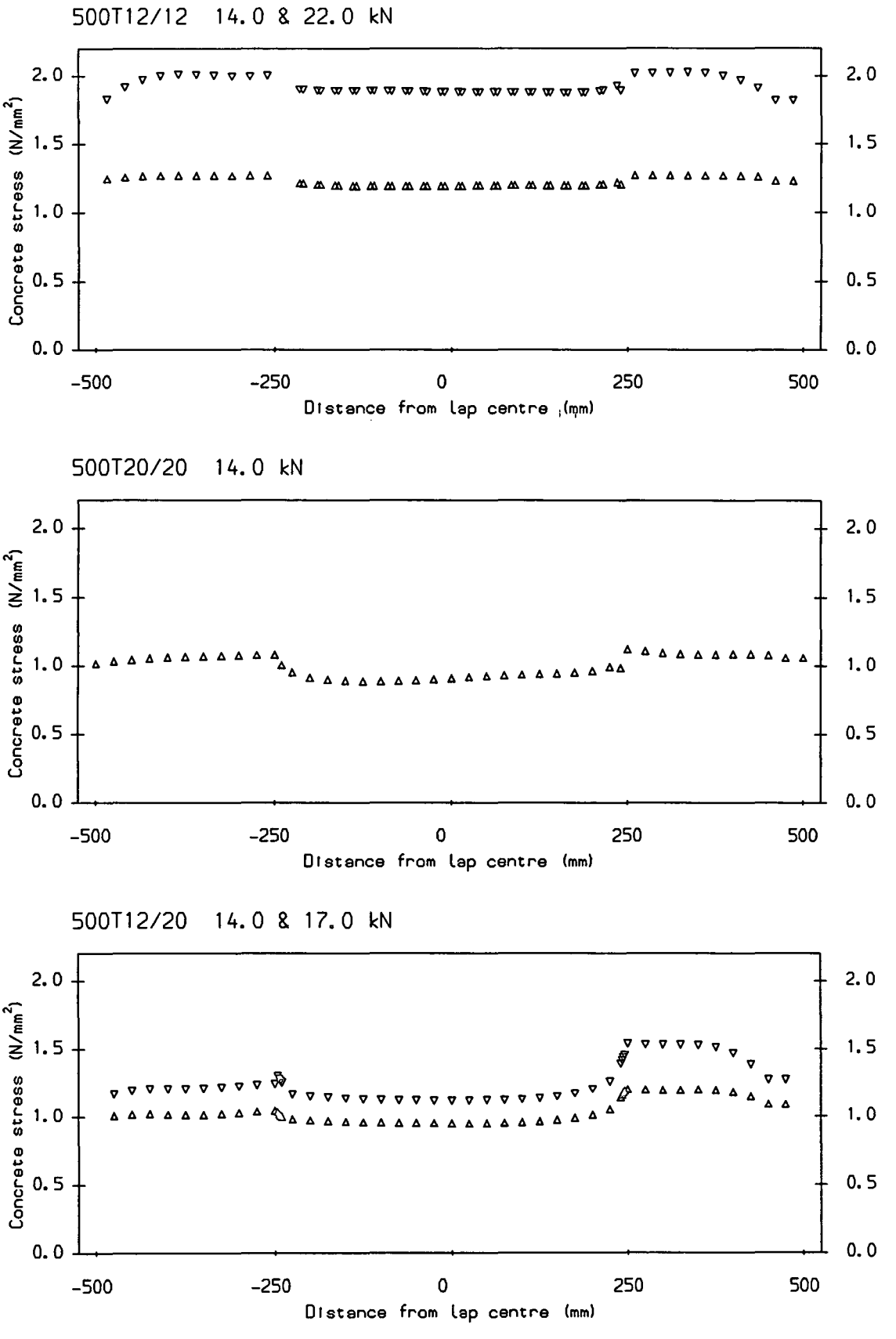

Fig. 6.14 Precrack Concrete Stress Distributions

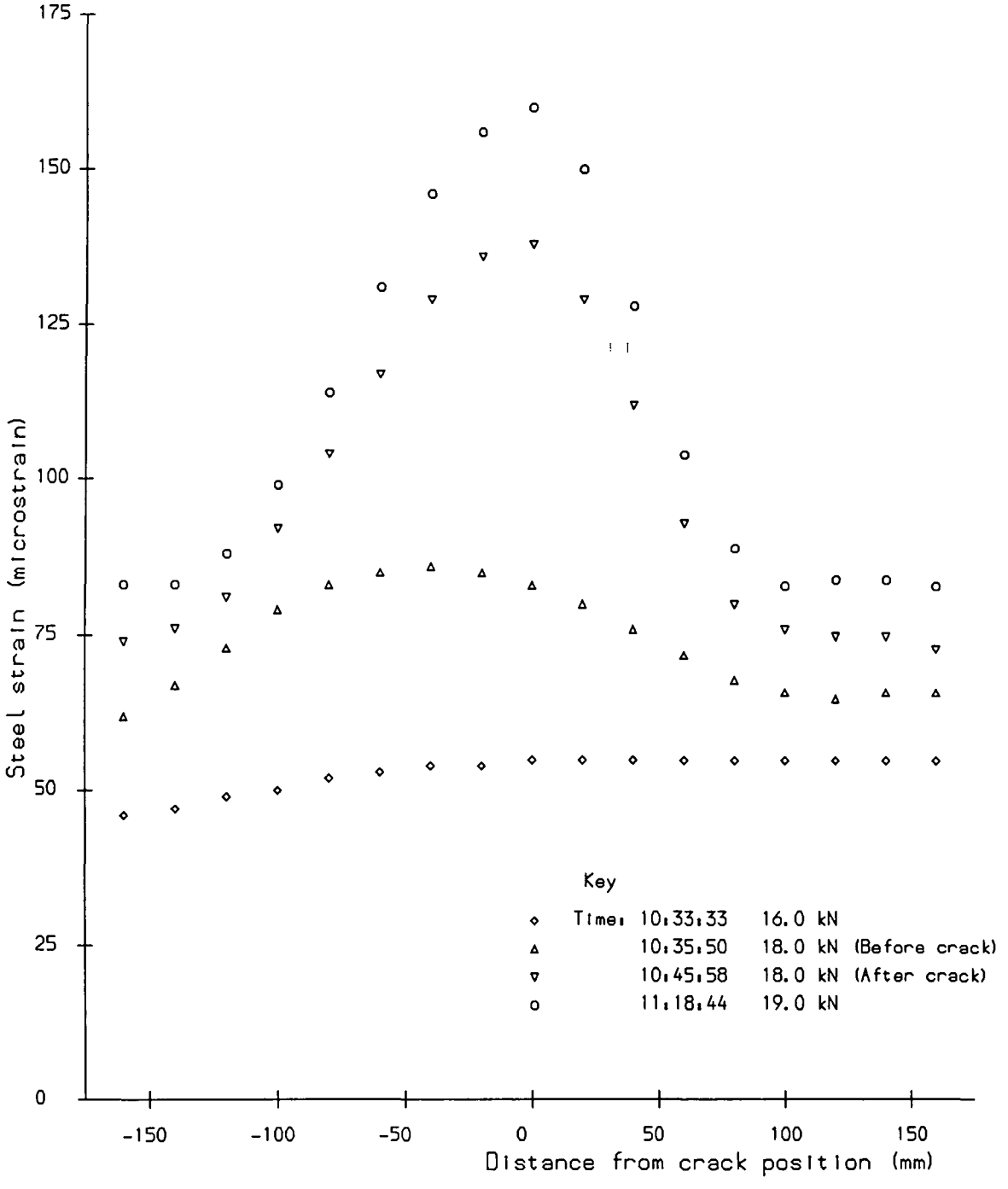

Fig. 6.15 Reinforcement Strains Specimen 250T20/20
(Before and after crack formation)

Specimen	No. of cracks	Average spacing (mm)	Maximum spacing (mm)	Minimum spacing (mm)
125T12/12	2	375	483	230
250T12/12	4	300	410	205
500T12/12	4	300	415	195
750T12/12	3	300	440	150
250T20/20	6	214	300	125
500T20/20	7	214	425	115
750T20/20	7	188	275	100
250T12/20(A)	6	214	285	155
250T12/20(B)	5	250	450	170
500T12/20	5	250	350	150
250T20/20(E)	8	167	240	100
250T20/20(L)	8	164	265	80
500T20/20(L)	10	136	240	100

N.B. 'High strain' cracks have been excluded.

Fig. 6.16 Crack Spacing

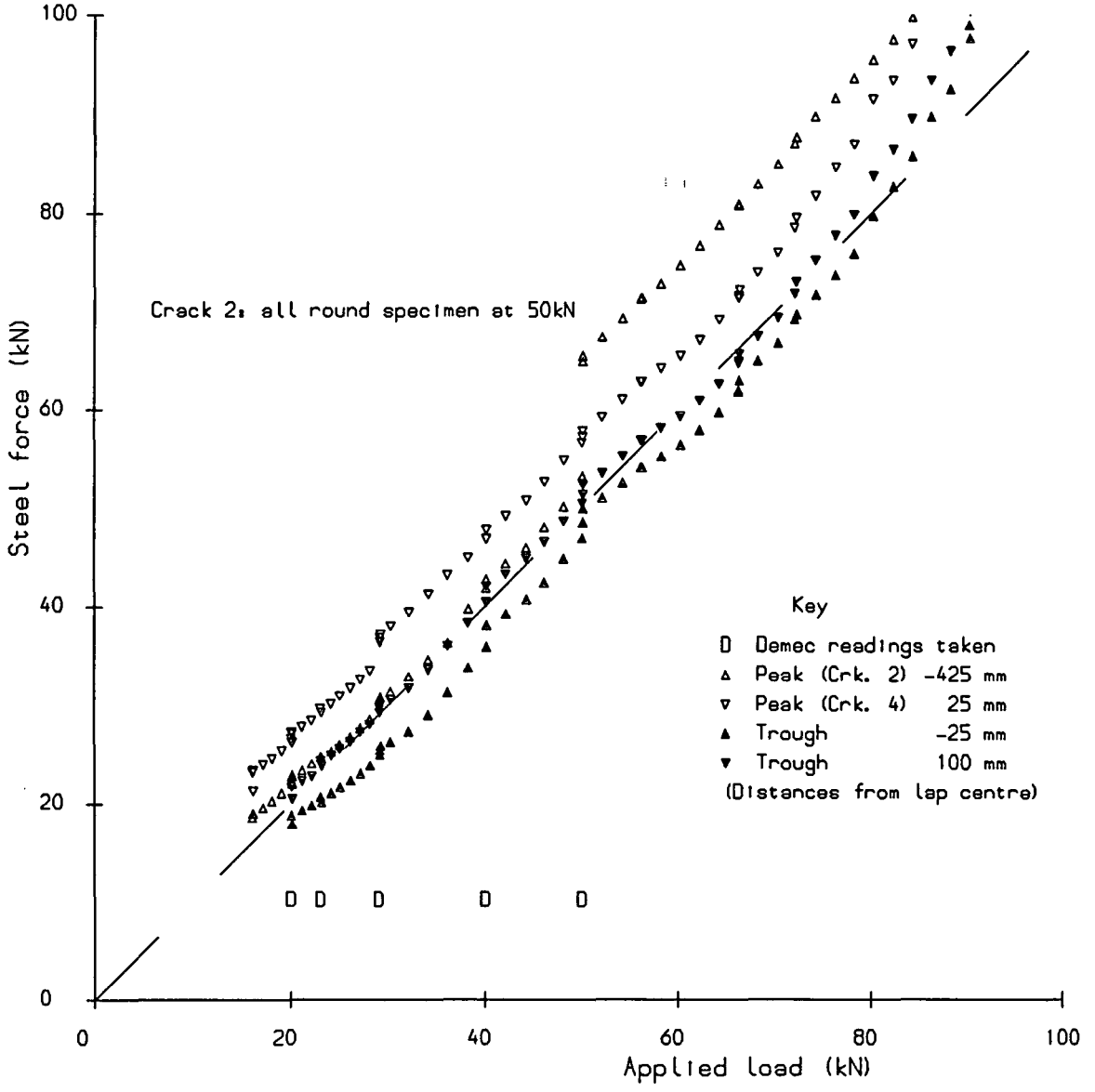

Fig. 6.17 Applied Load vs. Force in Steel Specimen 500T20/20

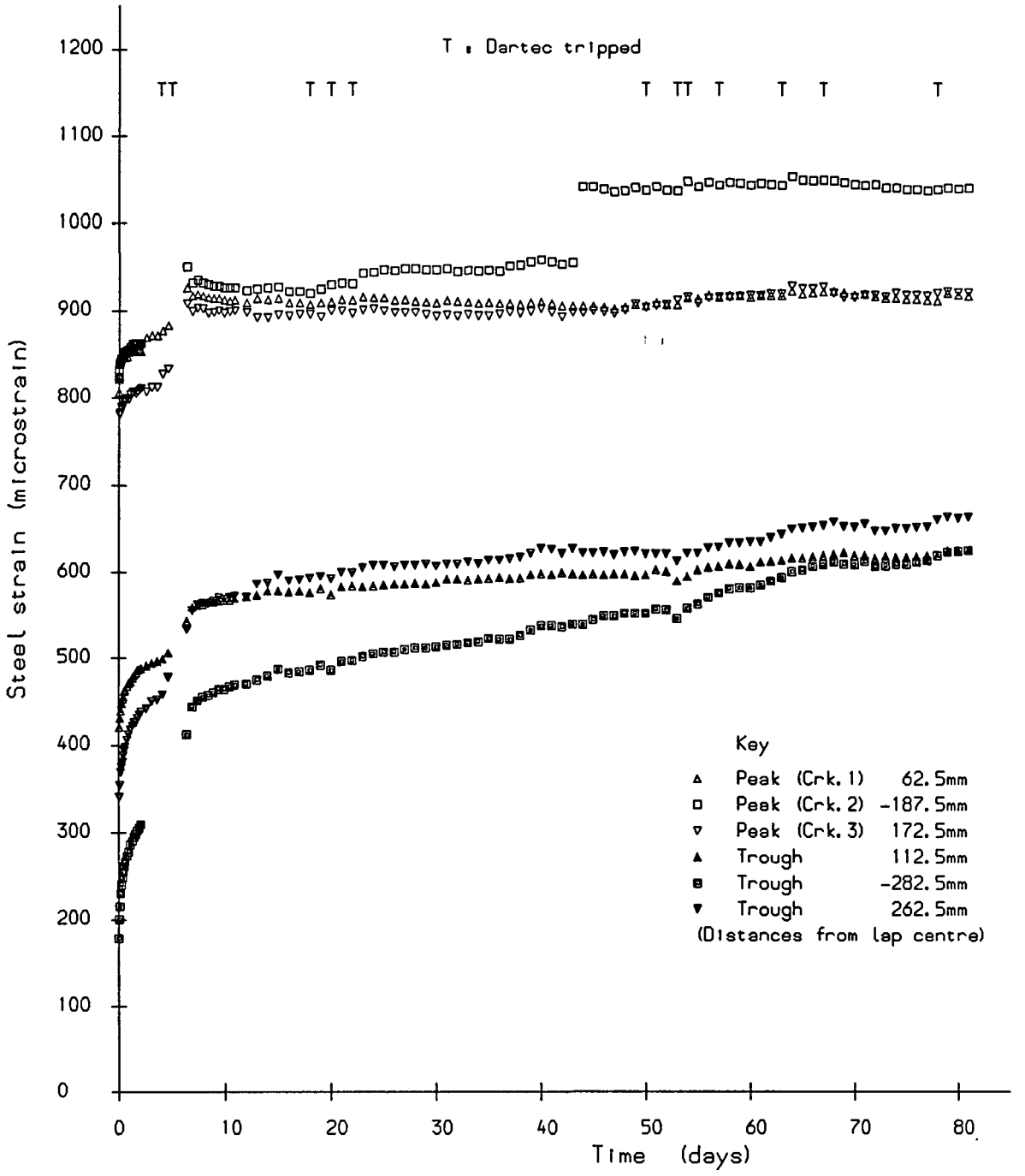

Fig. 6.18 Variation in Strains with Time
Specimen 125D12/12(L)

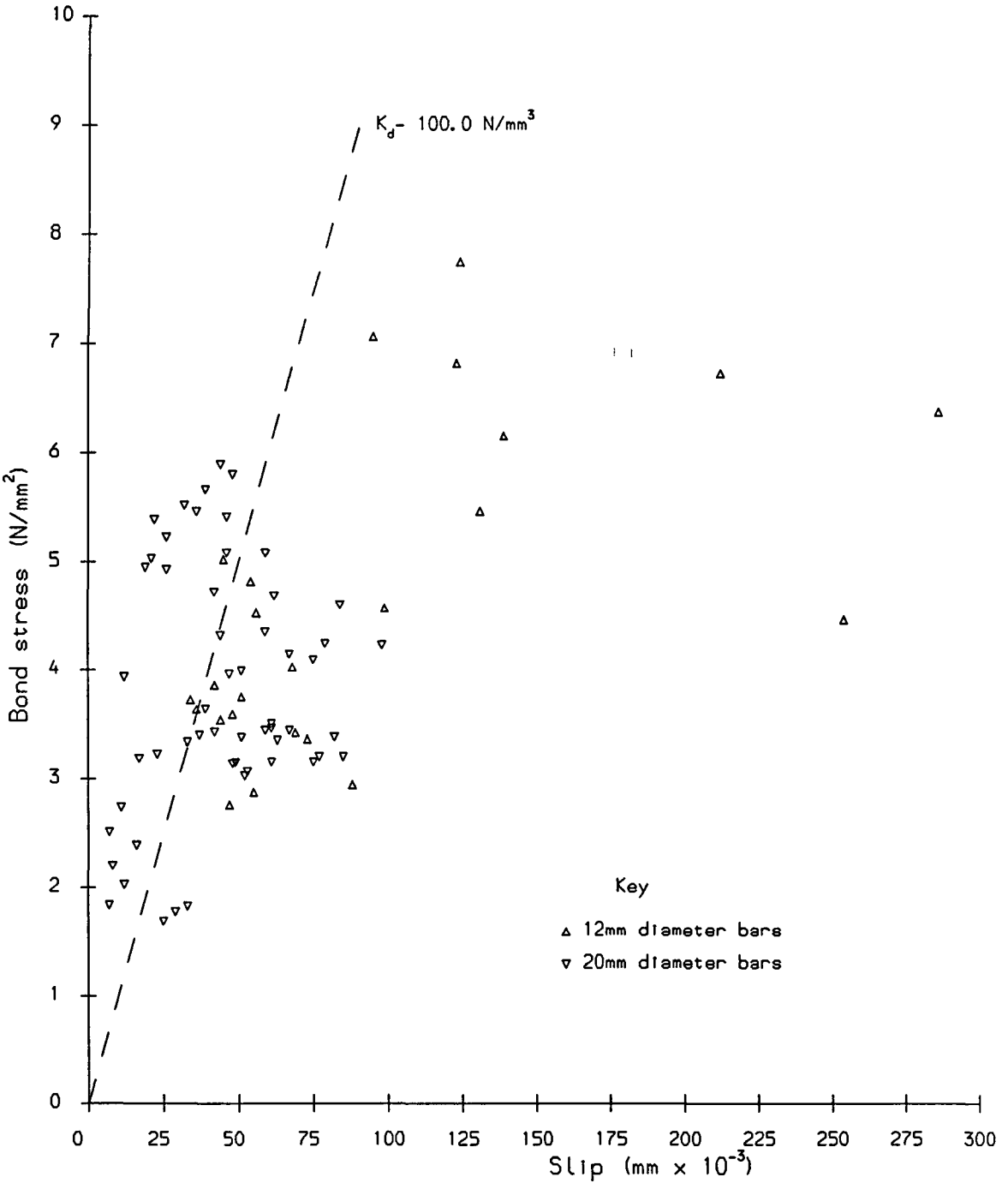

Fig. 6.19 Bond Stress/Slip Relationship

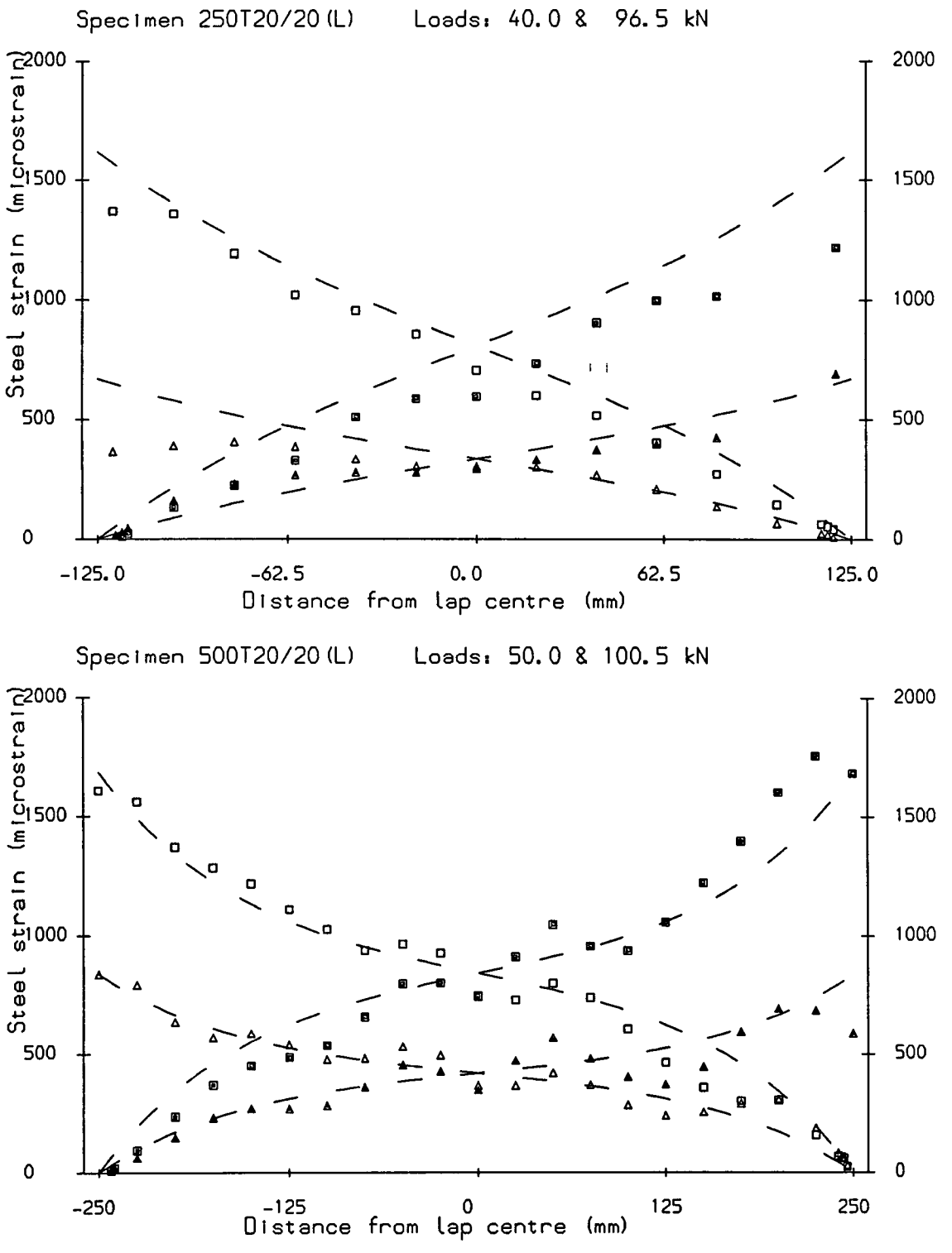

Fig. 6.20 Steel Strain Distribution along the Lap
(Dashed line refers to Tepfers analysis[51])

Specimen	Crack number 1		2		3		4		5		6		7		8		9		10		11
125T12/12	312.		377.																		
	2.6	*4.5*	*3.0*	*5.6*																	
250T12/12	–		432.		201.	L	309.		–		–										
	–	–	–	–	2.6	*3.8*	*4.1*	6.1	–	–	–	–									
500T12/12	284.		135.	L	397.		225.	L	373.												
	4.8	4.2	2.4	1.4	*4.2*	*6.1*	2.9	2.9	–	–											
750T12/12	190.		310.		150.	L	243.	L	227.	L											
	3.6	*4.2*	7.6	6.8	2.5	4.1	*2.7*	5.8	–	*4.8*											
250T20/20	–		–		29.		52.		36.	L	57.		–								
	–	–	–	–	0.7	1.0	2.3	–	1.4	1.4	2.0	2.1	–	–							
500T20/20	36.	L	59.		25.		58.	L	116.		117.		–		–						
	1.2	1.7	2.4	2.1	0.8	0.6	1.8	2.4	4.3	*3.7*	*2.5*	*3.4*	–	–	–	–					
750T20/20	54.		46.	L	30.	L	42.	L	89.		62.	L	62.	L	141.	L	307.		284.		
	–	1.8	1.7	2.2	1.4	1.0	1.5	1.9	3.7	*1.9*	2.2	*1.7*	*1.4*	*1.2*	*0.8*	*0.8*	*5.9*	*2.3*	*0.9*	–	
250T12/20(A)	–		35.		489.		113.	L	–		123.		–								
	–	–	1.2	1.9	–	–	2.8	2.1	–	–	3.5	3.3	–	–							
250T12/20(B)	84.	L	–		297.		88.		87.		531.	L	435.								
	2.5	2.0	–	–	4.7	5.4	3.9	5.0	2.9	3.3	–	–	–	–							
500T12/20	–		100.	L	339.	L	110.	L	108.												
	–	–	2.6	2.6	*3.3*	*7.2*	1.8	2.3	*2.1*	*4.0*											
250T20/20(E)	30.	L	–		47.		63.		96.		–		–		126.						
	1.8	1.4	–	–	2.1	1.7	3.1	3.1	4.1	4.2	–	–	–	–	5.0	5.1					
250T20/20(L)	–		28.	L	39.		66.		68.		39.		–		44.	L	115.		191.		
	–	–	0.7	0.7	1.6	1.3	3.1	3.1	*1.0*	2.5	1.1	–	–	–	*0.5*	*2.4*	*1.8*	*0.9*	*1.2*	*4.0*	
500T20/20(L)	–		25.	L	29.	L	33.	L	–		23.		23.		34.	L	67.		–		246.
	0.8	*2.5*	0.9	0.9	1.2	1.1	–	–	0.0	0.5	0.5	0.0	1.0	1.6	2.6	2.9	–	–	–	–	–	–
125D12/12	–		–																		
	–	–	–	–																	
125D12/12(L)	167.		170.		161.																
	6.5	7.2	4.2	4.4	4.2	3.6															
Key	A	B	A : Rod stress (N/mm^2)								B : L – denotes crack in lap						*Italics*: bond stress				
	C	D	C : Bond stress below crack (N/mm^2)								D : Bond stress above crack (N/mm^2)						influenced (see text)				

Fig. 6.21 Bond Stresses at Crack Formation

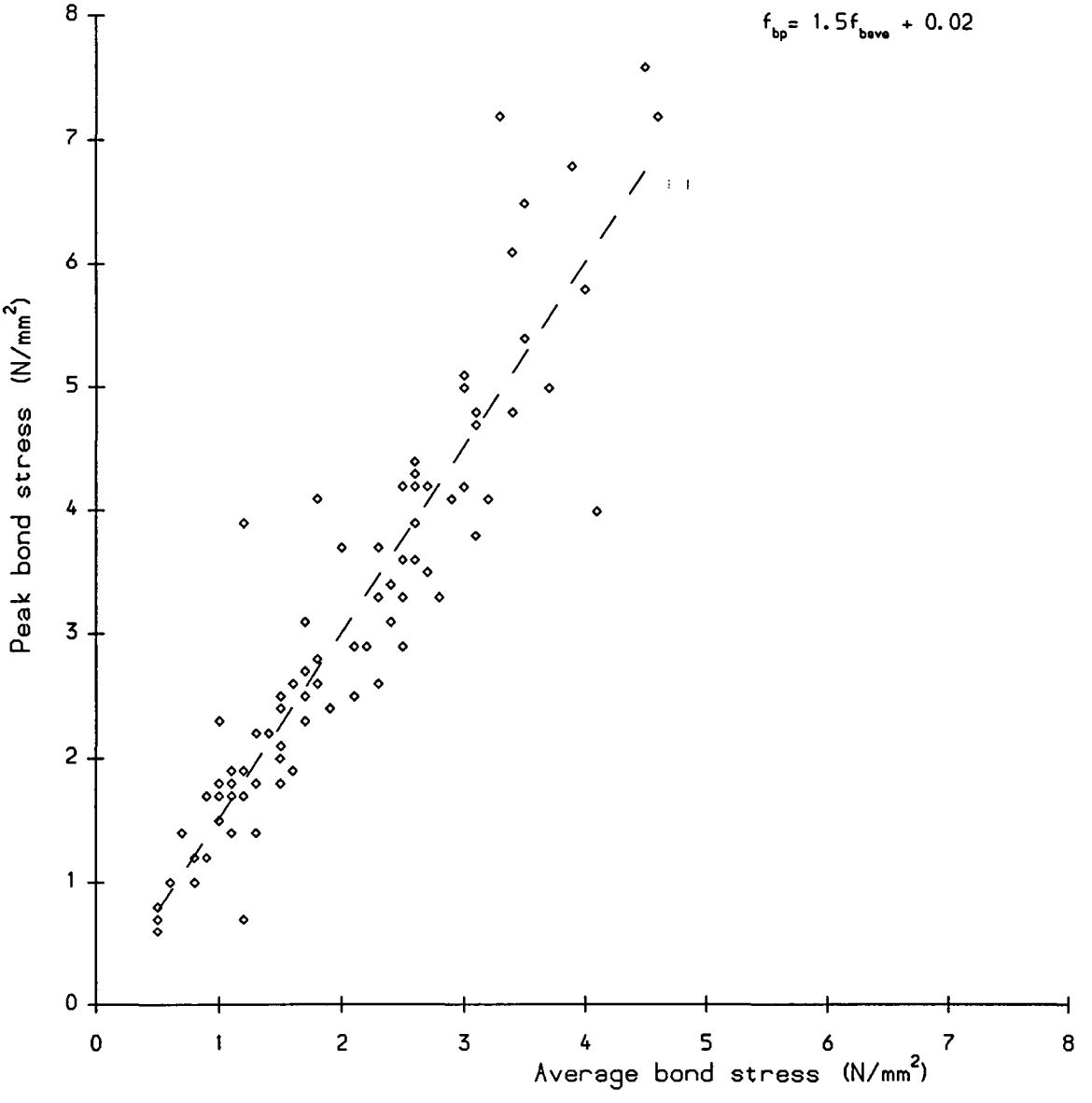

Fig. 6.22 Comparison of Peak and Average Bond Stresses near Transverse Cracks

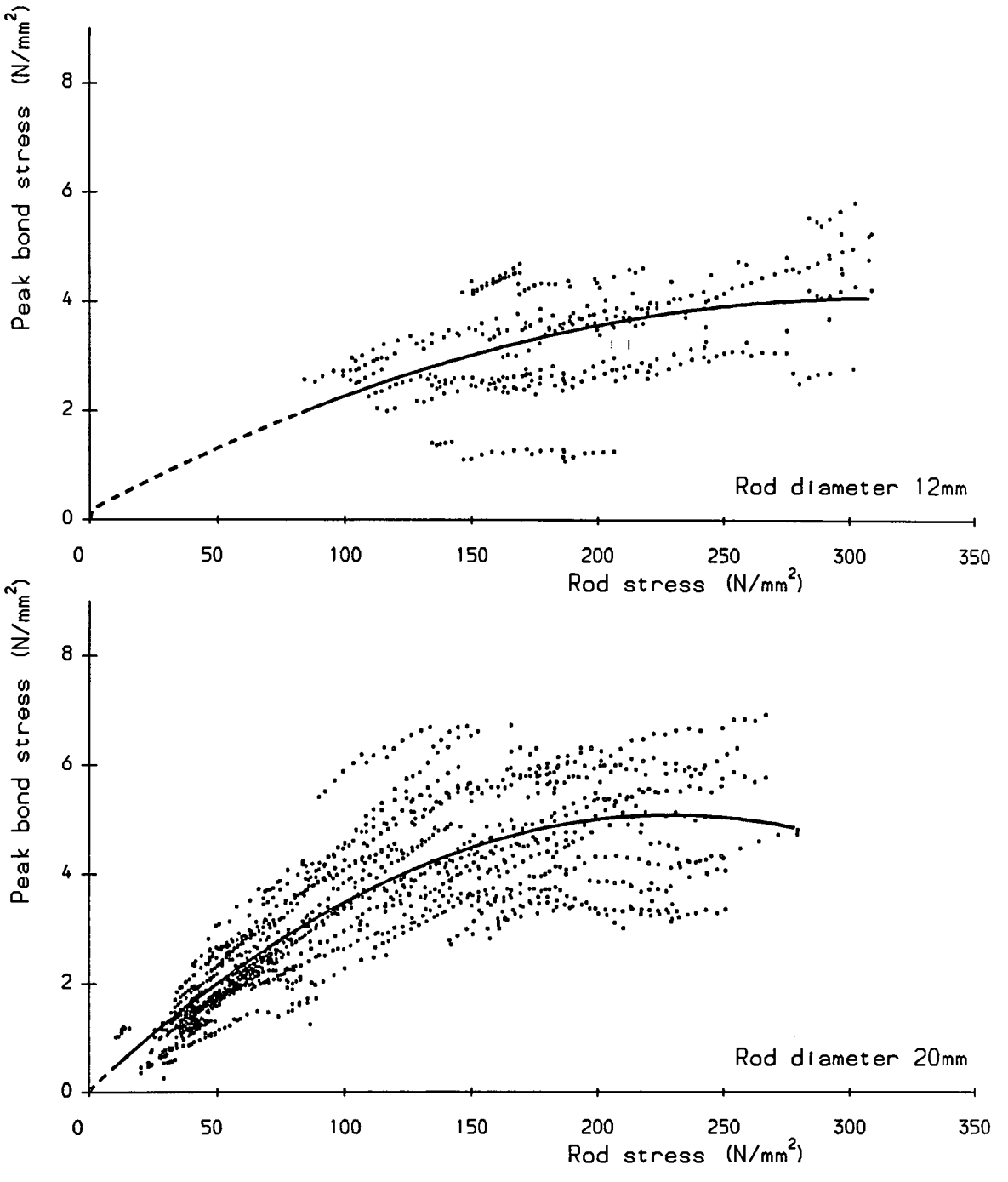

Fig. 6.23 Bond Stress/ Rod Stress Relationship

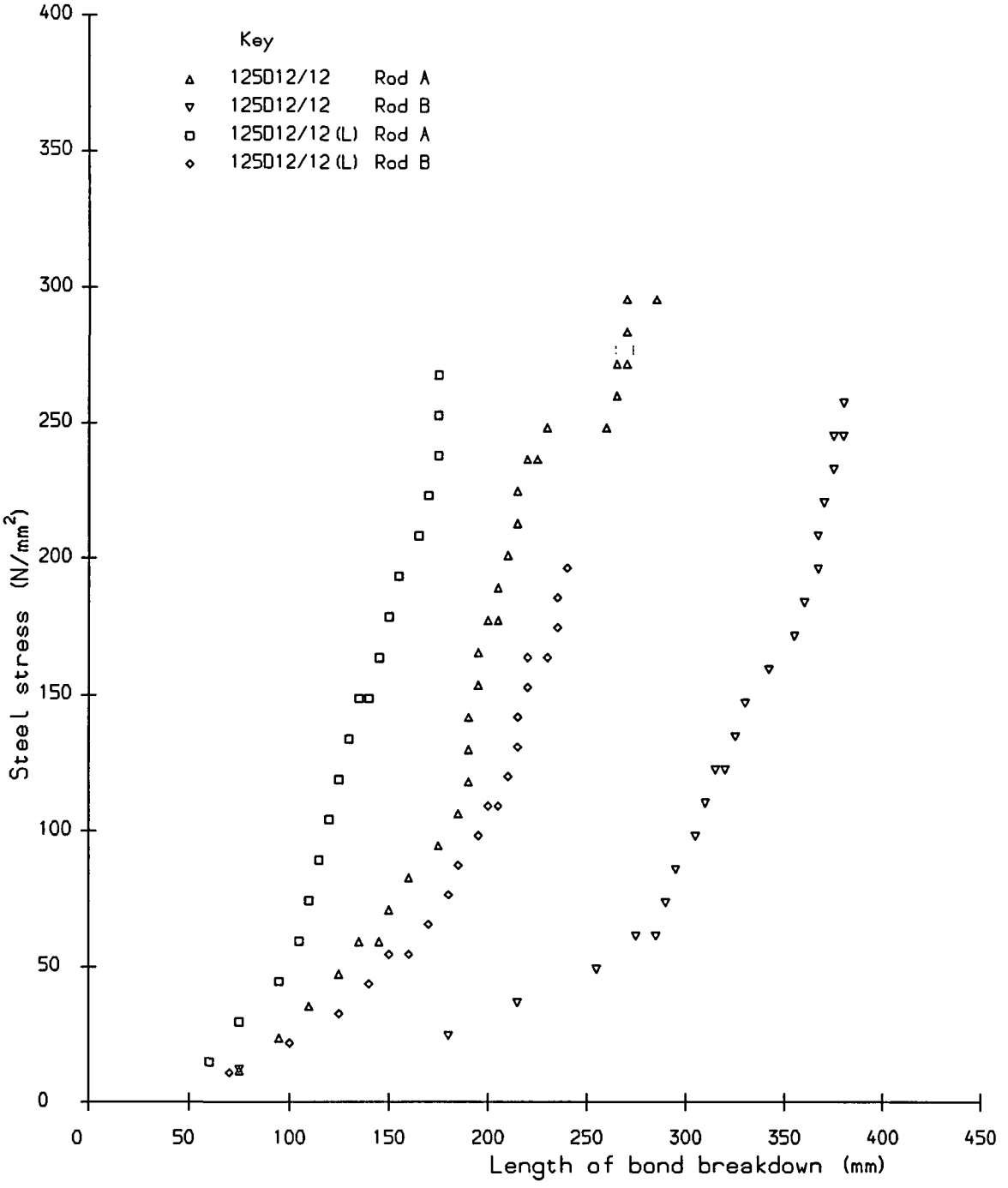

Fig. 6.24 Bond Breakdown at the Specimen End

Specimen	Maximum load (kN)	Failure (Yes/No)	Mean bond stress (N/mm^2)		Coefficient of variation (%)		Peak bond stress (N/mm^2)	
			A	B	A	B	A	B
125T12/12	32.0	Yes	Final strain distribution not recorded					
250T12/12	42.0	Yes	Final strain distribution not recorded					
500T12/12	40.0	No	3.6	2.4	57	48	8.6	3.8
750T12/12	48.0	No	3.5	3.1	77	73	10.5	8.5
250T20/20	66.0	Yes	3.8	5.0	51	56	6.3	13.3
500T20/20	90.3	Yes	3.6	3.6	22	47	6.2	6.7
750T20/20	100.5	No	2.7	3.6	62	64	6.1	8.4
250T12/20(A)	42.0	No	4.4	4.8	38	27	8.4	8.0
250T12/20(B)	42.0	Yes	3.5	5.9	67	33	7.4	8.2
500T12/20	40.0	No	2.5	2.7	47	55	4.4	6.3
250T20/20(E)	52.0	Yes	4.2	4.1	35	37	6.5	5.6
250T20/20(L)	96.5	Yes	3.5	4.4	52	54	6.6	6.9
500T20/20(L)	100.5	No	3.5	3.5	61	61	7.1	5.8
125D12/12	25.5	Yes	Final strain distribution not recorded					
125D12/12(L)	19.0	No	–	–	–	–	–	–

Fig. 6.25 Bond Stresses at Maximum Load

Specimen	Failure (Yes/No)	Maximum bond stress (N/mm^2)	Ultimate bond stress (N/mm^2)		
			BS8110	Reynolds	O.J.& B.
125T12/12	Yes	–	2.8	6.7	8.4
250T12/12	Yes	–	2.8	6.7	7.1
500T12/12	No	3.6	2.7	6.5	6.3
750T12/12	No	3.5	2.8	6.6	6.2
250T20/20	Yes	5.0	2.7	3.5	5.1
500T20/20	Yes	3.6	2.7	3.6	4.2
750T20/20	No	3.6	2.8	3.6	3.8
250T12/20(A)	No	4.8	2.5	6.0	6.5
250T12/20(B)	Yes	5.9	2.9	6.5	7.0
500T12/20	No	2.7	2.8	6.3	6.1
250T20/20(E)	Yes	4.2	2.9	3.8	5.5
250T20/20(L)	Yes	4.4	5.4	5.1	8.4
500T20/20(L)	No	3.5	5.5	4.9	6.6
125D12/12	Yes	–	2.7	6.4	8.1
125D12/12(L)	No	–	5.5	8.9	12.9

British Code (BS8110:1985:§3.12.8)[7]:

$$f_{bs} = 0.392\sqrt{f_{cu}} \qquad \text{(without links)}$$

$$f_{bs} = 0.7\sqrt{f_{cu}} \qquad \text{(with links)}$$

Constants exclude partial safety factor of 1.4.

Reynolds[31]:

$$f_{bs} = 0.25\sqrt{f_{cu}}\left(0.5 + \frac{c}{\phi}\right) + 22\left(\frac{A_{tr}}{s_v\,\phi}\right)$$

Orangun, Jirsa & Breen[30]:

$$f_{bs} = 0.22\sqrt{f_{cu}}\left(0.5 + \frac{c}{\phi}\right) + 3.72\sqrt{f_{cu}}\frac{\phi}{l} + 0.025\sqrt{f_{cu}}\left(\frac{f_{yt}\,A_{tr}}{s_v\,\phi}\right)$$

Constants have been converted from imperial units.

It is assumed that $f'_c = 0.8\sqrt{f_{cu}}$.

Fig. 6.26 Ultimate Bond Stresses

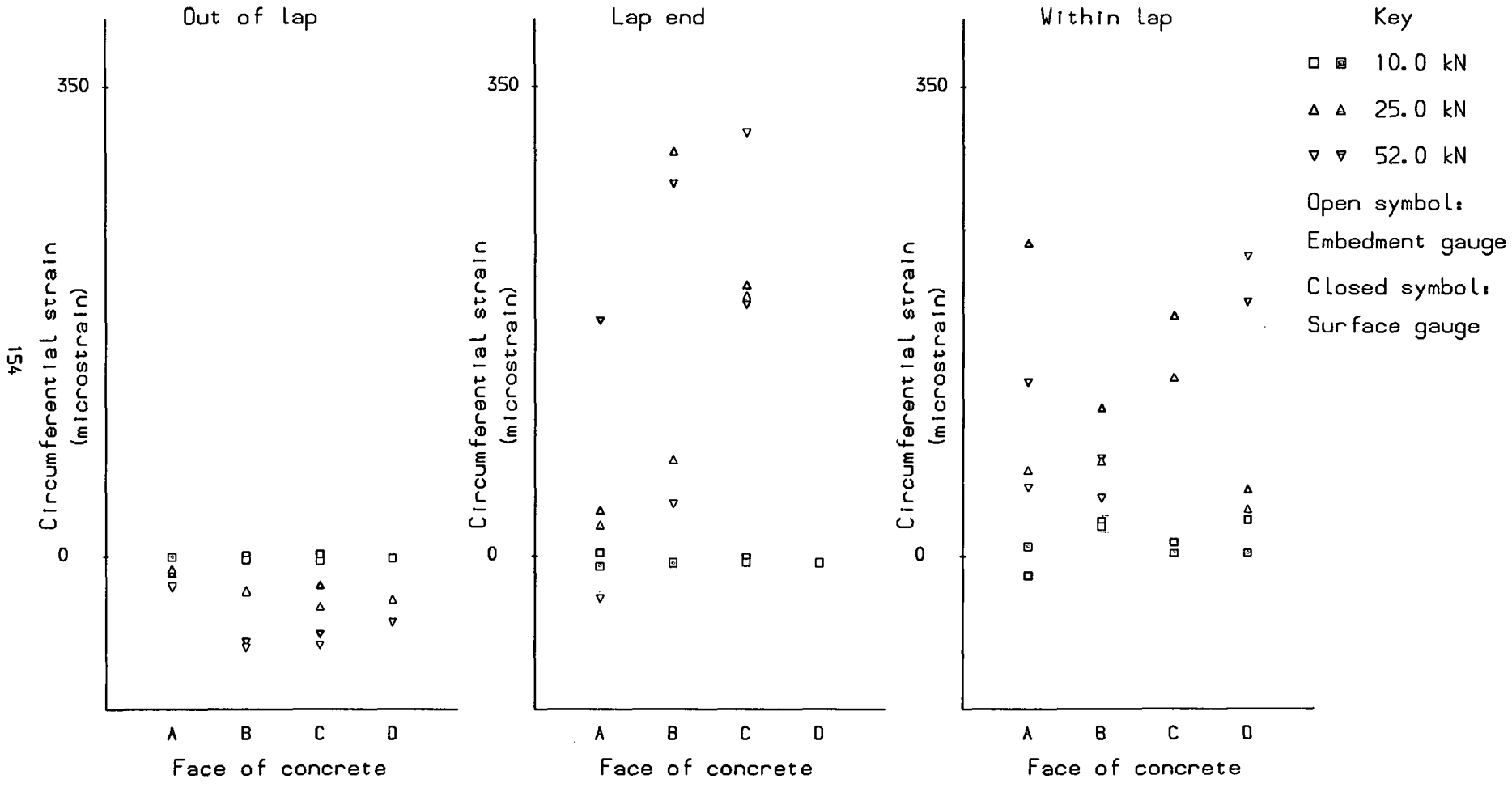

Fig. 6.27 Circumferential Strains Specimen 250T20/20(E)

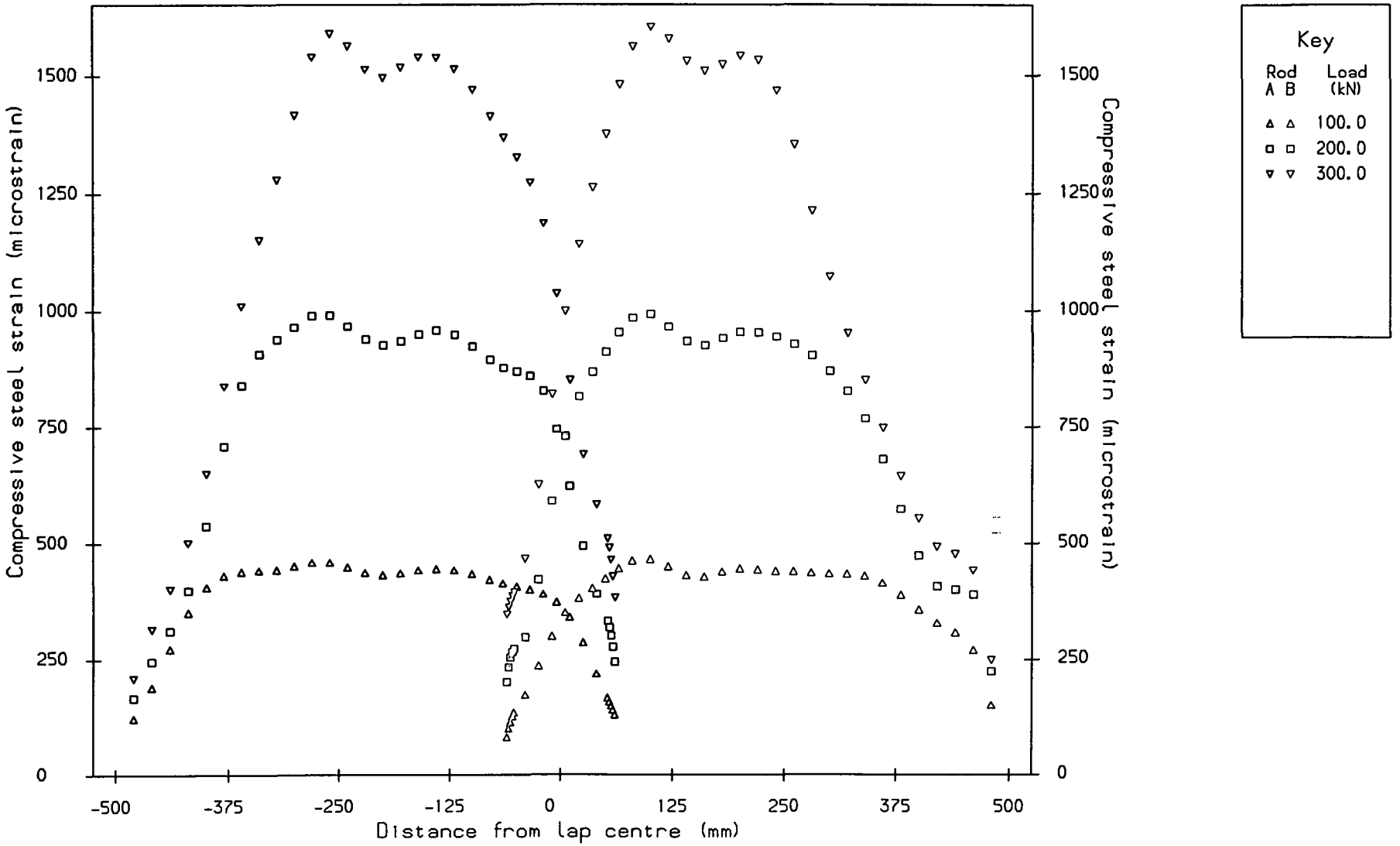

Fig. 7.1.1 Steel Strain Distribution Specimen 125C12/12

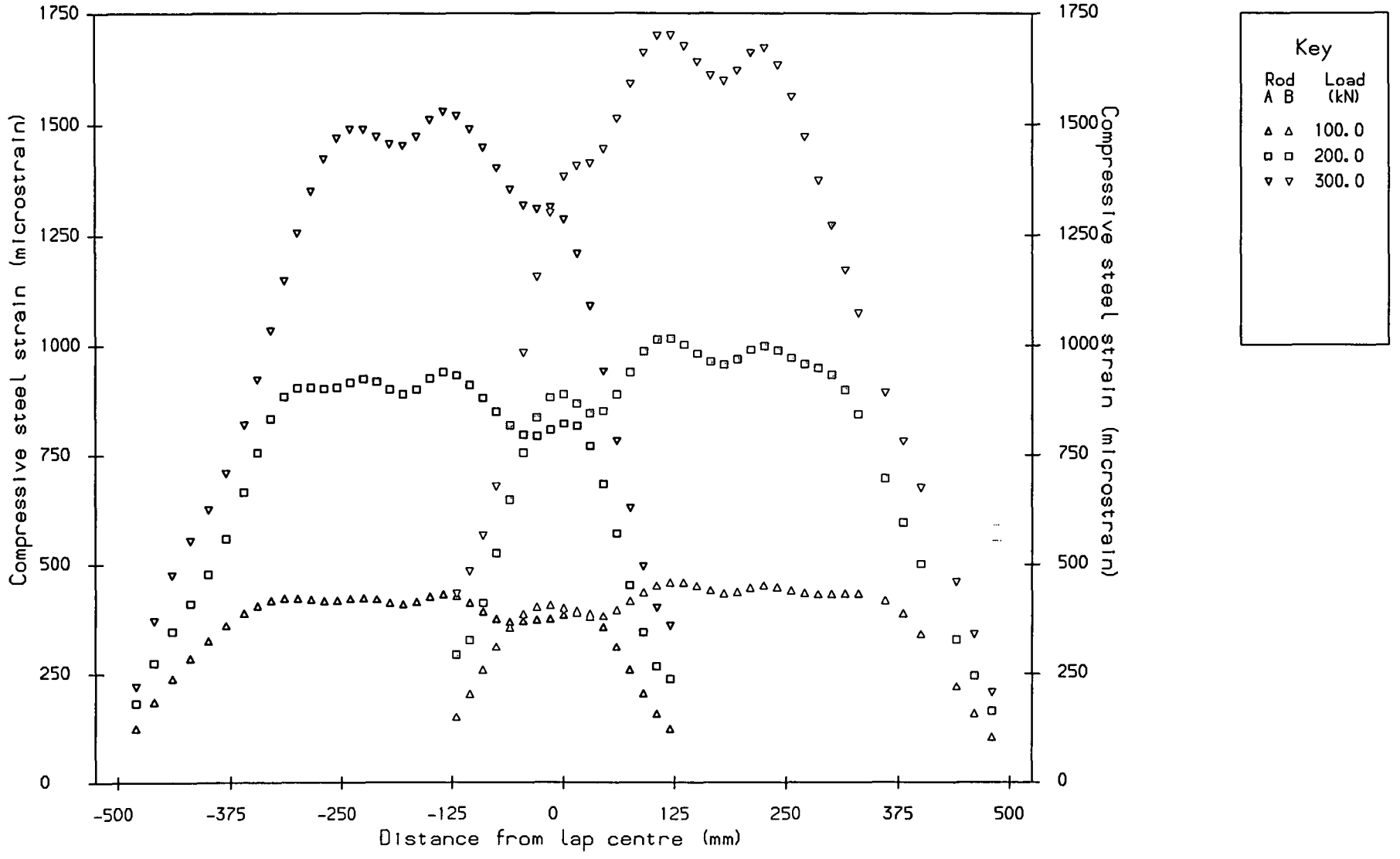

Fig. 7.1.2 Steel Strain Distribution Specimen 250C12/12(A)

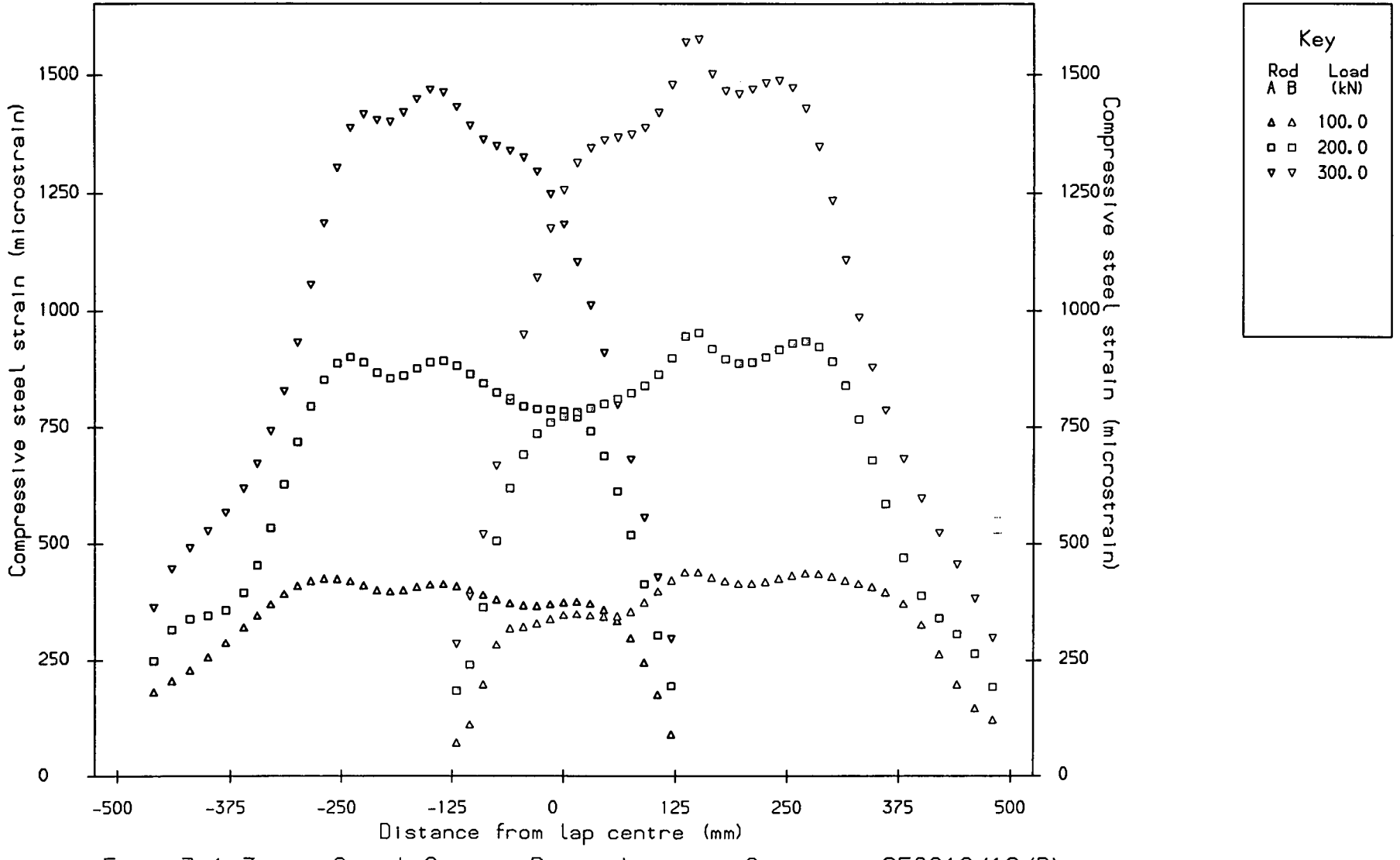

Fig. 7.1.3 Steel Strain Distribution Specimen 250C12/12(B)

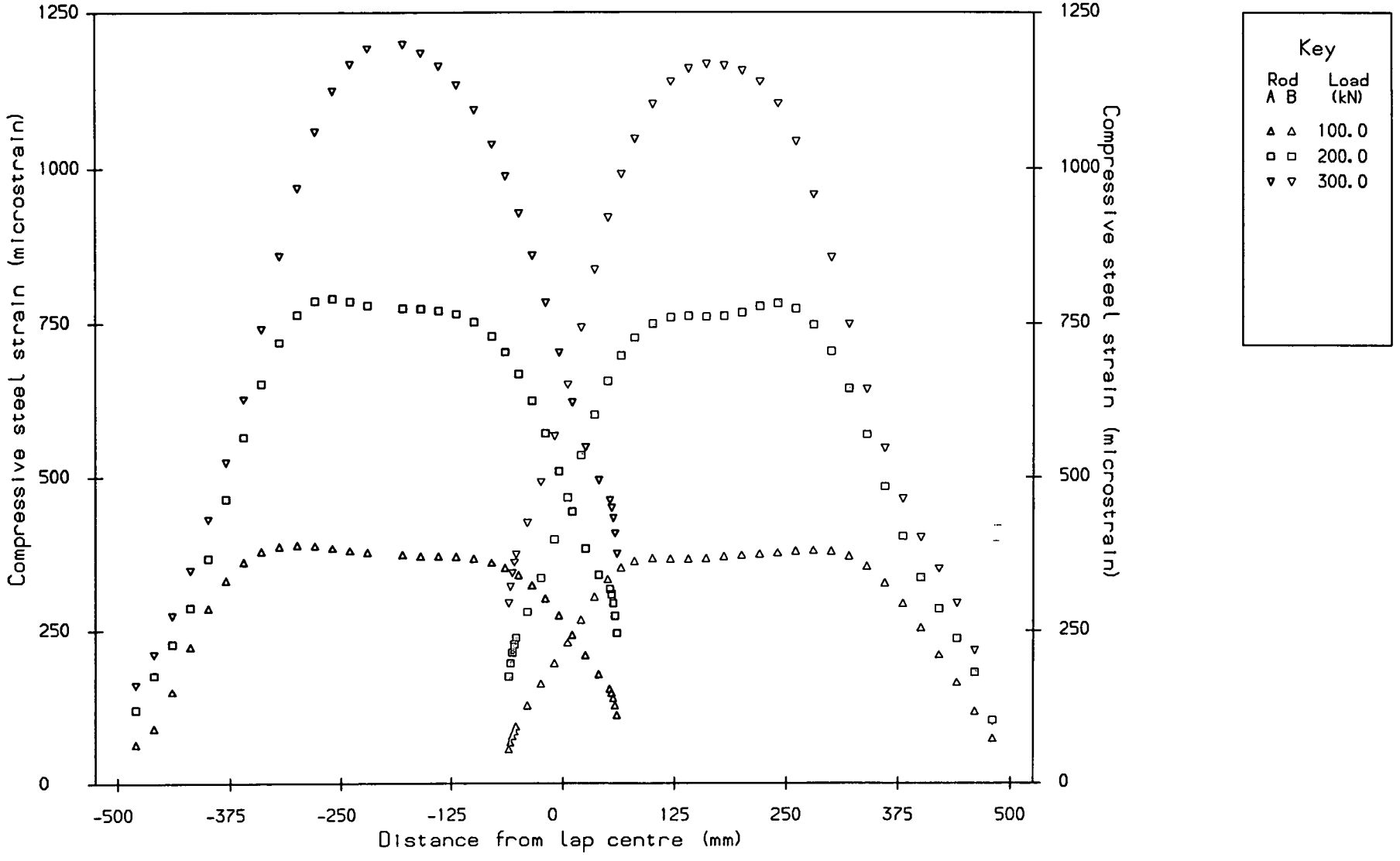

Fig. 7.1.4 Steel Strain Distribution Specimen 125C20/20

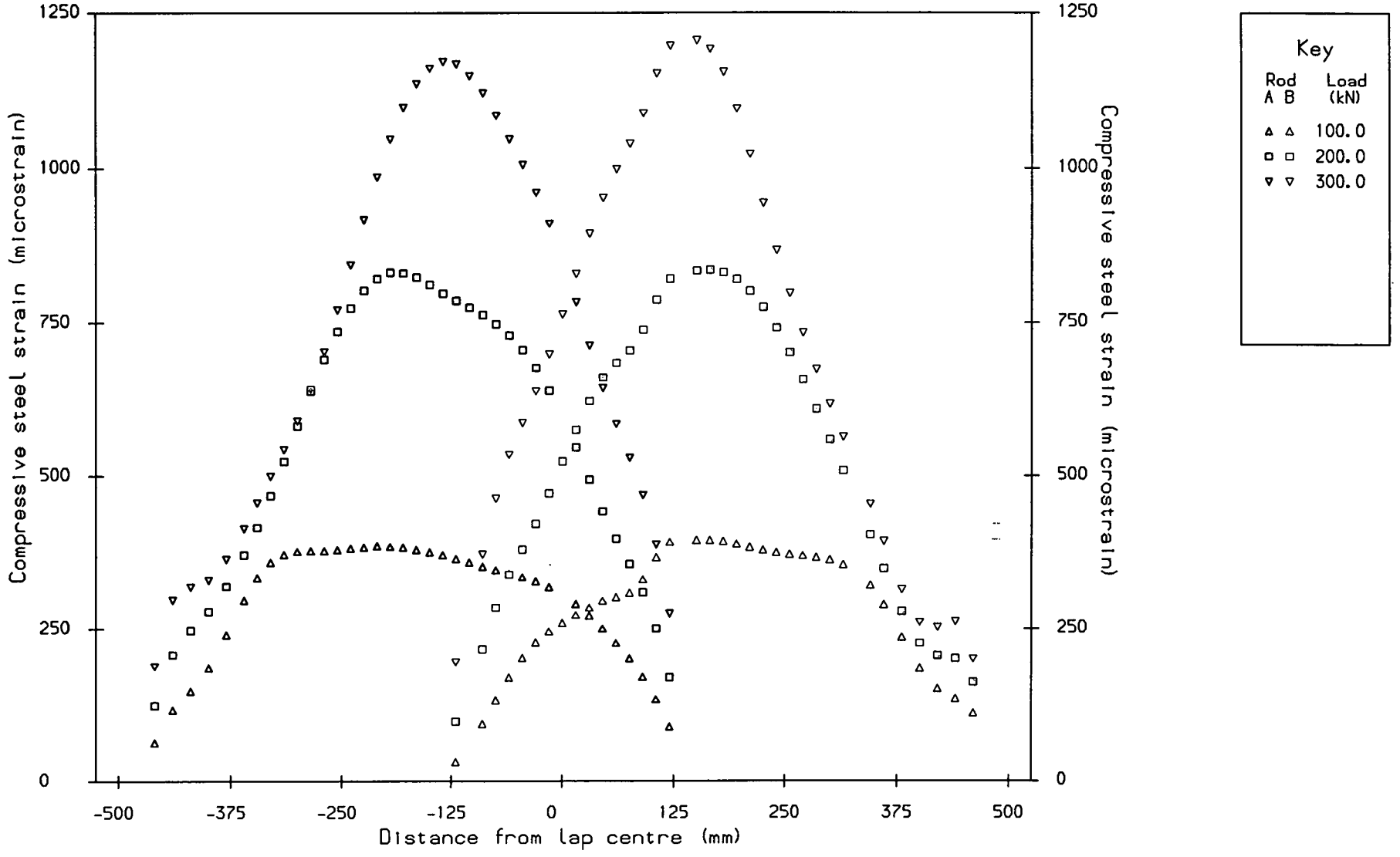

Fig. 7.1.5 Steel Strain Distribution Specimen 250C20/20(E)

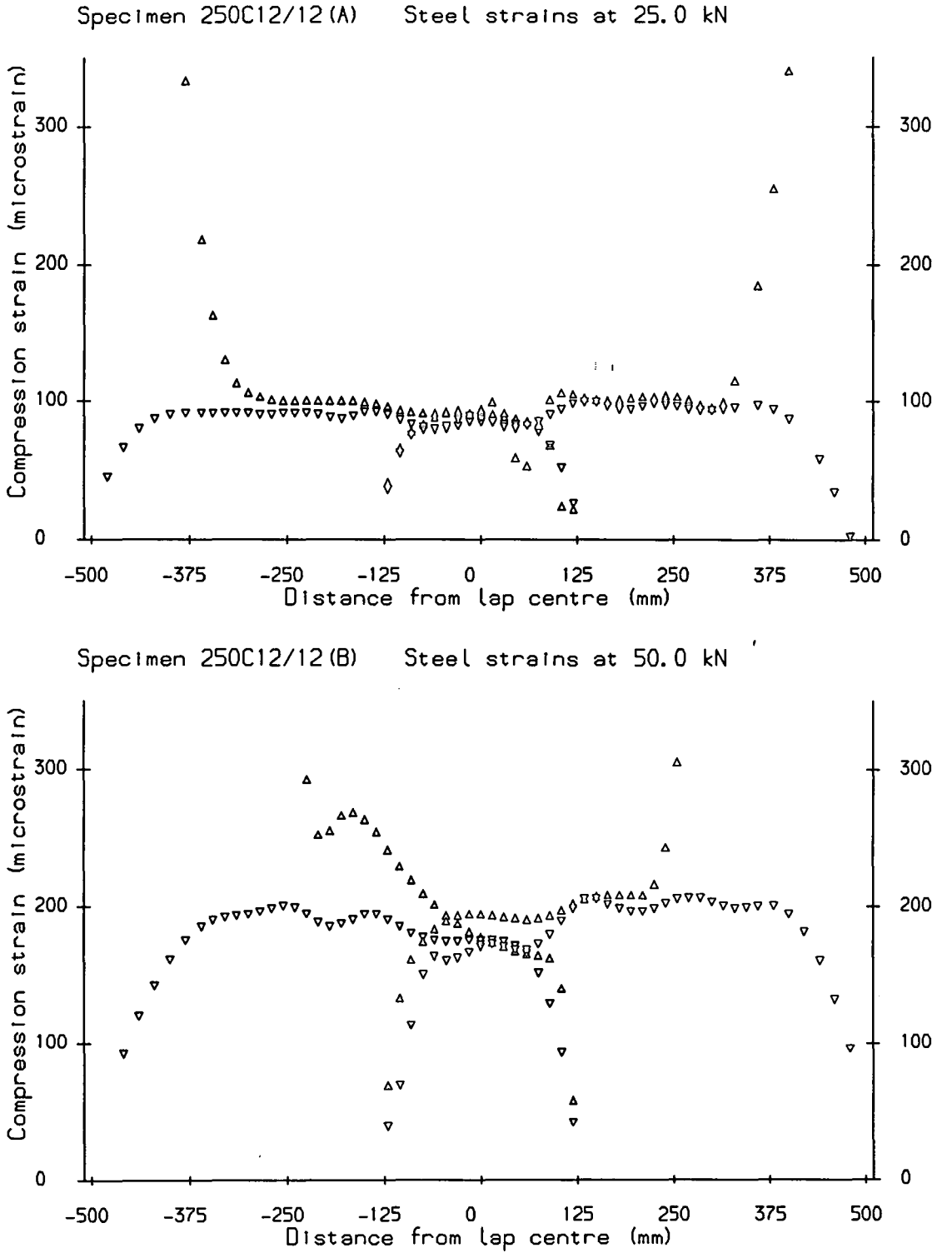

Fig. 7.2 Comparison of Loading Methods

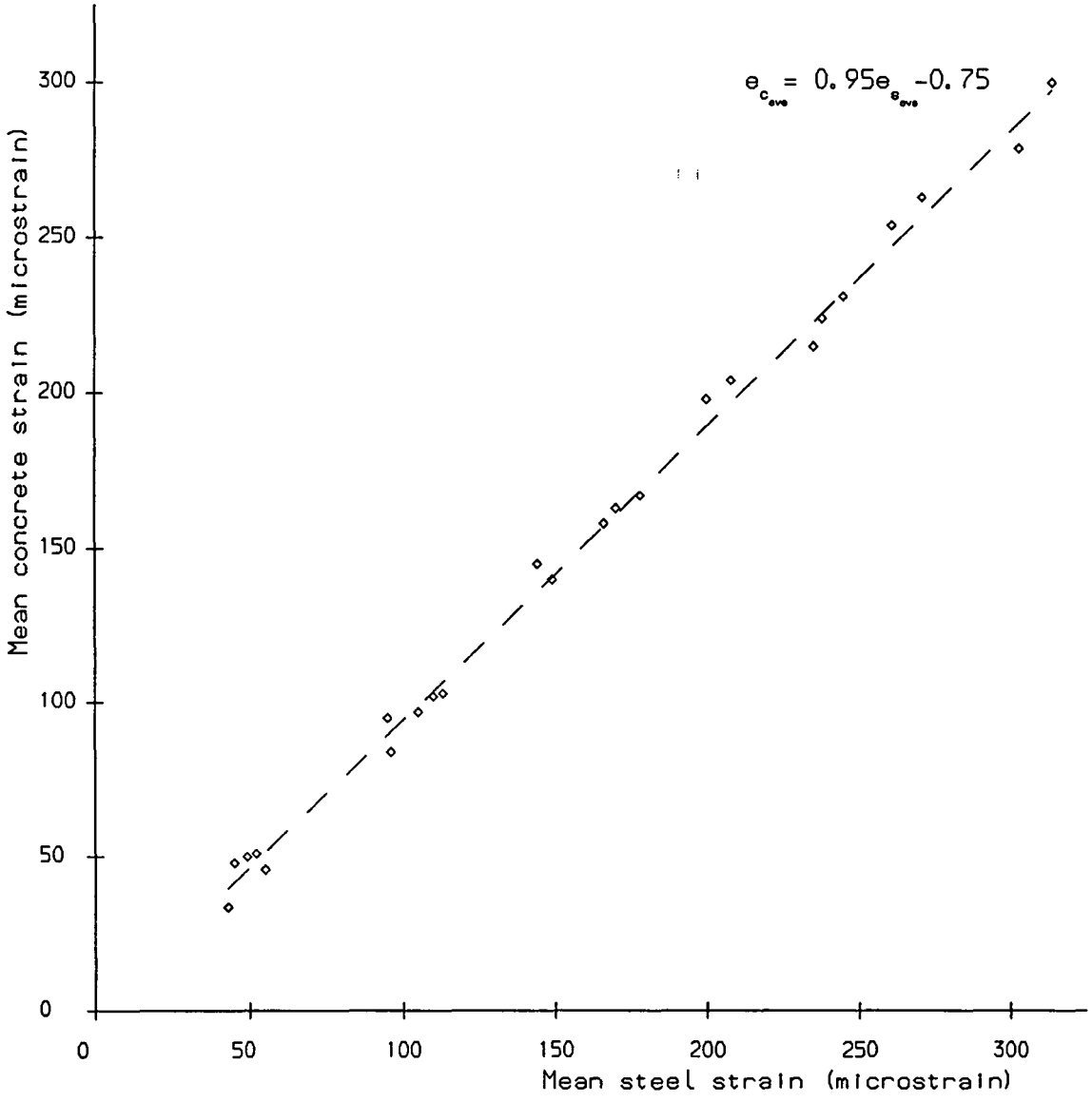

Fig. 7.3 Comparison of Steel and Concrete Strains

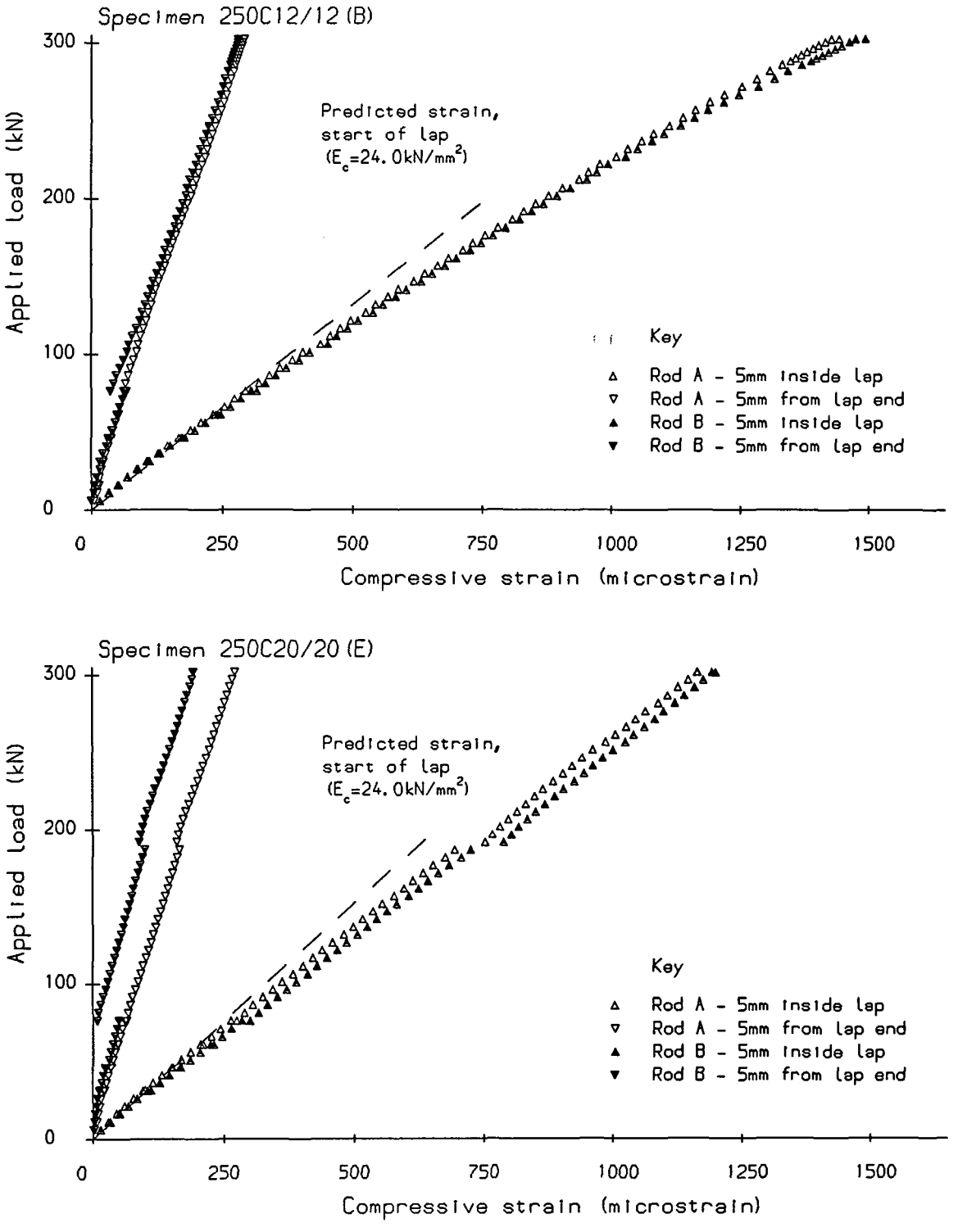

Fig. 7.4 Steel Strains at the Lap Ends

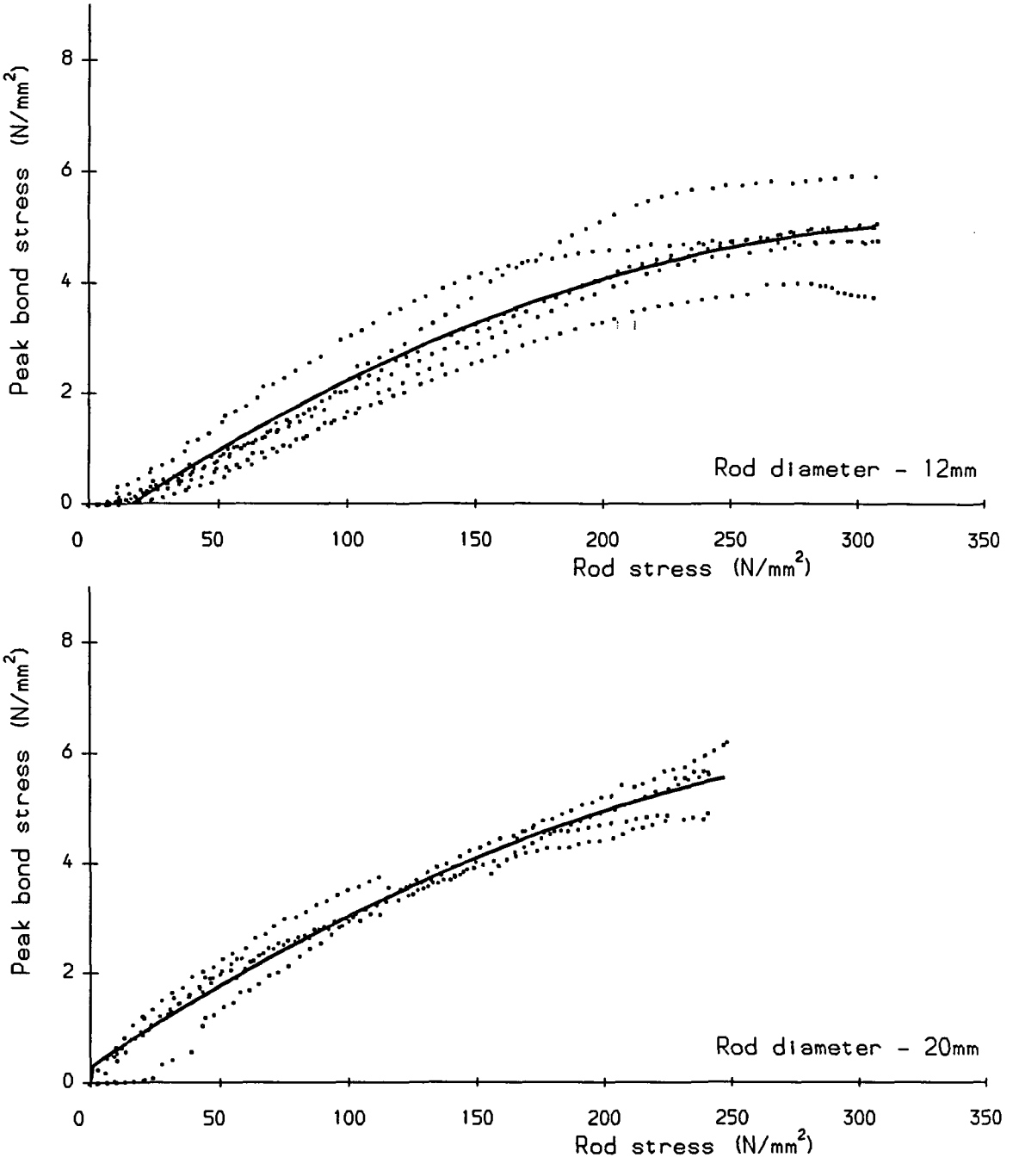

Fig. 7.5 Bond Stress/ Rod Stress Relationship

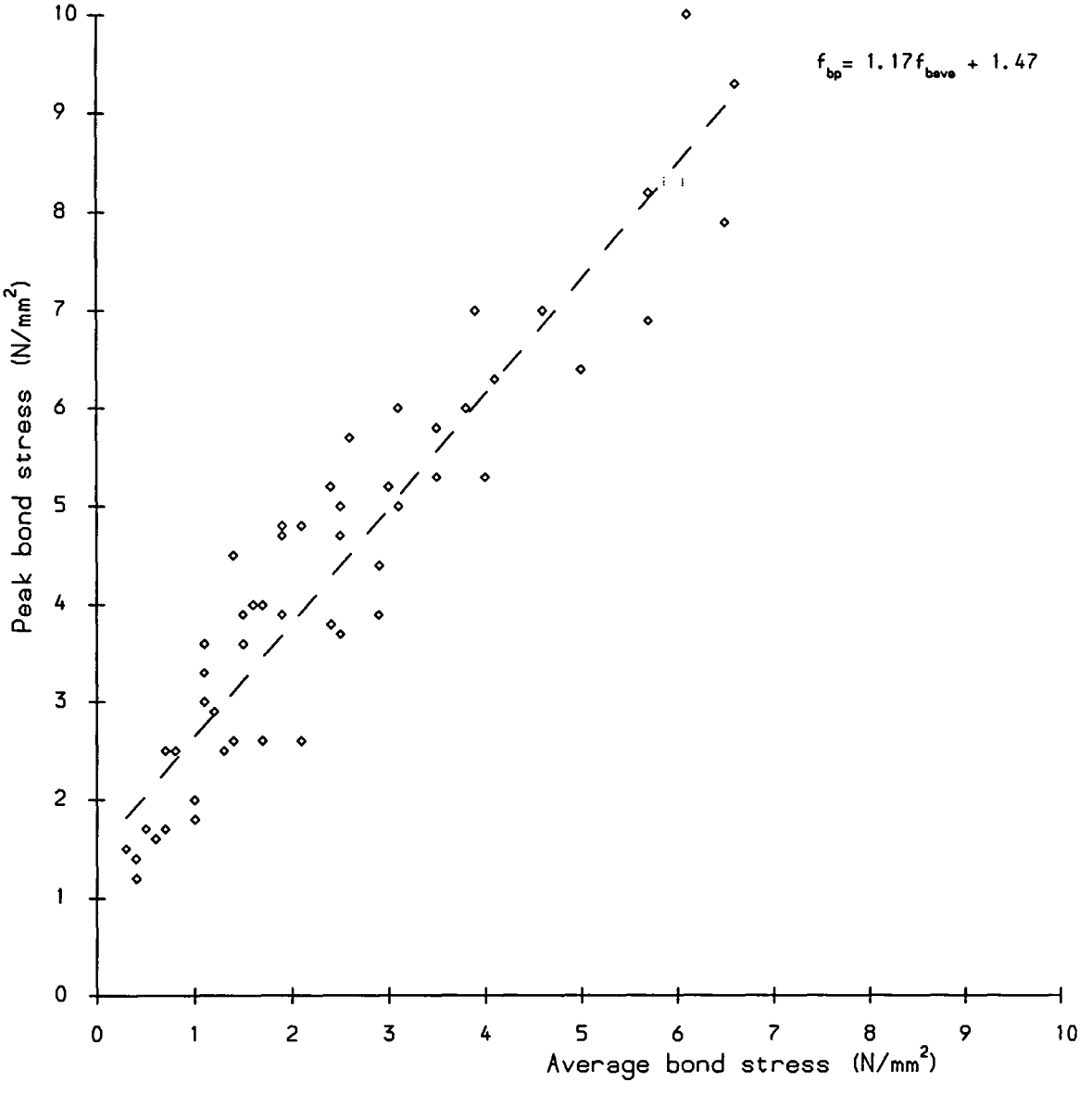

Fig. 7.6 Comparison of Average and Peak Bond Stresses (Compression Specimens)

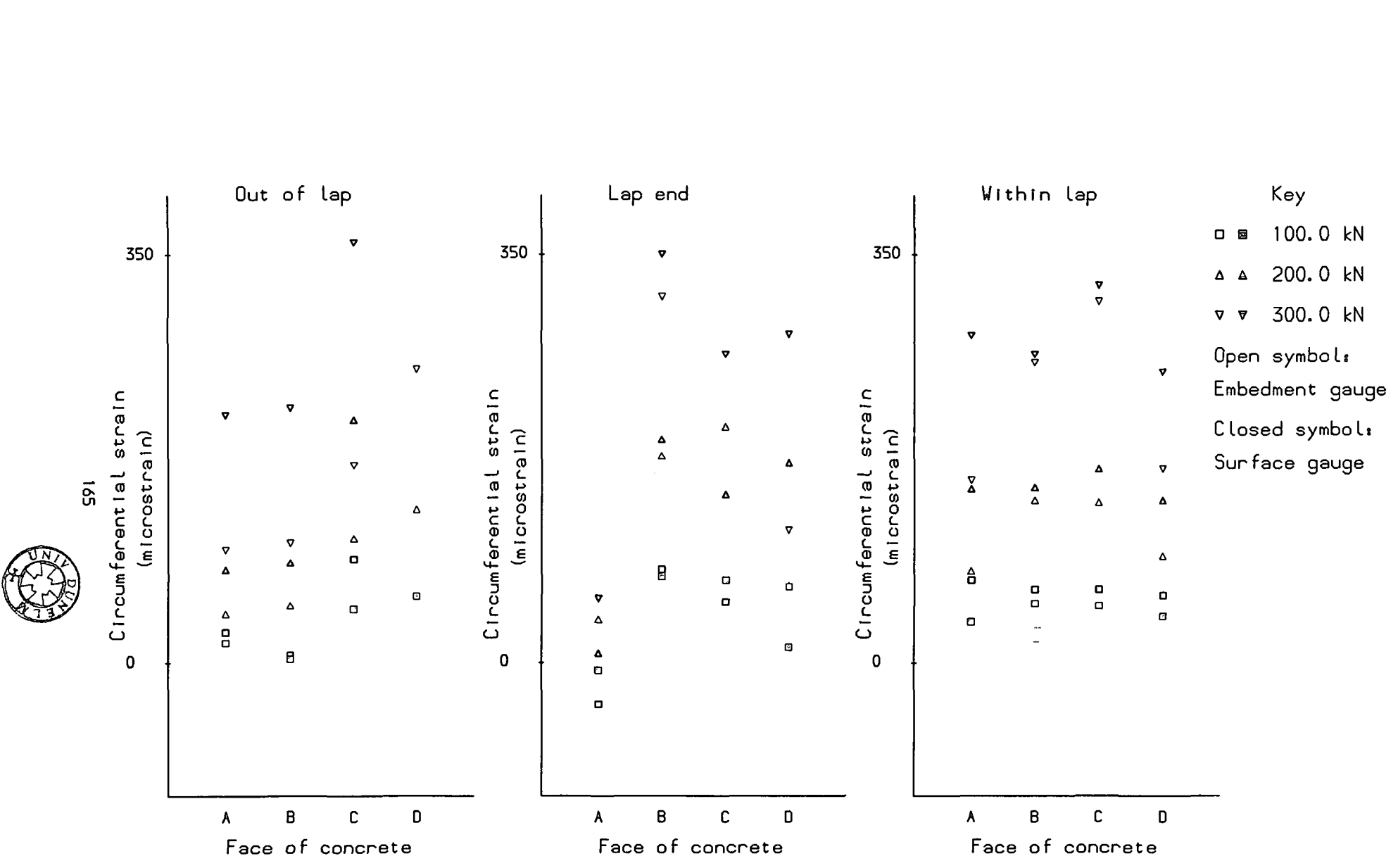

Fig. 7.7 Circumferential Strains Specimen 250C20/20(E)